Old Dominion University

ODU Digital Commons

Chemistry & Biochemistry Theses & Dissertations

Chemistry & Biochemistry

Spring 2021

Evaluating the Role of the Stringent Response Mechanism in *Clostridioides difficile* Survival and Pathogenesis

Astha Pokhrel
Old Dominion University, astha.pokhrel@gmail.com

Follow this and additional works at: https://digitalcommons.odu.edu/chemistry_etds

 Part of the Biochemistry Commons, Chemistry Commons, and the Microbiology Commons

Recommended Citation

Pokhrel, Astha. "Evaluating the Role of the Stringent Response Mechanism in *Clostridioides difficile* Survival and Pathogenesis" (2021). Doctor of Philosophy (PhD), Dissertation, Chemistry & Biochemistry, Old Dominion University, DOI: 10.25777/05ee-2b17
https://digitalcommons.odu.edu/chemistry_etds/56

This Dissertation is brought to you for free and open access by the Chemistry & Biochemistry at ODU Digital Commons. It has been accepted for inclusion in Chemistry & Biochemistry Theses & Dissertations by an authorized administrator of ODU Digital Commons. For more information, please contact digitalcommons@odu.edu.

EVALUATING THE ROLE OF THE STRINGENT RESPONSE MECHANISM IN *CLOSTRIDIOIDES DIFFICILE* SURVIVAL AND PATHOGENESIS

by

Astha Pokhrel
B.Sc. May 2015, Central Connecticut State University
M.S. May 2018, Old Dominion University

A Dissertation Submitted to the Faculty of
Old Dominion University in Partial Fulfillment of the
Requirements for the Degree of

DOCTOR OF PHILOSOPHY

CHEMISTRY

OLD DOMINION UNIVERSITY
May 2021

Approved by:

Erin B. Purcell (Director)

Lesley H. Greene (Member)

Alvin A. Holder (Member)

Patrick C. Sachs (Member)

ABSTRACT

EVALUATING THE ROLE OF THE STRINGENT RESPONSE IN *CLOSTRIDIOIDES DIFFICILE* SURVIVAL AND PATHOGENESIS

Astha Pokhrel
Old Dominion University, 2021
Director: Dr. Erin B. Purcell

The human pathogen *Clostridioides difficile* is increasingly tolerant of multiple antibiotics and causes infections with a high rate of recurrence, creating an urgent need for new preventive and therapeutic strategies. The stringent response, a universal bacterial response to extracellular stresses, governs antibiotic survival and pathogenesis in diverse organisms but has not previously been characterized in *C. difficile.* This dissertation explores the ability of *C. difficile* to mount the stringent response. The bacteria encode a full-length, canonical bifunctional Rel/Spo Homolog or RSH enzyme. *C. difficile* RSH is incapable of utilizing GTP as a substrate but readily synthesizes putative 5'-pGpp-3' alarmones. Transcription of *rsh* is stimulated by bacterial stationary phase onset, nutrient limitation, and exposure to the antibiotics clindamycin and metronidazole. Transcriptional suppression of *rsh* increases bacterial antibiotic susceptibility, suggesting that RSH contributes to bacterial antibiotic tolerance and survival. Chemical inhibition of RSH by the 5'-ppGpp-3' analog Relacin similarly increases antibiotic susceptibility in epidemic *C. difficile*, indicating that RSH inhibitors are a viable strategy for drug development against *Clostridioides difficile* infection. Finally, mechanisms contributing to *C. difficile* host colonization and aspects of bacterial behavior during infection remain unclear. Therefore, this dissertation also explores nutrient-derived motility regulation of the pathogen during host intestinal mucus colonization. An epidemic *C. difficile* strain suppresses motility in the presence of high unchained N-acetylneuraminic acid, an intestinal mucus component. The observed motility suppression is independent of bacterial tumbling but robust single-species biofilm formation by R20291 and motility suppression in response to high NEU5A concentration may be regulated by the same signaling network(s).

Copyright ©, 2021, by Astha Pokhrel, All Rights Reserved.

This dissertation is dedicated to
my loving and supporting parents.

ACKNOWLEDGEMENTS

Firstly, I would like to thank my advisor Dr. Erin B. Purcell, for giving me the opportunity and platform to pursue my Ph.D. research under her guidance. She has been a fantastic mentor to me. Her patience and diligence have been and will continue inspiring me. Above all, her support for my research ideas and goals was one of the most significant driving forces in my graduate student career. I sincerely thank her for being ever so welcoming and considerate.

I am sincerely thankful to my dissertation committee: Dr. Alvin A. Holder, Dr. Patrick C. Sachs, and Dr. Lesley H. Greene. Their invaluable contributions throughout the graduate school have helped mold me into the scientist I am today. I would also like to thank all the Purcell laboratory group members, including the undergraduate students, for their contribution and support in this work. Their discussions and feedback on my projects have been incredibly enriching throughout the years. I feel blessed to have gotten the opportunity to work with such a diverse, friendly, and extremely industrious group of individuals. I would particularly like to thank Dr. David S. Courson for his research-related counseling and guidance. I appreciate all his feedback on my work and for training me in Differential Interface Contrast microscopy as well as mammalian cell culturing. I am also thankful for some faculty and student bodies of the Chemistry and Biochemistry department at Old Dominion University for their collaborative work and help. I am thankful to Kory B. Castro for training me on High Performance Liquid Chromatography and Dr. Michael J. Celestine to train me on Isothermal Titration Calorimetry. I am also thankful to my friends and colleagues at Old Dominion to celebrate the lows and highs of my graduate student experience and share this journey with me. Furthermore, I would like to acknowledge Dr. Rita Tamayo (UNC-Chapel Hill), Dr. Bruno Dupuy (Institut Pasteur, France), Dr. Ravikanthreddy K. Marreddy (Texas-A&M), Dr. Fang Mingxu (UC-San Francisco), Dr. Carl E. Bauer (Indiana University), and Dr. Alex Goranov (Rensselaer Polytechnic Institute) for their helpful correspondence and consultations on some of my projects.

I am most thankful to my parents for their unconditional support throughout my educational career. I am indebted to my father, Resham Bahadur Pokhrel, and mother, Sushila Karki Pokhrel, for their love and making sacrifices to accommodate my academic aspirations since my childhood. I thank them for always prioritizing their children's education and ensuring that they reach the highest potential in life with grace and humility. I am grateful to my little sister, Cristina Pokhrel, for her moral support during this COVID-19-imposed pressing time. I thank her for the care she has shown and for making the last year of my graduate school extremely enjoyable. I am also thankful to my uncle, Dr. Shankar Karki, for his educational and professional advice that has been tremendously impactful through the years. Finally, I would like to thank my husband, Kamod Gautam, to share and support my vision. His unshaking faith in my aspirations and understanding nature has been highly encouraging, especially through challenging circumstances. I thank him for being the calm to my storm.

NOMENCLATURE

Abbreviations	Full forms/ definitions
CDI	*Clostridioides difficile* infection
CDC	Centers for Disease Control and Prevention
CA-CDI	Community acquired *Clostridioides difficile* infection
PaLoc	Pathogenicity locus
TcdA	Toxin A
TcdB	Toxin B
RT027	Ribotype 027
CdtLoc	*Clostridioides difficile* transferase locus
CDT	*Clostridioides difficile* transferase
IDSA	Infectious Diseases Society of America
SHEA	Society for Healthcare Epidemiology of America
rCDI	Recurrent *Clostridioides difficile* infection
FMT	Fecal microbiota transplantation
FDA	Food and Drug Administration
T3SS	Type III Secretion System
GlcNAc	N-acetylglucosamine
PTM	Post-translational modification
TFP	Type IV Pili
c-di-GMP	Cyclic diguanylate
ECM	Extracellular matrix
SLPs	S-layer proteins
FESEM	Field scanning electron microscopy
CLSM	Confocal laser scanning microscopy
SR	Stringent response
GMP	Guanosine-5’-monophosphate
GDP	Guanosine-5’-diphosphate
GTP	Guanosine-5’-triphosphate

ADP	Adenosine-5'-diphosphate
ppGpp	GDP-3'-diphosphate / gaunoisne tetraphosphate
pppGpp	GTP-3'-diphosphate / guanosine pentaphosphate
pGpp	GMP-3'-diphosphate
RSH	RelA/SpoT homolog
SAS	Small alarmone synthetase
SAH	Small alarmone hydrolase
HD	Hydrolase domain
SD	Synthetase domain
NTD	N-terminal domain
CTD	C-terminal domain
TGS	ThrRS, GTPase, and SpoT
ACT	Aspartate kinase, chorismate, and TyrA
GXP	GMP, GDP or GTP substrate
GppA	Guanosine pentaphosphate phosphohydrolase
NuDiX	Nucleoside diphosphate linked moiety X
RNAP	RNA polymerase
rRNA	Ribosomal RNA
30SIC	30S initiation complex
70SIC	70S initiation complex
IF2	Initiation factor 2
RF	Release factor
SETI	Structured enhancer of translational initiation
SPI-1	*Salmonella* pathogenicity island 1
TCP	Toxin-regulated pilus
SHX	Serine hydroxamate
NMR	Nuclear magnetic resonance spectroscopy
PPi	Inorganic pyrophosphate
Pi	Inorganic phosphate
(pp)pGpp	ppGpp, pppGpp, and pGpp
TLC	Thin layer chromatography

PEI-cellulose	Polyethyleneimine-cellulose
HPLC	High-performance liquid chromatography
Std	Standard
ITC	Isothermal titration calorimetry
Magic spot	Product catalyzed by RSH enzymes
Kbp	Kilo base pair
hrs / hr	Hours
KDa	Kilo dalton
MWCO	Molecular weight cut off
mAU	Milli absorbance unit
AU	Absorbance unit
~	Approximately/around
°C	Degree Celsius
OD	Optical density
PCR	Polymerase chain reaction
qRT-PCR	Quantitative reverse transcriptase- PCR
BHIS	Brain heart fusion supplemented with yeast extract
X g	Times gravity
ANOVA	Analysis of variance
DNA	Deoxyribonucleotide
cDNA	Complementary-DNA
RNA	Ribonucleotide
mRNA	Messenger RNA
RNAi	Ribonucleotide interference
asRNA	Antisense RNA
EDTA	Ethylenediaminetetraacetic acid
SDS	Sodium dodecyl sulfate
DTT	Dithiothreitol
PMSF	Phenylmethylsulphonyl fluoride
IPTG	Isopropyl β-D-thiogalactoside
SDS-PAG	SDS-polyacrylamide gel

ARA	Arabinose
GLU	Glucose
NEU5A	N-acetylneuraminic acid
sec	Second(s)
RSHCd	*C. difficile* RSH
RelQBs	*B. subtilis* RelQ
ON	Overnight
CL	Clarified lysate
L	Lysate
PCL	Prepped clarified lysate
FT	Flow through
5'UTR	5' untranslated region
P_{rsh}	Promoter region upstream of *C. difficile rsh*
P_{relQ}	Promoter region upstream of *C. difficile relQ*
P_{tet}	Promoter region of an empty tetracycline-inducible vector
ATc	Anhydrotetracycline
PBS	Phosphate buffered saline
w/v	Weight by volume
CV	Crystal violet
Ni-NTA	Nickel-nitrilotriacetic acid
LB	Luria Bertani
TY	Tryptone yeast
TEM	Transmission electron microscopy
DIC	Differential interface microscopy
K_m	Kinetic constant
K_{cat}	Constant for the turnover of substrate into product
[GDP]	Concentration of GDP
MIC	Minimum inhibitory concentration
MDCK	Madin-Darby canine kidney
DMEM	Dulbecco's modified eagle medium

TABLE OF CONTENTS

Page

Page

LIST OF TABLES

LIST OF FIGURES

Figure Page

CHAPTER I

INTRODUCTION

CLOSTRIDIOIDES DIFFICILE INFECTION

Clostridioides difficile (*C. difficile*), previously known as *Clostridium difficile* is a Gram-positive, obligate anaerobic bacillus that was discovered in 1935 and identified as a severe pathogen only in the late 1970s (1). Today, *C. difficile* is the most common cause of hospital-acquired infection and *C. difficile* infection (CDI) in several developed countries (2). The pathogen contributes to approximately 500,000 cases and 29,000 deaths annually in the United States alone and in 172,000 cases annually in Europe (3-6). According to the Antibiotic Resistance Threats in the United States 2019 report issued by the US Center for Disease Control and Prevention (CDC), *C. difficile* was responsible for ~223,900 hospital admissions cases and ~12,800 deaths in 2017. The economic impact of CDI is enormous. It has led to health care and medical expenditures of over one billion dollars and three billion euro per annum in the US and within the European Union, respectively (6-8). The CDC currently recognizes the pathogen as an urgent public health threat (9).

C. difficile persist as aerotolerant spores in aerobic environments (10). The spore is a metabolically dormant form of the bacterium that houses genetic entities preserved in a dense hydrophobic core, externally protected by a thick proteinaceous coat (11). Due to their dormancy and highly complex structure, *C. difficile* spores are intrinsically resistant to antibiotics, and defenses from the host's immune system (11). They are also tolerant to bleach-free as well as alcohol-based disinfectants commonly used in healthcare settings (11). Furthermore, *C. difficile* spores also survive heat assault, making their eradication extremely challenging from contaminated surfaces (12).

This Dissertation is formatted based on the Journal of Biological Chemistry.

Surfaces most frequently contaminated by *C. difficile* spores include toilet seats, sinks, call buttons, bed rails, and telephones, along with medical devices such as stethoscopes, blood pressure cuffs, and pulse oximeters (9). Other reservoirs for the bacteria include asymptomatic carriers, infected patients, and the animal intestinal tracts (13). Around 5% of adults and 15 to 70% of infants are colonized by *C. difficile*, with colonization prevalence being significantly higher in institutionalized patients, including adults with underlying health conditions (6,13). Notably, the community-acquired incidence of *C. difficile* infection has been increasing with an associated increase in mortality, morbidity, and clinical and economic burden (14,15). According to a CDC-based population surveillance from 2011 to 2017, the estimated burden of community-acquired CDI in the US did not decrease like healthcare-associated CDI and contributed to ~50% of CDI's total national burden in the year of 2017 (16).

Upon ingestion by susceptible hosts, *C. difficile* spores germinate into actively reproducing vegetative cells in the anaerobic mammalian gut. Spore germination is triggered in response to host-derived bile salts, including taurocholate, glycocholate, cholate and deoxycholate, and L-glycine, which is a more effective germinant than the other naturally occurring amino acids (11,17,18). Germination into oxygen-intolerant vegetative cells further leads to the secretion of exotoxins, toxin A (TcdA) and toxin B (TcdB) that are internalized by host intestinal epithelial cells (10). TcdA (308 kilodalton) and TcdB (270 kilodalton) are members of the large clostridial toxin family, encoded by *tcdA* and *tcdB* genes, respectively (10,19). These genes are part of a highly conserved 19.6-Kb pathogenicity locus (PaLoc) of toxigenic strains (19,20). In addition to *tcdA* and *tcdB* genes, three other open reading frames are associated with the PaLoc, including *tcdC, tcdD/tcdR,* and *tcdE* (19). TcdC is suggested to function as a negative regulator of toxin A and B production whereas TcdR acts as a DNA binding protein that positively regulates toxin gene expression and production (19,21). Finally, the gene encoding TcdE is homologous to holin proteins and is suggested to contribute to the release of the toxins through permeabilization of the bacterial cell wall (19,22).

After receptor-mediated endocytosis, both toxins transfer a UDP-glucose to Ras superfamily GTPases (Rho, Rac, and Cdc42), resulting in host cell morphological changes, inhibition of cell division, and blocking of membrane trafficking (19). Rho

GTPase is the primary regulator of the cellular actin cytoskeleton, which plays a critical role in forming and localizing stress fibers at the focal adhesion sites (19). Rho also regulates the formation of prejunctional rings at the apical side of epithelial cells such that inactivation causes epithelial cell rounding from disaggregation of the actin cytoskeleton as well as disruption of the epithelial tight junction (19,23). Consequently, neutrophils are recruited to the intestines, macrophages are activated, and pro-inflammatory cytokines are rapidly released to cause a massive host acute inflammatory response (19). In more severe cases, microulcerations covered with pseudomembranes made of destroyed intestinal cells, neutrophils, and fibrin begin to form on the intestinal mucosal surfaces (13). Unlike Rho, Rac and Cdc42 are involved in lamellipodium and filipodium formation that are structural extensions at the edge of migrating cells (19,24). Rac and Cdc42 facilitate cellular movement and sensing of environmental conditions during migration. Interestingly, TcdA and TcdB promote cell migration despite glycosylating Rac and Cdc42 GTPases (19). In terms of potency, initial studies based on animal models suggested Toxin A to be the dominant intoxicating glycosyltransferase encoded by *C. difficile* until TcdA-, TcdB+ strains became responsible for CDI outbreaks (10,13,25). Studies involving human colonic epithelial tissues and transplantation of human xenografts in immunodeficient animal models have identified Toxin B to be more potent, although both toxins can elicit CDI symptoms independently of one another (13,26,27).

The incidence of CDI has markedly increased in the last 20 years, largely due to the emergence and dissemination of the *C. difficile* polymerase chain reaction ribotype 027 (RT027) or R20291 (28). RT027, which was first isolated in North America and Europe back in the 2000s, is naturally hypervirulent (25,29). Hypervirulence of the strain is associated with reduced susceptibility to a wide array of antibiotics including fluoroquinolones (30). The strain also spreads more easily and rapidly within hospital settings as it can produce higher levels of spores and toxins (30,31). Importantly, RT027 strain produces an additional toxin called *C. difficile* transferase (CDT) or binary toxin, which is encoded by the *C. difficile* transferase (Ctd) locus (CdtLoc) (10). Unlike TcdA and TcdB glucosyltransferases, *C. difficile* CDT, is an ADP-ribosylating enzyme that disrupts the cytoskeleton of epithelial cells by inhibiting actin polymerization (10,19,30). Inhibition of actin polymerization consequently leads to excessive fluid loss, cell rounding,

and apoptosis (10). CDT (~43 kilodalton) comprises two separate components: CDTa and CDTb, where CDTb binds to gut epithelial cells resulting in the uptake of CDTa (30). CDT also induces the formation of thin microtubules that promote *Clostridia* adherence to host intestinal epithelial surfaces along with increasing TcdA and TcdB uptake (30,32). In the last decade, the percentages of CDI caused by the RT027 strain is reported to be 51% and 84% in the US and Canada, respectively (33,34).

The clinical manifestation of CDI ranges from asymptomatic carriage, mild or moderate diarrhea, to life-threatening fulminant colitis and toxic megacolon (13). Most patients experience mild diarrhea and recover spontaneously after 5 to 10 days of treatment withdrawal (13). In addition to watery stool, clinical features of CDI is accompanied by abdominal pain, fever, weakness, nausea and vomiting, and loss of appetite (13). Severe clinical presentations involve symptoms such as dehydration, hypoalbuminemia, and subsequent circulatory shock (13). Additional complications include colon perforation, intestinal paralysis, kidney failure, systemic inflammatory response syndrome, and septicemia (13).

The primary risk factor for CDI development is antibiotic exposure. However, other significant risk factors include advanced age, residence in long-term care facilities (hospitals and nursing homes), and prior medical conditions such as immunosuppression, inflammatory bowel diseases, and chronic kidney disease, and/or gastrointestinal procedures (6,13,35,36). Antibiotics have serious and long-lasting effects on the bacterial ecosystem of the host gut. The highly organized intestinal ecosystem comprises numerous bacterial species, mainly those belonging to the *Firmicutes* and *Bacteroidetes* phyla, whose concentration is heightened in the colon (6,37-39). The commensal microbiota plays a crucial role in maturating the immune system and protecting against enteric pathogens. Disruption of this well-balanced ecosystem via antibiotic exposure alters microbial diversity and composition, promoting *C. difficile* colonization (6). Antibiotics associated with the development and increased frequency of CDI include metronidazole, vancomycin, broad spectrum penicillins and cephalosporins, clindamycin, and fluoroquinolones (6,13). Cephalosporins are known to decrease members of the healthy *Clostridia, Lactobacilli*, and *Bifidobacteria* taxa, whereas clindamycin decreases species of the anaerobic *Bifidobacterium*, *Clostridium*, and *Bacteroides* genera (40,41).

Another significant role of commensal bacteria, particularly those in the *Lachnospiraceae*, *Ruminococcacae*, and *Blautia* families of *Firmicutes* as well as *Clostridium* spp., is to metabolize primary bile acids into secondary bile acids via deconjugation and 7-α-dehydroxylation mechanisms (42,43). As mentioned previously, *C. difficile* spores germinate into replicating vegetative cells in the presence of primary bile acids such as taurocholate and cholic acid to promote vegetative cell outgrowth (43). Secondary bile acids, on the other hand, inhibit *C. difficile* growth (44,45). Antibiotic-induced alterations of the intestinal microbiota cause an increase in the primary bile acids concentration and a concurrent decrease in secondary bile acids concentration, enhancing colonization. The commensal *Bacteroidetes* and *Firmicutes* phyla are depleted and changed, respectively, with a concurrent increase in pathogenic *Enterobacteriales* and *Proteobacteria* diversity in CDI patients (42,46).

C. difficile colonization is very common in the elderly population due to inadequate innate or humoral immune responses and loss of commensal bacterial diversity in this age group (6,47-51). Patients above 65 years of age carry an increased risk for CDI development, ~5 to 10-fold higher relative to younger patients (13). Although a significant portion of CDI incidence also occurs in the younger age group, the poor clinical outcome of the disease (higher severity and mortality) is directly associated with advanced age (13). Prolonged stay in healthcare institutions also corelates with CDI incidence. The incidence of bacterial colonization during the first few days of hospitalization ranges from 2.1 to 20% and gradually increases with extended stay (52-56). Furthermore, nursing home residents are also at high risk for CDI possibly due to older age, health comorbidities, frequent hospitalizations, and antibiotics exposure compared to the non-institutionalized population (13).

Prevention of CDI has mostly included the use of gloves and disposable gowns in healthcare settings since *C. difficile* spore transmission occurs from person to person contact and through the fecal oral route (13,35). After direct contact with CDI patients, it is recommended to wash hands with soap and water (57). Since alcohol-based disinfectants are ineffective at killing *C. difficile* spores, it is ideal to use chlorine-based solutions such as sodium hypochlorite for environmental cleaning (58). Treatment wise, primary therapy of moderate and severe CDI has included the use of metronidazole and

vancomycin (59). While the Infectious Diseases Society of America (IDSA) and Society for Healthcare Epidemiology of America (SHEA) guidelines issued in 2018 no longer recommends the use of metronidazole as a first-line treatment, multiply recurrent CDI (rCDI) is a significant problem associated with the use of vancomycin (4,29,36,60-63). The recurrence rate after the first bout of CDI treatment (or second episode within 8 weeks of discontinuing antibiotic therapy for primary infection) using vancomycin is ~10 to 35%, and that the risk for subsequent recurrences is at least 40% (36,59,64). Patients with three or more relapses often experience consecutive relapse episodes, leading to low quality of life with minimal therapeutic options (57,59). Unlike vancomycin, fidaxomicin is associated with a lower recurrence rate via the inhibition of *C. difficile* spore formation and toxin production (65,66). Fidaxomicin targets exosporium and spore coat proteins to inhibit germination and internalizes vegetative *C. difficile* cells (67). Furthermore, the use of fidaxomicin is also advantageous over vancomycin due to the twice-daily dosing regimen of the former antibiotic over quadrice-daily dosing (36). However, fidaxomicin is expensive, preventing its widespread use and resistance of the epidemic strains to the antibiotic has been reported in clinical trials (59,65,66,68). As *C. difficile* demonstrates high survival rates when treated with multiple classes of antibiotic, including beta-lactams, cephalosporins, clindamycin, and fluoroquinolones, microbiome restoration through fecal microbiota transplantation (FMT) continues to be the most effective therapy for rCDI (7,36,63,69,70). The introduction of suppressive bacterial species from screened and healthy donors to *C. difficile* colonized gastrointestinal tracts of infected patients has demonstrated between 80 to 90% success rate (57,71,72). Unfortunately, the technique carries an inherent risk of transmitting undetected pathogens and chemical agents to the recipient (73,74). Additionally, the long-term effect of the therapy remains to be determined (74). In 2019, two immunocompromised patients were reported to develop extended spectrum β-lactamase producing *Escherichia coli* infection post-FMT, which lead to the demise of one of the patients (75).

Another significant drawback of FMT is the heterogeneity associated with the methodological components of the procedure, including donor screening, donor and stool sample preparation, and instillation as well as patient follow-up (36). To establish standardization of the FMT technique for universal therapeutic usage, capsule-based

products such as CP101 (Phase II), RBX7455 (Phase I), SER-109 (Phase III), and enema-based RBS2660 (Phase II and III) have demonstrated appreciable efficacy in double-blinded randomized-controlled trial (36). Nevertheless, replacement of the conventional FMT with standardized microbiome restoration products appears to be encouraging also because patients' experience with and perception regarding traditional FMT is reportedly unpleasant (36,76).

Newer approaches to managing CDI and multiply rCDI have included the administration of monoclonal antibodies directed against *C. difficile* toxins in conjugation with antibiotic therapy. Bezlotoxumab is the United States Food and Drug Administration (FDA)-approved human monoclonal antibody that targets toxin B, and that is associated with a substantially lower rate of rCDI (63,77). Notably, some vaccines that have entered late-stage clinical trials include injectable anti-toxin vaccines and formalin-inactivated toxin A and B by Sanofi Pasteur (63). Genetically and chemically inactivated toxin A and B vaccine by Pfizer and a single recombinant fustian protein with segments of the bacterial toxins by Valneva have also entered Phase 3 clinical trials (63). The use of probiotics as an alternative to antibiotics and FMT is also being largely explored in the field. Much like the native intestinal microbiota, probiotics stimulate the host immune system, compete with enteric pathogens for nutrients, and inhibit colonization of foreign species (78,79). *Bifidobacterium* as well as the combination of *B. longum* and *B. bifidum* with prebiotics are known to be protective against *C. difficile* (80,81). Widely used *Lactobacilli* probiotics also inhibit *C. difficile* growth where *Lactobacillus rhamnosus* GG interfere with key metabolic pathways in the bacteria such as Stickland reactions and butyrate metabolism, resulting in the negative regulation of toxin production (82,83).

In summary, diverse approaches are available and under development for the management of CDI and rCDI. However, the development of more effective prevention and therapeutic strategies continues being urgent.

FACTORS PROMOTING *CLOSTRIDIOIDES DIFFICILE* VIRULENCE

Adhesion of bacteria to target cells is the first step in colonization and the establishment of pathogenesis. Therefore, it is imperative for *C. difficile* to find a way to get through the host intestinal lumen and into the mucosa to the epithelial cells for attachment and infection. Notably, mammalian epithelial mucosal tissues are coated by a high viscosity mucus layer composed of water and glycosylated mucin components (84). Hence, movement or motility through the mucus barrier to the epithelial lining is essential for successful colonization. The secretion of flagella provides many species with ability to be motile, to colonize abiotic and/or biotic surfaces, to optimize growth, and to survive attacks from the host (85,86). In a few gastrointestinal pathogens, including *Campylobacter jejuni* and *Vibrio cholerae*, flagella play roles in bacterial motility, adherence, and colonization (87-90). Therefore, flagellar mutations cause these bacteria to become less adherent and less pathogenic in nature (91-95).

The flagellum is constituted of a basal body which contains the reversible motor that anchors the structure to the cell membrane while powering organelle rotation, a hook that extends out from the top of the basal body, and the filament which extends ~20 μm from the hook to form the helical propeller when rotated (Fig. 1) (86,87,96). Self-assembly of the flagellum is a multi-stage hierarchical process that begins with the coordinated assembly of the flagellar type III secretion system (T3SS), the MS-ring in the cytoplasmic membrane, and the C-ring at its cytoplasmic face (87). In Gram-negatives, the MS- and C-rings form a scaffold for the assembly of the flagellar T3SS first followed by the assembly of the peptidoglycan-spanning P-ring and lipopolysaccharide-spanning L-ring (87). Notably, the L- and the P-rings are lacking in the structure of a Gram-positive flagellum (Fig. 1). Consequently, the activated T3SS recruits, unfolds, and exports proteins through the axial structure's hollow core in order to assemble the periplasm-spanning rod, the flagellar hook, and the filament in a highly coordinated fashion (87). As mentioned previously, the motor of the flagellar basal body is responsible for fueling flagellar rotation. This transmembrane protein complex transduces energy from the flow of H^+ or Na^+ ions across the inner membrane, causing a conformational change in the C-ring torque that is coupled to the rod, the hook, and the filament (87). The propulsive force

generated by the flagellar rotation subsequently leads to bacterial movement at speeds ranging from 25 to 160 µm/sec (87,97,98). Due to flagellar rotation that propels bacteria forward in the direction of suitable niches (swimming motility) and/or for adhesion and colonization sake, flagellated species do not rely on the Brownian motion (87).

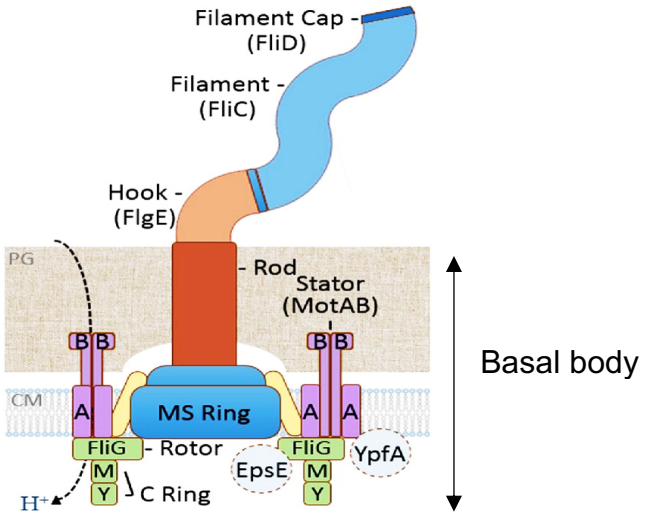

Figure 1. Diagram of a Gram-positive flagellum. Gram-positive flagellum showing the basal body, the hook, and the filament. Adapted from Purcell *et al.* 2016.

Several genes governing the structural integrity and function of the flagellum in relevant flagellated species have also been identified in different *C. difficile* strains (86). These genes are organized into three distinct loci called F1, F2, and F3 (61,86). The hierarchical transcription of flagellar genes is firstly initiated in the F3 regulon or *flgB* operon, which comprises early flagellar genes such as the *fliA* (86). This operon mainly encodes motor and structural components of the organelle along with the alternative sigma factor SigD necessary for flagellar assembly and bacterial movement. The SigD alternative sigma factor regulates the transcription of flagellar genes in the late-stage F1

and F2 operons (99,100). The F1 regulon houses three *ƒliA* promoter regions (86). The same operon also encodes flagellin FliC and the protein cap FliD, both of which are structural proteins critical for attaining complete flagellar functionality (86,101). Interestingly, variation in the F1 regulon between *C. difficile* strains have been recorded, supporting the findings that the R20291 strain is more motile with higher flagellar counts in comparison to the non-epidemic or historical strain *C. difficile* 630 (61,86,102). Lastly, genes in the F2 regulon encode proteins that play parts in filament glycosylation (86,90). Notably, the F2 operon of *C*. *difficile* 630 strain carries four genes encoding glycosyl transferases, whereas that of R20291 carries six (61).

Post-translational modification (PTM) of *C. difficile* flagella is critical for flagellar assembly and bacterial motility. In 2009, Twine and group determined that *C. difficile* flagellin undergoes modification by O-linked glycans and that this modification varies between *C. difficile s*trains (103). According to Twine *et al.,* the addition of N-acetyl hexosamine is dependent on the specific glycosyltransferase gene (CD0240) from *C. difficile* 630 F1 operon such that inactivation results in the loss of surface-associated flagellin protein and in impaired bacterial motility (103). Years later, Faulds-Pain *et al*. showed that a β-O-linked N-acetylglucosamine (GlcNAc) glycan is attached to either serine and/or methylated phosphor-threonine of the flagellin to induce PTM (104). Nevertheless, mutations in the CD0240 gene and those downstream of CD0240 in the F2 operon (with putative roles in flagellin modification) lead to bacterial autoagglutination, increased cellular binding to abiotic surfaces, and reduced colonization in a relapsing model of CDI (104). Autoagglutination is a process of bacterial cells either clumping together or with host cells. Several surface structures in bacteria influence autoagglutination. For instance, *C. jejuni* employs a flagellin-dependent autoagglutination strategy to promote virulence (86,105). The degree of autoagglutination in *C. difficile* is strain-specific and that this dependency is majorly due to differences in flagellar glycosylation pattern (61,86). Valiente *et al.* studied genes in RT027 with predicted roles in flagellar glycosylation and PTM (106). Mutation of two putative glycosyltransferase genes, GT2 and GT3 as well as those with predicted coding sequences of the F2 operon, immediately downstream of *ƒliC* gene demonstrated reduced motility but an increase in

autoagglutination (106). This suggests that the PTM of *C. difficile* flagellin influences pathogenesis.

Flagellum-mediated motility contributes to bacterial colonization and virulence in many species. Flagellar filaments are responsible for probing the host cell surface for contact and interaction with polymeric proteins, proteoglycans, glycolipids, and phospholipids (84). Flagella contributes to *C. difficile* adherence to epithelial cells *in vitro* and host colonization in a strain-specific manner. Mutation in the *ƒliC* gene of the RT027 strain has been shown to reduce bacterial adherence to mammalian cell lines and colonization in mouse models (107). Surprisingly, a mutation in the same gene from *C. difficile* 630Δ*erm* (RT012) strain, an erythromycin sensitive variant of the non-epidemic 630 isolate, increased bacterial adherence to mammalian cells without affecting colonization (107,108). This indicates that flagella-driven motility is not necessary for colonization in all genetic variants of *C. difficile,* but the flagellum can function as an adhesin is some, promoting bacterial interactions with the host (90). Aubury *et al*. also used 630Δ*erm* strain to generate early-stage flagellar gene mutants and late-stage *ƒliC* and *ƒliD* mutants (109). They found mutations in early stage flagellar genes to attenuate virulence in hamster models of infection, whereas *ƒliC* and *ƒliD* mutations lead to increased virulence and quick transitioning of infection models to a moribund state (109). The same study also recorded a decrease in toxin production due to early-stage flagellar gene mutations (109). The association between flagellar genes and toxin production can be explained by the role of the flagellar alternative sigma factor SigD. SigD regulates *tcdA* and *tcdB* gene expression and toxin production in *C. difficile* via *tcdR* activation such that *sigD* mutations lead to decreased toxin expression, production, and virulence during infection (109). Nevertheless, the flagellum is an essential organelle of *C. difficile* physiology with roles in bacterial motility and colonization, even motility-driven dispersal of cells to find new surfaces to colonize (87).

Another surface-associated protein encoded by many Gram-negative and select Gram-positive species is the Type IV pili (TFP) that regulate bacterial movement, adherence to host cells, DNA uptake, transformation, and protein secretion (Fig. 2) (110-112). TFP can also act as nanowires carrying electric current and that pilus biosynthesis occurs through the type II protein translocation pathway (112,113). This surface-

associated macromolecule is polymerized from an inner membrane-bound pool of pilin monomers (PilA) via the PilB ATPase, and is held to the pilus filament via hydrophobic interactions and assembly of the PilM, PilN, and PilO proteins required for extension (Fig. 2) (112). Retraction of the pilus, on the other hand, is controlled by the disassembly of the PilA pilin subunits into the inner membrane, a mechanism powered by the PilT ATPase (113).

In contrast to the flagellar filament, TFP make thinner and shorter filaments that extend from the bacterial surface (Fig. 3) (110). Interestingly, both flagellum and TFP can coordinate with each other to facilitate bacterial adhesion and colonization. In some cases, for instance, TFP reinforce flagella-mediated transient and reversible interactions of bacteria, resulting in more robust and permanent associations (110,114). Mechanistically, TFP promotes bacterial motility through the extension, attachment, and retraction of the pilin fiber along a solid surface (110). The TFP-based motility that aid in bacterial propulsion to reach target sites has been described in many species including, *Neisseria*, *Pseudomonas, Myxococus xanthus*, *C. difficile,* and *Clostridium perfringens* (115,116). Furthermore, in *C. difficile*, TFP contributes to *in vitro* cell aggregation in a 3'-5' cyclic diguanylate (c-di-GMP)-dependent manner (117). Inactivation of *pilA1* (encoding PilA monomer) and *pilB1* (encoding PilB ATPase) genes from the primary TFP loci hinders pilus formation and reduces *C. difficile* autoaggregation (117). c-di-GMP is a bacterial second messenger that regulates the switch of cells from motile, free-living, or planktonic state to sessile while playing multifaceted roles in bacterial physiology and virulence. The cytoplasmic levels of c-di-GMP is regulated by GGDEF-domain containing diguanylate cyclases and EAL or HD-GYP-domain containing phosphodiesterases that synthesize and hydrolyze the signaling molecule, respectively (110). In Gram-positives, two protein receptors for c-di-GMP have included the PilZ-domain protein and the transcription factor BidD. Furthermore, class I and II types of riboswitches have also been identified in different bacterial groups that bind c-di-GMP and regulate gene transcription (110). Importantly, the *C. difficile* 630 genome encodes 37 predicted c-di-GMP cyclases and phosphodiesterases (31 of which are conserved in R20291), one PilZ domain, 12 predicated class I, and four class II riboswitches (110). An increase in the intracellular c-di-GMP concentration via the overexpression of DccA synthetase (GGDEF-domain

carrying diguanylate cyclase) inhibits flagellar-driven motility and induces *C. difficile* cell clumping (117-119). According to Purcell and colleagues, repression of flagella-mediated motility at elevated c-di-GMP levels is due to the binding of c-di-GMP to the type I riboswitch located upstream of the *f*lgB flagellar biosynthesis operon (119). As mentioned previously, the *f*lgB or F3 operon includes *sigD*, which regulates *tcdA* and *tcdB* gene expression and toxin production via the *tcdR* of the PaLoc. Therefore, increased concentration of cytoplasmic c-di-GMP also inhibits *C. difficile* toxin production via premature transcription termination of the *sigD* (99). c-di-GMP-dependent motility suppression and induction of cell aggregation via the TFP has been reported to involve a c-di-GMP riboswitch that transcriptionally regulates TFP biosynthesis genes (117). Binding of c-di-GMP to the class II_4 riboswitch located upstream of the TFP primary locus facilitates *C. difficile* autoaggregation, which contributes to biofilm formation (117). In 2018, McKee *et al*. evaluated the role of TFP in the ability of *C. difficile* to adhere to and colonize the intestinal epithelial cells (120). Based on their observations, c-di-GMP promotes TFP-mediated attachment of *C. difficile* to colonic epithelial cells such that mutations in TFP genes (*pilA1* and *pilB1*) result in reduced bacterial adherence (120). Overall, these findings suggest that c-di-GMP signaling regulates virulence in *C. difficile* by inhibiting flagella-dependent swimming and enhancing TFP-dependent aggregation and biofilm formation in the colonic epithelial surface.

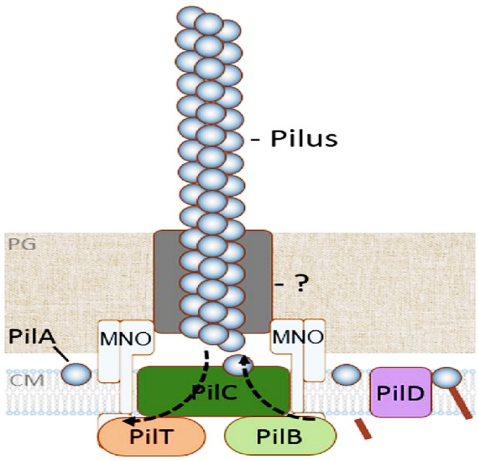

Figure 2. Diagram of Gram-positive Type IV Pili. PilB ATPase assembles PilA pilin subunits from the base to allow pilus extension. PilM, PilN and PilO form a membrane complex for pilus extension. Adapted from Purcell *et al*. 2016.

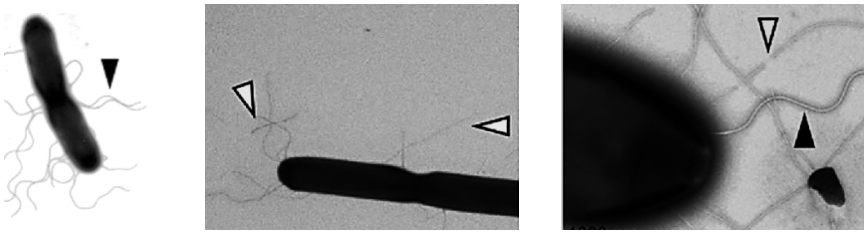

Figure 3. Comparison of *C. difficile* flagella and Type IV Pili using transmission electron microscope (TEM). Shown are the *C. difficile* flagella (black arrowheads) and TFP (white arrowheads). Image scale from left to right is 5 µm, 5 µm, and 100 nm. Adapted from Purcell *et al.* 2016.

Biofilms are the predominant state of most bacteria in natural environments (110). Biofilm formation is initiated by bacterial interaction with a surface where surface-adhesion is facilitated by flagella and TFP (121). Post-surface attachment, adherent cells secrete a dense and very protective extracellular polymeric substance or matrix (ECM) (121,122). The ECM comprises polysaccharides, proteins, lipids, complex sugars, extracellular DNA, and ions such as Ca^{2+} (121,123). The surface-attached cell mass also harbors many pathogenic species that are inherently more drug-tolerant than planktonic species, suggesting that biofilm plays a crucial role during host infection (122,124). Irreversible attachment and maturation of the biofilm through development of microcolonies ultimately results in a robust three-dimensional community of microorganisms (122). The major roles of the ECM include securing the biofilm community to the surface, trapping nutrients within, providing structural support, and protecting the community from host immune defenses as well as antimicrobial agents (122). Furthermore, the ECM is responsible for enabling cell-to-cell communication via autoinducer molecules and the exchange of genetic materials via horizontal gene transfer mechanism within the community (122). Upon maturation, to disperse bacterial infection, mature biofilms release cells from the main community so that free cells can swim to new locations for surface attachment (122).

Mechanisms contributing to bacterial drug tolerance and survival within a biofilm community include occlusion of the penetration of chemical agents by the thick ECM, sequestering of antimicrobial agents within the matrix, and the inner hostile environment of biofilms that reduce growth rate and render bacteria metabolically inactive (122,124). In humans, 80% of bacterial infections are due to biofilm-producing pathogens such as those belonging to the *Staphylococcus, Pseudomonas*, *Enterococcus*, and *Streptococcus* genera (124). Furthermore, biofilms also contribute to bacterial persistence and infection recurrence (90). Bacterial persistence is an antibiotic stress-response phenomenon in which a subpopulation of cells survives antibiotic exposure without acquiring genetic alteration(s) in their genome that can otherwise confer antibiotic resistance (125,126).

Over the years, biofilm formation has been characterized in a handful of anaerobic species that colonize the gut. Both *C. difficile* 630 and R20291 strains can form well-structured and thick biofilms *in vitro*, with the latter strain forming substantially more

biofilm (127). The biofilm matrix of *C. difficile* is mainly composed of glycoproteins, lipoproteins, phosphoproteins, and extracellular DNA in addition to fiber-like structures (127). The surface-structures flagella and TFP, and members of the S-layer regulate biofilm formation in *C. difficile.* The *C. difficile* S-layer is composed of S-layer proteins (SLPs) that present as heterodimeric complex with putative functions in bacterial adherence and evasion of the immune system (128). The maturation of the S-layer proteins is dependent on proteolytic cleavage by Cwp84. Therefore, isogenic mutants of *cwp84* and *fliC* dramatically suppress biofilm formation during the early and late stages of biofilm maturation, respectively (127). Quorum sensing, which is a process that permits bacteria to coordinate group behaviors for sharing information about cell density and gene expression, also influences biofilm formation (129). The role of quorum sensing regulators in biofilm production, such as *luxS* has been documented in *B. subtilis* and *C. perfringens* (130,131). Notably, *luxS* mutants in *C. difficile* also cause dramatic defects in biofilm formation, suggesting that the *luxS*-mediated quorum sensing system contributes to mature biofilm formation in this organism (127). Furthermore, the master regulator of the sporulation pathway called Spo0A is also involved in *C. difficile* biofilm formation *in vitro* (127). The biofilm environment is known to support sporulation processes making spores one of the members of the biofilm ecosystem, particularly under nutrient-limiting conditions (127,132). While Dapa *et al*. found *C. difficile* biofilms to contain significantly lower numbers of spores *in vitro*, other studies have found *C. difficile* biofilms to be densely populated with spores harnessing reduced germination efficiency (127,133). In agreement with precedent findings, Dawson and group recently demonstrated that both R20291 and 630 strains have significantly increased spore titers within the biofilm matrix compared to the planktonic phase (134). The discrepancy between these findings can be attributed to differences in strain types and growth conditions used in the studies (90).

Nevertheless, field emission scanning electron microscopy (FESEM) and confocal laser scanning microscopy (CLSM) based studies have revealed biofilms produced by *C. difficile* to contain mats of rod-shaped vegetative cells, spores, and sporulating cells interconnected through a network of ECM, and string-like materials connecting the cells (135). Arguably, it is reasonable for *C. difficile* biofilms to constitute a higher proportion of non-germinating spores since germination suppression enables more spore

dissemination and transmission. Spores are highly resilient to a vast range of environmental insults and it can persist in the gut to cause recurrent infection (136,137). Garth *et al*. have found fidaxomicin, an inhibitor of the sporulation process, to be more potent than metronidazole and vancomycin at penetrating and disrupting *C. difficile* biofilms *in vitro*, indirectly supporting precedent findings that *C. difficile* biofilms constitute a significant number of spores (137). Additionally, their study revealed surotomycin to be effective at disrupting *C. difficile* biofilms by killing vegetative cells within this community (137). Unfortunately, the development of surotomycin remains incomplete due to poor outcomes in a reported Phase 3 clinical trial (137,138). Nonetheless, the establishment of persistent cells and spores within the biofilms potentially cause rCDI. *In vivo*, *C. difficile* associates with commensal microbes within the mucus during CDI (139-141). Clumps or aggregates (containing polysaccharides and extracellular DNA consistent with a typical biofilm matrix) of *C. difficile* cells have also been observed in mouse models with damaged intestinal tissues (86,90,139,141,142). In support of these findings, Normington and group, using a model reflective of human colon, recently showed that *C. difficile* cells and spores associate with polymicrobial biofilm communities, which leave vancomycin and FMT treatments ineffective at depleting bacterial load (143). Composed of synergistic species, including *Candida parapsilosis*, *Staphylococcus warneri*, and *Bacteroides thetaiotaomicron*, the polymicrobial biofilms encase *C. difficile* via species-specific ECM and facilitate bacterial growth (143). Since 8 to 18% of FMT patients are reported to experience relapsing episode of CDI, it can be suggested that *C. difficile* within multi-species biofilm are responsible for causing rCDI (143).

In summary, *C. difficile* encodes flagella and TFP that aid in bacterial motility and attachment to surfaces of the intestinal epithelial cells. Various motility modes such as swimming, swarming, twitching, and gliding are coupled to signaling mechanisms and nutritional sources that promote bacterial colonization in the host (144). Bacterial flagella and TFP directly influence biofilm formation as deletion of either or both surface appendages cause serious impairments in cell attachment, growth, and virulence (135,144). Biofilm formation by *C. difficile* is further regulated by SLPs, Spo0A and the luxS-mediated quorum sensing system (135).

THE BACTERIAL STRINGENT RESPONSE

Bacteria are exposed to several adverse environmental conditions when colonizing a potential host, including nutrient limitation, heat, and pH changes, high osmolarity, reactive oxygen species, and antimicrobial peptides of the host innate immune system (145-147). Bacteria must respond and adapt to these conditions efficiently to maintain growth and survival (147). Therefore, bacteria have evolved several stress response pathways that enable adaptation and survival, including the ubiquitous stringent response (SR) mechanism (147). The SR is mediated by the nucleotide alarmones GDP-3'-diphosphate (5'-ppGpp-3') and GTP-3'-diphosphate (5'-pppGpp-3') produced from GDP and GTP, respectively (147-149). These nucleotides are produced by the members of the RelA/SpoT homolog (RSH) protein superfamily (149). Synthesis involves transferring a pyrophosphate group of ATP to the 3'OH group of the ribose moiety of GDP or GTP via a nucleophilic attack of the β-phosphate of ATP by the 3'OH group of the substrate (149,150). Furthermore, the presence of guanosine GMP-3'-diphosphate (5'-pGpp-3') has also been confirmed in numerous species, including *Mycobacterium tuberculosis*, *Enterococcus faecalis*, *Staphylococcus aureus*, *Mycobacterium smegmatis*, *Corynebacterium glutamicum*, and *Bacillus subtilis* (151-157). To produce pGpp, bacteria can directly utilize primary GMP and/or GMP that result from phosphatases-induced ester hydrolysis of GTP (151). All three nucleotides or small nucleotide messengers are collectively known as (pp)pGpp (149).

Three main groups of enzymes in the RSH superfamily regulate the intracellular levels of (pp)pGpp, including long RSH or full-length RSH enzymes, small alarmone synthetases (SAS), and small alarmone hydrolases (SAH) (148,149,158). Long RSH enzymes have a hydrolase domain (HD) and a synthetase domain (SD) in their N-terminal domain (NTD), and a regulatory C-terminal domain (CTD) (158). The CTD is comprised of ThrRS, GTPase, and SpoT (TGS), helical, conserved cysteine (CC), and aspartate kinase, chorismate, and TyrA (ACT) domains (158). The NTD contains RSHs' catalytic region where the hydrolase and synthetase domains act coherently to maintain an optimum level of cytoplasmic (pp)pGpp based on immediate environmental conditions (149,159-161). Binding of the substrate (GXP) and the ATP precursor to the synthetase

domain of long RSH enzymes alters protein conformation, resulting in the activation of the SD (149,162). Binding of ppGpp to the HD domain, on the other hand, induces conformational changes that inactivates the SD while activating the HD to facilitate nucleotide hydrolysis (149,162). Notably, the switch between domain activities is presumed to occur via protein-protein interactions or small-molecule binding by the enzymes' non-catalytical CTD (147,159,160,163-166). The model Gram-negative organism, *E. coli*, contains two long RSH enzymes. The monofunctional RelA has a catalytically inactive pseudo-HD domain, while the bifunctional enzyme SpoT exhibits weak synthetase activity and strong hydrolase activity (148,149). Gram-positive species such as *B. subtilis*, *Streptococcus equisimilis*, *S. mutans*, and bacteria outside the *β-proteobacteria* and *γ-proteobacteria* group also encode a single long RSH enzyme bearing great sequence homology to *E. coli* RelA and SpoT (149). Gram-positive bacteria also oftenly possess one or two monofunctional synthetases (167,168). The SASs lack a hydrolase domain and are divided into several subfamilies that are spread across species (169). RelQ and RelP from *Firmicutes* such as *B. subtilis* and *S. aureus* are the most extensively characterized SASs. Other SASs that have been studied include RelV from the *Proteobacterium V. cholerae*, and RelS as well as RelZ from the *Actinobacterium* group (155,170). RelZ encoded by *M. smegmatis* is the only SAS enzyme whose synthetase domain is fused to an RNase HII domain that separates RNA-DNA hybrid structures during DNA replication, repair, and transcription (171). The last group of RSH superfamily proteins is the SAH recently identified in *C. glutamicum* (172). *C. glutamicum* RelH is a member of the metazoan SpoT homolog 1 L (Mesh1-L) subgroup that lacks a SD and can hydrolyze (pp)pGpp *in vitro* (172). Interestingly, genes encoding for (pp)pGpp synthetases and hydrolases are conserved in a few plants, including green algae, *Physcomitrella patens* moss*, Oryza sativa*, and dicotyledon *Arabidopsis thaliana*, *Nicotiana tabacum*, and *Capsicum annnum* (173). According to Ito *et al*., RSH encoding genes were first introduced in proto-plant cells via the lateral gene transfer mechanism from different bacteria (173,174). Very recently, Ito and colleagues demonstrated that ppGpp accumulates in Mesh1 encoding *Drosophila* at all stages of metazoan development (175). As in bacteria, overaccumulation of ppGpp in *Drosophila* causes changes in cellular metabolome and cell death (175).

Proteins that are not members of the RSH superfamily can also metabolize (pp)pGpp in bacteria. For instance, *E. coli* encodes guanosine pentaphosphate phosphohydrolase (GppA) that lacks the enzymatic domains of the long RSH NTD (176). GppA converts pppGpp to ppGpp through its guanosine pentaphosphate phosphohydrolase activity, presumably to refine ppGpp potency (176-178). In *B. subtilis* and *Bacillus anthracis*, a nucleoside diphosphate linked moiety X (NuDiX) hydrolase called NahA degrades pppGpp and ppGpp to pGpp *in vitro* and *in vivo* (156,157). Hydrolysis of pppGpp and ppGpp between the 5'-α and 5'-β phosphate groups is postulated to fine-tune alarmone regulation in the bacterial cells (157). Interestingly, Gram-negative *E. coli* also encodes for NuDiX hydrolases such as MutT, NudG, and RppH to cleave pppGpp and ppGpp to 5'-pGp-3' *in vivo* (179,180). However, Gram-positive species are not yet reported to encode for GppA homolog(s) or enzyme(s) with identical GppA functionality (181).

Long RSH enzymes are regulated at the transcriptional level, with transcription increasing during the late exponential or stationary phase of bacterial growth or upon induced nutrient depletion by inhibitors of biosynthetic pathways (147,158,182-184). The specific nutrients that trigger (pp)pGpp synthesis also vary between bacteria (182,185-187). In *E. coli*, the *relA* gene is under the control of four promoters, two σ^{70}-dependent promoters, *relAP1* and *relAP2*, and σ^{54}-dependent P3 and P4 promoters (158,188). Transcription from *relAP1* is constitutive throughout growth, and activity is dependent on a UP element (158,188). Transcription from *relAP2* is induced when bacteria transition from exponential growth to stationary phase (158,188). Conversely, transcription from *relAP3* and *relAP4* is activated from nitrogen starvation in an NtrC-dependent manner where NtrC is a master regulator of nitrogen limitation in the niche (158,188). *E. coli relA* is further transcriptionally regulated by HipB, and 6S RNA. HipB is an anti-toxin component of the type II toxin-antitoxin module HipAB involved in *E. coli* persister cells formation (189,190). HipB negatively regulates *relA* transcription in *E. coli* by binding to a sequence upstream of the P3 promoter (189,190). 6S RNA is a small non-coding RNA that binds σ^{70}-RNA polymerase (RNAP) to suppress *E. coli relA* transcription (190). Amy *et al.* demonstrated that *E. coli* cells lacking 6S RNA present with increased transcription of *E. coli relA* and subsequent accumulation of cytoplasmic ppGpp (191).

Transcriptional regulation of Gram-positive long RSHs have not been characterized as extensively as that of *E. coli* RelA. Swantjie *et al*. evaluated the response of *S. aureus* to mupirocin or pseudomonic acid, which is a structural analog of isoleucyl-adenylate that binds eubacterial and archaeal isoleucyl-tRNA synthetases (192). Binding of mupirocin to isoleucyl-tRNA synthetases (which otherwise bind isoleucyl-tRNA-isoleucyl adenylate) restricts the charging of isoleucyl-tRNA with isoleucine, resulting in the accumulation of uncharged isoleucyl-tRNA (193,194). The increased concentration of uncharged tRNAs represents amino acid starvation in cells that triggers the stringent response. Therefore, the treatment of cells with mupirocin mimics amino acid limitation stress. According to Swantjie *et al*., mupirocin induces *S. aureus rel* transcription in the *S. aureus* background (192). In *M. tuberculosis*, *rel* gene encoding the long RSH enzyme is a part of the σ^E regulon, which is positively regulated by polyphosphate chains that serve as a phosphate donor to histidine Kinase MprB (158). MprB senses polyphosphate chains to phosphorylate MprA, resulting in the upregulation of SigE transcription (158). SigE is an alternative sigma factor, one of the master regulators of bacterial gene expression involved in bacterial survival during stressful conditions. In *M. tuberculosis*, SigE contributes to increased bacterial tolerance and persistence to antitubercular drugs (195). Based on a study conducted by Kamakshi and colleagues, MrpA-P-driven activation of SigE positively regulates *M. tuberculosis rel* transcription (196).

Transcriptional control of SASs has been elucidated for some Gram-positive bacteria. Under stresses, SAS genes from *B. subtilis* are differentially regulated during growth phases (158). The gene encoding *B. subtilis* RelQ (*relQ*) is transcriptionally regulated during exponential growth, with mRNA transcript levels decreasing as cells transition into the stationary growth phase (168). Conversely, the RelP encoding gene (*relP*) is induced in the late exponential phase when there is a concurrent decrease in *relQ* transcription (168). Of the seven identified sigma factors in the genome of *B. subtilis*, *relP* is part of the σ^M and σ^W-induced regulons (158,197,198). Both sigma factors respond to cell wall stresses, including vancomycin and alkaline shock, suggesting that SAS enzymes in this organism are activated from extracytoplasmic stresses (158,168). Transcription of *S. aureus relP* and *relQ* is also induced by vancomycin and exposure to ethanol, increasing *relP* transcription by more than 20-fold (199,200).

The intracellular accumulation of (pp)pGpp has a diverse range of biological consequences in bacteria. (pp)pGpp can control critical metabolic pathways and processes in a cell such as DNA replication, transcription, nucleotide synthesis, and translation or protein synthesis. In *E. coli*, ppGpp directly binds to and inhibits the priming activity of DnaG, a DNA primase that synthesizes RNA primers needed for DNA replication (201,202). In *B. subtilis*, pppGpp not ppGpp binds DnaG primase to inhibit replication elongation (203). Another consequence of (pp)pGpp accumulation during the SR is a rapid change in gene transcriptional profiles. Ribosomal RNA (rRNA) synthesis, tRNA synthesis, and transcription of genes involved in the metabolism of DNA and phospholipids are dramatically suppressed with a coincident increase in the transcription of amino acid biosynthesis genes and nutrient transporters (149,204). In all studied *Proteobacteria*, ppGpp directly interacts with RNAP to influence gene transcription (178). In *E. coli*, binding of ppGpp to RNAP σ^{70} holoenzyme in the presence of DksA transcription factor allosterically potentiates alarmone-mediated inhibition of gene transcription (204).

In contrast to *Proteobacteria*, (pp)pGpp in *Firmicutes, Actinobacteria*, and *Deinococcus Thermus* do not bind RNAP but indirectly contribute to transcriptional regulation (205). During the SR, the GTP nucleotide pool decreases due to the production of (pp)pGpp via RSH enzyme-catalyzed pyrophosphoryltransferase reaction. A decrease in the GTP pool is also attributable to the inhibition of GTP biosynthesis enzymes, including inosine monophosphate dehydrogenase (GuaB) and guanylate kinase by (pp)pGpp (157,206,207). In *B. subtilis*, a decrease in GTP levels reduces the transcription frequency of σ^{A} -dependent promoters at the +1 position during amino acid starvation that otherwise use GTP as a transcription initiating nucleotide (205,208). Similarly, GTP at +1 to +4 positions also have a role in *S. aureus* gene transcription during SR activation, suggesting that initial mRNA elongation step is also sensitive to the intracellular GTP pool (209). A global transcriptional repressor called CodY is also able to utilize GTP along with branched-chain amino acids as cofactors to regulate gene expression (210). Present only in Gram-positive species with low G + C content in their genomes, this nutritional regulator senses changes in nutrient availability such that when the GTP concentration is high, CodY binds the promoter regions of target genes to block the transcription of genes

involved in carbon and nitrogen metabolism as well as in amino acid biosynthesis and transport (210-212). When GTP levels are low, CodY-mediated repression of genes are de-repressed enabling the transcription and adaptation of bacteria to the immediate environment. In 2012, Geiger *et al*. demonstrated a direct association between the stringent response and the CodY regulon (213). They found that out of 150 genes in *S. aureus* that are upregulated during leucine and valine starvation, 143 are positively regulated from CodY de-repression (213).

(pp)pGpp alarmones also inhibit protein synthesis. During the SR, (pp)pGpp targets the guanine binding domain of translational GTPases initiation factor 2 (IF2) to prevent 30S initiation complex (30SIC) formation and translation (149,214,215). IF2 is the only initiation factor that binds ribosome to facilitate 30SIC formation and subsequent assembly of the 70S initiation complex (70SIC), which results in the formation of the initiation dipeptide and the ribosomal pretranslocation complex (215). (pp)pGpp also suppresses translation by targeting elongation factors EF-TU and EF-G. These elongation factors are essential for charged tRNA delivery and translocation of the peptide chain during protein synthesis (149). Additionally, (pp)pGpp inhibits the termination factor F3, which during termination plays a critical role in the removal of release factors (RF) 1 and 2 (that hydrolyze and release the completed nascent chain from the P-site tRNA) from the ribosome (149,216). Binding of ppGpp to RF3 reportedly slows down translation (216). Finally, (pp)pGpp halts protein synthesis via inhibition of ribosomal maturation. (pp)pGpp targets GTPases such as RsgA, RbgA, Era, HflX, and Obg that function in the maturation of individual 50S and 30S ribosomal subunits prior to the formation of mature 70S ribosomes (149,217).

Despite interfering with protein synthesis at different stages, (pp)pGpp can still activate the transcription and translation of several genes required for the SR cascade. Recently, Vinogradova and group showed that 30S-bound IF2 exhibits different tolerance to 5'-ppGpp-3' based on the mRNA present in the 30S pre-IC state (218). In *E. coli*, structured enhancer of translational initiation (SETI) confers ppGpp tolerance for *tufA* (encoding elongation factor EF-TU) and *rnr* (encoding RNase R) mRNA under physiological concentrations of GTP (218). According to Vinogradova and group, SETI-mRNA binds to 30S pre-IC complexed with ppGpp and enables the substitution of ppGpp

for GTP to allow translation (149,218). Furthermore, pppGpp bound to IF2 also enables the permissive synthesis of proteins, albeit at higher IF2 concentrations (149,218).

One of the most intriguing aspects of the stringent response is its association with virulence phenotypes (motility, adhesion, and invasion) and traits such as biofilm formation, sporulation, toxin production, and antibiotic survival (Table 1) (147,149,219). For instance, ppGpp is required for host cell invasion and regulation of virulence gene expression in *Salmonella typhimurium*. Using a (pp)pGpp-null mutant of *Salmonella enterica* subsp. *enterica* serovar Typhimurium, Pizarro *et al.* demonstrated that bacterial invasion of intestinal epithelial cells is attenuated in the animal infection model (220). Based on their study, a (pp)pGpp-null mutant exhibited reduced expression of *hilA* and *invF* that encode two essential transcriptional activators of the *Salmonella* pathogenicity island 1 (SPI-1) operon (220). SPI-1 encodes a type III secretion system responsible for secreting factors that support bacterial uptake and invasion (220). (pp)pGpp also binds to *S. typhimurium* SlyA transcriptional activator leading to SlyA dimerization *in vivo* (221). The SlyA dimers subsequently bind to the target promoter DNA and influence the transcription of the *pagC* virulence gene (221). PagC is an outer-membrane protein that confers an appreciable degree of serum resistance to *S. enterica* serovar Choleraesuis enabling infection establishment (222). The importance of (pp)pGpp to *Salmonella* invasion was further explored by Dasgupta and colleagues who discovered that a (pp)pGpp-null mutant strain displays decreased flagellar-motility and phagocytic uptake by macrophages owing to diminished bacterial adhesion (223). Additionally, the role of (pp)pGpp in bacterial invasion and intra-epithelial survival has been evaluated in *C. jejuni*. In *C. jejuni*, the stringent response is specifically regulated by SpoT, and according to Gaynor *et al.*, a *SpoT* mutant strain exhibits poor invasion of human epithelial cell lines, along with defects in host cell survival (224). Interestingly, the *ΔSpoT* strain also exhibits higher susceptibility to rifampicin in comparison to the WT strain, suggesting that the SR contributes to antibiotic resistance in *C. jejuni* (224).

The stringent response is critical for pathogenesis in *P. aeruginosa* as well. A *relA spoT* double mutant strain of *P. aeruginosa* is severely attenuated in virulence in animal models (225,226). According to Vogt *et al*., the double mutant strain secretes a reduced amount of virulence factors, including pyocyanin, elastase, and the siderophore

pyoverdine (225). Reduced production of these virulence factors is presumably due to altered expression of the Las and/or Rhl quorum sensing systems, suggesting that quorum sensing signaling also contributes to the ability of *P. aeruginosa* to cause chronic infection (225). The contribution of ppGpp in antibiotic tolerance to quinolone in *P. aeruginosa* has also been evaluated. Knockout mutants of *P. aeruginosa SpoT* and *dksA* appear to show higher survival rate in the presence of ofloxacin and ciprofloxacin compared to *relA* knockout strain, suggesting that lower levels of ppGpp in the later strain renders the mutant less tolerant to quinolones (227). Furthermore, the *relA spoT* double mutant displays impaired flagellum-mediated swarming and TFP-mediated motility compared to the WT strain, suggesting that (pp)pGpp is required for *P. aeruginosa* adhesion (225). Since biofilm formation is dependent on bacterial motility, adhesion, and translocation, the *relA spoT* double mutant strain of *P. aeruginosa* also exhibits reduced biofilm formation and cell viability (226).

The contribution of (pp)pGpp in biofilm formation has also been implicated in other species, including *E. coli*, *V. cholerae,* and *S. mutans* (228-230). In *E. coli*, fimbriae are important factors for bacterial attachment to host cells (149). The expression of type 1 fibrial genes in uropathogenic *E. coli* is upregulated by (pp)pGpp via transcriptional activation of the *ƒimB* gene whose protein product acts as a recombinase switch to turn on the *ƒimAICDFGH* operon (149,228). Activation of the *ƒimAICDFGH* operon promotes transcription of many fimbria-encoding genes with roles in bacterial adhesion and initial steps of biofilm formation (228). (pp)pGpp-null uropathogenic *E. coli* mutants fail to display fimbriae on their surface, resulting in impaired biofilm formation (228). In *V. cholerae*, genes involved in biofilm formation are regulated by the transcriptional activators *vpsR* and *vpsT* of the *Vibrio* exopolysaccharide operon, which in turn are regulated by the stationary phase sigma-factor σ^S (*rpoS*) (229). According to He *et al*., all three SR-mediating synthetases play a distinct role in the positive transcriptional regulation of *vpsR* and *vpsT*, suggesting that biofilm formation is controlled by (pp)pGpp (229). *S. mutans* form biofilms to tolerate pH changes and nutrient limitation in the human oral cavity (230). *S. mutans relA* insertional mutants also show a significant reduction in biofilm formation (230). Interestingly, Lemos and group found the biofilms of the *relA*

mutants to be more resistant to acid killing, suggesting that the physical barrier of biofilms contributes minimally to acid diffusion in this organism (230).

Apart from adhesion, antibiotic tolerance, and biofilm formation, (pp)pGpp also regulates sporulation and toxin production in bacteria. During amino acid starvation, a *relA* deletion mutant of *B. anthracis* demonstrates significantly reduced sporulation, notably, without affecting bacterial virulence in animal models of infection (231). Upon germination, *B. anthracis* produce toxins and a capsule where the toxin-form constitutes of a protective antigen (encoded by *pagA*) with either the lethal factor (encoded by *lef*) or oedema factor (encoded by *cya*) (231). The capsule, which is composed of poly-γ-D-glutamate aids in inhibiting bacterial phagocytosis during infection (231). Both toxins and capsule formation in the organism are regulated by AtxA (231). However, *relA* deletion does not impact *pagA* and *atxA* transcription, suggesting that the SR in *B. anthracis* is more critical in priming cells to sporulate than in virulence factors production during nutrient limitation (231). In *V. cholerae*, the toxin-coregulated pilus (TCP) and cholera toxin are major virulence factors responsible for host colonization and symptomatic infection (232). Expression of genes encoding these virulence factors is controlled by the ToxR regulon, which includes ToxR (encoded by *toxRS*), TcpP (encoded by *tcpPH*), and ToxT (encoded by *toxT*) transcriptional activators (232). Where ToxT directly initiates cholera toxin and TCP genes transcription, TcpP and ToxR control the expression of ToxT (232). TcpP is needed for bacterial colonization of the small intestine during early stages of infection so that toxin production can be enabled (232). Recently, Raskin and group, using *ΔrelAΔspoTΔrelV* strains demonstrated that *tcpPH* and *toxT* expression are decreased in cells devoid of (pp)pGpp with a corresponding defect in bacterial colonization and toxin production, suggesting that the SR regulates cholera toxin and TCP induction in *V. cholerae* (232).

Table 1.

Stringent response is widely conserved in bacterial groups. Summary of components of the stringent response that contribute to virulence traits and phenotypes in diverse bacterial species. Adapted from Dalebroux *et al.* 2010.

Pathogen	**RSH enzyme(s)**	**Phenotypes/traits**
Yersinia pestis	RelA, SpoT, DksA	Infection, dissemination
Legionella pneumophila	RelA, SpoT, DksA	Macrophage transmission
Shigella flexneri	RelA, SpoT, DksA	Intracellular spread
Mycobacterium tuberculosis	RelA	Persistence
Listeria monocytogenes	RelA, RelQ, RelP	Adherence, survival
Staphylococcus aureus	RelA, RelQ, RelP	Viability
Helicobacter pylori	SpoT	Macrophage survival

Due to the role of (pp)pGpp in bacterial virulence factor production, antibiotic tolerance, infection, and persistence, there has already been some interest in inhibiting the SR cascade. One of the first molecules to be synthesized for the targeted inhibition of the SR-regulating RSH enzymes is Relacin (233). Relacin is a ppGpp analog in which the molecule's pyrophosphate moieties at positions 5' and 3' are substituted with a glycyl-glycine dipeptide linked to the sugar ring by a carbamate bridge (Fig. 4) (233,234). Functionally, Relacin perturbs stationary phase onset and viability of Gram-positive *B. subtilis*, *Deinococcus radiodurans,* and *Streptococcus pyogenes* (233). *In vitro* analyses by Wexselblatt *et al.* also demonstrated that Relacin inhibits (pp)pGpp synthesis driven by *B. subtilis* RelA and *D. radiodurans* RelA in a dose-dependent manner (233). Furthermore, in *B. subtilis* and *B. anthracis*, Relacin largely inhibits sporulation by lowering the number of cells expressing sporulation-specific enzymes required in different

stages of the sporulation process (233). Relacin also reduces *B. subtilis* biofilm formation (233). *E. coli* RelA-mediated (pp)pGpp synthesis is also inhibited by Relacin *in vitro*, although the compound fails to inhibit *E. coli* growth and survival (233). Furthermore, Relacin has no effect on the (pp)pGpp synthetase activity of SAS family synthetases, indicating that the compound's activity is specific for long RSH enzymes (152).

Employing the crystal structure of the N-terminal catalytic fragment of the long RSH enzyme encoded by *S. equisimilis*, Wexselblatt and group also modeled the interaction of Relacin with the enzyme's SD to determine the molecule's mechanism(s) of inhibition (233). Based on their putative model, Relacin adopts an optimal conformation upon binding to the extremely polar Rel/Spo synthetase domain active site (233). In this conformation, Relacin forms a net of hydrogen bonds and strong hydrophobic interactions with relevant amino acid residues within the domain's GDP-binding pocket (233). Additionally, the hydrophobic isobutyryl group of the compound at position N2 of the guanosine base (Fig. 4, black dashed circle) makes contact with a defined hydrophobic patch within the SD active site, ensuring high-affinity interaction and effective occlusion of substrate binding (233).

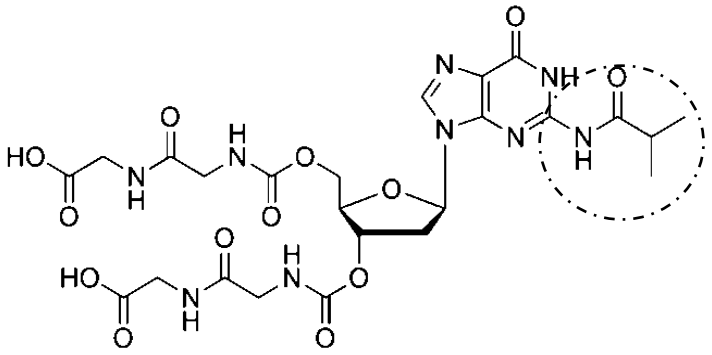

Figure 4. Chemical structure of Relacin. Relacin contains an isobutyryl group (dashed circle). Adapted from Wexselblatt *et al.* 2012 and 2013.

Despite its efficacy at inhibiting RSH/Rel-mediated (pp)pGpp synthesis *in vitro* and *in vivo,* and the long-term survival strategies employed by some deadly pathogens, Relacin is only effective at millimolar concentrations. Therefore, efforts have been made to increase the potency of Relacin by synthesizing analogs of the molecule (235,236). Wexselblatt *et al.* synthesized a series of analogs that were symmetrically substituted with several amino substituents (Fig. 6) in place of the moieties at positions 5' and 3' deoxyribose ring of Relacin (Fig. 5) (235). The activity of the inhibitors was also tested *in vitro* using Rel enzymes encoded by *B. subtilis*, *D. radiodurans,* and *E. coli*. According to Wexselblatt *et. al*., of all the symmetrically substituted analogs, compounds 2a and 2d demonstrated highest inhibitory activity, potentially due to the replacement of basic dimethylamino groups with carboxylic acid(s) (Fig. 6) (235). Between compounds 2a and 2d that only differ in the number of negatively charged species and in bulkiness, compound 2a reduced intracellular levels of serine hydroxamate (SHX)-induced (pp)pGpp levels in *B. subtilis* (235). SHX is a derivative of L-serine that serves as a completive inhibitor of seryl-tRNA synthetases, mimicking amino acid starvation in bacterial cells and evoking the SR (237). Compound 2d deemed significantly more effective at reducing *B. subtilis* (pp)pGpp levels *in vivo* (235). Furthermore, compound 2d was more effective at inhibiting (pp)pGpp synthesis via *E. coli* RelA and *D. radiodurans* Rel/Spo *in vitro* (235). The efficacy and potency of compound 2d are directly attributable to the two glutamyl-glutamic acid moieties of the analog (235). The six-total number of carboxylic acids in this analog makes it more acidic and voluminous than the parent Relacin molecule, enabling more hydrogen bonding and electrostatic salt bridges formation during interaction with bacterial RSH synthetase domain (235).

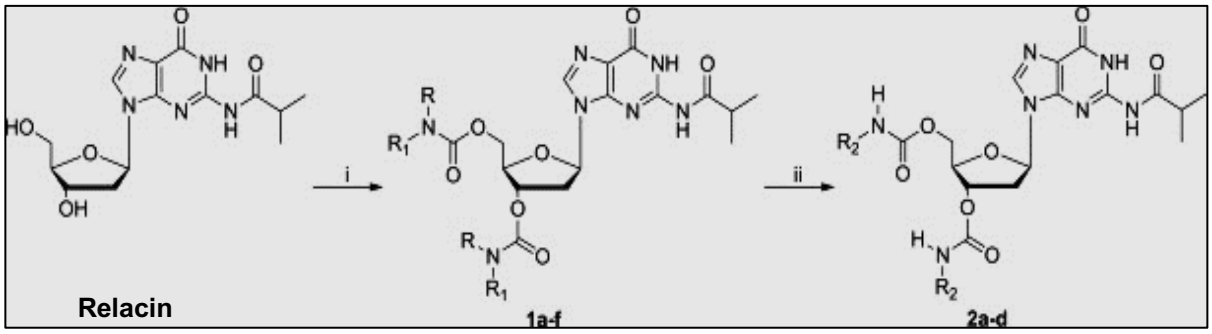

Figure 5. Schematic representation of the synthetic route employed for symmetric compounds analogous to Relacin. Reaction conditions as mentioned in the reference Wexselblatt *et al.* 2013 from which the figure has been adapted.

Comp.	R	R1	Comp.	R2
1a	H	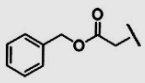	2a	
1b	H	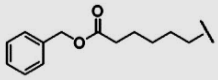	2b	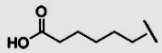
1c	H	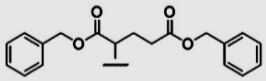	2c	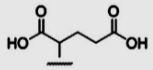
1d	H	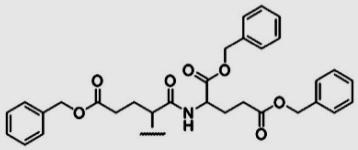	2d	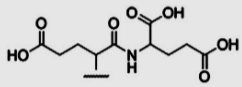
1e	H			
1f	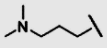	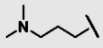		

Figure 6. Summary of symmetric substituents on the 3' and 5' positions of Relacin deoxyguanosine ring to synthesize Relacin analogs. Adapted from Wexselblatt *et al.* 2013.

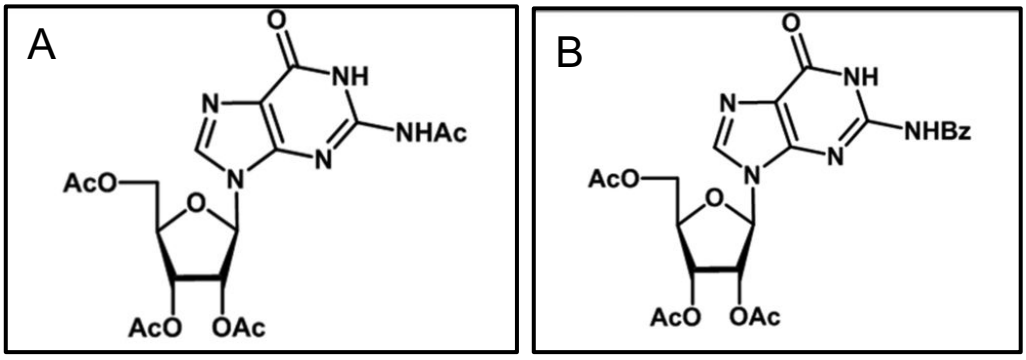

Figure 7. Modification of Relacin isobutyryl group. Analogs of Relacin where the isobutyryl group have been substituted with (A) acetylated compound and (B) acetylated benzoylated compound. Adapted from Sayal *et al.* 2017.

Syal *et al*. substituted the isobutyryl group at the second position of Relacin guanosine base with either a bulkier benzoyl group or a less bulkier acetyl group called acetylated benzoylated compound (AB) and acetylated compound (AC), respectively (Fig. 7) (236). They found both compounds to inhibit *M. smegmatis* Rel-driven pppGpp synthesis *in vitro* and *in vivo*, with compound AB being a more potent inhibitor of the bacterial Rel protein (236). The group further demonstrated that both synthetic compounds affect long-term *M. smegmatis* survival and biofilm formation (236). These nontoxic and cell permeable agents also disrupt preformed biofilms produced by *M. smegmatis* and arrest biofilm formation in *M. tuberculosis* (236). Overall, the chemical modifications of Relacin render the molecule more potent, providing further modification opportunities so that inhibitor activity in the nanomolar range can be attained for use in the clinical settings.

Apart from Relacin and its structural analogs, molecules that interfere with the bacterial SR have included vitamin C and an inhibitor peptide called peptide 1018 (234). Vitamin C is an antioxidant agent that has roles in strengthening host immune system, speeding recovery from a tuberculosis infection, and impeding pathogen progression,

even killing *M. tuberculosis* (238). Vitamin C also alters regulatory pathways linked to bacterial stress response and dormancy (238). Structurally, vitamin C has a furan ring with 1,2 dihydroxy ethyl moiety that bears remarkable similarity to the chemical structure of GDP. Sayl *et al.* showed that vitamin C inhibits (pp)pGpp synthesis *in vitro* in a dose-dependent manner and *in vivo* via direct interaction with *M. smegmatis* Rel enzyme (238). Furthermore, vitamin C lowers bacterial viability and the ability of *M. smegmatis* to form biofilms, suggesting that vitamin C affects the SR in this organism by altering the levels of (pp)pGpp (238). Unlike Relacin, Relacin derivatives, and vitamin C, synthetic peptide 1018 directly targets (pp)pGpp nucleotides (239,240). Peptide 1018 is a board-spectrum anti-biofilm agent that prevents biofilm formation by diverse species, including *P. aeruginosa*, *S. enterica*, *E. coli*, *S. aureus*, *Klebsiella pneumoniae*, *Burkholderia cenocepacia,* and *Acinetobacter baumannii* at concentrations as low as 10 µg/mL (240). During the stringent response, peptide 1018 specifically binds ppGpp as per co-precipitation and nuclear magnetic resonance spectroscopy (NMR)-based analyses (240). Peptide-bound ppGpp nucleotides in *P. aeruginosa* undergo rapid molecular degradation, leading to the inhibition of biofilm formation, cell death within biofilm communities, and dispersal in matured biofilms (240). This suggests that peptide 1018 prevents (pp)pGpp signaling and the consequences of the signaling cascade, such as virulence factors production in pathogenic strains. The synergistic effects of peptide 1018 against biofilms in conjugation with conventional antibiotics have also been investigated (239). Reffuveille *et al.* demonstrated that peptide 1018 in combination with ciprofloxacin, ceftazidime, imipenem, or tobramycin prevents biofilm formation and disrupts preformed biofilms in a diverse group of bacteria (239). Furthermore, interaction between the peptide and antibiotics results in a considerable decrease in antibiotic concentrations needed to inhibit biofilm production (239). Notably, the peptide and ciprofloxacin combination substantially increases the susceptibility of planktonic *P. aeruginosa* cells during SHX-induced stringent response, suggesting that the targeted degradation of (pp)pGpp by peptide 1018 contributes to one, increased antibiotic susceptibility and two, decreased biofilm production (239).

Recently, a diterpene analog, 4-(4,7-Dimethly-1,2,3,4-tetrahydroNapthalene-1-yl)Pentatonic acid or DMNP was shown to suppress *M. smegmatis* persistence and

biofilm formation at concentrations as low as 0.14 mM (~14 X less than the efficacious dose of Relacin) (241). The synthetic DMNP compound targets *M. smegmatis* Rel and SAS (RelZ) to inhibit (pp)pGpp synthesis while also increasing bacterial antibiotic susceptibility to streptomycin and rifampicin (241). Taken together, the bacterial SR mechanism is a largely conserved stress signaling with diverse triggering factors. The hallmark of the stress response, (pp)pGpp, which is metabolized by enzymes of the RSH superfamily and beyond, have distinct but partially overlapping functions in bacterial physiology. Due to the contributions of the stringent response in bacterial stress tolerance, survival, and pathogenesis, both RSH enzymes and small alarmone nucleotides catalyzed by RSHs are targets for pharmaceutical and pharmacological interventions.

THE SCOPE OF THIS DISSERTATION

The main objectives of the work presented in this dissertation are to:

1. Investigate whether *Clostridioides difficile* can mount the stringent response using recombinant gene expression and protein purification techniques; confirm protein function and perform biochemical characterization of *C. difficile* full-length RSH enzyme using thin layer chromatography assays and high-performance liquid chromatography (Chapter II). This chapter is based on the publications Pokhrel *et al.* 2018 and Pokhrel *et al.* 2020.
2. Characterize full-length RSH-mediated (pp)pGpp signaling in *C. difficile* using quantitative reverse transcriptase-polymerase chain reaction and an oxygen-independent fluorescent transcriptional reporter. Bacterial response to stationary phase onset, nutrient limitation, and antibiotics exposure was examined (Chapter III). This chapter is majorly based on the publication Pokhrel *et al.* 2020.
3. Evaluate the effect(s) of disrupting the stringent response in *C. difficile* stress tolerance and survival using Relacin and RNA interference gene-silencing tool (Chapter IV). This chapter is based on the publication Pokhrel *et al.* 2020.
4. Evaluate nutrient-derived motility regulation and single-species biofilm formation by *C. difficile* using a home-built rose cell chamber for single cell motility analyses and

plate-based biofilm production assays (Chapter V). Major aspects of this chapter are based on the publication Courson *et al.* 2019.

Overall, this dissertation aims to introduce the ability of *Clostridioides difficile* to elicit the stringent response pathway via the synthetase activity of its long RSH enzyme. The research herein allows a greater understanding of a ubiquitous signaling system that is also significant for the survival and pathogenesis of *C. difficile*. Additionally, this dissertation aims at expanding the knowledge about factors contributing to *C. difficile* host colonization and virulence factors production, such as motility and biofilm. These data provide the foundation necessary for the synthesis and screening of small molecule inhibitors of the enzyme that demonstrate high specificity. The use of *C. difficile* RSH-specific inhibitors in place of antibiotics or in conjugation with clinically available antibiotics could significantly minimize antibiotics-induced risk factor development for CDI, along with the side effect of bacterial antibiotic resistance in the host. The development of an alternative therapy will alleviate the international health and economic burden associated with *C. difficile* infection.

CHAPTER II

BIOCHEMICAL CHARACTERIZATION OF FULL-LENGTH *CLOSTRIDIOIDES DIFFICILE* RSH

OVERVIEW

The stringent response is a globally conserved stress signaling pathway, primarily characterized by the cytoplasmic accumulation of ppGpp and pppGpp alarmones. ppGpp and pppGpp are produced by members of the RSH superfamily from GDP and GTP, respectively (149,158). The presence of pGpp (formed from GMP and/or degradation of ppGpp and pppGpp has also been confirmed in several species (149). Together, (pp)pGpp regulates key physiological processes within the cells, including the inhibition of DNA replication, nucleotide synthesis and protein synthesis, with a concomitant increase in the transcription of amino acid biosynthesis and transport genes (149). Importantly, (pp)pGpp downregulates transcription of factors needed for growth and division, while upregulating stress response and virulence genes (182). Genes encoding proteins for (pp)pGpp metabolism are common in the genomes of *Proteobacteria*, *Eubacteria*, and eukaryote*s* as well as metazoa (160,175).

Most Gram-positive RSH exhibit net (pp)pGpp hydrolysis activity under normal growth conditions. The first crystal structure of the N-terminal catalytic fragment of full-length *S. equisimilis* Rel (RelSeq) revealed two conformations of the fragment, hydrolase-OFF/synthetase-ON and hydrolase-ON/synthetase-OFF (159). Of the two conformations, RelSeq assumes the default (pp)pGpp-hydrolase-ON/(pp)pGpp-synthetase-OFF state until substrate binding to either catalytic site induces a mechanical switch of the conformational state; a process controlled by the enzyme's CTD (159,160,242). The catalytical domain (aa residues 1- 347) and regulatory domain (aa residues 363 – 739) of RelSeq is presumed to be linked by a solvent-exposed, flexible hinge (160,242). When the two enzymatic domains of the NTD are aligned with one another and to the CTD, the hydrolase domain is activated (160). However, when the contact between the NTD and

CTD is perturbed, the NTD folds and undergoes a conformational change that leads to the activation of the synthetase domain (160).

For instance, full-length RelSeq exhibits weak pyrophosphoryl transfer activity for basal (pp)pGpp synthesis due to its interaction with the CTD. However, the transferase reaction is activated ~12-fold in the absence of the C-terminal region of the enzyme *in vitro*, suggesting that the CTD of RelSeq participates in the reciprocal regulation of the two opposing catalytic activities of the NTD (160). Unlike RelSeq, *M. tuberculosis* Rel (RelMtb) catalyzes both transferase and hydrolase reactions at the maximal rate *in vitro* (243). But binding of full-length RelMtb to a complex containing uncharged tRNA, ribosome, and mRNA results in a 20-fold increase in the rate constant for the catalytic conversion of GXP to (pp)pGpp with a concurrent 2-fold decrease in the K_{cat} for (pp)pGpp hydrolysis (243). The presence of uncharged tRNAs, which is caused by amino acid limitation in bacterial cells, rapidly increases bifunctional Rel/RSH-catalyzed (pp)pGpp synthesis while exhibiting an opposite effect when treated with charged tRNAs (243). The regulation of the opposing catalytic activities of full-length RSH enzymes is extremely critical since equally active, unregulated hydrolase and synthetase domains would catalyze a futile cycle of alarmone synthesis and hydrolysis (242). Too much synthetase activity would elevate cytoplasmic (pp)pGpp levels provoking the SR, whereas too little (pp)pGpp from uncontrolled hydrolysis activity would restrict cells from responding appropriately to extracellular stresses (242). Gram-positive bacteria also oftenly encode one or two SAS enzymes that lack both N-terminal hydrolase and C-terminal regulatory domains of the long RSHs (158). Studies have shown that deletion of RelQ, RelP or both while leaving an intact RSH enzyme has minimal effects on the intracellular (pp)pGpp accumulation during the stringent response (167,168). However, in the absence of an intact long RSH enzyme, constant yet low production of alarmones by SAS results in an increased basal (pp)pGpp levels in *E. faecalis*, suggesting that SASs contribute to basal levels of (pp)pGpp under normal physiological conditions (244-246).

The synthetase reactions catalyzed by RSH and SAS enzymes are universally dependent on Mg^{2+} cofactor(s) although both enzymes differ in their catalytic mechanism of (pp)pGpp synthesis. According to Sajish *et al*., a charge reversal in the highly conserved RXKD motif of the long RSH synthetase domain to EXDD in the SAS domain

contributes to the differential effect of metal cofactor and also impacts substrate preference (151,247). When concentrations of Mg^{2+} are higher than that of the total nucleotide pool, binding of Mg^{2+} to the full-length RSH enzyme presumably causes a protein conformational change that occludes substrate binding, resulting in the inhibition of (pp)pGpp synthesis (160,243,247). Using fluorescent-based nucleotide binding assays and circular dichroism studies, Sajish and group revealed that the RXKD motif of bifunctional RSH enzymes contribute to poor nucleotide binding and structural transitioning of the catalytic loop (α-13/β-4 loop of the SD as per the crystal structure of the N-terminal catalytic domain of RelSeq) strongly in favor of an alpha-helix in the presence of high Mg^{2+} (159,247).

Of note, high Mg^{2+} concentrations do not affect enzyme-catalyzed reactions for proteins employing a dual-divalent cation mechanism (247). The closest structural relative to the SD of RelSeq is the palm domain of mammalian DNA polymerase β (polβ) (159). Of the three highly conserved aspartate amino residues that coordinate two Mg^{2+} ions in polyβ, only two carboxylic acid groups (D264 and E323) are conserved in the RelSeq synthetase domain, suggesting that the absence of a third carboxylic group potentially enables a single-divalent cation mechanism for RSH-mediated (pp)pGpp catalysis (159,247). In the contrary, high Mg^{2+} concentrations appear to have no effect on SAS-mediated (pp)pGpp synthesis (247). The two additional negative charges in the EXDD motif of SAS enzymes create a second Mg^{2+} binding site lacking in the RXKD motif, suggesting that SASs follow a dual-divalent cation-mediated catalysis (247). Furthermore, the charge reversal in the RKXD motif of long RSH proteins to EXDD in SASs also influences substrate specificities. Full-length RSH proteins with an RXKD motif preferentially utilize GTP to produce pppGpp, whereas SASs with an EXDD motif prefer GDP as the primary substrate to produce ppGpp (151).

During host colonization and infection, *C. difficile* encounters and adapts to environmental changes using different stress response pathways. We have found that *C. difficile* genome encodes a putative long RSH and a SAS, RelQ, suggesting that the organism is capable of mounting the SR (147). The long RSH protein contains the well-conserved RXKD motif and we predict the enzyme to be bifunctional (147). To determine the substrate preference and kinetics of RSH encoded by *C. difficile* (RSHCd), we

expressed hexa-histidine tagged recombinant RSHCd in a non-native background and purified the enzyme using metal affinity chromatography (248). We subsequently performed *in vitro* (pp)pGpp synthesis reactions in the presence of guanosine phosphate derivatives and commercially available γ-^{32}P-ATP or 32P-ATP and monitored enzyme-catalyzed pyrophosphoryl transfer activity using thin layer chromatography (TLC) (147,248). While characterizing the contribution of RSHCd to (pp)pGpp synthesis *in vitro*, we found RSHCd incapable of utilizing GTP and GMP (147). Based on the enzyme's strict GDP utilization unlike its Gram-positive full-length RSH homologs, we previously reported that RSHCd produces 5'-ppGpp-3' (147,248). We also found GDP utilization by RSHCd to be independent of environmental pH and to lack metal cofactor specificity (147).

We initially predicted that the production of ppGpp by RSHCd is either due to the exclusive utilization of GDP or rapid degradation of unstable pppGpp to ppGpp under the experimental conditions used although RSHCd binds GTP with poor affinity, indicating that the interaction likely doesn't occur *in vivo* (147). In Gram-negative bacteria, pppGpp is broken down to ppGpp via GppA, whose homologs remain to be identified in Gram-positive species. Very recently, Yang *et al.* identified NahA, a NuDiX hydrolase encoded by *B. subtilis* and *B. anthrasis* to be able to hydrolyze pppGpp and ppGpp to pGpp (157). Like other SR-regulating alarmones, pGpp regulate purine nucleotide biosynthesis in bacterial cells without interacting with GTPases (157). To confirm that the exclusive 5'-ppGpp-3' synthesis is a unique feature of RSHCd, we have used purified RelQ from *B. subtilis* (RelQBs) as a positive control to detect the products catalyzed by *in vitro* (pp)pGpp synthesis reactions using anion exchange chromatography. We found that incubation of RelQBs with GTP and GDP results in the formation of pppGpp and ppGpp, respectively (Poudel *et al.* in preparation). Unexpectedly, high performance liquid chromatography showed that the consumption of ATP by RSHCd occurred concurrently with the apparent formation of triphosphate species, leading us to hypothesize that RSHCd produces pGpp instead of ppGpp in the presence of GDP substrate. In support of this hypothesis, our thin layer chromatography assay demonstrated that incubation of RelQBs with GMP and 32P-ATP results in the formation of spot (representing pGpp) that in polyethyleneimine (PEI)-cellulose plate migrates similar distance with putative pGpp produced by RSHCd (Poudel *et al.* in preparation). The principal rule governing (pp)pGpp

synthesis requires a pyrophosphate moiety from ATP to be transferred to the 3'-OH group of GMP, GDP or GTP substrate by members of the RSH superfamily (243). Based on this rule, we postulate that GDP is being degraded to GMP, enabling RSHCd to catalyze an ATP-dependent pyrophosphate transfer to synthesize pGpp (Poudel *et al.* manuscript in preparation). Additionally, we postulate that RSHCd hydrolysis activity requires regulation by the CTD via interaction with branched-chain amino acids and that the enzyme harnesses a default synthetase activity in isolation or independent of biological effectors. We found that the overexpression of the monofunctional RSH-REL domain is extremely toxic to bacterial cells, suggesting that the CTD and the HD domain of full-length RSH coordinate to prevent excessive intracellular accumulation of (pp)pGpp in *C. difficile*.

Overall, this chapter focuses on characterizing the synthetase activity of full-length *C. difficile* RSH, which is predicted to be regulated by the enzyme's intact hydrolase and C-terminal regulatory domains. Segments of this chapter previously appeared as articles in the references (248) and (147). The rights and permission to use the materials of the publications is given in Appendix M. Published figure numbers and formats have been modified unless stated otherwise in the legends.

METHODS AND MATERIALS

Overexpression and purification of C. difficile RSH

Restriction enzymes and DNA ligase used in this study were purchased from New England Biolabs (NEB). Phusion DNA polymerase for polymerase chain reactions (PCR) was purchased from Themro Fisher Scientific. *rsh* (CDR20291_2633) gene was amplified from the genomic DNA of *C. difficile* R20291 using primers (Appendix B) that added a C-terminal hexa-histidine tag, ligated into the pMMBneo expression vector at the KpnI and PstI restriction sites, and transformed into *E. coli* BL21. The plasmid was confirmed by PCR using *rsh* gene-specific primers (Appendix B).

E. coli expression strain carrying pMMBneo vector ligated with hexa-histidine tagged *rsh* gene was grown in Luria Bertani (LB) treated with 50 µg/mL kanamycin (Kan_{50}) at 37 degrees Celsius (°C) to an optical density (OD) of 0.16 to 0.25 at 600 nm (if OD_{600} reached above this range, cell cultures were back diluted into fresh LB-Kan_{50} at the

desired OD value or range), at which point the temperature was dropped to 30°C and expression was induced using 0.5 mM isopropyl β-d-1-thiogalactopyranoside (IPTG) for 16 hours (hrs). Cells were lysed by sonication in the lysis buffer composed of 10 mM Tris-HCl pH 7.8, 300 mM NaCl, 5 mM $MgCl_2$, 50 mM NaH_2PO_4, 10% glycerol, 0.5 mg/mL lysozyme, 10 mM imidazole, 0.25 mM dithiothreitol (DTT) and 5 mM phenylmethylsulphonyl fluoride (PMSF). After treatment with the lysis buffer, the lysates were clarified by centrifugation and subsequently transferred to a gravity column filled with 1 mL of HisPure Ni-nitrilotriacetic acid (Ni-NTA) resin (G-Biosciences). Protein purification was conducted according to the manufacturer's protocol. Notably, all purification buffers included 5 mM $MgCl_2$ which was found to be critical for protein stabilization and purification. Purification fractions were run on a Sodium dodecyl sulfate polyacrylamide gel (SDS-PAG) (4% stacking and 10% separating) via electrophoresis to resolve the elutant fractions. Purified RSHCd (elutant fraction 2) was dialyzed overnight (ON) at 4°C against dialysis buffer composed of 15.7 mM Tris-HCl pH 7.6, 471.9 mM NaCl, 15.69 mM $MgCl_2$, 1.57 mM DTT, 1.5 mM PMSF, and 15.7% glycerol. A 30 kilodalton (KDa) molecular weight cutoff (MWCO) dialysis membrane (Spectra/Por Spectrum® Laboratories Inc.) was used for protein dialysis. Concentration of *C. difficile* RSH was determined from Beer's law by measuring the absorbance at 280 nm and using the calculated molar extinction coefficient 82085 $M^{-1}cm^{-1}$. Aliquots of the protein were stored at -80°C for subsequent use.

Purification of B. subtilis RelQ

Plasmid bearing *E. coli* BL21 strain (received from the Bauer laboratory, Indiana University, USA) were grown to OD_{600} of 0.4 in LB-Kan_{50} before ON induction for protein expression at 16°C with the addition of 0.2 M IPTG. Cells were collected by centrifugation and resuspended in StrepTactin wash buffer (IBA Lifesciences) composed of 0.1 M Tris-HCl pH: 8.08, 0.15 M NaCl, 1 mM ethylenediaminetetraacetic acid (EDTA), and 20% glycerol. Cells were lysed by sonication and the lysates were clarified by centrifugation at 12,000 revolutions per minute (RPM) (Beckman coulter JA 12.0 rotor) at 4°C prior to loading onto a StrepTactin resin column (IBA Lifesciences). The column was washed with the wash buffer (IBA Lifesciences) followed by protein elution with elution buffer

composed of 0.1 M Tris-HCl pH: 7.92, 0.15 M NaCl, 1 mM EDTA, and 2.5 mM desthiobiotion (IBA Lifesciences). The elutants were collected in three separate fractions and stored at - 80°C in 5 to 10 µL aliquots to be used for subsequent enzymatic assays. When necessary, fractions were combined, and spin concentrated at 4,500 RPM (Beckman Coulter JA-12 rotor) for 15 minutes (mins) using a 10 KDa MWCO spin concentrator (Sartorius). Concentration of *B. subtilis* RelQ was determined spectrophotometrically.

Overexpression and purification of C. difficile RSH-REL

rsh-rel, a truncation construct of the full-length *rsh* gene, was amplified from pMMBneo::*rsh* expression vector using primers (Appendix B) that also added a C-terminal hexa-histidine tag. The amplicon was subsequently digested and ligated into pMMBneo vector at the KpnI and PstI cut sites and transformed into *E. coli* DH5-α background. The plasmid was confirmed by PCR using *rsh-rel*-specific primers (Appendix B). Amplified *rsh-rel* was also digested and ligated into pBAD33 vector at the KpnI and PstI sites. The plasmid pBAD33::*rsh-rel* (Appendix A) was subsequently transformed into DH5-α first, followed by plasmid extraction from DH5-α background and transformation into *E. coli* BL21. The plasmid was confirmed by PCR using *rsh-rel*-specific primers (Appendix B).

For RSH-REL purification, *rsh-rel* was amplified from pMMBneo::*rsh* expression vector using primers (Appendix B), digested and ligated at the NdeI and XhoI cut sites into pET24a vector fused with a hexa-histidine tag. The plasmid, pET24a::*rsh-rel* (Appendix A) was transformed into *E. coli* BL21 expression strain. Transformation was confirmed using gene-specific primers (Appendix B). The expression strain was eventually grown in LB-Kan_{50} supplemented with 0.5% casamino acid (CAA) and 0.5% glucose (GLU) at 37°C ON. The following day, the ON starter culture was spun at 4°C using a JA-12 rotor (Beckman Coulter) at 500 RPM for 30 mins. The pellet was resuspended in plain LB-Kan_{50} medium and allowed to grow till the cell density reached 0.5 to 0.8 at 600 nm. At this point the cells were diluted down in fresh plain LB-Kan_{50} to bring the OD_{600} at ~0.14. When the new OD_{600} value was between 0.14 to 0.16, the temperature was dropped to 30°C and expression was induced using 0.5 mM IPTG ON

(16 to 20 hrs). After induction, cells were lysed by sonication in the lysis buffer composed of 10 mM Tris-HCl pH 7.8, 300 mM NaCl, 5 mM $MgCl_2$, 50 mM NaH_2PO_4, 10% glycerol, 0.5 mg/mL lysozyme, 10 mM imidazole, 0.25 mM DTT, and 5 mM PMSF after which the lysates were clarified by centrifugation and subsequently purified using HisPure Ni-NT resin (G-Biosciences) according to the manufacturer's protocol. Like RSHCd purification, all RHS-REL purification buffers included 5 mM $MgCl_2$. Purification fractions were run on a 4% stacking and 12% separating SDS-PAG via electrophoresis. Concentration of the elutant fraction (resolving in a clean band) was determined spectrophotometrically. Purified RSH-REL were stored at -80°C in 5 to 10 µL aliquots to be used for enzymatic assays.

Growth curves

Growth curve was performed using a 96-welled microtiter plate (BrandTech) after the induction of *C. difficile rsh* in *E. coli* DH5-α background. Log phase cultures of *E. coli* cells were inoculated in LB-Kan_{50} in the presence or absence of 0.5 mM IPTG inducer. The plate was incubated at 37ºC shaking for a total of 12 hrs. Growth of induced vs uninduced cells were monitored every 30 mins. Growth curve assays following the induction of *C. difficile rsh-rel* in *E. coli* DH5-alpha background was also conducted in the same manner. Supplementation with nutrient sources, including CAA and GLU were initiated from time point 0 mins for both pMMBneo::*rsh* and pMMBneo*::rsh-rel* vector carrying strains in the presence of the 0.5 mM IPTG inducer.

In vitro measurement of RSHCd synthetase activity using Thin layer chromatography (TLC)

RSHCd synthetase assays were conducted in buffer containing 10 mM Tris-HCl (pH 7.5), 5 mM ammonium acetate, 2 mM KCl, 0.2 mM DTT and 0.12 mM ATP (ATP at the working concentration of 0.6 mM can also be used). A 5X buffer stock was mixed with the indicated concentrations of GDP/GTP/ADP (0.2 – 0.6 mM), $MgCl_2$ always 2X more than the concentration of GXP or AXP, and 1.0 µCi of γ-^{32}P-ATP. The use of 32P-ATP radioisotope was presented as a proposal to and approved by the University's Radiation Safety Office committee prior to experiment designing and conduction (Appendix L).

Pyrophosphate transfer reactions were initiated by adding RSHCd at a final concentration of 3.0 µM and a reaction volume of 10 µL. Post-incubation at 37°C for indicated time points, reactions were stopped by spotting 2 µL samples on PEI-cellulose plates, allowing the spots to dry. The plates were subsequently developed in 1.5 M KH_2PO_4 (pH 3.64 ± 0.05) and autoradiographed using the Storm 860 Phosphorimager from GE Healthcare Life Sciences. RSHCd-catalyzed product signal was quantitated using ImageJ software as previously described (249). RSHCd synthetase activity was expressed as the percentage of 32P-ATP converted into inorganic phosphate (Pi) for alarmone synthesis (Appendix C).

Allosteric feedback regulation of RSHCd by 5'-ppGpp-3' was evaluated in the same manner in the presence of 0 to 10 µM of exogenous ppGpp (TriLink). Furthermore, the effect of different divalent metal cations as well as buffer pHs on RSHCd synthetase activity were also investigated under reaction conditions mentioned above. Metal cofactors studied included Mg^{2+}, Mn^{2+}, Co^{2+}, Cu^{2+}, Zn^{2+}, Ni^{2+}, Ca^{2+}, and Fe^{2+} at the working concentration of 1.2 mM. Buffer pH studied included values of 5.0, 6.0, 7.5, 9.0, and 10.0. The effect of both metal cations and pH values on RSHCd pyrophosphoryl transfer activity was assayed at least three times. Post-incubation, the reaction mixtures were spotted on PEI-cellulose plates to perform the standard one-dimensional TLC assay.

High-performance liquid chromatography (HPLC)

Instrumentation for all HPLC analyses included the use of a dual-pump Ultra-High-Performance Liquid Chromatograph system with ultraviolet detectors (Schimazdu). The analytical column used for running nucleotide samples was a strong anion exchange DNAPac™ PA100 (4 x 250 mm) column with a guard column (4 x 50 mm) from ThermoScientific. HPLC mobile phase buffer A and B was composed of 50 mM KH_2PO_4 and 500 mM KH_2PO_4 and 500 mM Na_2SO_4, respectively. The buffers were adjusted to a neutral pH (7.00 ± 0.09) using HPLC grade concentrated orthophosphoric acid and potassium hydroxide. The following sections include a detailed procedure for the use of the HPLC system for the analysis of various samples.

A. *Nucleotide standards run*

Nucleotide standards, including GDP (Alfa Aesar), GTP (BioBasic), and GMP (BioWorld) at the concentration of 20 µM were separated using a gradient elution at the flow rate of 1.0 mL/min and absorbance at 252 nm. Total run duration was set at 22 mins per sample.

B. *Sample preparation for the analysis of intracellular (pp)pGpp in RSH-REL expressing E. coli cells using HPLC*

For analysis of intracellular (pp)pGpp in RSH-REL-induced *E. coli* cells, ON starter cultures of *E. coli* strain carrying either empty vector pBAD33 or pBAD33::*rsh-rel* were inoculated in LB medium treated with 10 µg/mL chloramphenicol. Cultures were allowed to grow till OD_{600} reached ~0.5. At mid log phase, cells were induced with 0.5% arabinose (ARA) for 3 hrs at 30°C. Post-induction, cell densities were remeasured (OD_{600} 1.1 – 1.3) followed by spinning the cells at the maximum speed using a JS 5.3 rotor (Beckman Coulter). The supernatants were discarded appropriately, and cell pellets were stored in -20°C ON. The following day, pellets were thawed and resuspended in extraction buffer composed of MeOH/ acetonitrile/ Millipore water at the ratio of 40:40:20 with 0.1 N formic acid by vigorous shaking or vortexing. The pellets were incubated in the extraction buffer at -20°C for 30 mins by positioning the conical tubes upright. The resuspensions were subsequently transferred into new Eppendorf tubes on ice and cell debris were pelleted by centrifugation at 13,000 RPM for 5 mins at 4°C using a benchtop centrifuge. Post-centrifugation, ~200 µL of the extractions were recovered which underwent neutralization with 4 µL of 15% NH_4HCO_3 (pH 7.0 – 7.7) per 100 µL of sample. After neutralization, samples were filter sterilized with 0.45 µm filter units and speed vacuumed for over 30 mins. Samples were finally diluted in Millipore water and stored in -20°C ON prior to running through an anion exchange column.

For HPLC, a gradient elution was set up where the concentrations of mobile phase Buffers A and B were changed accordingly for a total run duration of 31 mins per sample. Samples were separated at a flow rate of 1.5 mL/min and absorbance at 260 nm was used to detect the eluted nucleotides.

C. Analysis of in vitro RSHCd and RelQBs synthetase reactions using HPLC

RSHCd synthetase activity was separately conducted in a buffer composed of 10 mM Tris-HCl (pH 7.5 ± 0.02), 5 mM ammonium acetate, 2 mM KCl, 0.2 mM DTT, 0.12 mM ATP (ATP up to 0.6 mM can also be used), 0.2 or 0.6 mM GXP, and 1.2 mM $MgCl_2$. Reactions were started by adding RSHCd at a final concentration of 3.0 µm and incubated at 37°C on a portable heat block for a total duration of 30 mins. After 30 mins, ~100 µL samples were transferred into a VIVA SPIN 500 spin column (Corning) with a MWCO of 30 KDa and spun at 12,000 times gravity (X g) for 5 mins at 20°C. The filtrates were saved in a new Eppendorf tube and stored in -20°C ON to run through the anion exchange column the next day.

Likewise, RelQBs synthetase activity was separately conducted in a buffer composed of 10 mM Tris-HCl (pH 7.5), 5 mM ammonium acetate, 2 mM KCl, 0.2 mM DTT, 0.12 mM ATP, 0.2 mM GDP or GTP, 5 mM $MgCl_2$, and 3.0 µM RelQBs. Reactions were incubated at 37°C on a portable heat block for 30 mins. Post-30 mins, ~45 µL samples were transferred into a VIVA SPIN 500 spin column (Sartorius) with a MWCO of 10 KDa and spun at 12,000 X g for 5 mins. The filtrates were saved in a new Eppendorf tube and stored in -20°C ON to run through the anion exchange column the next day. Notably, all samples were run on the HPLC system using a gradient elution profile where absorbance at 252 nm was used to detect enzyme-catalyzed (pp)pGpp alarmones.

C. Analysis of in vitro RSHCd hydrolase reactions using HPLC

RSHCd hydrolysis activity was conducted against a buffer containing 50 mM Tris-HCl (pH 7.52), 25 mM ammonium acetate, 10 mM KCl, 1 mM DTT, 0.2 mM ATP, 0.1 mM exogenous 5'-ppGpp-3' (Trilink), and 0.2 mM $MnCl_2$ in a mini plastic vial. Reactions were initiated by adding RSHCd at a final concentration of 0.6 µM into a dialysis tubing with a MWCO of 12 to 14 KDa (Spectra/Pro) and incubated at 37°C. The whole reaction was conducted within an incubator (Thermofisher) set at 37°C for a total duration of 4 hrs in a manner similar to the standard dialysis procedure. At 0 and 4 hrs time points, ~20 µL samples were drawn from the hydrolase reaction mixture outside of the membrane tubing and pipetted into mini HPLC-grade vials (AQ Brand) to run through the anion exchange

column at 1.0 mL/min flow rate. Absorbance at 260 nm was used to detect the reduction in ppGpp signal between 0 and 4 hrs of reaction incubation.

LiCl-based extraction of radiolabeled nucleotides for RSHCd hydrolysis activity

RSHCd pyrophosphate transferase reaction was conducted separately in the order mentioned above and separated on a PEI-cellulose plate. The plate was left to dry after which the retention factor of RSHCd-catalyzed product was manually calculated. Radioactive strips corresponding to the radiolabeled spots was subsequently cut from the plate using sterile scissors. The strips were then immersed in 15 mL of 4 M LiCl into a 50 mL conical tube. The strips were incubated in the LiCl solution for 15 mins at room temperature. The solution was then filter sterilized using a 45 mm, 0.2 µm filter. The pH of the solution was measured and adjusted to 7.24 with concentrated formic acid and ammonium hydroxide. After acid-base neutralization, the solution was aliquoted into 1.5 mL Eppendorf tubes (9X) and spun at 4,000 X g using the benchtop centrifuge. Following centrifugation, the precipitates were washed with 95% ethanol (5 mL total) to remove residual LiCl. The ethanol washed-radioactive nucleotides were centrifuged for 5 mins at 4,000 X g and finally suspended in Millipore water to store in -20°C for further use.

Measurement of in vitro RSHCd hydrolysis activity using TLC

In vitro hydrolase assay was conducted in a buffer containing 10 mM Tris-HCl (pH 7.5), 5 mM ammonium acetate, 2 mM KCl, 0.2 mM DTT and 0.12 mM ATP. A 5X buffer stock was mixed with ~0.5 µL of radiolabeled LiCl-extracted nucleotide product in the presence of 1.2 mM $MnCl_2$. The use of 32P-ATP for the synthetase and hydrolase reactions was approved by the University's Radiation Safety Office committee (Appendix L). Reactions were initiated by adding RSHCd at a final concentration of 3.0 µM and a total reaction volume of 10 µL. Reactions were stopped by spotting 2 µL samples on a PEI-cellulose plate, allowing the spots to dry for at least 10 mins. The plate was subsequently developed in 1.5 M KH_2PO_4 (pH 3.64). The plate was exposed to the phosphor cassette for at least 4 hrs and autoradiographed using the Storm 860 phosphorimager from GE Healthcare Life Sciences.

Isothermal Titration Calorimetry (ITC)

ITC analyses were conducted using an ITC200 Micro-Calorimeter from Malvern. 300 µL of purified RSHCd was added onto the cell component of the instrument and the syringe was filled by 40 µL of GXP ligand. Protein and ligand were prepared in the same buffer composed of 10 mM Tris-HCl (pH 7.5), 5mM ammonium acetate, 1.2 mM MgCl2, 0.2 mM DTT, 0.012 mM ATP, and 2 mM KCl. 1.2 µM protein and 12 µM ligand concentrations were used in the interaction analysis experiments at 37ºC. ITC experiments were repeated at least three times where the heat of dilution obtained through the titration of ligand into the reference solution was used as a blank and subtracted from all binding curves attained in the presence of RSHCd and GXP. The data obtained were fitted using a single-binding-site model by Origin Software. The same software was also used for peak integration and thermodynamics calculation.

RESULTS

C. difficile has conserved (pp)pGpp metabolism genes

The complete genome sequence of *C. difficile* strain R20291 has been searched for homologs to the conserved (pp)pGpp synthetase domain of RelA/SpoT-like proteins in diverse bacteria. The analysis has identified two putative open reading frames, *rsh* (KEGG ID, CD2633) in an operon with predicted beta-lactamase gene and a gene for tRNA metabolism, D-aminoacyl-tRNA deacylase *dtd* (148). *C. difficile* R20291 also encodes a conserved SAS, *relQ* (KEGG ID, CD1607) in a predicted operon with a putative beta-lactamase gene (148). As both *rsh* and *relQ* share predicted operons with yet to be characterized beta-lactamase like proteins, it can be suggested that the proteins may confer bacterial tolerance in *C. difficile* to beta-lactam family of antibiotics such as ampicillin and penicillin (Fig. 8A) (147). The product of *rsh* is a putative Rel/SpoT homolog (RSHCd) with two conserved N-terminal synthetase and hydrolase domains and ACT and TGS C-terminal regulatory domains (Fig. 8B) (147). *C. difficile* RelQ (RelQCd) is a proposed single-domain small alarmone synthetase (Fig. 8B). Based on our bioinformatics analysis, both *rsh* and *relQ* genes are completely conserved between the non-epidemic 630, 630Δ*erm*, and the epidemic R20291 strain (147).

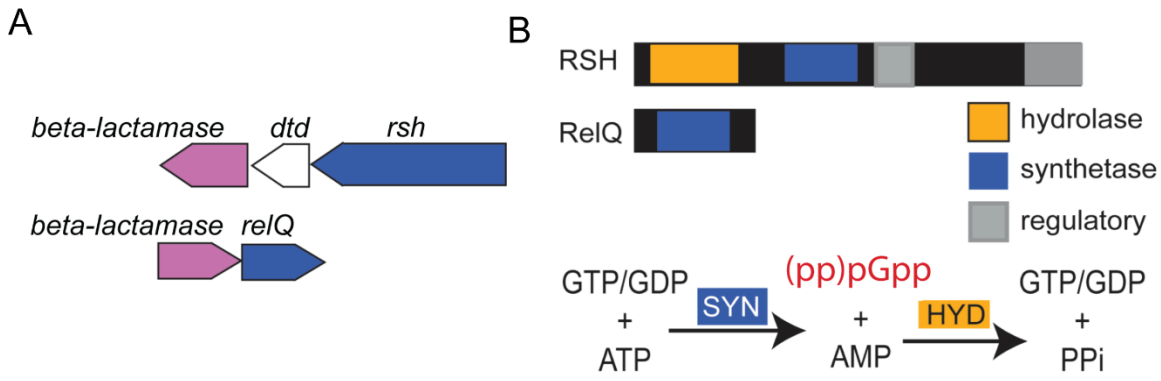

Figure 8. (pp)pGpp metabolism in *C. difficile.* (A) Operons of predicted (pp)pGpp metabolism genes (blue) and beta-lactamase like proteins encoding gene (pink). (B) Domain organization of predicted (pp)pGpp metabolism. Figure adapted from Pokhrel *et al*. 2020.

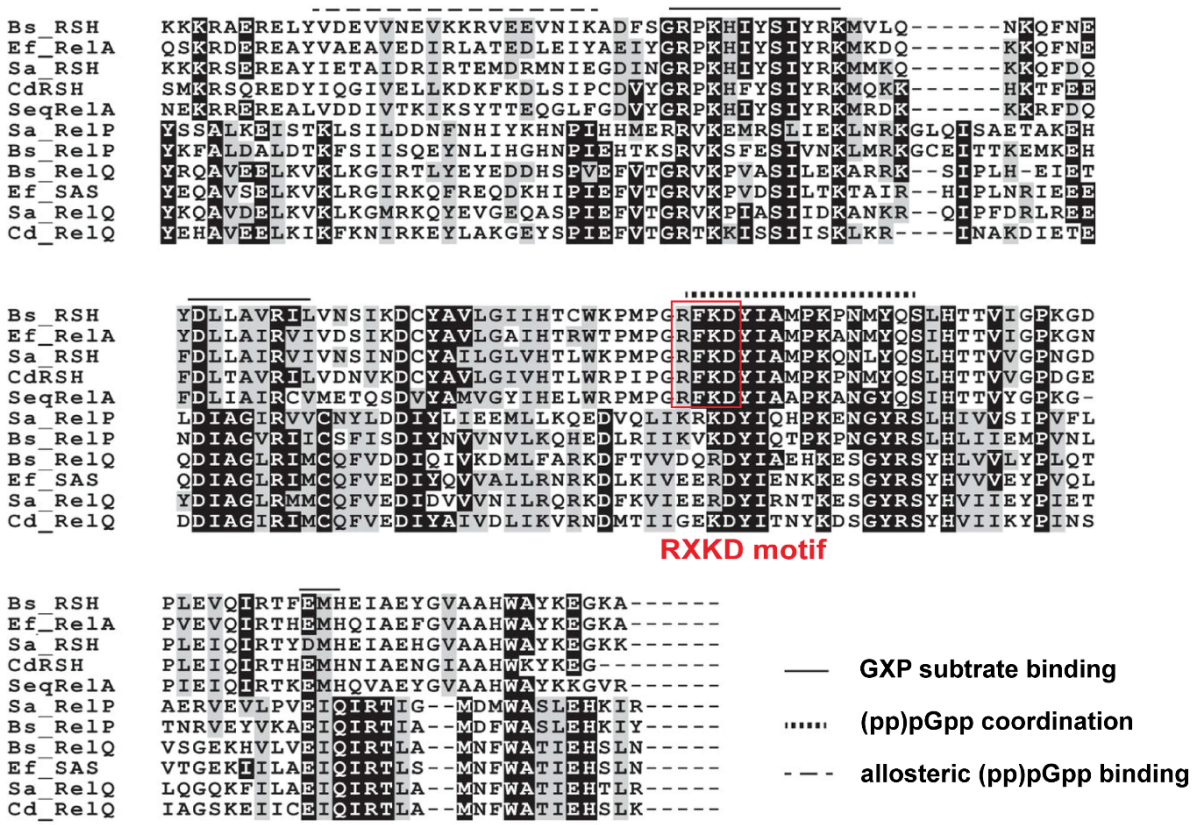

Figure 9. Alignment of amino acid sequences of the catalytic synthetase domain RSHCd with the primary sequence of other RSH family enzymes. Alignment of RSHCd and RelQCd with RelP/RelQ/SAS enzymes from *B. subtilis*, *E. faecalis*, *S. aureus*, and *S. equisimilis*. Adapted from Pokhrel *et al.* 2020.

Table 2.

Sequence alignment summary between RSHCd synthetase domain with its relatives. RSHCd synthetase domain sequence shares high % identity and similarity with those of RelA and RSH/Rel encoded by *S. equisimilis* and *B. subtilis*, respectively. Table adapted from Pokhrel *et al.* 2020.

	% Identity	% similarity
S. equisimilis RelA	43.6	62.9
B. subtilis Rel or RSH	50.7	69.4

Alignment of the amino acid sequence of RSHCd with those of known proteins belonging to the RSH superfamily of enzymes revealed that the sequences exhibit high similarities, particularly to the substrate binding and product coordination regions of the N-terminal synthetase domain (Fig. 9) (147). Many functionally significant and charged amino acid residues, including D264, Y308, E323, G240, H342, and A335 from *S. equisimilis* RelA (RelSeq; GenBank accession no. X72832) are conserved in RSHCd, suggesting that the enzymes share functional, and presumably structural homology (Fig. 9) (147,159,168). Several hydrophobic amino acid residues found in the synthetase domain of *B. subtilis* Rel/RSH (GenBank accession no. U86377), which are predicted to coordinate Relacin binding to the active site, are also conserved in the RSHCd synthetase domain (Table 2) (147,168). The great percentage identity and similarity between RSHCd and *B. subtilis* RSH suggests that RSHCd can potentially be inhibited by Relacin in a manner comparable to *B. subtilis* RSH inhibition (Table 2) (147).

Expression of RSHCd causes partial growth arrest in E. coli

Precedent studies have revealed that the intracellular accumulation of (pp)pGpp, as a result of amino acid starvation, leads to a delayed bacterial growth phenotype in exponentially growing *E. coli* cells (242,250). Upon the IPTG-dependent induction of full-length *C. difficile rsh,* we also observed a partial growth inhibition of exponentially growing *E. coli* cells (Fig. 10) (147). The observed inhibition of *E. coli* growth suggests that RSHCd mediates the production and cytoplasmic accumulation of (pp)pGpp while also inducing native *E. coli* stringent response. We found that the partial growth arrest of cells due to the overaccumulation of (pp)pGpp can be rescued through supplementation with CAA (Fig. 10B) (147). This shows that *C. difficile* potentially responds to amino acid starvation via activation of the stringent response, followed by RSH-mediated (pp)pGpp synthesis, which slows growth and rapid division, favoring survival (147).

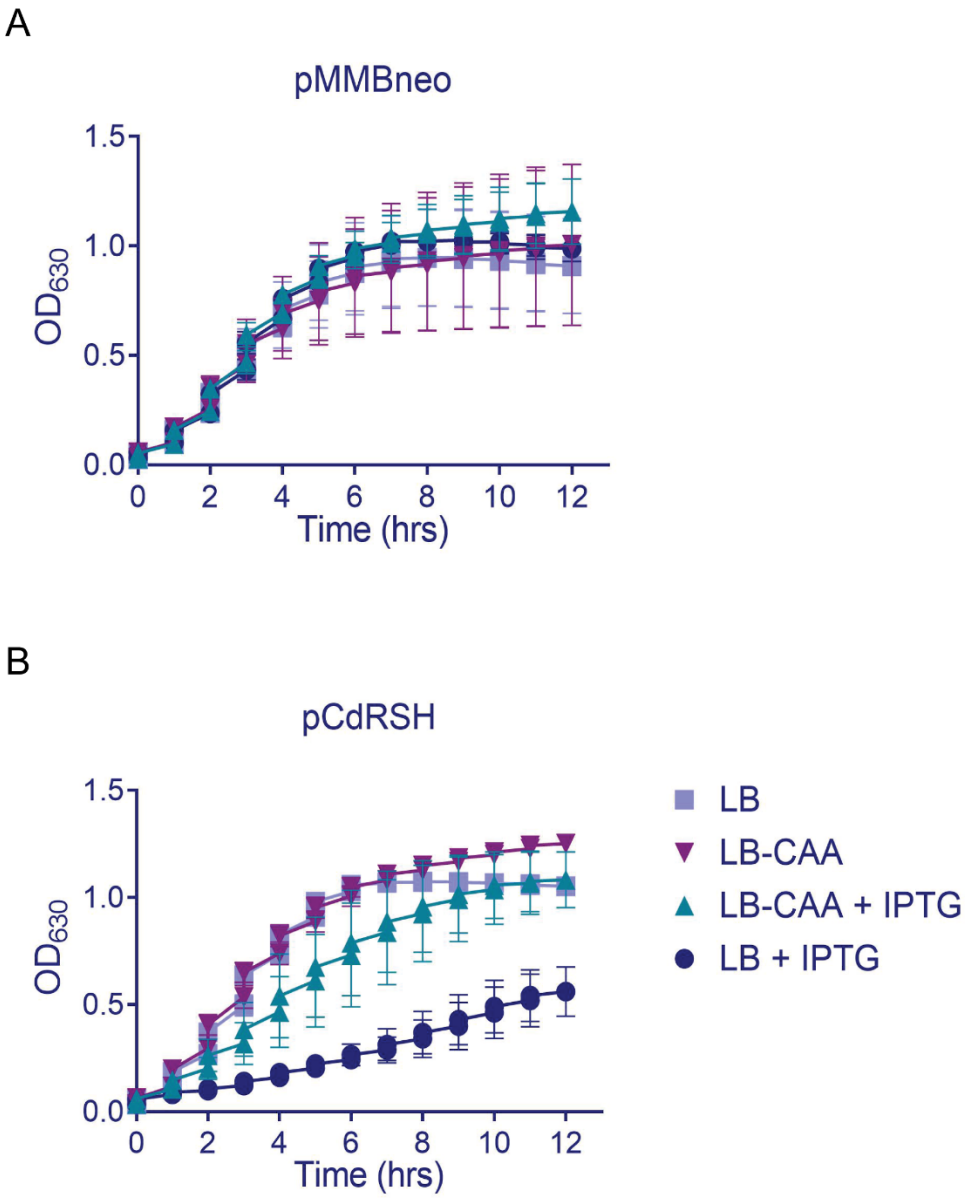

Figure 10. Overexpression of RSHCd partially arrests bacterial growth. Growth curves of *E. coli* strain carrying either empty pMMBneo vector (A) or IPTG-inducible *rsh*-ligated pMMBneo expression vector (B) in plain LB medium or LB supplemented with CAA in the presence or absence of 0.5 mM IPTG. Adapted from Pokhrel *et al.* 2020.

RSHCd exclusively utilizes GDP to produce magic spot in vitro

The enzymatic activity of full-length RSHCd has also been studied to confirm that the enzyme is a (pp)pGpp synthetase (248). Hexa-histidine-tagged *C. difficile* R20291 *rsh* has been expressed in *E. coli* and its product purified using nickel affinity chromatography and SDS-PAG electrophoresis in the presence of 5 mM $MgCl_2$ (Fig. 11) (248). We found that failure to include $MgCl_2$ results in the loss of protein activity even upon including the metal cation in the activity buffer, indicating that the divalent cation plays a crucial role in protein folding and stability in addition to enzyme catalysis. To confirm the synthetase activity of RSHCd, radiolabeled y-^{32}-PATP has been utilized to directly monitor the transfer of a radiolabeled pyrophosphate group from ATP to the non-radiolabeled GDP substrate (248). Thin layer chromatography has been used subsequently to separate and quantify radiolabeled alarmones using autoradiograms (248). Nearly five decades ago, *E. coli* responding to amino acid starvation lead to the production of molecules, which in TLC autoradiograms "magically" appeared as spots that weren't synthesized by non-starving bacterial cells (242,251). Since the molecules hadn't yet been characterized to be the derivatives of GDP and GTP, researchers began denoting the spots of the autoradiograms as "magic spot". We also denote the RSHCd-produced alarmones collectively as the magic spot in this dissertation. For quantification purpose, magic spot signal was presented as a percentage of the total radioactive signal (Fig. 13 and 14B, Appendix C) (248). By doing so, we ensured for data reproducibility and prevented the introduction of random noises (which can be caused from pipetting errors and/or radioactive decay) in our analyses (Appendix C) (248).

Based on the primary sequence of RSHCd N-terminal synthetase domain, the enzyme contains the well conserved RXKD domain (Fig. 9). Consistent with precedent observations regarding the effect of increasing metal ion concentrations on basal RelSeq and RelMtb synthetase activity, we found that RSHCd also exhibits reduced magic spot synthesis in the presence of higher Mg^{2+} concentrations (Fig. 12) (247). This finding suggests that RSHCd depends on a single-divalent cation mechanism to synthesize the magic spot. Furthermore, inhibition of enzyme catalysis at higher Mg^{2+} concentrations also suggests that the RXKD motif of RSHCd negatively impacts GDP binding of the

protein while potentially causing a conformational change in the predicted synthetase domain catalytical loop as reported for RelMtb (247).

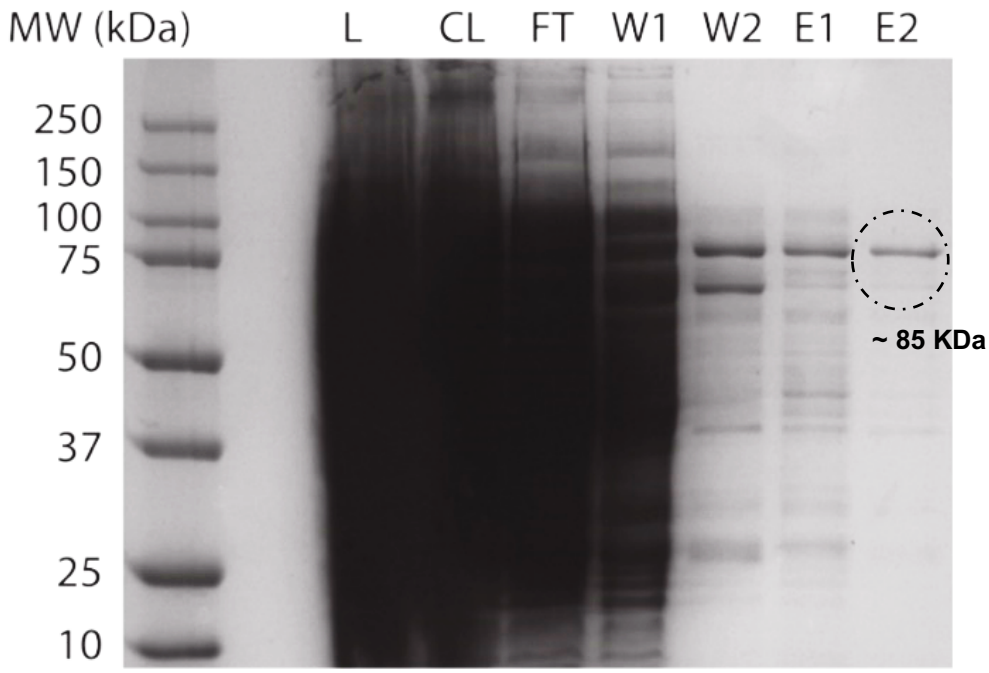

Figure 11. Purification of full-length RSHCd. Coomassie-stained SDS-PAG showing lysate (L) and clarified lysate (CL) of induced BL21 strain carrying the expression vector as well as flow-through (FT), wash 1 (W1), wash 2 (W2), and elution fractions 1 (E1) and 2 (E2) after nickel affinity purification. RSHCd is ~85 KDa in molecular weight (dashed black circle). Adapted from Pokhrel *et al.* 2018.

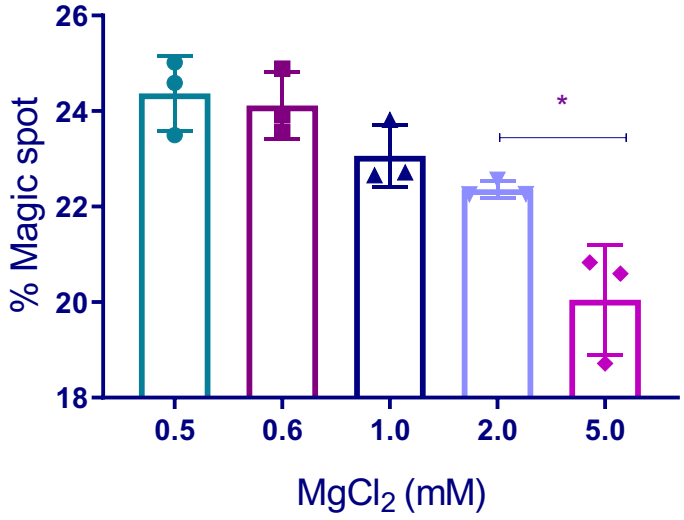

Figure 12. Effect of increasing concentrations of Mg^{2+} on RSHCd-mediated magic spot synthesis. Reaction was incubated at 37°C for 60 mins with 0.6 mM GDP, 3.0 μM RSHCd, 0.12 mM ATP, and indicated concentrations of $MgCl_2$. TLC assay was performed to quantitate magic spot synthesis. One-Way ordinary ANOVA analysis with Turkey's multiple comparisons test. Adjusted * *P* 0.0253. Error bars indicate standard deviations from three independent reactions.

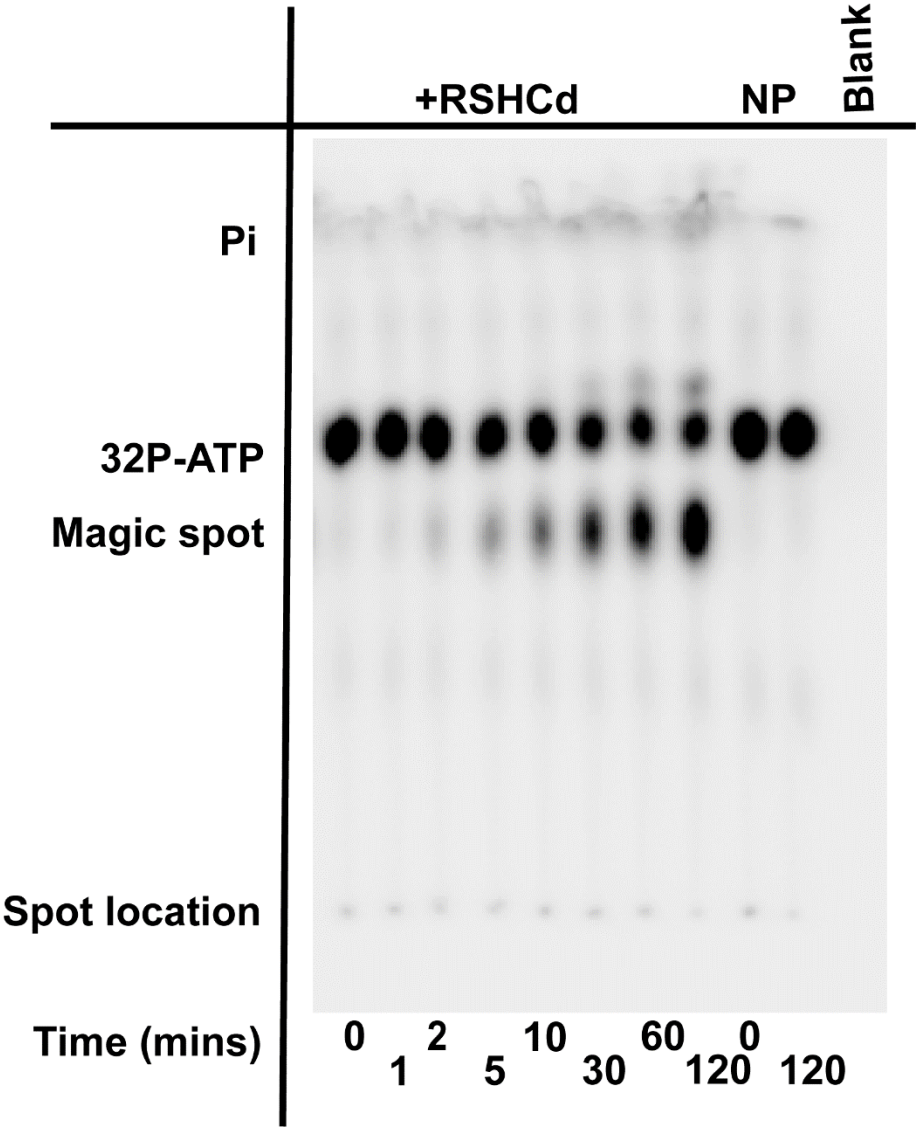

Figure 13. A typical autoradiogram of TLC assay. PEI-cellulose plate depicting the 32P-ATP spots, magic spots, and spot origin or location of a reaction carried out using purified RSHCd in the presence of GDP substrate. NP denotes no protein. Adapted from Pokhrel *et al.* 2018.

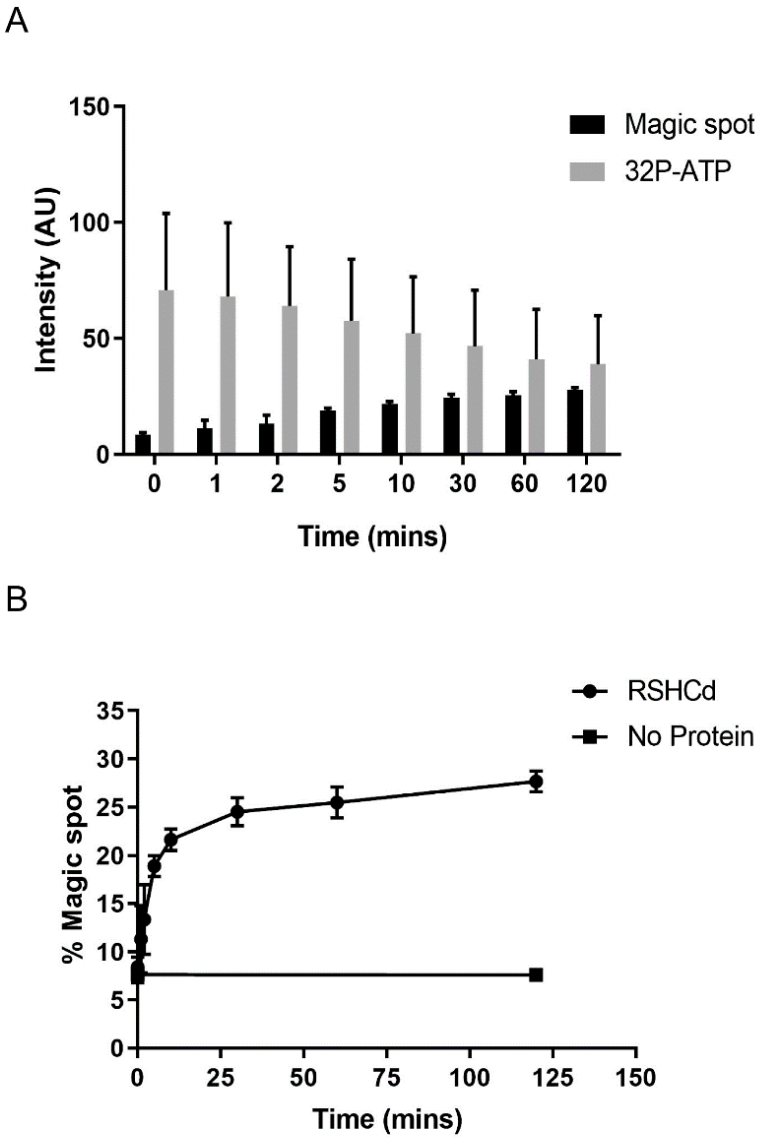

Figure 14. Functional characterization of RSHCd. (A) Absolute signal intensities of 32P-ATP and the magic spot as a function of time. (B) Magic spot synthesis is represented as percentages of the total radioactive signal. Adapted from Pokhrel *et al.* 2018.

Interestingly, the RXKD motif of RSHCd appears to have no influence on the enzyme's substrate preference as is the case for RelSeq and RelMtb (151,247). Unlike RelSeq and RelMtb, RSHCd does not utilize GTP to synthesize pppGpp (Fig. 15) (147). Notably, GTP appears to stimulate ATP hydrolysis by RSHCd, which corresponds to the robust inorganic phosphate (Pi) spots in the autoradiogram, suggesting that the enzyme recognizes the substrate but cannot accommodate the triphosphate form of the nucleotide in its active site to enable pyrophosphate transfer (147). Furthermore, SAS enzymes from *E. faecalis* and *B. subtilis* can also utilize GMP to produce pGpp, but RSHCd does not utilize GMP either, demonstrating high specificity for GDP (Fig. 15) (147,152,168).

The finding that RSHCd does not utilize GTP despite carrying the highly conserved RXKD motif in its synthetase domain was further explored. RSHCd was incubated with a mixture of GDP and GTP at the ratio of either 1:1 or 1:2 in the presence of ATP. Reaction products were subsequently separated using TLC. Based on the TLC autoradiogram, RSHCd failed to utilize GTP at equimolar concentration of GDP and at an excess concentration of GTP in the same reaction mixture (Fig. 16) (147). Furthermore, commercially available GMP, GDP, and GTP nucleotide standards were also run separately through an anion exchange column in the HPLC system. We found that the GTP peak resolves in the chromatogram completely devoid of contaminants and derivative compounds (Fig. 17) (147). This suggests that the inability of RSHCd to utilize GTP is not due to substrate impurity and/or degradation (147).

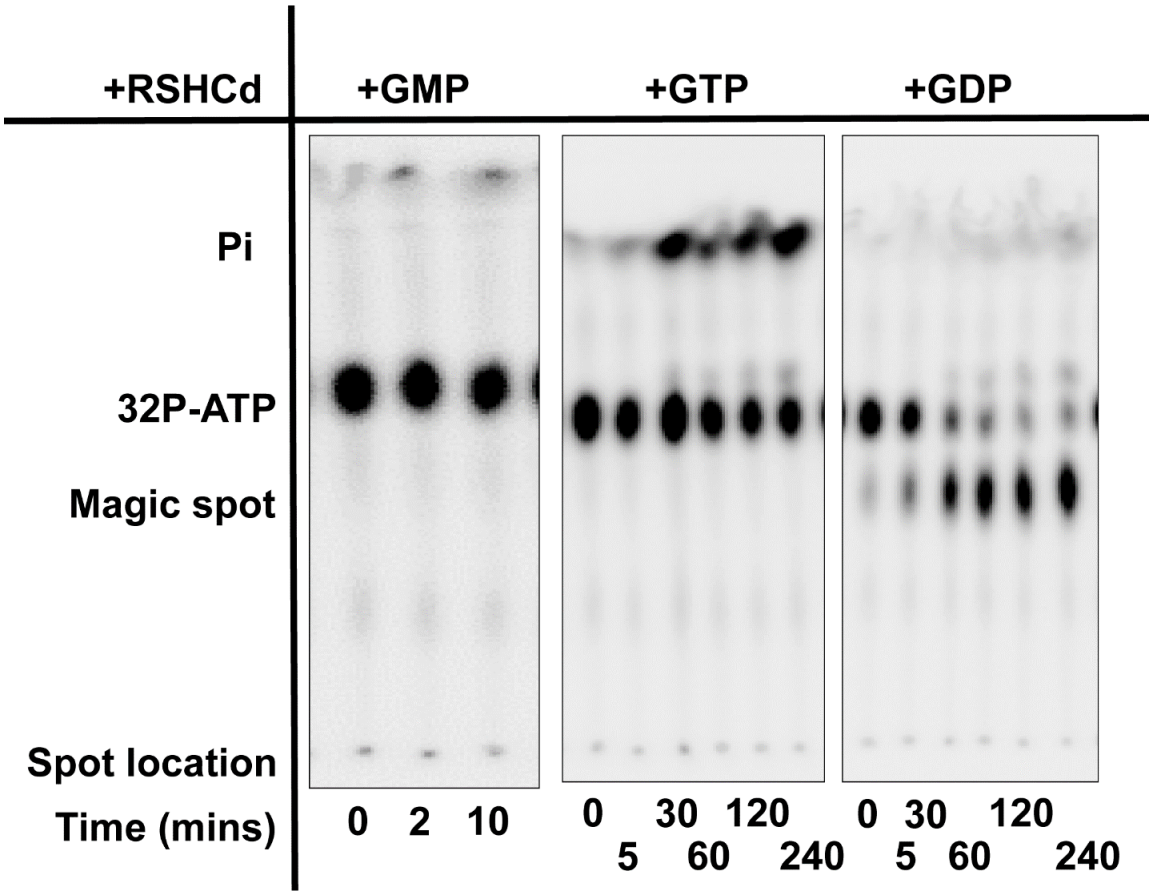

Figure 15. Analysis of substrate preference and utilization of RSHCd. TLC autoradiogram of *in vitro* RSHCd transferase activity using different substrates. RSHCd readily transfers radioactive pyrophosphate from 32P-ATP to GDP but cannot utilize GMP or GTP as a substrate. ATP hydrolysis appears to increase Pi levels in the presence of GTP. Adapted from Pokhrel *et al.* 2020.

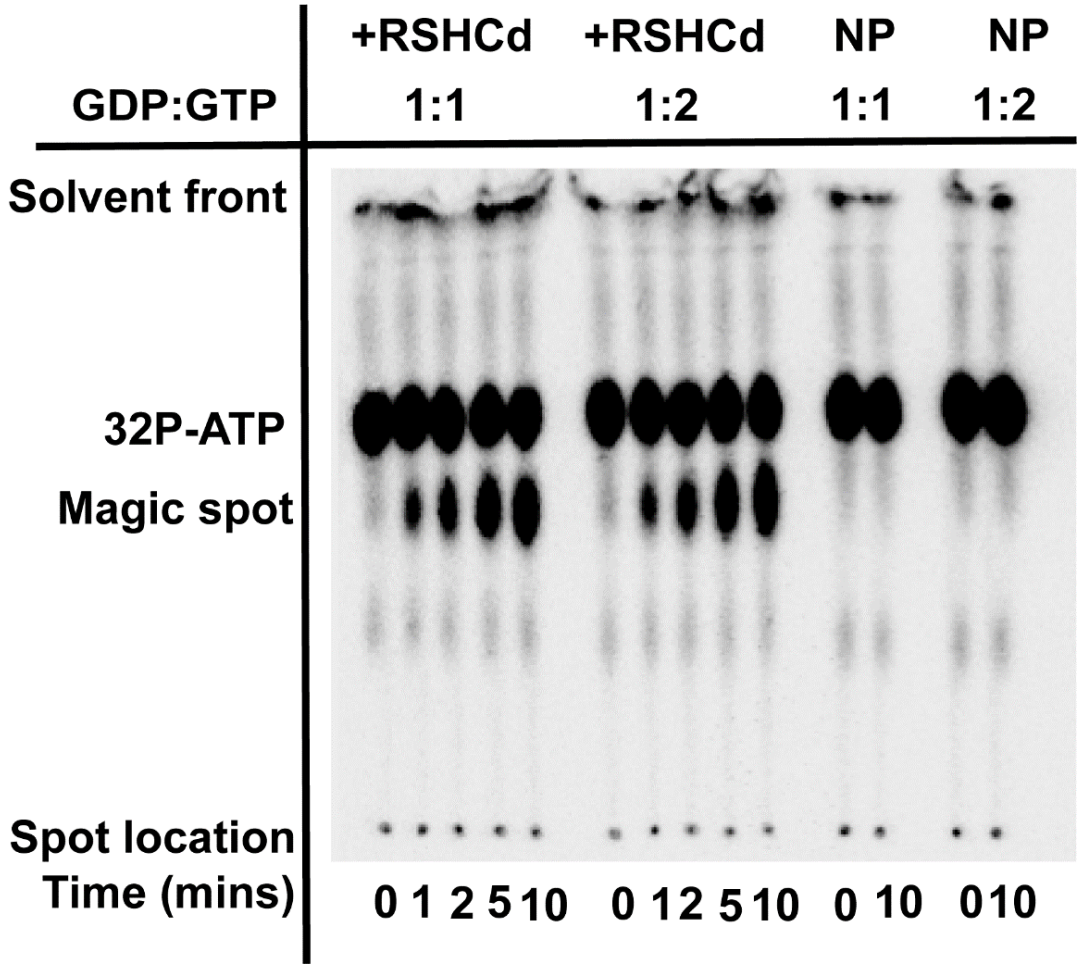

Figure 16. TLC autoradiogram of *in vitro* RSHCd transferase activity at different GDP:GTP ratio. *In vitro* transferase reaction using equimolar concentration of GDP and GTP (0.15 mM each) and 2X more GTP (0.2 mM) than GDP (0.1mM) keeping the total substrate concentration equivalent to 0.3 mM. NP denotes no protein. Adapted from Pokhrel *et al.* 2020.

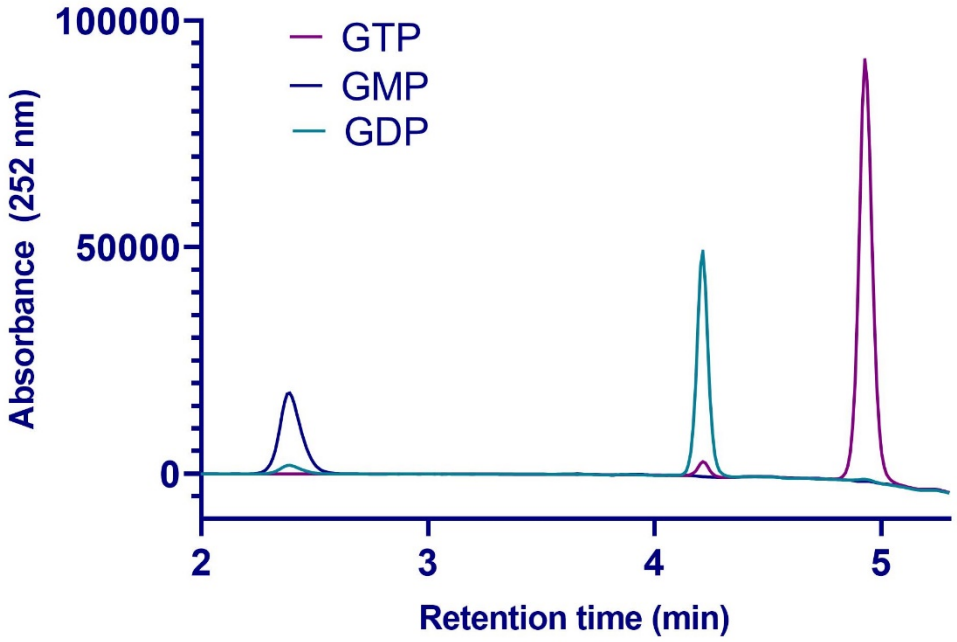

Figure 17. HPLC chromatogram of GTP, GDP, and GMP standards. Standards were run separately at the concentration of 20 μM as 252 nm readout. Adapted from Pokhrel *et al.* 2020.

Biochemical characterization of RSHCd synthesis activity

We found RSHCd to exclusively utilize GDP, therefore, we next measured the kinetic constant (K_m) for the RSHCd-mediated (pp)pGpp synthetase reaction. The synthesis reaction that was assayed involved the incubation of RSHCd at 3.0 μM with 0.12 M ATP and 1.0 μCi 32P-ATP in the presence of various concentrations of GDP. Based on our reactions, the ability of RSHCd to convert GDP and excess radioactive ATP to the magic spot increases with increasing concentrations of GDP (Fig. 18A and 18B) (147). As a magic spot synthetase that only utilizes GDP for a substrate, we found that RSHCd binds GDP with a K_m of 95 μM (Fig. 18C), which is physiologically relevant to the levels of GDP (< 128 μm) in the cytoplasm of exponentially growing *E. coli* cells (147,252).

Furthermore, ppGpp and pppGpp is a positive allosteric regulator of magic spot synthesis catalyzed by *E. coli* RelA and *B. subtilis* SAS, respectively (150,253). In *E. coli*, rapid production of ppGpp resulting in the activation of a positive feedback response is postulated to concurrently activate a fast-coordinated response that is mediated by the SpoT enzyme (253). As a strong (pp)pGpp hydrolase, *E. coli* SpoT serves as a threshold filter that controls cells from committing to full stringency during the SR cascade (253). Since RSHCd is a putative bifunctional enzyme with an intact synthetase and hydrolase domains, we investigated whether its synthetase activity (in the presence of GDP) is allosterically regulated by the ppGpp product. Upon incubation of RSHCd with GDP, ATP, and increasing concentrations of exogenous 5'-ppGpp-3' (Trilink), we found that the magic spot synthesis activity of RSHCd is not regulated by a positive feedback mechanism (Fig. 19) (147).

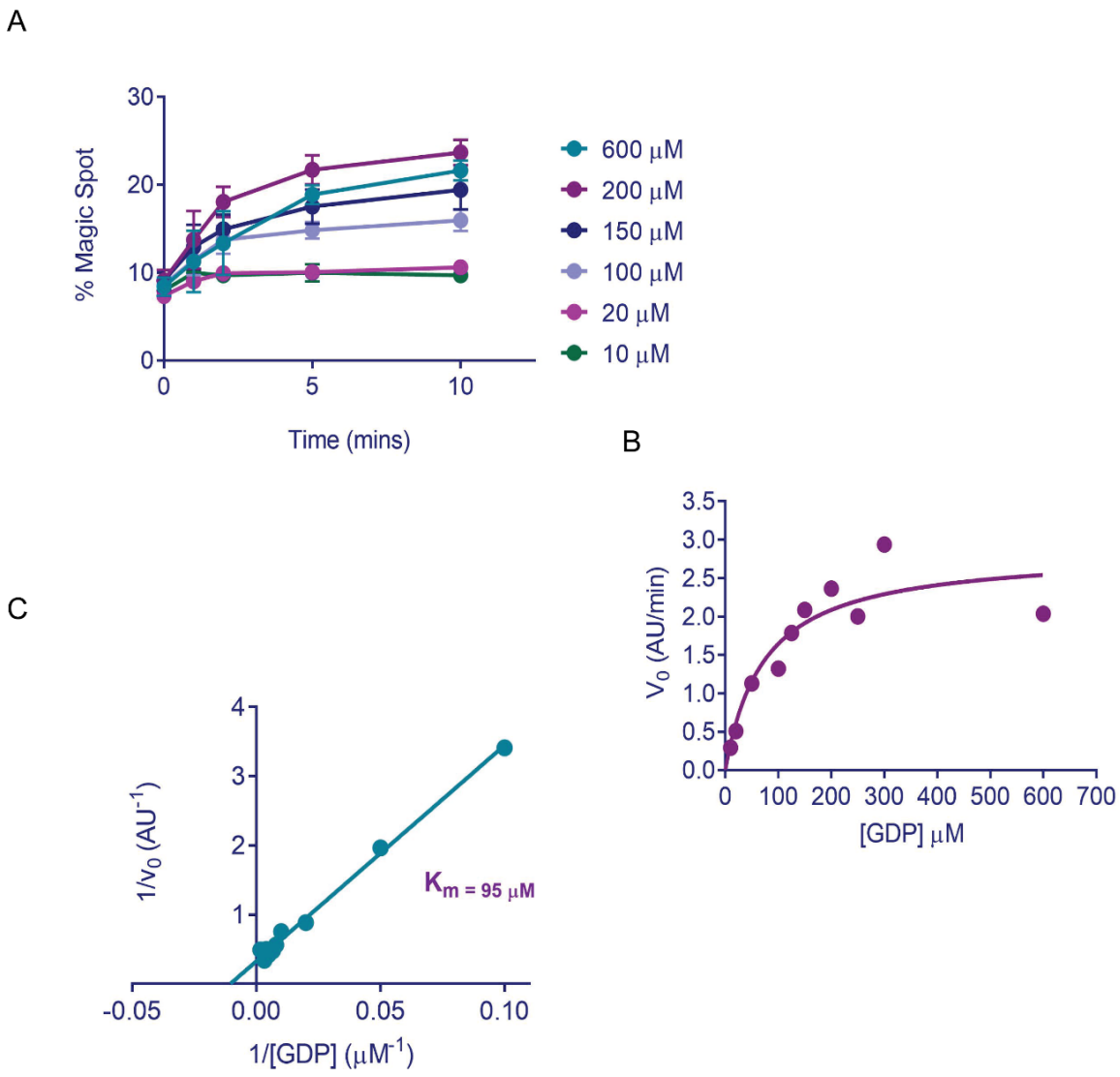

Figure 18. Biochemical characterization of RSHCd. (A) Conversion of radiolabeled ATP to magic spot increases with a corresponding increase in GDP concentrations. (B) Nonlinear fit of velocity vs [GDP]. (C) Lineweaver-Burk plot of RSHCd activity. K_m of RSHCd for GDP is 95 μM. Figures A and C adapted from Pokhrel *et al.* 2020.

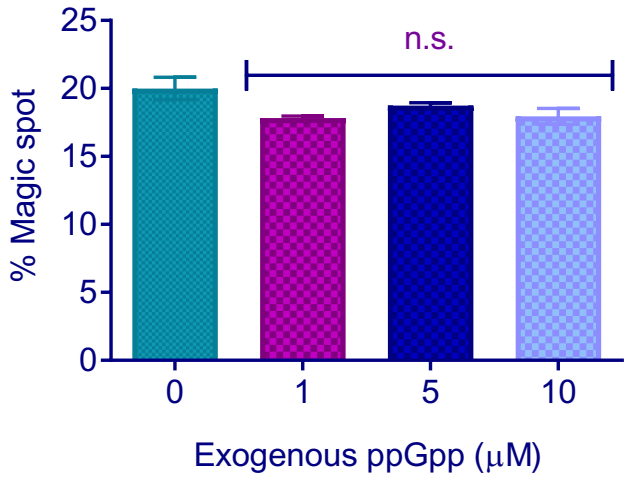

Figure 19. Evaluating allosteric regulation of RSHCd. RSHCd activity in the presence of increasing concentrations of exogenous 5'-ppGpp-3'. Enzyme activity at different 5'-ppGpp-3' concentrations were compared by One-Way ANOVA analysis of variance. n.s., not significant. Adapted from Pokhrel *et al.* 2020.

RSHCd synthetase activity is unaffected by pH or the type of metal ion cofactor

Like several biochemically characterized long RSH enzymes, RSHCd is an overall basic protein with an isoelectric point of 8.81 (147,160,254). RSHCd synthesizes magic spot, presumably ppGpp, in the presence of GDP at a buffer pH of 7.5 (147,248). Notably, a pH of 7.5 is a value that corresponds to the pH range (7.1 - 7.5) of the normal colonic perimucosa (147,255). To investigate the effect of environmental pH on the substrate utilization of RSHCd, *in vitro* pyrophosphate transfer reactions were carried out separately in various buffer pH values, including 5.0, 6.0, 7.5, 9.0, and 10.0. (Fig. 20). We found that RSHCd synthesizes magic spot at all buffer conditions studied but fails to utilize GTP at any tested pH value (Fig. 20) (147). This finding suggests that RSHCd cannot bind to or accommodate GTP regardless of the titration status or the ionic strength of the SD amino acid residues (Fig. 20) (147) .

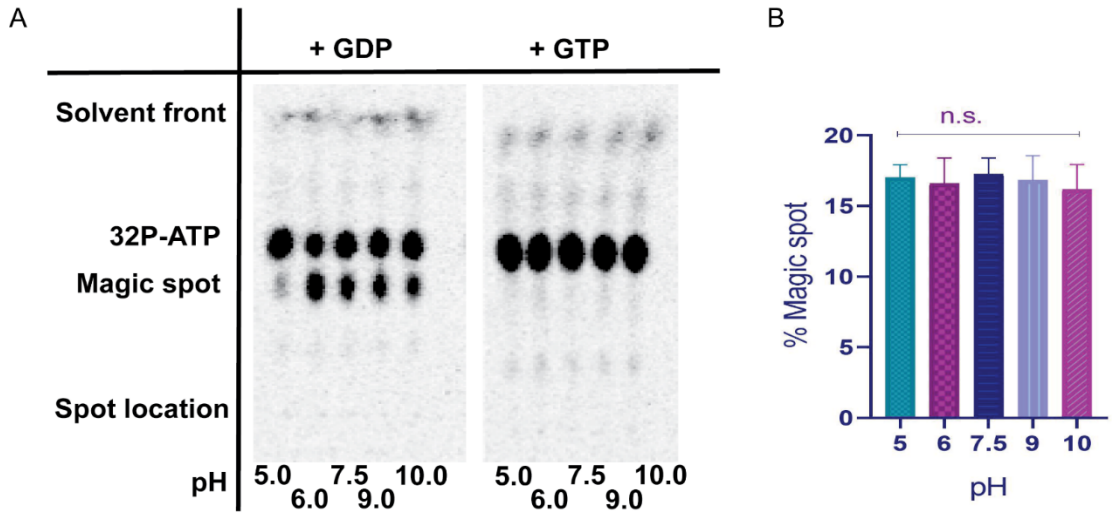

Figure 20. Effect of pH on RSHCd synthetase activity. TLC autoradiograms (A) showing the accumulation of magic spot in the presence of GDP or GTP at any given pH value. Graphical representation of the GDP autoradiogram (B) demonstrating that RSHCd utilizes GDP without exhibiting any pH specificity. Magic spot synthesis at various pH values was compared to that at pH 7.5 by One-Way ANOVA. n.s., not significant. Adapted from Pokhrel *et al.* 2020.

Pyrophosphokinases and nucleic acid-metabolizing enzymes need metal cofactor(s) to coordinate negative charge(s) for enzymatic reactions (147). Magnesium is abundantly present in the bacterial cytoplasm (~100 mM) and is the most utilized ion for nucelotidyl transfer reactions (147,256). Previous studies have shown that Mg^{2+} is employed by RelMtb and RelSeq for the optimal synthesis of (pp)pGpp *in vitro* (159,160,243,257). Recently, *Methylobacterium extorquens* RSH was shown to synthesize pppGpp more efficiently in the presence of Co^{2+} than Mg^{2+} (147,258). The catalytic palm domain of human DNA polymerase β bears structural kinship with the active site of RelSeq synthetase domain (147,159,247). According to Vashistha *et al.*, human Polβ can use Zn^{2+}, Mn^{2+}, and Co^{2+} along with Mg^{2+} to catalyze primer extension (147,259,260). Notably, Zn^{2+}, Mn^{2+}, and Co^{2} have an ionic radius similar to that of Mg^{2+} (147,259,260). Ca^{2+} has an ionic radius that is significantly larger than that of Mg^{2+} and does not enable primer extension, suggesting that the human Polβ exhibits selectivity for specific metal cofactors (260).

To investigate the metal cofactor selectivity of RSHCd, we performed *in vitro* pyrophosphate transfer reactions in the presence of different divalent cations (Fig. 21) (147). Of the eight metals tested, including Mg^{2+}, Mn^{2+}, Co^{2+}, Cu^{2+}, Fe^{2+}, Zn^{2+}, Ni^{2+}, and Ca^{2+}, only Cu^{2+} significantly yet modestly reduced RSHCd-driven magic spot synthesis (Fig. 21) (147). This suggests that the enzyme readily employs a wide array of structurally diverse cations for a cofactor to catalyze pyrophosphate transfer (147). We postulate that the substitution of Mg^{2+} with different cations becomes most relevant to *C. difficile* under environmental condition(s) where specific metal ions are depleted and/or during competition for metals with host-metal sequestering proteins (147).

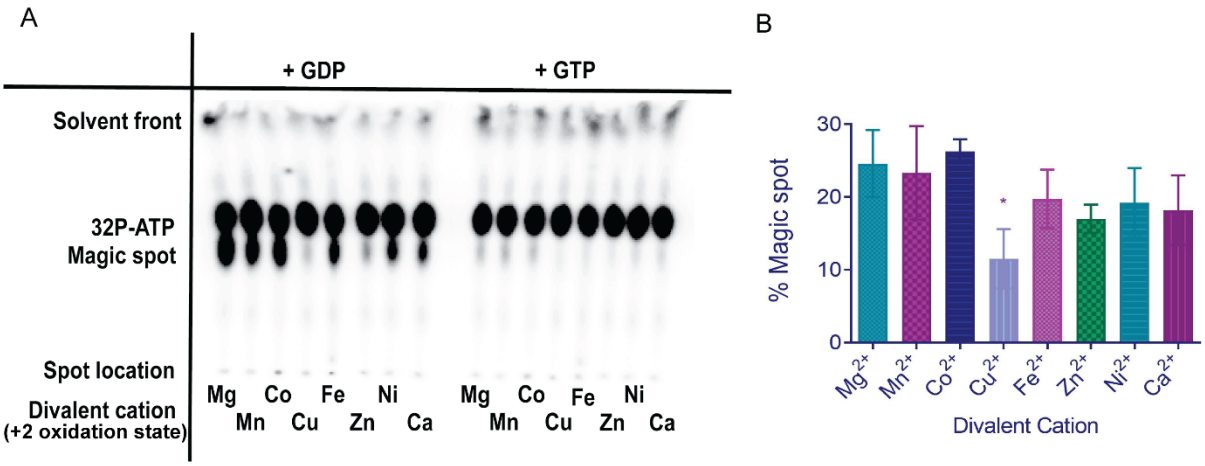

Figure 21. Effect of divalent metal cations on RSHCd synthetase activity. TLC autoradiogram (A) showing the accumulation of magic spot in the presence of GDP or GTP in the presence of different metal ion cofactors at a buffer pH of 7.5. Graphical representation of the GDP autoradiogram (B) demonstrating that RSHCd utilizes GDP without exhibiting any metal ion specificity. Levels of magic spot synthesis were compared by One-way ANOVA. * $P < 0.01$. Adapted from Pokhrel *et al.* 2020.

RSHCd binds GTP with poor affinity

To further investigate the lack of GTP utilization by RSHCd, we examined the interaction of RSHCd with GDP and GTP using isothermal titration calorimetry (147). Based on our ITC data, we found that RSHCd binds to GDP and GTP with an association constant of 31.9 M^{-1} (Fig. 22) and 25.1 M^{-1} (Fig. 23), respectively (147). This finding indicates that RSHCd interacts with GTP despite failing to catalyze the synthesis of pppGpp. During exponential growth, bacterial cells maintain GTP at concentrations ranging from 900 to 1,100 μM, a 2 to 10-fold excess compared to the concentrations of GDP (147,252,261,262). During stationary phase onset, both ATP and GTP are rapidly depleted, with ATP levels recovering more faster from the conversion of guanosine nucleotides to (pp)pGpp (252,262). Despite interaction, we found the binding affinity of RSHCd for GTP to be lower than that for GDP (147). During stationary phase, the physiological concentrations of GDP is relatively higher than that of GTP, indicating that RSHCd can preferentially utilize GDP as a substrate due to its abundancy and availability (147). Notably, we found RSHCd to bind GTP at a protein to substrate ratio of 1:10 (147). However, failure to utilize GTP to produce pppGpp was observed at a much larger protein to substrate ratio of 1:200 (147). Nevertheless, these results suggest that RSHCd may transiently bind to GTP at different stages of bacterial growth, but the consistent abundancy of GDP in the bacterial cytoplasm potentially enables the enzyme to readily respond to the substrate for enzyme catalysis (147). Furthermore, the “K” value from our ITC data represents the association constant computed from a single-site-binding model (Fig. 22 and 23) (147). We observed that the K value of RSHCd for GDP is lower than the K_m value of 95 μM quantitated through TLC (147). We hypothesize that the observed variation in K values is arising from nonspecific interaction of GDP with the C-terminal domain of full-length RSHCd (147,163).

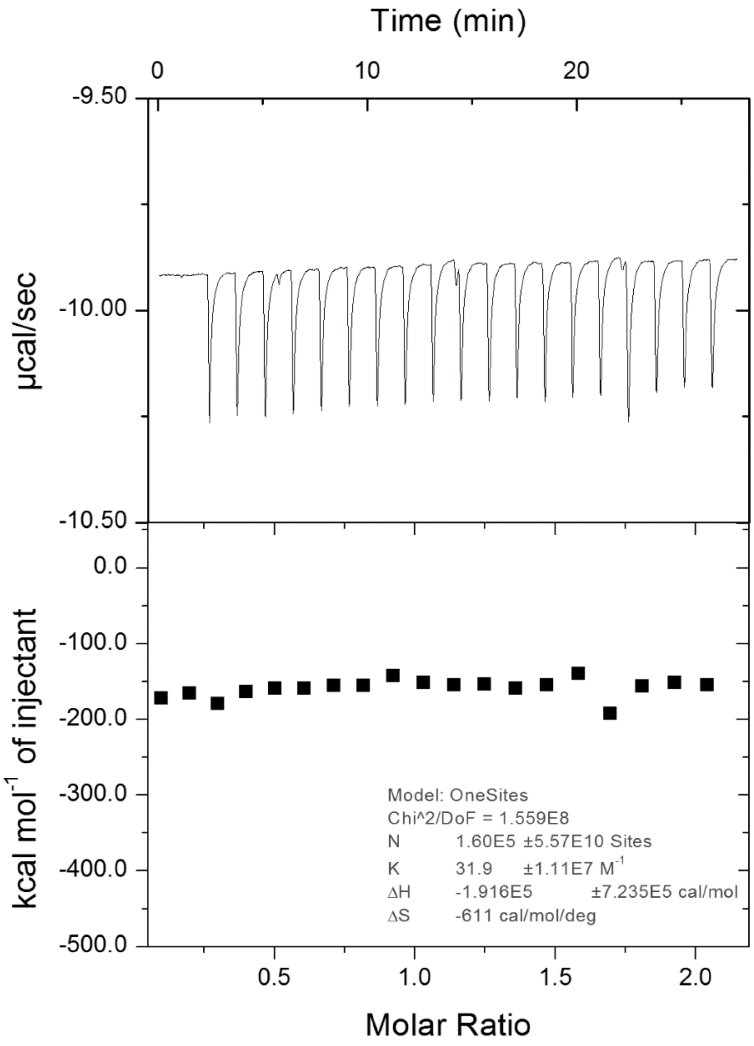

Figure 22. Interaction analysis of RSHCd with GDP. Isothermal titration calorimetry thermogram (top) and Wiseman plot (bottom) of RSHCd interaction with GDP at 37°C. The upper panel shows the raw data for titration of GDP with RSHCd, and the lower panel shows the integrated heats of binding obtained from the raw data. The data were fitted to a single-binding model. Each value is the average of three repeat experiments and the standard deviation ± are shown. RSHCd binds to GDP at a K value of 31.9 M^{-1}. Adapted from Pokhrel *et al.* 2020.

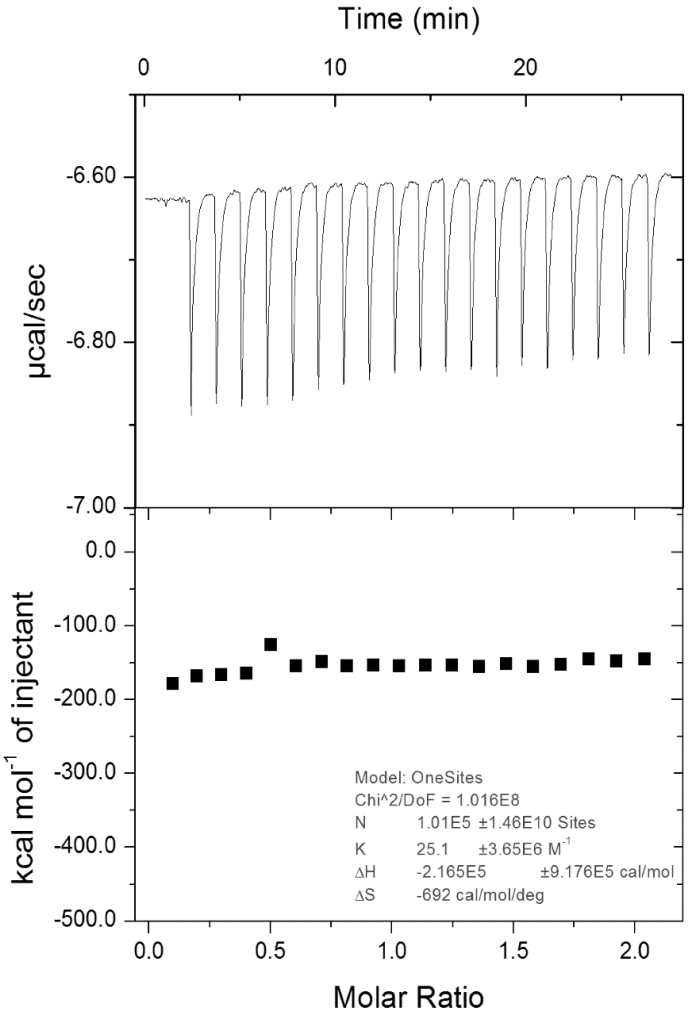

Figure 23. Interaction analysis of RSHCd with GTP. Isothermal titration calorimetry thermogram (top) and Wiseman plot (bottom) of RSHCd interaction with GTP at 37°C. The upper panel shows the raw data for titration of GTP with RSHCd, and the lower panel shows the integrated heats of binding obtained from the raw data. The data were fitted to a single-binding model. Each value is the average of three repeat experiments and the standard deviation ± are shown. RSHCd binds to GTP at a K value of 25.1 M^{-1}. Adapted from Pokhrel *et al.* 2020.

RSH-REL lacks regulation by the HD and CTD of full-length RSHCd

As mentioned previously, the C-terminal regulatory domains of long RSH enzymes control the opposing hydrolase and synthetase activity of the N-terminal region (159,160). In *E. coli* (pp)pGpp synthesis is negatively regulated by the CTD either by mediating RelA oligomerization or via intramolecular interaction with the enzyme's N-terminal domain (160,263,264). However, upon binding to uncharged (non-aminoacyl) tRNA in complex with ribosomes, CTD positively regulates RelA-mediated (pp)pGpp synthesis (264). RelSeq and RelMtb NTD are also positively regulated by the enzymes' CTD in the presence of uncharged tRNAs such that (pp)pGpp synthesis increases when uncharged tRNAs are bound to a complex of ribosome + mRNA (160,243). Interestingly, regulation of the Rel/RSH hydrolase domain, capable of hydrolyzing the small molecule alarmones, also appears to involve the CTD in diverse bacterial species. Fang *et al.* demonstrated that the ACT domain present in *Rhodobacter capsulatus* Rel, along with *S. equisimilis* Rel, *B. subtilis* Rel and *E. coli* SpoT bind branched-chain amino acids to stimulate its hydrolysis activity (166). Very recently, Shin and colleagues solved the atomic structure of the interaction between valine and the ACT domain of RelMtb using NMR, confirming the role of the CTD of bifunctional RelMtb in the positive allosteric regulation of (pp)pGpp hydrolysis (265).

In order to determine whether RSHCd synthetase domain activity is regulated by the RSHCd CTD, we designed and cloned a truncation construct of RSHCd called RSH-REL, which is a monofunctional synthetase derivative of the full-length RSHCd (Fig. 24A). Overexpression of RSH-REL appeared to be extremely toxic to *E. coli* even in the absence of the IPTG inducer, suggesting that the enzyme is hyperactive (Fig. 24B) (147). It is so active that trace transcription of *rsh-rel* from an uninduced, leaky promoter results in sufficient RSH-REL protein product to produce inhibitory/potent levels of magic spot (147). RSH-REL-driven toxicity can be partially rescued by supplementation with 1% CAA and is further enhanced by the additional supplementation with 1% GLU (Fig. 24B) (147). The finding that full-length RSHCd slows *E. coli* growth while RSH-REL completely arrests it suggests that (pp)pGpp toxicity is modulated by the presence of and the activity of the regulatory CTD and/or activation of the hydrolase domain in RSHCd (147).

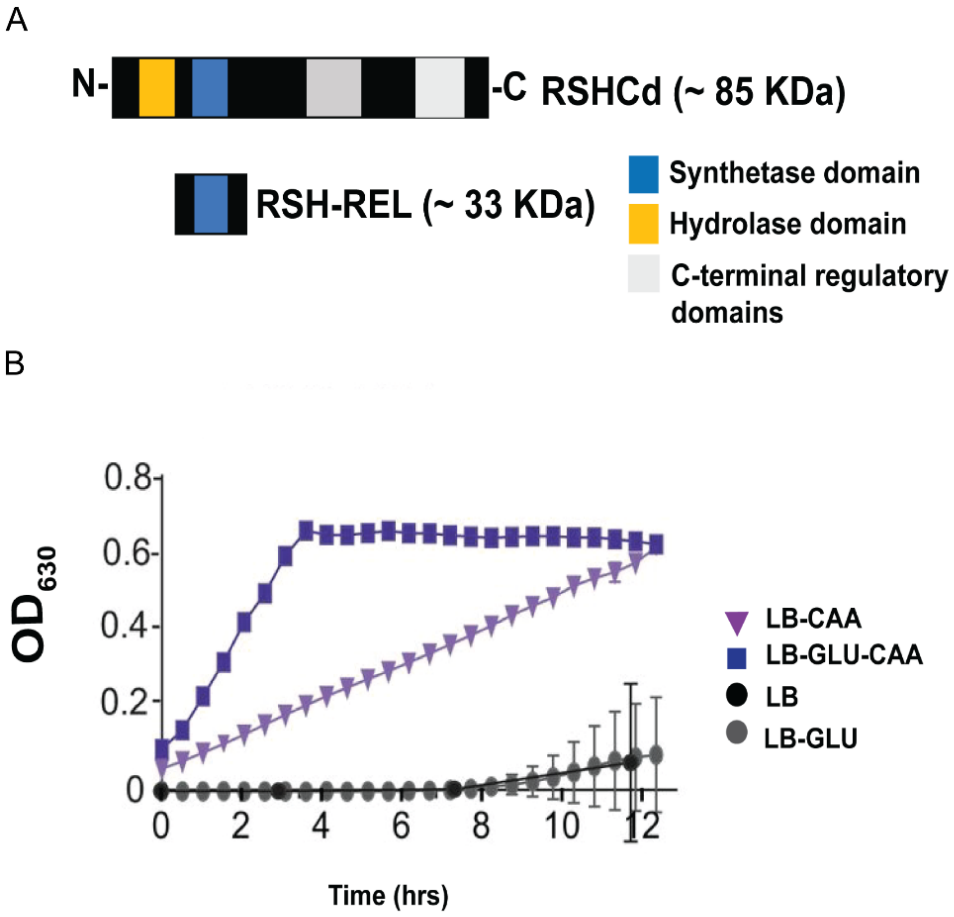

Figure 24. Cloning and overexpression of RSH-REL. (A) Schematic representation of full-length RSHCd (1-735 amino acid residues) alongside the truncation construct; RSH-REL (amino acid residues 113–388). The theoretical molecular weight of the construct is provided (~33 KDa). Growth of *E. coli* cells carrying pMMBneo::*rsh-rel* vector in LB medium supplemented with Casamino acids (LB-CAA), glucose (LB-GLU) or both (LB-GLU-CAA). Bottom figure adapted from Pokhrel *et al.* 2020.

RSH-REL produces magic spot in vitro

To confirm the functionally of RSH-REL enzyme, recombinant RSH-REL was purified using metal affinity chromatography. We found that the protein runs at a higher molecular weight (MW) (between 40 and 45 KDa) on a 4% stacking, 12% separating SDS-PAG (Fig. 25A). This finding suggests that the enzyme could be undergoing post-translational modification such as glycosylation and phosphorylation or the protein is interacting with potential binding partners, contributing to its increased weight. Peptide amino acid composition has been directly linked to the difference between SDS-PAGE-displayed MW and the theoretical MW of enzymes. Guan *et al.* demonstrated that the difference in MW of several enzymes is linearly correlated with the percentage of acidic amino acid that fits the equation y = 276.5x - 31.33 (where x represents the percentage of D and E amino acids combined, and y represents the average ΔMW per amino acid residue) (266). Based on the equation, y = 0 when x = 11.3% in which case the observed MW on an SDS-PAG is identical to the enzyme's theoretical MW (266). RSH-REL constitutes approximately 16% acidic amino acids in its primary sequence and with the application of the "y = 276.5x - 31.33" equation, it can be inferred that the band size discrepancy is not due to PTM. The calculated ΔMW (~5 KDa) also corresponds to the approximate added weight to the theoretical MW of RSH-REL enzyme (Fig. 25A). Like full-length RSHCd, RSH-REL enzyme utilizes GDP and ATP to produce the magic spot but appears to be incapable of utilizing GTP (Fig. 25B). Furthermore, expression of RSH-REL results in the cytoplasmic accumulation of ppGpp in *E. coli* cells (Fig. 25C).

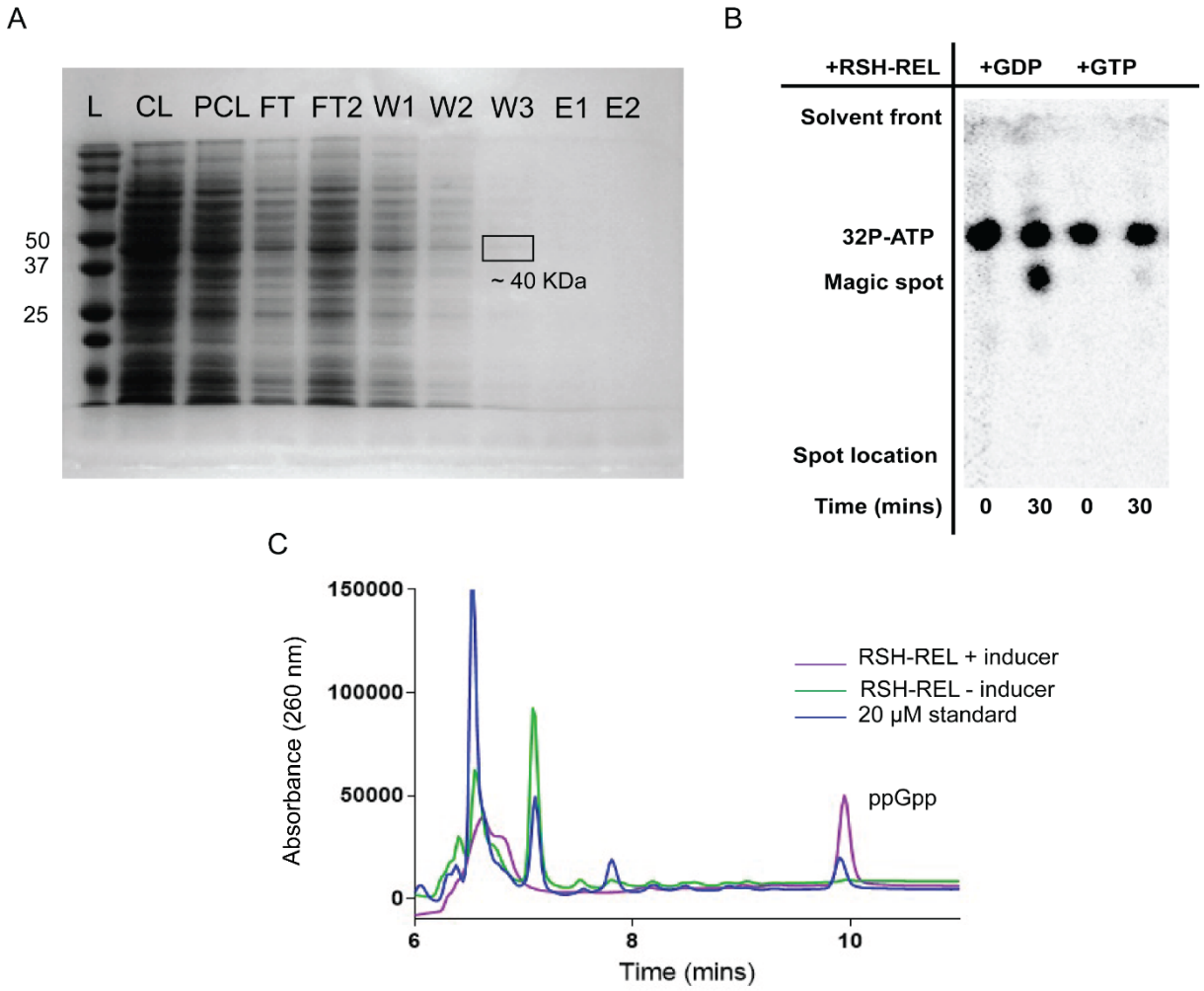

Figure 25. Overexpression, purification, and functional characterization of RSH-REL. (A) 4%, 12% SDS-PAGE gel image of purified RSH-REL protein. Lanes 1 through 10 were loaded with marker (L), clarified lysate (CL), prepped CL, flow-through (FT), CL FT2, wash 1 FT, wash 2 FT, wash 3 FT, elute 1 (E1), and elute 2 (E2). (B) TLC autoradiogram of RSH-REL protein utilizing GDP for reaction catalysis. (C) HPLC chromatogram of 5'-ppGpp-3' detected in exponentially growing *E. coli* cells expressing RSH-REL in the presence of the IPTG inducer. Filtered cell extracts post-induction were run through a strong anion exchange column at the flow rate of 1.5 mL/min. Sample readouts were obtained at 260 nm.

RSHCd HD requires activation by biological effectors of the CTD

The differential regulation of the synthetase and hydrolase domain activities in bifunctional *S. aureus* Rel (RelSau), RelSeq and RelMtb has been characterized (160,164,243). Like *E. coli*, the synthetase domain activity of RelMtb is activated in the presence of uncharged tRNAs alone or from an imbalance in the ratio of uncharged tRNAs to charged tRNAs, which is characteristic of cytoplasmic amino acid depletion (243). But *in vitro* synthetase activity significantly increases in the presence of and upon complex formation of RelMtb with ribosome, uncharged tRNA, and mRNA (243). Similarly, the synthetase domain of RelSeq, an enzyme exhibiting a net specific activity strongly in favor of (pp)pGpp degradation, is also activated in a stalled ribosome-dependent manner (159,160). The CTD of RelSeq is directly involved in the reciprocal regulation of the two opposing activities in the NTD of RelSeq (160). Free RSHCd optimally utilizes GDP to produce basal levels of magic spot at Mg^{2+} concentrations approximately 2-fold higher than the concentration of GDP substrate (147,248).

To investigate how the opposing synthesis and hydrolysis activities of RSHCd are differently regulated, we evaluated the hydrolase activity of RSHCd. The hydrolase assay involved the extraction and use of radiolabeled magic spot (product of a separate pyrophosphate transfer reaction) as a substrate, Mn^{2+} metal cofactor, and full-length RSHCd for pyrophosphohydrolase catalysis. Based on literature evidence, Mn^{2+} optimally coordinates (pp)pGpp to the hydrolase domain of long RSHs (160,243). For instance, RelSeq in the presence of Mn^{2+} optimally catalyzes (pp)pGpp hydrolysis at 2 to 3-fold molar excess over the total concentration of nucleotide substrate at pH values ranging from 7.2 to 9.5 (160). However, we found RSHCd to exhibit a net synthesis activity in isolation (Fig. 26). The failure to hydrolyze the magic spot to yield inorganic pyrophosphate (PPi), suggests that the hydrolase domain requires regulation by branched-chain amino acids and/or yet to be characterized biological effector(s) of alarmone metabolism. Analysis of *in vitro* RSHCd pyrophosphohydrolase activity through HPLC also resulted in a modest reduction of the exogenous ppGpp signal after 4 hrs of reaction incubation, further suggesting that the hydrolase domain of RSHCd requires regulation by the CTD, presumably via interaction of the ACT domain with branched chained amino acids, including valine, isoleucine, and leucine (Fig. 27).

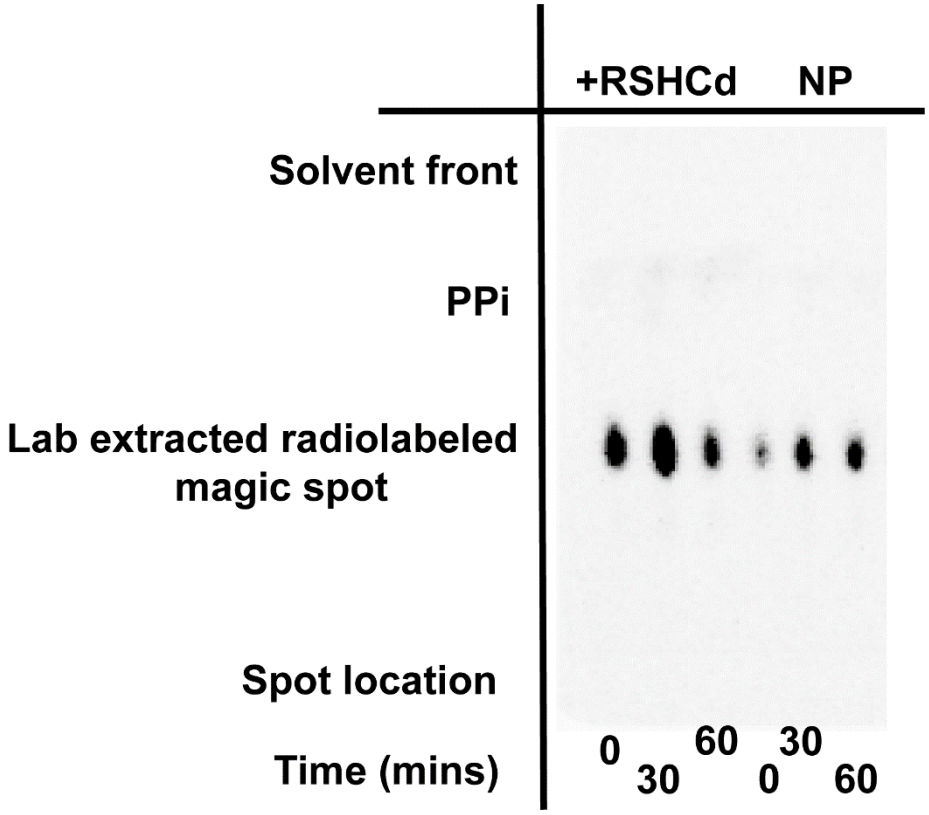

Figure 26. Characterization of *in vitro* RSHCd hydrolase activity using TLC. Autoradiogram of RSHCd hydrolase activity with Mn^{2+}, full-length RSHCd, and radiolabeled magic spot. Radiolabeled magic spots were extracted using Li^{2+} from a separate synthetase reaction. Failure to detect the hydrolysis product in the autoradiogram suggests that the reaction requires effectors of the CTD domain to produce detectable levels of PPi.

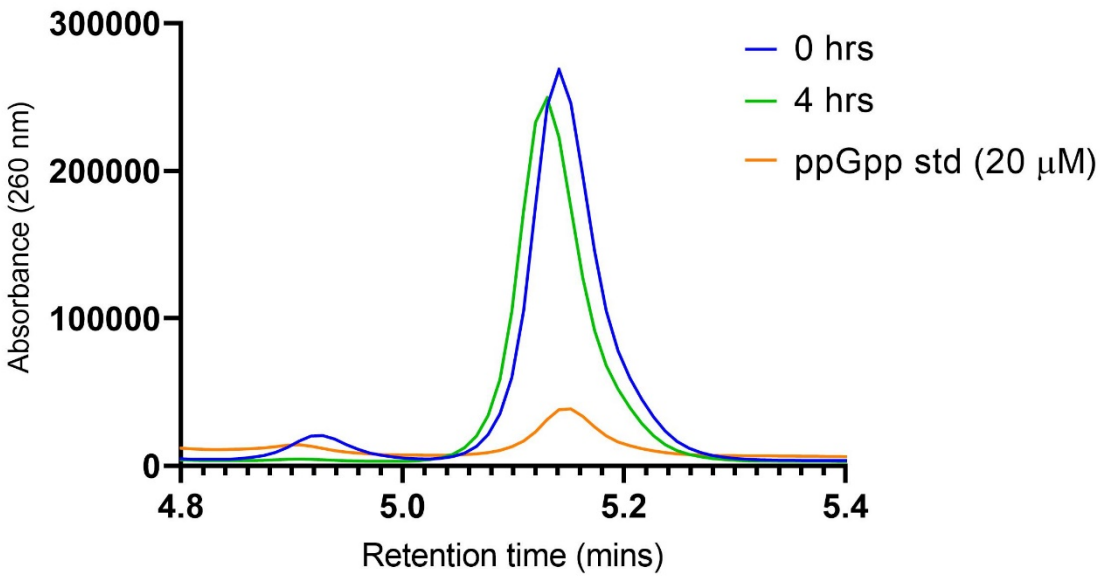

Figure 27. Analysis of *in vitro* RSHCd hydrolase activity via HPLC. HPLC chromatogram comparing 5'-ppGpp-3' signal between 0 and 4 hrs of RSHCd-mediated hydrolysis reaction *in vitro*. Reaction mixture after 0 and 4 hrs of incubation were run separately through a strong anion exchange column at the flow rate of 1.0 mL/min. Sample readout was obtained at 260 nm.

RSHCd produces triphosphate product in the presence of GDP

The unique finding that RSHCd utilizes only GDP for a substrate was further evaluated through the functional characterization of RelQ from *B. subtilis*. RelQBs is a small alarmone synthetase that shares the conserved synthetase fold with the long RSH/ Rel enzyme. Unlike monomeric Rel/RSH proteins, RelQBs forms highly symmetric homotetramers and binds ATP and GXP in a sequential order to catalyze pyrophosphate transfer (150). A unique feature of the RleQBs homotetramer is the presence of a cleft in its center that enables the binding of two allosteric pppGpp molecules (150). Cell wall antibiotics and perturbations of cell envelope from alkaline stress induce *B. subtilis relQ* expression, leading to a strong accumulation of (pp)pGpp, which can be detected via high performance liquid chromatography-coupled mass spectrometry (168,198).

Recently, Fung *et al.* demonstrated that the expression of gene encoding RelQBs also results in the accumulation of 5'-pppApp-3' in addition to (pp)pGpp *in vivo* (267). The increase in the levels of these alarmones are dramatically suppressed in a synthetase mutant strain of RelQBs (SAS^{D87G}), suggesting that the accumulation of multiple alarmones apart from (pp)pGpp are also dependent on the magic spot synthesis activity of RelQBs (267). Of the multiple alarmones, pGpp is the most strongly induced small alarmone nucleotide for several reasons (267). Firstly, ppGpp is rapidly degraded to pGpp by the NuDiX family hydrolase, NahA (156). Secondly, RelQBs is capable of directly producing pGpp through the utilization of GMP for a substrate as *ΔnahA* strains accumulate lower but detectable levels of pGpp (156). Fung *et al*. also reported that the accumulation of diverse alarmones corresponds with changes in the levels of intracellular purine nucleotide (267). Rapid depletion of GTP is postulated to occur from the inhibition of GMP kinase by pGpp, suggesting that (pp)pGpp target de novo purine biosynthesis enzymes (156,267). Based partially on the purification protocol established in Fang *et al.* 2018 as well as direct consultations with the first author of the publication, we purified RelQBs from an *E. coli* expression strain and performed *in vitro* pyrophosphate transfer reactions to subsequently run reaction products through an anion exchange column in the HPLC system (Fig. 28) (166). We also incubated RelQBs and RSHCd separately with GMP, GDP, GTP or ADP (RSHCd only), 1.0 µCi γ-^{32}P-ATP, and ATP at 37°C to subsequently perform one-dimensional TLC assay (Appendix D). As expected, RelQBs

synthetized pGpp, ppGpp, and pppGpp from GMP, GDP and GTP, respectively (Appendix D). RSHCd specifically utilized GDP to synthesize magic spot (Appendix D). However, RSHCd-produced magic spot ran parallelly with RelQBs-produced pGpp as depicted in the autoradiograms, indicating that RSHCd is not producing ppGpp alarmone (Appendix D). To confirm that RSHCd-mediated catalysis is yielding a triphosphate product rather than a tetraphosphate product using GDP as the substrate, we tested the ability of RSHCd to utilize ADP (Appendix D). *B. subtilis* RelQ can utilize ADP as a substrate to yield 5'-diphsophate-adenosine-3'-diphosphate (5'-ppApp-3'), which migrate similar distances to guanosine-three phosphate alarmones on a PEI-cellulose plate (258,267). The similarity in the retention factor or migration of ppApp with guanosine-three phosphate molecules is due to the steric hindrance imposed by or the higher mass of the guanosine base in comparison to the adenosine base. Since mobility of molecules in TLC is dependent on its molecular weight as much as its affinity for the stationary phase, and since RSHCd does not utilize GMP, we hypothesized that RSHCd uses ADP to produce ppApp (248). Contrary to our hypothesis, we found that RSHCd fails to utilize ADP, confirming that RSHCd is producing guanosine-triphosphate alarmone in the presence of GDP under the experimental conditions used (Appendix D).

Analysis of *in vitro* RSHCd and RelQBs-mediated (pp)pGpp synthesis via the highly sensitive HPLC technique also revealed that RSHCd produces a triphosphate alarmone that co-elutes with the GTP standard (Fig. 28). We postulate that the minor discrepancy in the retention times between RSHCd-produced alarmone and the GTP standards is due to slight variations in the pH value of the mobile phase buffers, which are prepared fresh and filter sterilized every time prior to sample running. The pH values of the mobile phase buffers can also change overtime if the buffers are stored at room temperature, which contributes to minor changes in the retention time of same compounds run through a column on different experimental days.

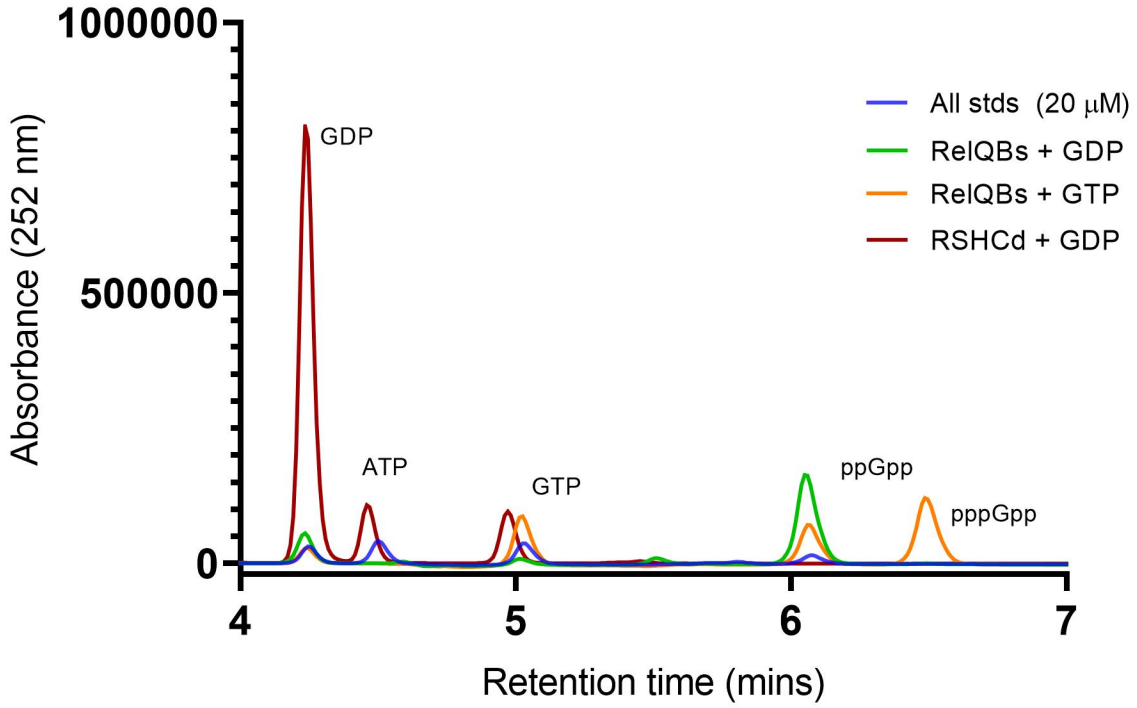

Figure 28. Analysis of RelQBs and RSHCd-catalyzed pyrophosphoryltransferase reactions *in vitro* using HPLC. Reactions were conducted separately in the presence of the indicated substrate with either 3.0 μM RSHCd or RelQBs. The sample filtrates alongside the standards were run through a strong anion exchange column using a gradient elution at the flow rate of 1.0 mL/min. Absorbance at 252 nm as a readout is presented showing that RelQBs produces ppGpp and pppGpp from GDP and GTP, respectively. Whereas RSHCd produces triphosphate alarmones in the presence of GDP that co-elute with the GTP standard. This experiment was conducted by and chromatogram produced by Astha Pokhrel (Poudel *et al.* manuscript in preparation).

Members of the RSH superfamily synthesize (pp)pGpp and (p)ppApp via the transfer of a pyrophosphoryl group from ATP to the 3'-OH group of GXP and/or AXP (148,149,158). Under the experimental conditions used in our pyrophosphate transfer reactions, RSHCd appeared to produce triphosphate products in the presence of GDP (Appendix D and Fig. 28). Contrary to the fundamental reaction mechanism of RSH-catalyzed reactions to produce (pp)pA/Gpp, RSHCd synthesizes magic spot with a guanosine entity bound to three phosphate groups even when GDP is the substrate. Therefore, based on our TLC and HPLC data, we currently hypothesize that RSHCd is producing a three-phosphate alarmone using GDP as a substrate in an ATP-dependent manner via non-canonical mechanism(s). The enzyme catalysis is potentially driven by the initial hydrolysis of GDP to GMP followed by the addition of a pyrophosphate moiety from ATP to the 3'-OH of GMP.

We believe that RSHCd itself could be responsible for the hydrolysis of GDP, which the enzyme utilizes to produce putative 5'-pGpp-3' for two reasons. One, purification of RSHCd from *E. coli* cells can result in the copurification of contaminant GDPases that hydrolyze GDP during pyrophosphoryltransferase reactions. But the use of hexa-histidine specific nickel affinity purification technique followed by a stringent protein dialysis procedure out rules the possibility of contamination by native *E. coli* GDPases. Two, the notion that RSHCd is either directly producing GTP from GDP in the presence of radiolabeled ATP or a byproduct of ppGpp synthesis reaction appears to hold untrue in this case. Sobala *et al.* demonstrated that *M. extorquens* RSH (RSHMex) produces ppGpp and pppGpp in the presence of ATP and GDP or GTP, respectively, in addition with γ-^{32}P-GTP (258). According to their findings, γ-^{32}P-GTP migrates slowly on PEI-cellulose plates than pGpp and ppGpp when run in 0.85 M KH_2PO_4 mobile phase buffer (258). We found that RSHCd-synthesized magic spot co-migrates with RelQBs-synthesized pGpp in 1.5 M KH_2PO_4. Furthermore, RSHCd does not produce ppGpp in the presence of GDP unlike RSHMex. This suggests that RSHCd carries an intrinsic GDPase activity and is able to synthesize the magic spot via non-conventional mechanism(s). Furthermore, *E. coli* GppA and NuDiX family hydrolases degrade pppGpp and ppGpp to ppGpp and pGp, respectively (176,179,180). This means that even if RSHCd were contaminated with native *E. coli* hydrolases that metabolize (pp)pGpp, the

contaminants would not yield radiolabeled pGpp products that are clearly visible as spots in our autoradiograms.

SUMMARY

Here we show that the full-length RSH homolog of *C. difficile* exhibits a strict utilization preference for GDP *in vitro* (147). The enzyme may transiently bind GTP but failure to produce pppGpp suggests that the enzyme is unable to accommodate a pyrophosphate transfer from ATP to GTP (147). Furthermore, the enzyme also fails to utilize GMP and ADP for a substrate but readily utilizes GDP at a wide range of environmental pHs without demonstrating any metal cofactor specificity (147). We previously concluded that the full-length enzyme produces ppGpp in the presence of GDP substrate (147,248). However, our more recent *in vitro* pyrophosphotransferase reactions using RelQBs as a positive control and full-length RSHCd indicate that the latter enzyme is in fact producing a triphosphate alarmone. HPLC analyses using an anion exchange column to separate and resolve RSHCd and RelQBs-catalyzed products further revealed that the alarmone synthesized by RSHCd co-elutes with the GTP standard, confirming that the protein is catalyzing the synthesis of small alarmone triphosphate nucleotide in the presence of GDP. This finding is unique as it indicates that RSHCd produce magic spot via non-conventional route(s), not previously reported in the analyses of other RSH-family enzymes. Furthermore, we postulate that the alarmone synthesis activity of RSHCd is regulated by the hydrolase domain and/or the CTD. Expression of RSH-REL is extremely toxic to bacterial growth and just like its full-length counterpart, RSH-REL can only produce magic spot in the presence of GDP. Additionally, we were able to detect intracellular ppGpp upon expression of RSH-REL in *E. coli* cells. Based on our TLC assay, however, RSH-REL does not produce ppGpp. Therefore, we believe that the intracellular ppGpp extracted and detected using HPLC is actually due to the production and accumulation of ppGpp by *E. coli* cells as a consequence of growth phase-induced nutrient starvation and cytoplasmic changes (Fig. 25C). ppGpp is a more potent effector of the SR in stressed *E. coli* cells, indicating that the bacteria produce detectable levels of ppGpp (178).

We also speculate that the HD of RSHCd requires regulation by the CTD, presumably via interaction with branched-chain amino acids. Based on the mobility of RelQBs-produced pGpp (where GMP is the substrate) and RSHCd-produced magic spot (where GDP is the substrate) in our TLC autoradiograms, we believe that RSHCd exclusively synthesizes pGpp. Nonetheless, analysis of RSHCd catalyzed magic spot using more sensitive techniques such as LC-MS along with the structural analysis of the magic spot through ^{31}Phoshporus NMR will also deem essential in confirming the alarmone identity.

CHAPTER III

CHARACTERIZATION OF RSH-MEDIATED MAGIC SPOT SIGNALING IN *CLOSTRIDIOIDES DIFFICILE*

OVERVIEW

Long RSH enzymes are transcriptionally regulated, with transcription increasing during late exponential phase or stationary phase, or upon induced nutrient deprivation by inhibitors of biosynthetic pathways (147,158,182-184). The specific nutrients whose limitation triggers RSH-mediated (pp)pGpp synthesis vary between bacterial species (158,182,183,185). In *E. coli,* the SR is triggered by amino acid starvation, which results in RelA-mediated (pp)pGpp synthesis. Interestingly, fatty acid starvation and iron limitation specifically induce *E. coli* SpoT-dependent accumulation of (pp)pGpp and ppGpp, respectively (268,269). In *B. subtilis*, the SR is also stimulated in response to lipid starvation (185). Since Gram-positive organisms typically encode one or two SASs in combination with a long RSH enzyme, the SASs in *B. subtilis* are transcriptionally regulated during bacterial growth phase where *relQ* expression is upregulated during exponential phase and *relP* expression is upregulated in the late exponential phase (158,168). Furthermore, genes encoding *S. aureus* RelQ and RelP are also regulated at the transcriptional level by vancomycin, exposure to ethanol and alkaline shock (158,199).

Clostridioides difficile genome encode a monofunctional RelQ and a bifunctional RSH (147). We have shown that full-length RSHCd produces putative pGpp, not ppGpp in the presence of GDP substrate via yet to be determined mechanism(s). To investigate whether the extracellular signals that regulate *C. difficile rsh* transcription include bacterial stationary phase onset, nutrient limitation, and exposure to antibiotics, we have employed highly sensitive and quantitative molecular tools such as quantitative reverse transcriptase-PCR (qRT-PCR) and a fluorescent translational reporter (147). Through qRT-PCR, we have analyzed the mRNA transcript levels of *C. difficile rsh* and *relQ* at

different phases of bacterial growth to find that *rsh* transcription is positively regulated by stationary phase onset (147). Unlike *rsh*, *relQ* transcription is not affected by growth phase, suggesting that *C. difficile relQ* expression is potentially induced by factors that cause cell wall stresses (147). Notably, bacterial stationary growth phase is associated with many adverse conditions, including nutrient limitation, accumulation of waste and metabolic byproducts and alterations in environmental pH (270). To evaluate whether nutrient limitation during bacterial stationary phase onset contributes to the positive regulation of *C. difficile rsh* transcription, we have used qRT-PCR to study *rsh* and *relQ* mRNA transcript fold-change in bacterial cells cultured in different media conditions, including regular Brain heart infusion medium supplemented with 5% yeast extract (BHIS), spent BHIS, and phosphate buffered saline (PBS). In this case, growth of *C. difficile* 630Δ*erm* strain in regular BHIS corresponded with normal growth conditions, whereas spent medium represented nutrient limited growth conditions. Based on our analysis, we found that *C. difficile rsh* is positively regulated by starvation stress, suggesting that nutrient limitation is one of many factors that triggers the stringent response in this pathogen.

Previous studies have also employed antibiotics as a stress inducer in *Clostridioides difficile*, notably, without directly demonstrating *rsh* and *relQ* transcriptional regulation. For example, Emerson *et al*. demonstrated that exposure of *C. difficile* 630 strain to amoxicillin, clindamycin, and metronidazole results in the general upregulation of numerous transcriptional and translational machineries (271). Microarray analyses revealed that amoxicillin upregulates *rpoB*, *rpoC* and *rpoA* (encoding components of the RNA polymerase) and ribosomal protein-encoding genes, along with tRNA synthetases and genes encoding tRNA-associated enzymes (271). Transcripts of putative ppGpp metabolizing enzymes are also significantly upregulated upon exposure to amoxicillin and clindamycin (271). Furthermore, expression of genes encoding bacterial cell wall proteins and those involved in peptidoglycan synthesis pathways are induced by ampicillin, clindamycin, metronidazole, and mainly amoxicillin (271). Interestingly, components of the secretion apparatus (*secE, secY, and secA2*) are also upregulated by these antibiotics, suggesting that *C. difficile* alters the composition of its cell wall to withstand the pressures exerted by and to reduce the penetration of antibiotics (271). Notably,

changes in the cell wall composition in response to antibiotics confer intermediate vancomycin resistance in *S. aureus*, suggesting that antibiotics cause changes in bacterial transcriptional profiles, leading to the development of virulence traits such as antibiotic tolerance (271,272).

To investigate whether antibiotics play a role in the transcriptional regulation of *C. difficile rsh* and *relQ*, we utilized an anaerobic fluorescent transcriptional reporter incorporating the oxygen-independent flavoprotein phiLOV2.1 (147,273). We placed the *phiLOV2.1* gene under the control of the *rsh* and *relQ* promoter regions from 630Δ*erm* and R20291 strains to monitor *rsh* and *relQ* transcription in two genetic variants of *C. difficile* upon exposure to sublethal concentrations of clindamycin and metronidazole (147). We found that the activity of the magic spot synthetase promoters in the presence of clindamycin is stimulated in a strain-specific manner (147). We also found that *rsh* transcription is positively regulated by exposure to metronidazole in the hypervirulent R20291 background, suggesting that the transcriptional regulation of full-length *rsh* in *Clostridioides difficile* is a general response to antibiotic stresses rather than a response to the inhibition of a specific synthetic pathway (147). Since the use of clindamycin is associated with risk factor development for CDI and metronidazole is losing clinical significance for CDI treatment, we postulate that the expression of *rsh* upon exposure to these antibiotics contributes to *C. difficile* tolerance and survival in the host.

In summary, this chapter focuses on elucidating environmental stimuli that positively regulate *rsh* gene transcription, resulting in the cytoplasmic accumulation of putative pGpp. All aspects of this chapter previously appeared as an article in the reference (147). The rights and permission to use the materials of the publication is given in Appendix M. Figure numbers and formats have been modified from the publication.

METHODS AND MATERIALS

Plasmid and strain construction

The plasmid pRF185::*phiLOV2.1* (provided by Gillian Douce, University of Glasgow), containing the *phiLOV2.1* gene under the control of the tetracycline-inducible promoter P_{tet}, was digested with BamHI and KpnI to remove the original promoter

(Appendix A). The predicted promoters upstream of *rsh* (CD630_27440 and CDR20291_2633) and *relQ* (CD630_03450 and CDR20291_0350) were amplified from 630Δ*erm* and R20291 genomic DNA using promoter-specific forward and reverse primers (Appendix B). P_{rsh} (promoter upstream of *rsh*) was amplified separately from 630Δ*erm* and R20291 genomic DNA, while P_{relQ} (promoter upstream of *relQ*) which is fully conserved between the two strains, was amplified only from 630Δ*erm* background. The primers introduced cut sites for BamHI and KpnI, which were used to digest the amplified promoters. The promoters were subsequently ligated into the digested pRF185_*phiLOV2.1* plasmid to yield $P_{rsh630\Delta erm}$::*phiLOV2.1*, $P_{rshR20291}$::*phiLOV2.1*, and $P_{relQ630\Delta erm}$::*phiLOV2.1* plasmids (Appendix A). These plasmids were PCR verified for promoter insertion using vector-specific as well as promoter-specific primers (Appendix B). The reporter plasmids were then individually transformed into competent *E. coli* HB101 cells (NEB) carrying the helper plasmid pRK24. HB101 with pRK24 were conjugated with *C. difficile* 630Δ*erm* and R20291 strains as described in details elsewhere (119). $P_{rsh630\Delta erm}$::*phiLOV2.1* and $P_{rshR20291}$::*phiLOV2.1* were conjugated into their isogenic background strains and $P_{relQ\Delta erm}$::*phiLOV2.1* was mated into both *C. difficile* strains. After conjugation, transconjugants were selected on BHIS agar treated with 10 µg/mL thiamphenicol and 100 µg/mL kanamycin (*E. coli* sensitive). Finally, transconjugants were verified by PCR using both promoter-specific and vector-specific primers (Appendix B).

Promoter activity analysis using fluorescent phiLOV reporter constructs

C. difficile strains containing phiLOV reporter plasmid (Appendix A) were grown anaerobically at 37°C in BHIS-Tm_{10} for 12 to 16 hrs. To monitor growth phase-dependent promoter activity of *rsh* and *relQ* genes, ON cultures of 630Δ*erm* were inoculated at the ratio of 1:20 into fresh BHIS-Tm_{10} media the next day and grown with OD measured at 600 nm. Samples were collected when cultures reached the OD_{600} of 0.8 (exponential phase) and 1.2 (stationary phase onset). When cultures at the final volume of 3 mL reached the target OD_{600} values, cell numbers in each sample for fluorescence measurements were normalized to cell culture OD of 0.20 at 600 nm. To monitor antibiotic-induced promoter activity, ON starter cultures were inoculated 1:50 into fresh

BHIS-Tm_{10} media containing metronidazole and clindamycin at the indicated concentrations and grown for ~2 hrs (Appendix E). OD_{600} was recorded for each sample to monitor growth. To minimize variations in fluorescence signal from background cellular autofluorescence, cell numbers in each sample were equalized on collection in the manner reported elsewhere (273). Each sample was collected at a volume that would give a cell count equivalent to 3 mL of the culture with the lowest OD_{600}. After collection, cells were pelleted in a microcentrifuge and suspended in 400 µL of reduced 1X PBS within the anaerobic chamber. Duplicate 200 µL samples were also aliquoted into a clear-bottomed black 96-wells microplate (ThermoFisher Scientific) for the purpose of measuring sample fluorescence intensity. Sample fluorescence and sample OD_{630} were measured using 440/30 excitation and 508/20 nm emission filters on a plate reader from BioTek. The instrumental parameters for all fluorescence measurements included a sensitivity limit of 65. Fluorescence measurements were blanked against 1X PBS and were reported as E_{508}/A_{630} absorbance units (AU).

Bacterial strains and growth conditions

Appendix A lists the bacterial strains and plasmids used herein. *C. difficile* 630Δ*erm* and R20291 were grown at 37°C in tryptone yeast (TY) medium or in BHIS, as indicated. The strains were grown in an anaerobic chamber (Coy Laboratory Products, Grass Lake, MI) with an atmosphere of 85% N_2, 10% CO_2, and 5% H_2. Bacterial strains carrying the respective phiLOV2.1 plasmid were maintained in 10 µg/mL thiamphenicol (Alfa Aesar), and 50 or 100 µg/mL kanamycin (Bio Basic Canada Inc). To study the effect of antibiotics on the promoter activity of *rsh* and *relQ* genes, 0.3 µg/mL metronidazole (Beantown Chemical) or 16 µg/mL clindamycin (Tokyo Chemical Industry) was used. The sublethal concentrations of the antibiotics used are included in Appendix E.

RNA isolation and real-time quantitative PCR

Total RNA from *C. difficile* 630Δ*erm* cultured in BHIS was isolated as previously described (119). Primers were designed using the PrimerQuest tool from IDT DNA technologies. Samples for RNA isolation were collected when cultures reached OD_{600} of 0.8, 1.2 and 1.6 (stationary phase). Samples were also collected after culturing in spent,

plain BHIS media and PBS. Complementary DNA (cDNA) samples were prepared from 200 ng RNA using random hexamers and the Tetro cDNA synthesis kit (Bioline). Real-time PCR reactions were performed with 2 ng of cDNA template using the SensiMix SYBR and fluorescein kit (Bioline). Primers (Appendix B) were designed using PrimerQuest tool from IDT DNA. The *rpoC* mRNA transcript was measured and used as an internal control for normalization. Controls with no reverse transcriptase were also included for all templates and primer sets. For data analysis, the standard $2^{-\Delta\Delta Ct}$ method was employed with normalization to *rpoC* and at OD_{600} of 0.8.

RESULTS

C. difficile rsh transcription is induced by stationary-phase onset

Transcription of *relA*/*rsh* gene in *E. coli* and several stringent response mounting organisms is induced by nutrient limitation during the onset of stationary phase of growth. To confirm that *C. difficile rsh* transcription is also regulated by bacterial growth phase, we have examined the transcript levels of *rsh* and *relQ* at cell culture optical densities (OD_{600}) of 0.8, 1.2, and 1.6, corresponding to exponential growth, stationary phase onset, and stationary phase, respectively (147). qRT-PCR-based analysis revealed that *rsh* transcription increases ~3-fold when cells leave the exponential growth phase and remains elevated in the stationary phase (Fig. 29A). In the contrary, *relQ* transcription is unaffected by bacterial growth phase, suggesting that transcription of *C. difficile rsh* is a response to changes in bacterial growth once the cells enter into the stationary phase, which is characterized by many adverse conditions (Fig. 29A) (147). We also utilized our phiLOV-based transcriptional reporter strain (630Δ*erm*) to examine the transcriptional regulation of *C. difficile rsh* in response to stationary phase onset. Strains carrying the respective fluorescent transcriptional reporter were grown at OD_{600} of 0.8 and 1.2 (147). Supporting our qRT-PCR data, we found *rsh* promoter activity to be induced by ~3-fold upon onset of stationary phase (Fig. 29B) (147). Notably, the promoter activity from the tetracycline-inducible control and from P*relQ* appeared to be unaffected by growth phase, suggesting that *C. difficile relQ* does not respond to growth phase but potentially to cell wall stresses (Fig. 29B) (147).

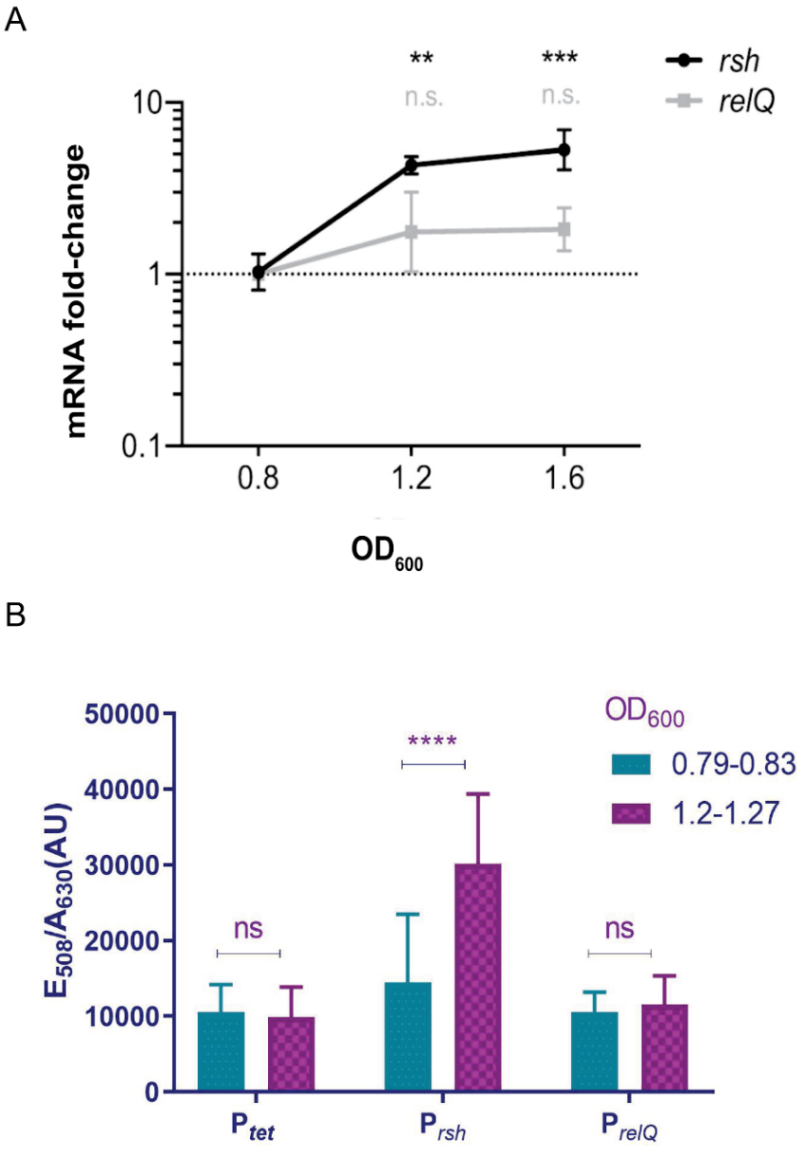

Figure 29. Stationary phase onset stimulates *C. difficile rsh* transcription. (A) qRT-PCR analysis shows that *rsh* mRNA levels increase by ~3-fold upon stationary phase onset, representative of bacterial OD_{600} of 1.2. (B) The fluorescent phiLOV transcriptional reporter also shows a 3-fold increase in the promoter activity of *rsh* between exponentially growing cells and cells entering stationary phase at an OD600 of 1.2. Adapted from Pokhrel *et al.* 2020.

rsh transcription is stimulated by nutrient limitation

To evaluate nutrient limitation as a candidate for the activation of the stringent response in *C. difficile*, we used qRT-PCR to compare the mRNA transcript levels of *rsh* and *relQ* in cells cultured either in plain BHIS, spent BHIS, or PBS media. When cultured in spent media, we found *rsh* gene transcription to be positively regulated with ~10-fold increase in the transcript levels compared to those from cells cultured in plain BHIS media (Fig. 30). We also found that *relQ* transcription is unchanged in spent media, suggesting that nutrient limitation induces the stringent response in *Clostridioides difficile* via upregulation of the *rsh* gene (Fig. 30).

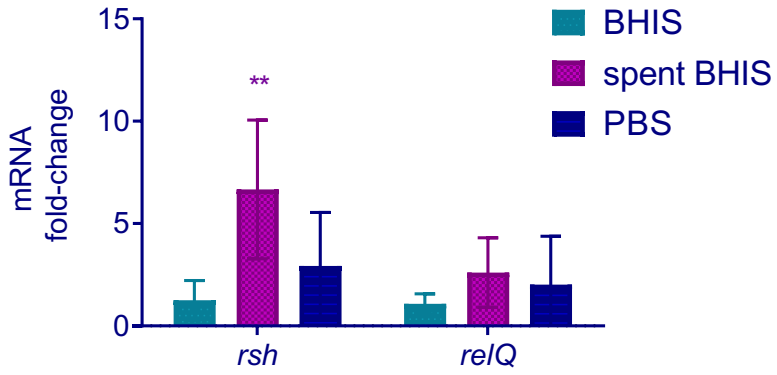

Figure 30. Nutrient limitation induces *C. difficile rsh* transcription. qRT-PCR analysis shows that transcription levels of *rsh* increases by ~10-fold when *C. difficile* cells are cultured in spent medium, representative of nutrient limitation or starvation condition. *relQ* transcription in unaffected by nutrient limitation. Multiple t test comparison between BHIS and spent BHIS. ** *P 0.001220*. This experiment and figure are the courtesy of Dr. Erin B. Purcell.

rsh and relQ transcription is induced by antibiotic stress

Adeo *et al.* demonstrated that antibiotic stress induces the stringent response in methicillin-resistant *S. aureus*, contributing to the pathogen's antibiotic tolerance phenotype (274). To confirm that antibiotic-induced stress regulates *C. difficile rsh* and *relQ* transcription, we used the phiLOV2.1 reporter to monitor the transcription of *rsh* and *relQ* upon treatment with sublethal concentration of clindamycin and metronidazole (Appendix E) (147). Notably, *rsh* promoters that control the expression of the *rsh* gene are differentiated by a single purine substitution in the 630Δ*erm* and R20291 genomes, whereas the *relQ* promoters are 100% identical in both genetic variants of the pathogen (Fig. 31) (147). Therefore, we constructed two translational reporters in which the *phiLOV2.1* gene was placed under the control of *rsh* promoter from both 630Δ*erm* and R20291 strains (147). As expected, we found that the promoter activity in the tetracycline-inducible negative control was unaffected by clindamycin in both genetic variants (Figure 32A) (147). But the activity of *rsh* and *relQ* promoters was increased in a strain-specific manner from clindamycin exposure (Fig. 32A) (147). The *rsh* promoter activity was uninduced by clindamycin exposure in the 630Δ*erm* background while demonstrating a 50% increase in promoter activity in the R20291 background (Fig. 32A) (147). *relQ* promoter activity, on the other hand, was upregulated 2.8-fold in 630Δ*erm* background but remained uninduced in R20291 (Fig. 32A) (147). To investigate if magic spot synthesis can also be stimulated by exposure to metronidazole, we repeated this assay by exposing cells to sublethal concentration of metronidazole (Appendix E). The tetracycline-inducible control promoter was uninduced by metronidazole treatment. Interestingly, both *rsh* and *relQ* promoter activities remained unaffected by metronidazole exposure in the 630Δ*erm* background (Fig. 32B) (147). However, *rsh* promoter activity increased by 80% in the R20291 background, while *relQ* promoter showed no activity (Fig. 32B) (147). These findings suggest that the epidemic strain responds to stress induced by different types of antibiotic via upregulation of *rsh* gene expression. The non-epidemic strain, on the other hand, does not respond to metronidazole via *rsh* or *relQ* transcription but induces transcription of *relQ* when exposed to clindamycin.

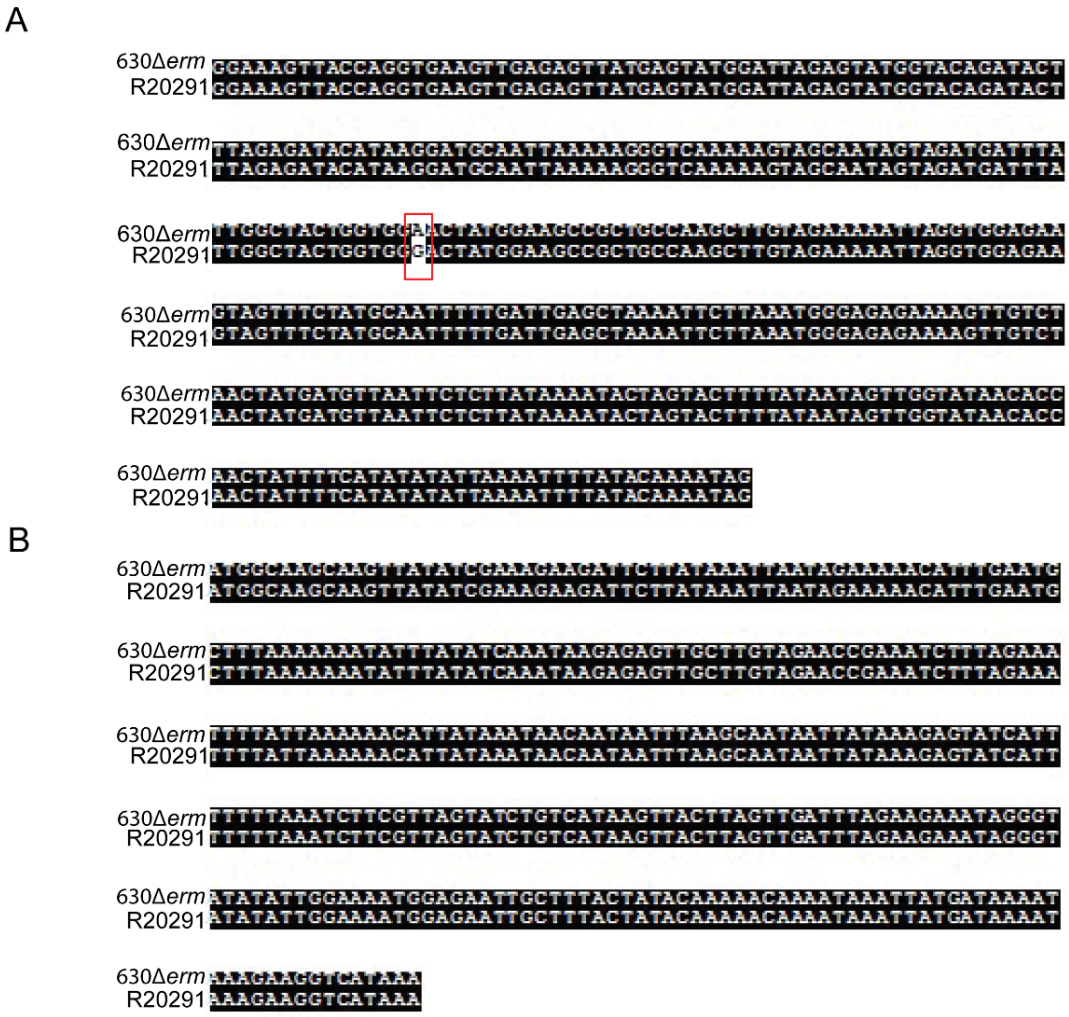

Figure 31. Sequence alignment of the upstream promoter regions. The sequence of promoters used in the (A) P*rsh* and (B) P*relQ* translational reporters are provided. A purine base substitution in the promoter sequences of *rsh* between R20291 and 630Δ*erm* is depicted in a red box. Adapted from Pokhrel *et al.* 2020.

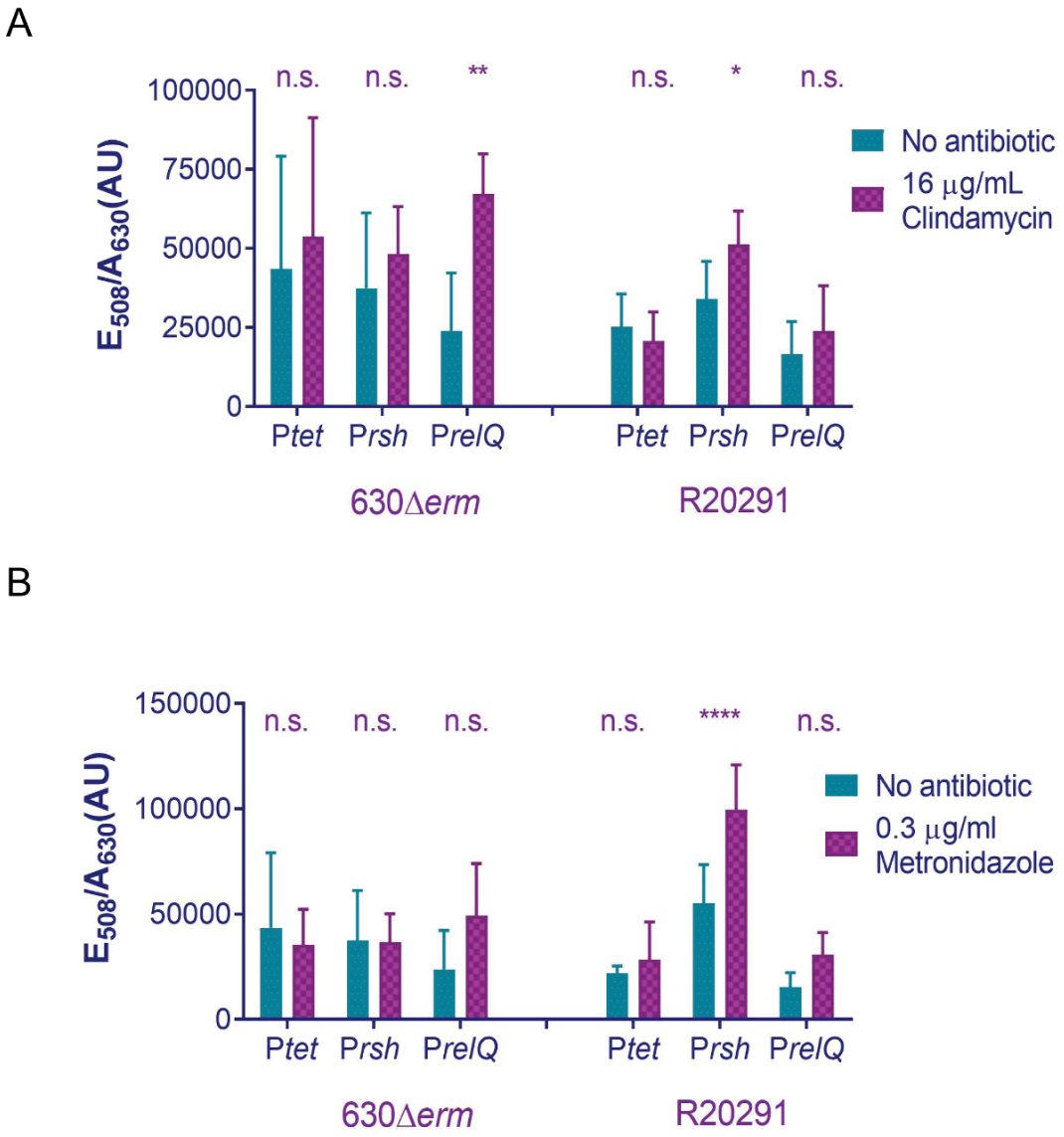

Figure 32. *C. difficile rsh* and *relQ* transcription is induced by antibiotic stress. PhiLOV2.1 transcriptional reporter activity after two hours of exposure to 16 μg/mL clindamycin (A) and 0.3 μg/mL metronidazole (B) in the *C. difficile* 630Δ*erm* and R20291 genetic backgrounds. Fluorescence activity normalized by cell density in the presence and absence of antibiotics was compared by Two-Way ANOVA. n.s., not significant, * $P < 0.05$, ** $P < 0.01$, **** $P < 0.0001$. Adapted from Pokhrel *et al.* 2020.

SUMMARY

The stringent response is a ubiquitous stress signaling in bacteria, which is regulated by different combinations of RSH superfamily enzymes (158). These enzymes are in turn differentially regulated by factors, including nutrient limitation or starvation, antibiotic and alcohol exposure, alkaline shock and oxidative stress (149,158). Regulation of RSH/SAS-mediated (pp)pGpp signaling occurs either at the transcriptional level or post-translational level (158). Long RSH enzymes are known to be transcriptionally regulated by stationary growth phase and nutrient limitation induced by inhibitors of biosynthetic pathways such as mupirocin and serine hydroximate (269). We have identified that stationary phase onset and nutrient limitation also induce *C. difficile rsh* transcription (147). Furthermore, we have identified antibiotic exposure as a stimulus that positively regulates *C. difficile rsh* transcription in a strain- and stress-dependent manner (147). The non-epidemic 630Δ*erm* and epidemic strain R20291 appear to exhibit different transcriptional responses to clindamycin and metronidazole (147). Notably, R20291 contains an intact *ermB* gene that renders the strain resistant to erythromycin (147). Therefore, we postulate that the presence of an intact *ermB* gene in R20291 potentially influences the strain's perception of antibiotic-induced stress and phenotypes (147). Nevertheless, clindamycin and metronidazole have distinct mechanism of antimicrobial action against pathogens, suggesting that *C. difficile rsh* transcription could be the predominant and a general response to extracellular stress caused by different classes of antibiotic in this organism (147).

CHAPTER IV

EFFECTS OF DISRUPTING THE STRINGENT RESPONSE IN *CLOSTRIDIOIDES DIFFICILE* STRESS SURVIVAL

OVERVIEW

Transcriptional regulation of *rsh* (and *relQ* in some) is not the only mechanism by which bacterial cells mediate (pp)pGpp signaling. The activity of other intracellular proteins can also influence alarmone levels in response to post-translational regulation by extracellular stimuli (275,276). Furthermore, stringency or stress response in bacteria doesn't always involve (pp)pGpp alarmones as the key pleiotropic effector for reprogramming cellular processes (277). Therefore, it is critical to define RSH's contribution, independently from RelQ's, in the accumulation of putative pGpp as well as the biological consequences of the alarmones in stressed *C. difficile* cells. It is also important to determine whether (pp)pGpp signaling stimulates *C. difficile* virulence traits such as antibiotic resistance, sporulation, and toxin production, even biofilm formation. One such way to determine the contribution of (pp)pGpp in *C. difficile* physiology during stresses is by disrupting alarmone synthesis via RSH inhibitors such as Relacin and/or by suppressing *rsh* and *relQ* genes at the transcriptional and translational level.

As mentioned previously, SASs in Gram-positive bacteria are known to respond to cell wall stressors, including β-lactam family of antibiotics, heat, and alkaline shock (158). Based on our fluorescent translational reporter assays, transcription of *C. difficile relQ* is not induced by bacterial stationary phase onset or nutritional depletion in the environment. We also found that *C. difficile relQ* responds to clindamycin and metronidazole antibiotics in a strain-specific manner (147). Notably, both clindamycin and metronidazole are cytoplasmic antibiotics that inhibit bacterial protein synthesis and DNA replication, respectively. Given that Gram-positive SASs respond to cell wall/envelope stresses, we postulate that *C. difficile relQ* is transcriptionally regulated by ampicillin exposure and/or is responsible for alarmone-driven bacterial beta-lactam tolerance. On the other hand,

positive transcriptional regulation of *C. difficile rsh* appears to be a general response of the bacteria when exposed to different classes of antibiotic, suggesting that *rsh* transcription contributes to general antibiotic tolerance in *C. difficile* R20291 variant (147).

To determine the significance of *rsh* and *rsh* translation in *C. difficile* survival during antibiotic stress, we have employed an RNA-based gene-silencing tool called RNA interference (RNAi) that suppresses the molecular translation of targeted genes (68,147). Through this tool, we have induced the expression of antisense RNA (asRNA) complementary to the 5'untranslated region (5'UTR) of the *rsh* mRNA in the epidemic R20291 strain using genomic and molecular cloning techniques described elsewhere (68). We found that induction of the asRNA specific to the mRNA of *C. difficile rsh* using a sublethal concentration of anhydrotetracycline (Appendix F) suppresses R20291 accumulation upon exposure to metronidazole (147). While the observed effect on bacterial accumulation is modest, we believe that *rsh* plays a direct role in *C. difficile* metronidazole tolerance and survival.

Due to the role of (pp)pGpp in bacterial survival and virulence factors production, compounds targeting RSH enzymes and (pp)pGpp alarmones have been screened, developed, and characterized (233,235,236,240,278-280). The ppGpp structural analog, Relacin competitively inhibits the activity of most full-length RSH family synthetases (233,235). The compound reduces (pp)pGpp accumulation, stationary phase onset and survival, biofilm formation, and sporulation in *Bacillus* species (233). Notably, Relacin does not affect the activity of SAS family synthetases or inhibit *in vivo* (pp)pGpp accumulation in *E. coli*, indicating that anti-stringent response inhibitors are not universally effective (233). To study the inhibitory effects of Relacin on RSHCd magic spot synthesis activity *in vitro* and *in vivo*, we have conducted pyrophosphate transfer reactions in the presence of increasing concentrations of Relacin (147). We found that Relacin inhibits the magic spot synthesis activity of RSHCd in a dose-dependent manner (147). We also found that Relacin independently has no discernible effect on the accumulation of *C. difficile* R20291 *in vivo*, however, the compound increases bacterial antibiotic susceptibility to both clindamycin and metronidazole (147). This suggests that Relacin is active against RSHCd during antibiotic-induced stringent response mechanism in *Clostridioides difficile*.

In summary, this chapter focuses on the effects of disrupting the RSH-mediated stringent response mechanism in *C. difficile* antibiotic stress tolerance and survival. All aspects of this chapter previously appeared as an article in the reference (147). The rights and permission to use the materials of the publication is given in Appendix M. Figure numbers and formats have been changed unless stated otherwise in the figure legends.

METHODS AND MATERIALS

Overexpression and purification of C. difficile RSH

Restriction enzymes and DNA ligase used in this study were purchased from New England Biolabs. Phusion DNA polymerase for polymerase chain reactions was purchased from ThermoFisher Scientific. *rsh* (CDR20291_2633) was amplified from the genomic DNA of *C. difficile* R20291 using primers (Appendix A) that added a C-terminal hexa-histidine tag, ligated into the pMMBneo expression vector at the KpnI and PstI restriction sites, and transformed into *E. coli* BL21. The plasmid was confirmed by PCR using *rsh* gene-specific primers (Appendix B).

E. coli expression strain carrying pMMBneo vector ligated with hexa-histidine tagged *rsh* was grown in LB-Kan_{50} at 37°C to an OD of 0.16 to 0.25 at 600 nm (if OD_{600} reached above this range, cell cultures were diluted into fresh LB-Kan_{50} at the desired OD value), at which point the temperature was dropped to 30°C and expression was induced using 0.5 mM IPTG for 16 hrs. Cells were lysed by sonication while suspended in the lysis buffer composed of 10 mM Tris-HCl (pH 7.8), 300 mM NaCl, 5 mM $MgCl_2$, 50 mM NaH_2PO_4, 10% glycerol, 0.5 mg/mL lysozyme, 10 mM imidazole, 0.25 mM DTT and 5 mM PMSF. Post-lysis buffer treatment, the lysates were clarified by centrifugation and subsequently transferred to a gravity column filled with HisPure Ni-NTA resin (G-Biosciences). Protein purification was conducted according to the manufacturer's protocol. Notably, all purification buffers included 5 mM $MgCl_2$ which was found to be critical for protein stabilization and purification. Purified RSHCd was dialyzed ON at 4°C against a dialysis buffer composed of 15.7 mM Tris-HCl (pH 7.6), 471.9 mM NaCl, 15.69 mM $MgCl_2$, 1.57 mM DTT, 1.5 mM PMSF, and 15.7% glycerol. Concentration of the

protein was determined spectrophotometrically. Protein aliquots were stored at -80°C for subsequent use.

In vitro measurement of RSHCd synthetase activity

Synthetase assays in the presence of Relacin (a gift from Sigal Ben-Yehuda, Hebrew University of Jerusalem) were conducted in a buffer composed of 10 mM Tris-HCl (pH 7.5), 5 mM ammonium acetate, 2 mM KCl, 0.2 mM DTT and 0.12 mM ATP. A 5X buffer stock was mixed with the indicated concentrations of GDP (0.2 to 0.6 mM), with covarying $MgCl_2$, 1.0 µCi of γ-^{32}P-ATP (approval to use 32P isotope is presented in Appendix L), and concentrations of Relacin ranging from 0 to 5 mM (233). Reactions were initiated by adding RSHCd at a final concentration of 0.6 µM and a reaction volume of 10 µL. Reactions were stopped by spotting 2 µL samples on a PEI-cellulose plate, allowing the spots to dry. The plates were subsequently developed in 1.5 M KH_2PO_4 (pH 3.64) and autoradiographed using the Storm 860 phosphorimager (GE Healthcare Life Sciences). Magic spot signal was quantitated using ImageJ software. RSHCd activity was reported as the percentage of magic spot produced.

Construction of RNAi strains

The vector pMSPT (Appendix A) was a gift from Dr. Julian G. Hurdle (Texas A&M University). It was used to express anhydrotetracycline (ATc)-inducible asRNA to the mRNA of *C. difficile rsh*. The pMSPT vector we received was derived by cloning a paired termini region (synthesized by GenScript) into pUC57 at BamHI/SacI sites of pRPF185 as reported elsewhere (68). Antisense fragments were designed and synthesized to span ~50 base pairs (bp) upstream and downstream of the start codon in order to mimic naturally occurring bacterial asRNAs that block translation upon binding to the ribosome binding site (RBS). The antisense fragment synthesized by GenScript was amplified using gene-specific primers (Appendix B), digested, and cloned into the SphI/ XhoI sites of empty pMSPT vector. The derived construct or plasmid, termed as pMSPT::*as_rsh* (Appendix A) contained the gene with its own RBS expressed from the P*tet* promoter. The plasmid was subsequently PCR verified for antisense gene insertion using vector-specific primers (Appendix B). The RNAi plasmid and the empty vector plasmid were both

individually electroporated into *E. coli* HB101 cells (NEB) carrying the helper plasmid, pRK24. HB101 with pRK24 were conjugated with *C. difficile* R20291 strains as described elsewhere (119). Transconjugants were selected on BHIS agar supplemented with 15 µg/mL thiamphenicol and 100 µg/mL kanamycin. Finally, transconjugants were verified by PCR using *C. difficile relQ* gene-specific and pMSPT vector-specific primers (Appendix B). *C. difficile relQ* primers were used in colony PCR to confirm that the transconjugants were *C. difficile*, whereas the vector-specific primers were used to confirm the success of the conjugation process.

Bacterial strains and growth conditions

Appendix A lists the bacterial strains and plasmids used herein. *C. difficile* R20291 strain was grown at 37°C in TY medium or BHIS medium, as indicated. The strain was grown in an anaerobic chamber (Coy Laboratory Products, Grass Lake, MI) with an atmosphere of 85% N_2, 10% CO_2, and 5% H_2. Wild type R20291 strain as well as bacterial strains carrying the pMSPT*::as_rsh* or pMSPT empty plasmid were maintained using the following antibiotics in the indicated concentration: 15 µg/mL thiamphenicol (Alfa Aesar), 50 or 100 µg/mL kanamycin (Bio Basic Canada Inc), 0.075 or 0.3 µg/mL metronidazole (Beantown Chemical), or 16 µg/mL clindamycin (Tokyo Chemical Industry) as indicated in Appendix E.

End-point growth/ cell accumulation assay using R20291 and RNAi strains

ON starter cultures of wild type R20291 strain was inoculated 1:50 into fresh TY medium and grown till OD_{600} ~0.8 (exponential phase). At this point, using a 96-welled microtiter plate, the starter cultures were added to reduced TY medium treated with 2 mM Relacin, with or without 16 µg/mL clindamycin or 0.3 µg/mL metronidazole from time point 0 min. The plate was subsequently incubated anaerobically at 37°C for 12 to 18 hrs. Post-incubation, the plates were taken out of the anaerobic chamber and OD_{630} was measured using a plate reader (BioTek) to measure cell accumulation.

For the RNAi strains, growth following the induction of asRNA to the mRNA of *C. difficile rsh* was performed by using the standard media dilution technique using a 96-welled microtiter plate. To determine the sublethal concentration of ATc to use for

inducing *as_rsh* without inhibiting bacterial growth and viability, increasing concentrations of ATc were added to BHIS medium in the absence of antibiotics (Appendix F). Plate was incubated for 24 hrs after which the sublethal concentrations of ATc that partially inhibited growth was recorded (Appendix E). The concentration of ATc (0.5 µg/mL) that moderately inhibited growth was further used to induce *as_rsh* in assays where the growth of unstressed vs stressed strains using 0.075 µg/mL metronidazole was monitored after 12 hrs of anaerobic incubation at 37°C in BHIS medium treated with 15 µg/mL thiamphenicol.

RESULTS

Relacin inhibits RSHCd synthetase activity in vitro and reduces bacterial antibiotic survival in vivo

Relacin inhibits (pp)pGpp synthesis in *B. subtilis* and *D. radiodurans* by competitively binding to the SD active site of the bifunctional RSH enzymes *in vitro* (233). Upon incubating purified RSHCd with GDP, ATP, and increasing concentrations of Relacin, we found that Relacin also inhibits RSHCd synthetase activity in a dose-dependent manner *in vitro* (Fig. 33) (147). Notably, Relacin appears to inhibit RSHCd pyrophosphoryltransferase activity in millimolar concentrations consistent with its efficacious dose against other RSH/REL enzymes, indicating that the molecule itself is not a promising candidate to use in the clinical settings for the management of CDI (147). We also investigated the effects of Relacin on the accumulation of R20291 cells over a period of 12 hrs (147). We treated cells with 2 mM Relacin in the absence of any stringent response inducing factors and found that Relacin does not affect bacterial survival under normal growth conditions (Fig. 34A) (147). Interestingly, when R20291 cells are pretreated with 16 µg/mL clindamycin or 0.3 µg/mL metronidazole, the compound appears to increase bacterial susceptibility to both antibiotics (147). The intracellular accumulation of (pp)pGpp causes a delayed growth phenotype in bacterial cells and puts cells in a state of quiescence, which notably, contributes to bacterial antibiotic tolerance (242). We found that treatment with clindamycin and metronidazole appears to suppress R20291 accumulation overtime, which could be due to the production and intracellular accumulation of the putative pGpp alarmones (Fig. 34B and 34C). But bacterial

accumulation was further suppressed in the presence of Relacin, suggesting that the molecule specifically targets RSHCd during the stringent response cascade in *C. difficile* (Fig. 34B and 34C) (147).

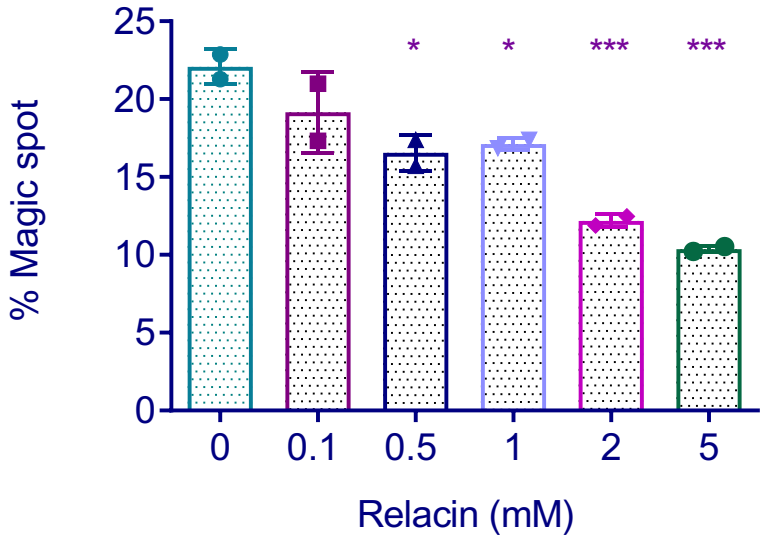

Figure 33. Relacin affects RSHCd synthetase activity *in vitro*. Relacin inhibits the activity of RSHCd in a dose-dependent manner. Activity at each Relacin concentration was compared to that in the 0 mM Relacin condition by ordinary One-Way ANOVA. * *P 0.0173, * P 0.0279, *** P 0.0009, **** P 0.0004.* Adapted from Pokhrel *et al.* 2020.

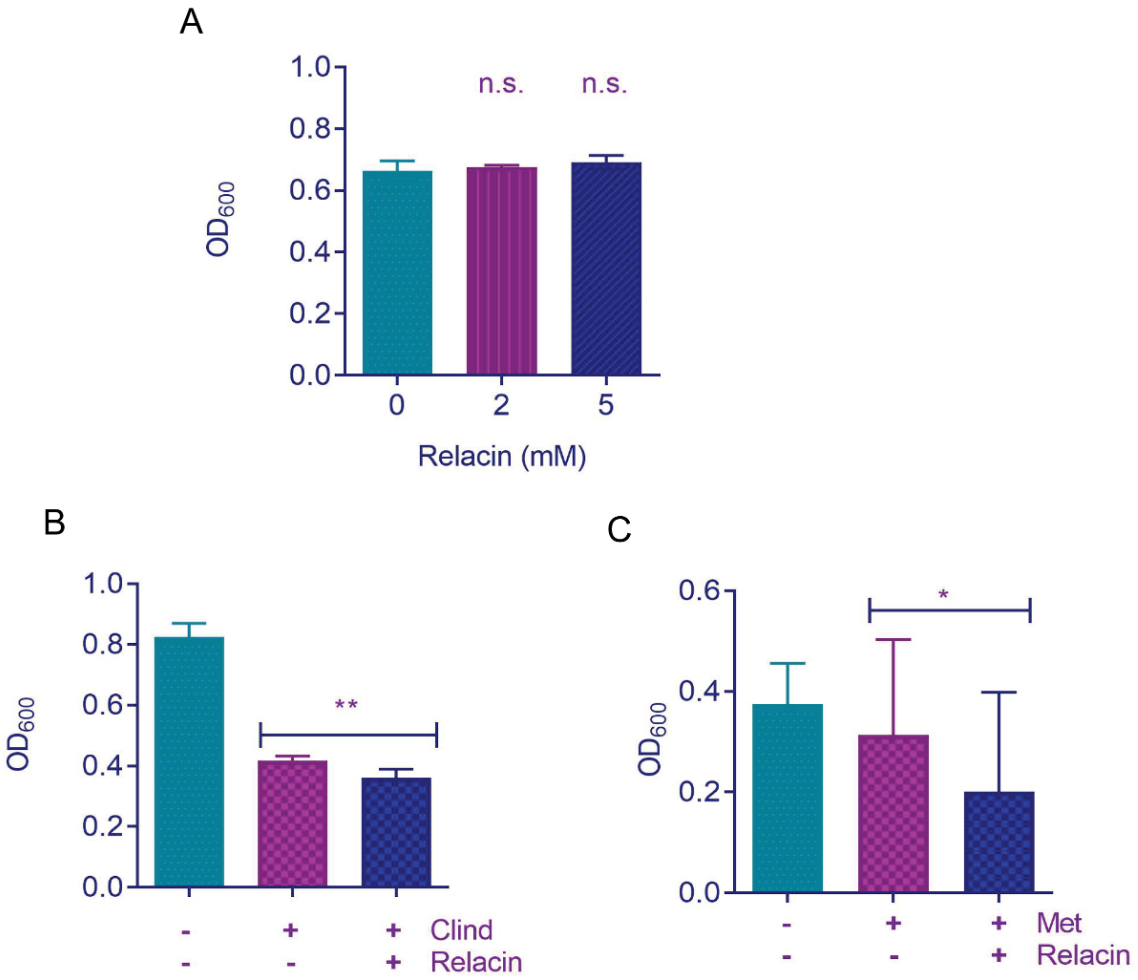

Figure 34. Effect of disrupting RSH-regulated stringent response mechanism in *C. difficile* antibiotic survival. (A) Relacin alone has no impact on the ON accumulation of *C. difficile* R20291. Cell density after overnight growth was compared with and without Relacin by ordinary One-Way ANOVA. (B-C) 18 hrs cell density in the presence of sublethal clindamycin (B) and metronidazole (C) with and without Relacin. The cell density of antibiotic treated samples with and without Relacin were compared by Unpaired t test. n.s., not significant, * $P < 0.05$, ** $P < 0.01$, *** $P < 0.001$. Adapted from Pokhrel *et al.* 2020.

rsh plays a role in bacterial antibiotic tolerance and survival in vivo

Due to the observed modest effect of Relacin on metronidazole treated hypervirulent R20291 strain, we investigated the significance of RSH for *C. difficile* survival during metronidazole-induced stress. We induced the expression of asRNA specific to the mRNA of *rsh* using our pMSPT::*as_rsh* vector carrying R20291 RNAi strain (Appendix A) (147). Induction of the asRNA has previously been shown to deplete mRNA transcript levels and to knock down translation in *C. difficile* (68,147). Upon silencing *rsh* translation *in vivo* in the epidemic strain pre-treated with sublethal concentration of metronidazole, we found R20291 accumulation to be dramatically suppressed overtime (Fig. 35) (147). This suggests that *rsh* and its gene product contribute to the accumulation and survival of *C. difficile* cells during metronidazole-induced stress (147). We also postulate that *rsh* confers metronidazole tolerance in *C. difficile*, further establishing that the antibiotic is no longer effective at killing the pathogen.

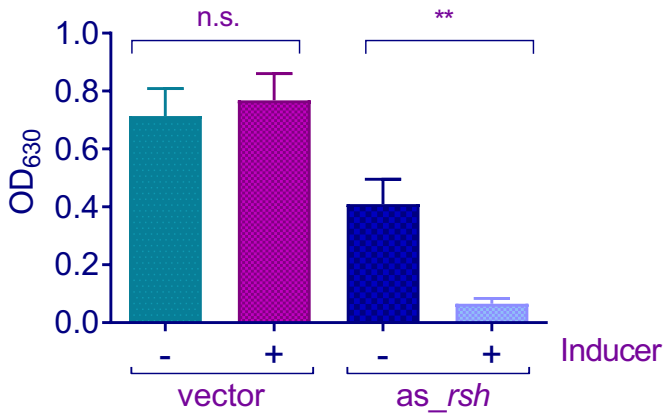

Figure 35. Significance of *rsh* in antibiotic stress survival. Knock down of *C. difficile rsh* gene with ATc inducer (0.5 µg/mL) negatively impacts the accumulation of R20291 strain in the presence of metronidazole (0.075 µg/mL). The cell densities of antibiotic treated samples with and without ATc were compared by ordinary One-Way ANOVA. n.s., not significant, ** *P 0.0042*. Adapted from Pokhrel *et al.* 2020.

SUMMARY

The stringent response governs virulence traits and phenotypes in many organisms, including biofilm production, spore formation, virulence factor expression, and survival of pharmacological and immune stresses (149). We have found that Relacin is effective at inhibiting RSHCd synthetase activity in a dose-dependent manner *in vitro* (147). While Relacin does not have any effect against bacterial accumulation and survival under normal growth conditions, we found that inhibition of RSHCd synthetase activity, mediated by Relacin, amplifies the potency of both metronidazole and clindamycin against *C. difficile* R20291 strain (147). Notably, we found the effect of Relacin on antibiotic efficacy to be modest (147). Furthermore, we found Relacin to be effective against RSHCd synthetase activity in millimolar concentration, suggesting that the

molecule is not a suitable candidate for clinal use in managing CDI. Furthermore, knock down of R20291 *rsh* gene in the presence of metronidazole substantially reduced bacterial accumulation, confirming that *rsh* translation and subsequent production of putative pGpp is required for *C. difficile* to respond to and survive antibiotic stress in the host (147).

CHAPTER V

NUTRIENT-SPECIFIC MOTILITY AND BIOFILM REGULATION OF *CLOSTRIDIOIDES DIFFICILE*

OVERVIEW

Clostridioides difficile is an obligate anaerobic pathogen that persists as dormant spores in the aerobic environment (13). Once ingested by the host, the pathogen germinates into rapidly reproducing vegetative cells that can secrete toxins (13). The clinical spectrum of *C. difficile* infection ranges from asymptomatic colonization to life-threatening pseudomembranous colitis, toxic megacolon, sepsis and death (13). CDI is defined when patients experience symptomatic diarrhea and test positive for *C. difficile* toxin A and/or B or the presence of toxin-producing strains in the stool (6,42). Pseudomembranous colitis or colonic histopathological characteristics revealed by endoscopy also defines CDI (6,7,281). But bacterial colonization without the onset of symptoms, which still leads to disease progression remains an unclear aspect of *C. difficile* pathogenesis. Studies have revealed that *C. difficile* colonizes between 0 to 17.5 % of healthy individuals without causing clinical signs of CDI (6,282,283). Notably, a high prevalence of asymptomatic colonization is found in institutionalized patients, particularly with underlying medical conditions, or in health-care workers (6,284-286). Furthermore, asymptomatic colonization can also be found in infants and neonates, mainly during the first four weeks of life (6,287). Analysis of PCR ribotypes have shown that individuals from different age groups are colonized with identical toxigenic strains of *C. difficile* without showing any clinical signs of CDI (288,289). Whether symptomatic or asymptomatic, colonization of *C. difficile*, nevertheless, serves as a reservoir of the pathogen and a mean of bacterial transmission from one host to another (6).

One of the key mechanisms regulating *C. difficile* colonization in the host is the disruption of the indigenous microbiota community (42). The intestinal microbiota is a complex ecosystem consisting of numerous bacterial species (6). In healthy adults, the

intestinal microbiota is predominantly constituted of species belonging to the *Bacteroidetes* and *Firmicutes* phyla, with roles in metabolism, nutritional function, maturation of the immune system, and conferring host colonization resistance to enteric pathogens (6,42,290). Due to the beneficial contributions of the indigenous microbiota to the host, disruption or dysbiosis of the microbiota community negatively impacts microbiota structure and functions (6). Consequently, host colonization resistance is attenuated, resulting in the germination, growth, and rapid multiplication of *C. difficile* within the host intestine (6). Factors such as diet, geography, antibiotic use, and the development of gastrointestinal complications influence microbiota diversity between individuals (6,291).

Antibiotic exposure (especially cephalosporins, penicillins, and fluoroquinolones) is the primary risk factor for CDI development and is postulated to increase host susceptibility to CDI by disrupting the intestinal microbiota community (6,292,293). The impact of antibiotic administration on the host microbial structure and composition has been studied extensively. CDI patients exhibit changes in the gut microbiota composition, including a significant decrease in *Bacteroidetes* family species with an increase in the members of the *Proteobacteria* such as *Pseudomonadales* (6,42). Within the *Firmicutes* phylum, CDI patients report a decrease in butyrate producing *Ruminococcacea* and *Lachnospiraceae*, *Bacteroidaceae*, and *Clostridia* cluster IV and XIVa with a corresponding increase in *Lactobacillales* (42,294). In animal models of infection, prior clindamycin exposure has confirmed the findings for human patients and demonstrated a decrease in the abundance of commensal species (295). Similarly, animal models lacking pre-antibiotic treatment fail to exhibit the debilitating symptoms of CDI, presumably owing to an undisrupted microbiota community (42,295,296). Changes in the gut microbiota of asymptomatic carriers of *C. difficile* are less defined but studies have shown that there is a comparable decrease in microbial diversity and species structure in both CDI and asymptomatic carrier groups in contrast to the healthy group (42,297). Interestingly, the structure of the microbial communities are strikingly different among CDI patients and asymptomatic carriers (42). Indigenous microbiota of the carrier group is dominated by *Firmicutes* and *Bacteroidetes*, suggesting that the composition of microbiota in this group resembles that of healthy individuals (42,297). Studies using

murine models of infection also support the findings that colonization with certain bacterial taxa such as *Lachnospiraceae* prevents the progression of CDI from symptomatic or asymptomatic colonization (42,298).

Apart from altering the native microbiota structure and composition, antibiotic treatment also induces substantial changes in the gut metabolome. The intestinal microbiota is responsible for fermenting carbohydrates and amino acids into short chain fatty acids (SCFAs) (299,300). Furthermore, the microbiota metabolizes lipids, amino acids, and proteins, ensuring a balanced colonic health that affects the growth and survival of enteric pathogens (300,301). However, antibiotic-induced disruption of the normal microbiota results in a metabolic environment that largely favors the colonization and spread of enteric pathogens. Theriot *et al*. reported that cefoperazone treatment in murine models increases the concentration of primary bile acids, including taurocholate, taurocholenate sulphate, and tauroursodeoxycholate, with a corresponding decrease in secondary bile acid, deoxycholate (300). To establish colonization, *C. difficile* spores must germinate into vegetative cells using primary bile acids as germinant. Therefore, antibiotic-induced increase in the concentrations of primary bile acid promotes *C. difficile* germination in animal models, further indicating that antibiotics disrupt members of the commensal microbiota with roles in the metabolism of primary bile acids into secondary bile acids, which inhibit *C. difficile* growth (44,45,300). Theriot *et al*. also reported that cepfoperazone treatment increases the level of sugar alcohols and carbohydrates in murine models, including mannitol, sorbitol, arabitol, xylitol, ribitol, gluconate, sucrose, raffinose, stachyose, galactose, lactate, and fructose (300). The reported increase in the levels of carbohydrates and alcohols coincided with a decrease in free short-chain fatty acids, including acetate, propionate, butyrate and valerate, suggesting that indigenous microbiota-mediated fermentation of carbohydrates is decreased from antibiotic exposure (300). Upon testing the ability of *C. difficile* to utilize these sugars and alcohols both independently and in conjugation with murine cecal contents, it was revealed that *C. difficile* successfully germinates and outgrows in a niche that is rich in these metabolites (300).

According to Theriot *et al*., antibiotic treatment also increases the concentration of N-acetylneuraminic acid (NEU5A) or sialic acid in the gut (300). NEU5A is a branched

carbohydrate and a component of the O-glycosylated MUC2 core protein, which is largely constituted by mucins of the intestinal mucus (302). *C. difficile* adheres to gut mucins *in vitro* and has been observed within the mucus of mice and humans *in vivo*, suggesting that *C. difficile* colonizes the intestinal mucus (302-309). In addition to NEU5A, the mucin is O-glycosylated with GlcNAc, N-acetylgalactosamine, galactose, and fucose (302,310,311). These O-glycosylated carbohydrates are degraded and released as free glycans via hydrolase enzymes encoded by mucin-degrading native species (302,311,312). Notably, free glycans serve as nutrients to the commensal microbes as well as to colonic enteric pathogens, including *V. cholerae*, *C. jejuni*, and *S. typhimurium* that swim towards the intestinal mucus to compete with and outnumber the native microbiota community (302,313-316). Like many motile bacteria, these organisms regulate their motility in response to nutrients by controlling the activity of motor complexes that rotate their flagella. According to Courson *et al.*, long periods of flagellar rotation cause unidirectional runs, whereas transient changes in rotational direction causes tumbles that reorient cells to run in new directions (317). Furthermore, sustained runs cause bacterial dispersal, but frequent tumbles reduce run lengths and confine cells in one region of the niche or locality (317). The speed of flagellar rotation can also influence bacterial dispersal (317). Nevertheless, bacteria alter their tumbling frequency and/or velocity to control their motility towards a more concentrated source of nutrients or chemoattractants (317). Notably, *C. difficile* also readily responds to nutrient availability in the niche. Sporulation, toxin production, and metabolism of c-di-GMP in this organism are influenced by the nutrient composition of the bacterial growth medium (317-319).

Like many motile intestinal pathogens, *C. difficile* produce flagella and can swim through liquid and semi-solid media (119,317). This bacterium also moves on solid surfaces with the aid of TFP (111,317). To investigate if nutrients regulate *C. difficile* R20291 motility, we have designed and constructed portable rose cell chambers that can be used in any inverted microscope under aerobic conditions (317). At the single-cell level, we found that free NEU5A glycans reduce bacterial swim velocity and displacement without affecting bacterial tumbling frequency (317). Since NEU5A is associated with *C. difficile* colonization *in vivo*, we postulated that the reduction in bacterial motility and biofilm formation by R20291 may be coordinately regulated by the same signaling

mechanism(s). Biofilm is a virulence factor that enables bacteria to resist stresses from antibiotics and host immune system. Very recently, Engevik *et al*. demonstrated that *C. difficile* RT027 strain chemotaxes toward and adheres to MUC2 of the intestinal mucus layer in murine models (302). Chemotaxis is defined as the directed movement of bacteria in response to chemical gradients that facilitate movement toward and away from favorable and unfavorable conditions, respectively. According to Engevik *et al.,* NEU5A is the least preferred chemoattractant for *C. difficile* followed by GlcNAc, and mannose (302). However, culturing of *C. difficile* cells in a minimal medium supplemented with each monosaccharide as the primary source of carbon demonstrated that all mucin sugars facilitate bacterial growth, resulting in a delayed stationary phase-onset (302). Based on Engevik *et al.,* mannose is the most preferred chemoattractant exhibiting maximal bacterial growth. But supplementation of a growth medium made from the cecal contents of gnotobiotic mice (also depleted in amino acids and carbohydrates) with GlcNAc and NEU5A has previously been reported to enable *C. difficile* division (317,320). These findings show that *C. difficile* respond to unchained NEU5A as a food source.

Engevik and group additionally reported that *C. difficile* interacts with mucus-associated and mucin-degrading microbes within biofilms such as *Bacteroides*, *Ruminococcus*, and *Akkermansia* in the antibiotic-treated gut (302). Given that *C. difficile* does not code for glycosyl hydrolases responsible for cleaving O-glycosylated mucin components, the pathogen depends on glycosyl hydrolases-encoding species to utilize free monosaccharides, suggesting that mucin degradation is a crucial step in the mucosal colonization and growth of *C. difficile* (302). To investigate whether *C. difficile* R20291 directly assembles as biofilm in the presence of high NEU5A concentration, we conducted the standard plate-based biofilm assays requiring crystal violet staining. Based on our analyses, *C. difficile* R20291 forms biofilm in BHIS medium independently of a GLU, GlcNAc, and NEU5A gradient. However, the strain appears to produce significantly robust single-species biofilm at 32 mM NEU5A, suggesting that NEU5A-specific motility suppression of the hypervirulent strain may be regulated by signaling network(s) that also inversely regulate biofilm formation.

In summary, this chapter focuses on evaluating nutrient-regulated motility stimulation and/or suppression of *C. difficile* R20291 strain. Antibiotic-induced shifts of

the colonic microbiome and metabolome create a niche suitable for *C. difficile* germination, growth and colonization (300). Therefore, this chapter focuses on nutrient-dependent colonization mechanisms adopted by *C. difficile* which ultimately contribute to virulence and/or transmission. Several aspects of this chapter, including the methods and materials section previously appeared as an article in the reference (317). The rights and permission to use the materials of the publication is given in Appendix M. Figure numbers and formats have been modified from the actual publication unless stated otherwise in the figure legends.

METHODS AND MATERIALS

Bacterial strains and growth conditions

C. difficile strain R20291 was grown in BHIS medium in an anaerobic chamber at 37°C maintained at an atmosphere composed of 85% N_2, 10% CO_2, and 5% H_2. Migration assays were performed in BHIS and BHIS with 0.3% agar in the presence of GLU, ARA, or NEU5A at the indicated concentrations. Growth curves were performed in BHIS supplemented with the indicated metabolites to a final concentration of 32 mM and inoculated at the ratio of 1:20 with ON cultures of R20291. Doubling times were calculated using the Prism (GraphPad) software and the non-linear curve fits to the exponential growth equation $Y = Y_0$*expo (K*X) where Y_0 denotes the initial optical density, Y is the measured optical density, and X is time. Doubling times were determined by fitting the data between 0 and 5 hours in order to exclude entry of bacterial cells into the stationary phase of growth.

Macroscopic motility assays

Macroscopic motility assays were carried out in supplemented or unsupplemented BHIS medium with 0.3% agar. ARA, GLU, or NEU5A was added to the molten agar to the indicated final concentration. Plates were prepared outside of the anaerobic chamber and left to dry ON, then transferred to the anaerobic chamber to equilibrate for at least 24 hours prior to use. Sterilized and O_2 reduced toothpicks were used for inoculation of individual colonies of R20291 into the motility agar. Each toothpick was used to stab a

soft agar (which was divided into two even sections using a sharpie on the plate base) twice to allow for duplicate measurements. Migration or bacterial swarm diameters were measured manually using a ruler after 12 and 24 hrs of incubation at 37°C. The mean diameters and standard deviations of four biologically independent samples measured in duplicate (total of 8) were reported. One biological replicate had to be excluded from the 24 hrs plain BHIS condition because cell populations grew into each other, spread across the agar, and made measurements of motility impossible.

Rose cell imaging chamber construction

As mentioned elsewhere, sealed rose cell chambers with gas impermeable gaskets were constructed for the imaging of anaerobic bacteria using an aerobic microscope (321). Aluminum top and bottom plates with imaging windows and 25 mm square glass coverslips were prepared for use with a Nikon Ti-E inverted microscope. Screw holes were milled into each corner of the top and bottom aluminum plates. Gaskets were cut from 3 mm thick rubber with a central circular or square opening (18 mm diameter). The screw holes in the gaskets were aligned to those in the aluminum chamber plates. Before use, all components of the rose cell chambers were sterilized in 10% bleach followed by rinsing in deionized water. The components were left to dry prior to use.

Sample preparation for imaging

Starter cultures of *C. difficile* R20291 were grown ON in BHIS medium. These cultures were diluted 1:50 and allowed to grow for ~3 hrs the following day so that the cells will have entered exponential growth phase. 150 µL of dilution culture was then mixed with fresh BHIS medium and nutrient supplement at desired concentrations for a total sample volume of 1,500 µL. Within the chamber, the sample was injected through the bottom port of the chamber through the rubber gasket using a 1 mL syringe until all gas escaped from the top needle. After sample injection, both top and bottom needles were removed, allowing the holes in the rubber gasket to seal on its own. The edges of the imaging chamber were parafilmed and removed from the anaerobic chamber, sprayed with 10% bleach and 70% ethanol for sterilization purpose before imaging. Microscopy

was initiated roughly 8 mins after chamber assembly for every single-cell analysis experiments.

Microscopy set-up

Live-cell, time-lapse differential interference contrast microscopy was performed on a Nikon Ti-E inverted microscope equipped with Nikon Perfect Focus System, apochromat TIRF 60X Oil Immersion Objective Lens (numerical aperture of 1.49), a condenser (numerical aperture of 0.52), pco.edge 4.2 LT sCMOS camera, and SOLA SE II 365 Light Engine along with complementary DIC components. Stage temperature was maintained at 36.5^{o}C ± 0.5^{o}C to monitor bacterial motility at 37^{o}C using a Nevtek Air Stream microscope stage warmer and a microscope enclosure prepared in house. 100 µs exposures at a frame rate of 10 frame/sec for 10 seconds was used to record movies of bacterial motility. Three biologically independent samples were imaged in each medium condition; 600 X 600-pixel windows were imaged at three randomly selected locations per sample. The first ten cells that entered the field of view were analyzed.

Decontamination of the rose cell chambers

After each imaging experiment, the microscope stage and sample holder were wiped with 10% bleach and 70% ethanol. The parafilm wrap was peeled off the rose cell chamber and placed into biohazard waste bin. The sample chamber was submerged in a 50% bleach solution and disassembled. All components of the chamber were allowed to soak in the bleach solution for at least 10 mins. Glass coverslips were gently removed and discarded as biohazardous waste. Aluminum and rubber components were rinsed with deionized water and then soaked in ~117 mM sodium thiosulfate for at least 30 mins to neutralize bleach. Components were subsequently washed with ethanol and dried prior to reusing.

Single-cell analysis

Image analysis was performed using a bunch of Nikon Elements imaging Suite and the ImageJ software. The line segment tool was used in ImageJ to measure unidirectional run of each bacterial cell over time from which the velocity and

displacement factors were calculated. Each reorientation was considered the peak as well as the end of a run but the start of a new one. Only runs whose beginnings and ends took place within the field of view and the plane of focus were considered for motility measurements. For each cell, the run lengths, run durations, and number of tumbles were recorded. Swimming velocity was calculated by dividing displacement by time.

Plate-based, single-species biofilm assay

ON cultures of *C. difficile* R20291 were diluted 1:100 into fresh buffered BHIS (38.7 mM NaH_2PO_4 and 11.3 mM Na_2HP0_4 at pH 7.43 ± 0.05) media. A total of 2 mL samples per well was deposited in 24-well polystyrene non-treated plates (Costar, USA) with 0 mM, 4 mM, 8 mM, 16 mM, and 32 mM of GLU, NEU5A and GlcNAc. The 24-well plates were always reduced for at least 72 hrs prior to setting up single-species biofilm assays. The stock solution of each metabolite was prepared as a 10X stock in plain BHIS media, filtered sterilized, and stored in aliquots in –20 °C for long-term use. Prior to plate set up, buffered BHIS, plain BHIS and 10X stock solutions of all sugar metabolites were taken into the chamber to reduce overnight. Post-set up, the plates were incubated at 37°C within the anaerobic chamber for at least 48 hours. Once incubation was complete, the plates were taken out of the anaerobic chamber and placed on a portable rack. Spent media from the plates were subsequently removed via pipetting and wells were gently washed once with filter sterilized 1X PBS. Biofilms were air dried for 5 to 10 mins and stained with crystal violet (CV; 0/1% w/v) for 30 mins. CV stain was removed through pipetting after which the wells were washed twice with PBS then air-dried for ~10 mins. Dye bound to the biofilm biomass was solubilized with 70% reagent alcohol and the absorbance, corresponding to the biofilm biomass, was measured at 570 nm with a plate reader (BioTek). When necessary, the solubilized CV dye was diluted for all readings to remain in the linear range of the spectrophotometer. Autoclaved BHIS and same media condition with different sugar metabolite was used for blanking in the assays. Biofilm assays using NaCl were conducted in the same manner at the indicated concentrations of the non-sugar osmolyte.

RESULTS

C. difficile regulates motility in a nutrient-specific manner

The *C. difficile* genome encodes a predicted methyl-accepting chemotaxis protein (CDR20291_0463) within a putative chemotaxis operon (CDR20291_0458 to CDR20291_0467), suggesting that the bacteria could regulate flagella-dependent motility to respond to unknown nutrients (317). The levels of NEU5A increases in animal models as a result of cefoperazone-induced dysbiosis of the gut microbiome and metabolome (300). To investigate if NEU5A regulates the motility of *C. difficile* R20291, we inoculated individual colonies of the strain into BHIS medium with 0.3% agar that has a level of viscosity comparable to that of the intestinal mucus and measured bacterial dispersal from the site of inoculation (317,322-324). We performed these macroscopic motility assays because available nutrients that bacteria can metabolize suppress motility by de-motivating bacteria to seek new territories. We found that BHIS medium supplemented with 1% of any metabolite reduces R20291 dispersal post-12 hrs of incubation (Fig. 36A) (317). Notably, NEU5A appeared to reduce migration of inoculated colonies from the inoculum site most dramatically (Fig. 36A) (317).

Supplementation of BHIS medium with arabinose also reduced motility of R20291 after 12 hrs of incubation (Fig. 36A) (317). This shows that the addition of substrates that are not metabolizable to the bacteria still contributes to motility suppression at earlier timepoints, potentially due to the impact of high carbohydrate concentration on the osmolarity of the medium (317,325). After 24 hrs of growth, however, migration through the agar in the presence of arabinose had no effect on the swarm diameter, suggesting that the bacteria eventually adapt to the nutrient-independent effects of the medium supplemented with ARA (Fig. 36B) (317). Nonetheless, by including arabinose in our motility analyses, we have controlled for the possibility of observing an osmolarity response of cells vs nutrient-derived response in the presence of GLU and NEU5A. Hence, supplementation with 1% GLU and NEU5A reduces migration by 22% and 69%, respectively, after 24hrs of incubation, suggesting that the presence of metabolically accessible nutrients in the niche inhibits *C. difficile* dispersal (Fig. 36B) (317).

To ensure that the observed motility differences from supplementation with 1% monosaccharide were not due to differences in the molar concentrations of each supplement tested, we remeasured bacterial swarm diameters on soft agar supplemented with 32 mM ARA and 32 mM GLU (where 32 mM concentration corresponds to 1% NEU5A) (Fig. 36C and 36D) (317). As expected, neither ARA nor GLU at 32 mM caused any significant motility suppression post-12 and 24 hrs of incubation (Fig. 36C and 36D) (317). This suggests that the inhibition of bacterial swarming on the soft agar is specific to high NEU5A concentration in the environment.

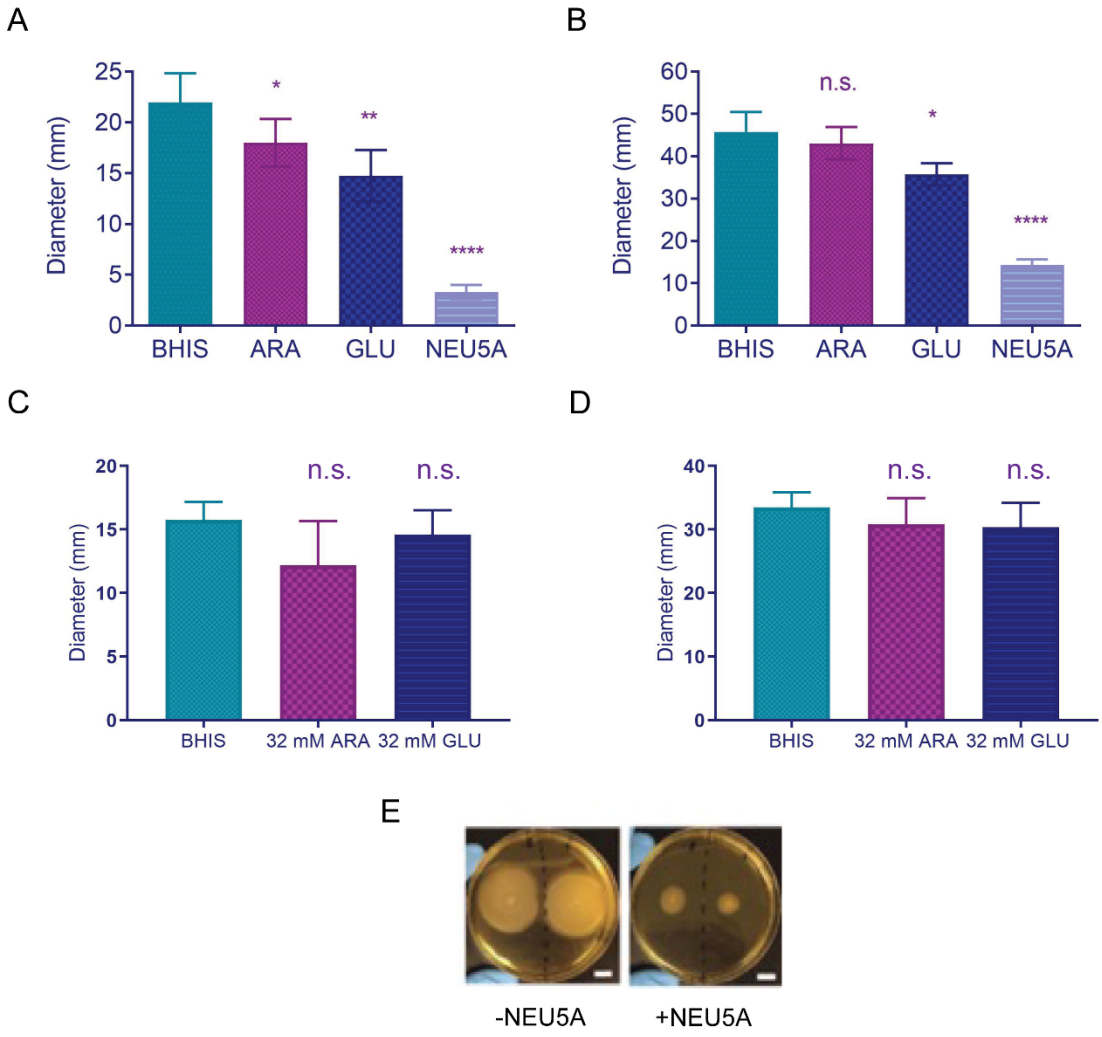

Figure 36. *C. difficile* motility through soft agar is regulated by nutrients. (A, B) Migration of *C. difficile* R20291 through BHIS, 0.3% agar supplemented with 1% ARA, GLU or NEU5A. (C, D) Migration of R20291 through BHIS, 0.3% agar supplemented with 32 mM of ARA or GLU. Swarm diameters were measured post-12 (A, C) and 24 (B, D) hrs of inoculation. Measurement of four biologically independent swarms per condition (X2). Motility in each medium was compared to migration in BHIS-agar by Unpaired t-test; n.s., not significant, * $P < 0.05$, ** $P < 0.01$, **** $P < 0.0001$. (E) Representative images of *C. difficile* R20291 24 hrs after inoculation. Adapted from Courson *et al.* 2019.

To confirm that motility suppression regulated by NEU5A or suppression of migration of *C. difficile* R20291 on the soft agar is not due to bacterial growth inhibition, we monitored bacterial growth in the presence of various monosaccharides at 32 mM concentration over the course of 12 hrs (317). We found that none of the monosaccharides slowed growth in liquid culture, confirming that the observed effect of nutrient supplementation in the motility agar (Fig. 36E) is due to motility suppression rather than suppression of cell division and growth (Fig. 37A) (317). The calculated doubling times of R20291 in BHIS supplemented with the indicated sugar are comparable to each other (Table 3). The findings that the bacteria exhibit a normal growth phenotype in the presence of all sugars studied at 32 mM concentration but substantially reduces motility in response to NEU5A, suggest that *C. difficile* R20291 senses nutrient availability in the niche and reduces its motility away from sites that are rich in specific nutrients (317).

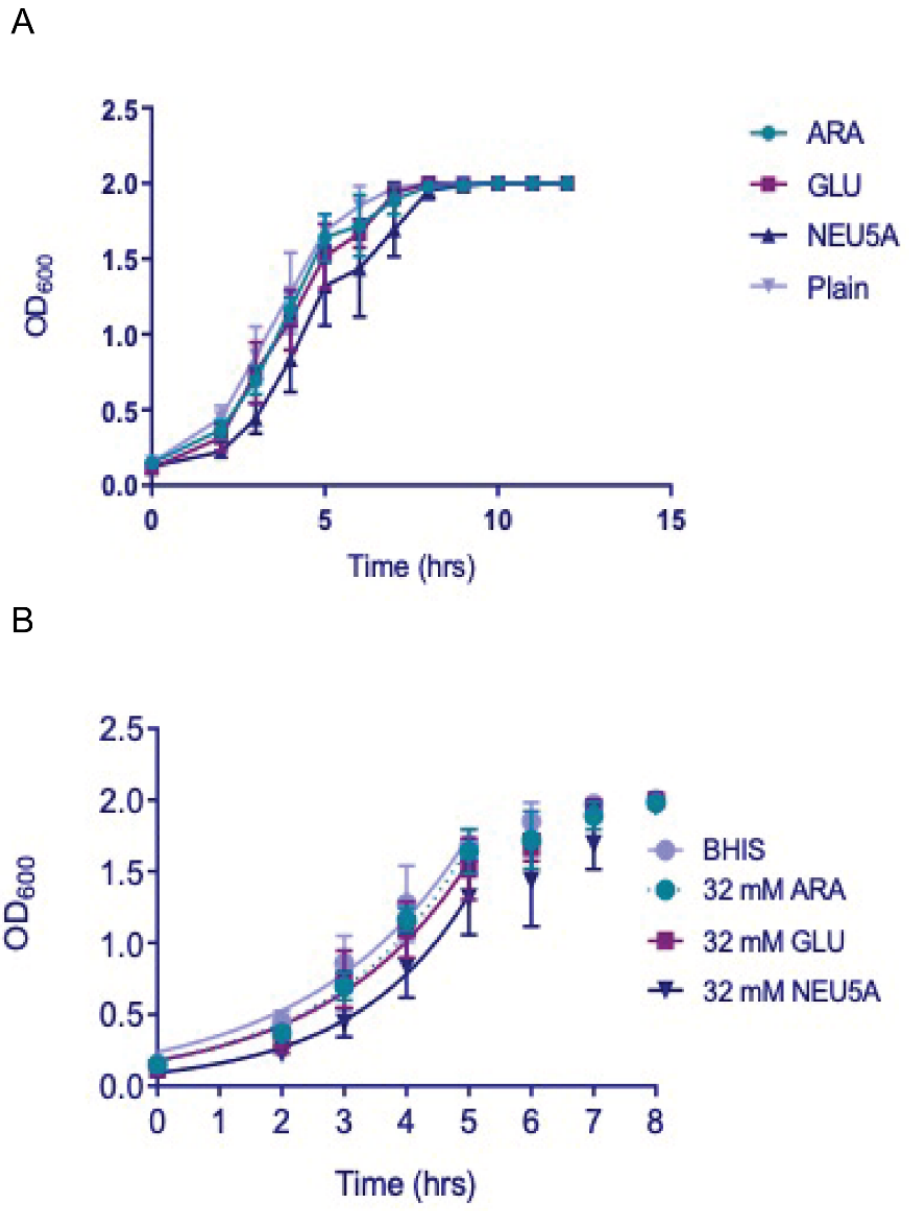

Figure 37. *C. difficile* growth in the presence of different sugars at 32 mM concentration. (A) Growth curves in medium supplemented with either 32 mM ARA, GLU or NEU5A are comparable to the growth of the bacteria in plain BHIS medium. (B) Growth curve as in (A) showing how the doubling times were calculated between 0 and 5 hrs of growth in the respective media. Adapted from Courson *et al.* 2019.

Table 3.

***C. difficile* replicates normally in the presence and/or lack of different metabolites.** Doubling times of *C. difficile* R20291 in BHIS with 32 mM supplementation of either ARA, GLU or NEU5A. Doubling times were calculated between 0 and 5 hrs of growth in plain BHIS or BHIS supplemented with the respective metabolite. Adapted from Courson *et al.* 2019.

Medium	Doubling time (hrs)
Plain BHIS	1.74
+ 32 mM ARA	1.54
+ 32 mM GLU	1.59
+ 32 mM NEU5A	1.30

Imaging of live C. difficile R20291 cells using home-built portable rose cell chambers

Based on our macroscopic motility assays, NEU5A specifically suppresses R20291 motility or swarming from the initial site of inoculation on a soft agar. To verify this finding on the single-cell level, we have utilized a rose cell chamber (317). The use of a rose cell chamber involves assembling a gas impermeable rubber gasket with a central hole that is sandwiched immediately between two glass cover slips followed by two aluminum plates at the top and bottom (Fig. 38A) (317). The rubber gasket is pierced with two standard needles, one that allows gas and fluid exchange to occur with the surrounding and another that allows for venting displaced air along with sample injection into the assembled chamber (317). Assembled chambers are reduced in the anaerobic chamber (although time consuming, the chamber can be assembled within the anaerobic chamber itself) and injected with liquid culture after which the needles are removed to allow the bacterial culture to be sealed inside of the rose cell chamber (317). The chamber is then placed on an aerobic inverted microscope and maintained at 37°C (317). By doing so, we found that within this device, *C. difficile* R20291 can grow and multiply normally overtime (317) (Fig. 38B). As depicted in the figure, growth is indicated by an increase in bacterial cell density as a function of time (Fig. 38B). We recorded images at various time points while the cells grew and found that after 6 hrs, bacteria continued swimming and multiplying, confirming that the home-built rose cell chambers preserve R20291 growth and viability (Fig. 38B) (317).

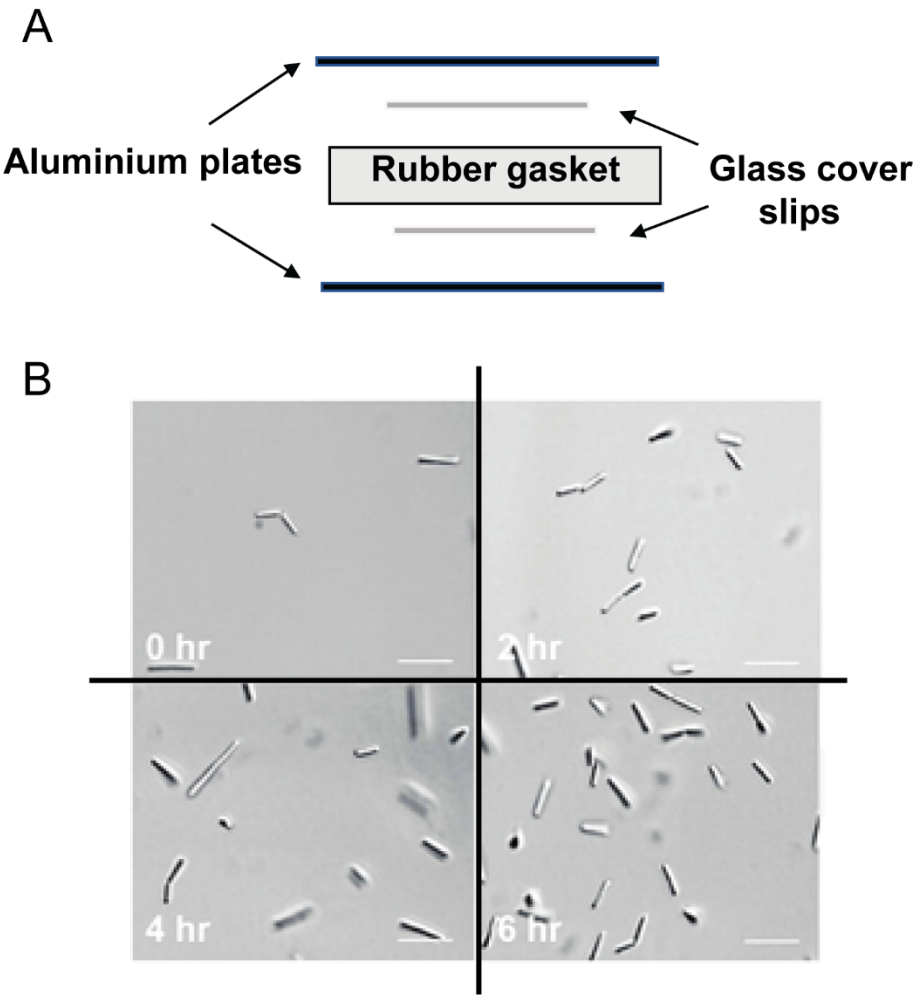

Figure 38. Extended live-cell microscopy of *C. difficile* R20291 using a rose cell chamber. (A) Side view of rose cell chamber assembly. (B) Cell division and growth of R20291 within the imaging chamber in BHIS medium. Panels show the time course in which the cells were incubated at 37°C within the chamber. Scale bar indicated at 10 μm. Adapted from Courson *et al*. 2019.

Analysis of C. difficile R20291 motility at the single-cell level

To measure motility in BHIS media supplemented with increasing concentrations of NEU5A, we recorded fast time-lapse videos (317). To prepare cultures for imaging, ON cultures of R20291 were diluted 1:50 into fresh BHIS media and allowed to grow for ~3 hrs, letting cells to reach late lag or early exponential phase of growth (317). Chambers were subsequently injected with BHIS supplemented with indicated concentrations of NEU5A (0, 10, 16, 25, and 32 mM) and 1:10 dilutions of the early exponential phase culture (317). To quantify bacterial motility within the chamber, we measured net displacement, unidirectional run length, and velocity during unidirectional runs of at least ten randomly selected cells within each movie (317). We found that supplementation with 10 mM NEU5A exhibited no significant effect on displacement, while 16 mM NEU5A caused a modest but significant increase in bacterial displacement (Fig. 39A) (317). At 32 mM concentration, however, bacterial displacement was significantly inhibited (Fig. 39A). At 25 mM, NEU5A reduced net displacement by 20% from 88.4 μm to 71.0 μm, and at 32 mM, NEU5A further reduced displacement. The motility videos used for the quantification of displacement are included in Courson *et al.* and that the link to the videos is included in Appendix G.

To verify if reduction in displacement caused by increasing NEU5A concentrations is due to reduction in bacterial swimming speeds, we calculated the flagella-dependent swimming velocities of each cell (317). We measured run velocity only during unidirectional runs even if that required us to include multiple frames of movement in the same direction (317). We found that NEU5A reduced swimming velocity at concentrations higher than 25 mM since 10 mM and 16 mM NEU5A had no significant effect on velocity (Fig. 39B) (317). Supplementation of BHIS medium with 25 mM and 32 mM NEU5A reduced velocity from 21.3 μm/sec to 15.8 μm/sec and 75% to 5.4 μm/sec, respectively (Appendix G, movies 2-5) (317).

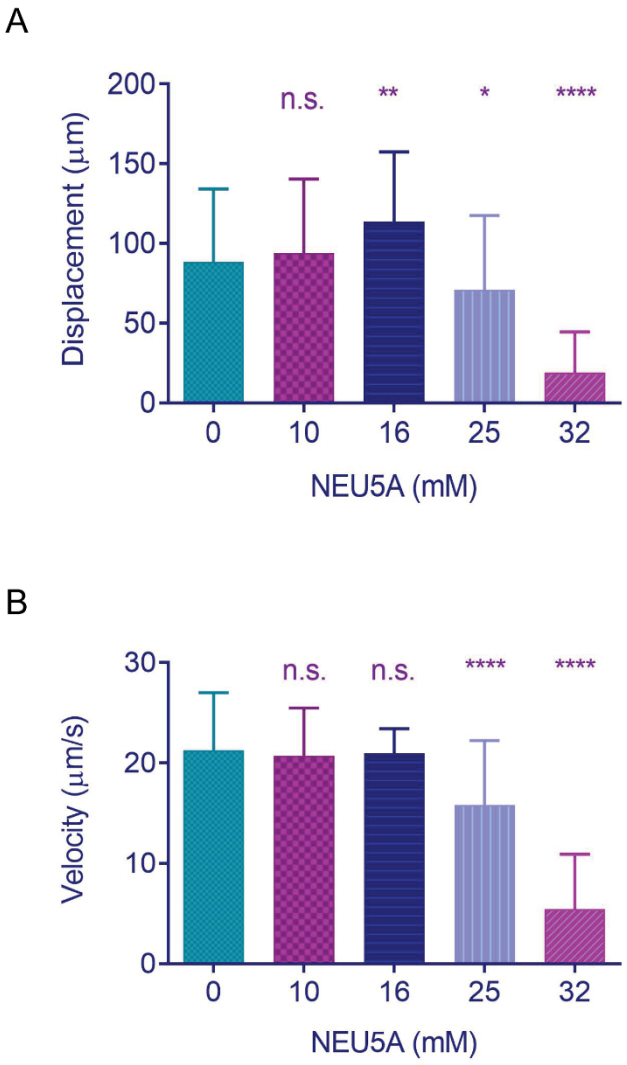

Figure 39. NEU5A reduces net displacement and velocity. (A) Net displacement (B) linear swimming velocity of R20291 during unidirectional runs within 10 sec in BHIS with indicated concentrations of NEU5A. Means and standard deviations of 49-146 cells are shown per condition. One-Way ANOVA analysis of variance comparing displacement and velocity of cells in supplemented media to those in plain BHIS. Turkey's multiple comparison test., n.s., not significant; **** $P < 0.0001$. Adapted from Courson *et al.* 2019.

Analysis of C. difficile R20291 motility via the tumbling mechanism

To quantify bacterial motility within the rose cell chamber, we also measured bacterial tumbling frequency of cells within each movie (317). Notably, reducing swimming velocity is not the only mechanism that bacteria employ to limit dispersing away from regions of high nutrient concentration or availability in the niche (317). Bacteria can stay closer to nutrient-rich sites by increasing flagella-dependent tumbling (317). To determine if *C. difficile* also alters its tumbling frequency in the presence of high NEU5A concentration, we quantified the reorientations of individual cells in the movies (317). We reported the number of tumbles per second of recorded motility because not all the cells analyzed managed to stay within-frame for the full 10 secs exposure duration (317). Upon doing so, we found that the average tumble frequency was not affected by supplementation with NEU5A at any concentrations tested (Fig. 40A) (317). The majority of cells did not tumble and supplementation with NEU5A appeared to make no difference in the observed trait (Fig. 40A) (317). Of the subset of cells that tumbled and were analyzed separately to study the effect of NEU5A, we found that NEU5A decreases tumbling frequency rather than increasing it (317). Tumbling cells in all medium conditions tumbled at the rate of 0.1-0.25 times/sec (Fig. 40B) (317). Only 7.3% of cells incubated in 32 mM NEU5A tumbled more than 0.25 times/sec in comparison to 10-20% of cells that tumbled in other media (Fig. 40B) (317). The average reorientation frequency of tumbling cells in 32 mM NEU5A was 0.22 tumbles/sec, which notably was lower than 0.32 tumbles/sec in plain BHIS or in any of the other media conditions supplemented with lower NEU5A concentrations (Fig. 40C) (317). These findings suggest that *C. difficile* R20291 senses high NEU5A concentration in the niche as is the case post-antibiotic treatment, notably without changing its tumbling frequency.

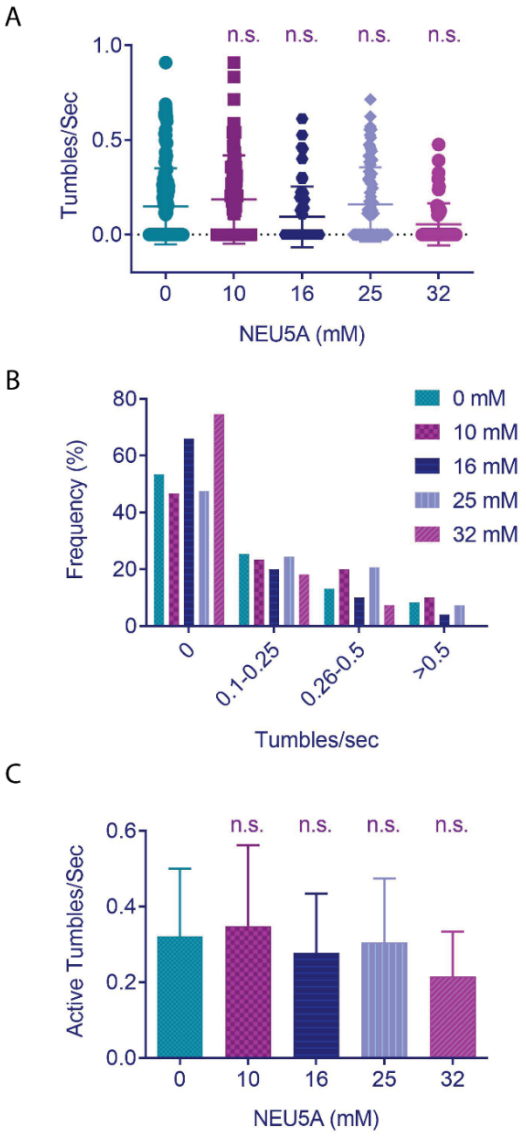

Figure 40. NEU5A has no effect on *C. difficile* R20291 tumbling. (A) Tumble frequency of *C. difficile* R20291 in BHIS supplemented with indicated concentrations of NEU5A. Tumble counts were normalized by the duration of each cell's motility to control for cells that left the field of view during 10 secs exposure. (B) Percentage of the total cells exhibiting the indicated number of tumbles/secs in each condition is given. (C) Normalized frequency of cells that show a non-zero rate of tumbling. Turkey's multiple comparison test., n.s., not significant. Adapted from Courson *et al.* 2019.

High NEU5A concentration regulates biofilm formation by C. difficile R20291

Since flagellum-dependent motility and TFP-mediated biofilm formation are inversely regulated by c-di-GMP in *C. difficile*, we investigated the impact of high NEU5A concentration in bacterial biofilm formation. We hypothesized that NEU5A serves as a potential signal in the host during *C. difficile* infection that regulates intracellular c-di-GMP pool and the associated physiological responses. Using plate-based biofilm assays, we found that *C. difficile* R20291 forms relatively more biofilm in media supplemented with NEU5A, GlcNAc, and GLU metabolites than in unsupplemented medium (Fig. 41). Notably, the bacteria formed single-species biofilm in the presence of both GLU and GlcNAc regardless of the monosaccharide concentrations (Fig. 41). However, the bacteria produced significantly more biofilm biomass at the highest NEU5A concentration tested (Fig. 41). This suggests that *C. difficile* responds to NEU5A abundancy and availability in the niche by producing biofilms above the threshold levels.

Previous studies have demonstrated that *C. difficile* 630 forms higher amounts of biofilm in BHIS supplemented with fermentable sugar such as GLU, fructose, and ribose in the presence of stress-causing insults (326). Since we were evaluating the impact of glucose in bacterial biofilm formation to determine if there is a correlation between motility suppression and sessile biofilm production in response to nutrients, we did not include glucose in our biofilm media. According to Dapa *et al*., both glucose and 0.3 M NaCl induce biofilm formation by 630 and R20291 strains where 0.3 M NaCl slightly inhibits biofilm production in caparison to 100 mM GLU (127). Consistent with literature evidence, we found that *C. difficile* R20291 form biofilm in the presence of increasing concentrations of NaCl (Fig. 42A), however, 32 mM NEU5A causes R20291 to produce more biofilm than does 0.3 M NaCl (Fig. 42B). Observed significant loss of biofilm during PBS washes led to this measurement which, notably, under-reports the amount of biofilm actually produced by R20291 in the presence of 32 mM NEU5A. Higher ionic strengths reduce the repulsion between a bacterial cell and a material surface, and that osmotic stress caused by NaCl promotes biofilm formation in Gram-positives such as *Staphylococcus* species and *Listeria monocytogenes* (327). The finding that *C. difficile* R20291 forms more biofilm in 32 mM NEU5A than in 0.3 M NaCl suggests that while osmolytes generally induce biofilm formation, the bacteria is also responding to NEU5A as a nutrient. We have

shown that 32 mM NEU5A does not impact bacterial growth negatively but inhibits dispersal from the site of inoculation on a soft agar (317). We have also shown that higher NEU5A concentration suppresses displacement and swimming velocity without affecting bacterial tumbling (317). Together, these observations indicate that NEU5A is not a repellent and rather a food source that promotes R20291 auto- aggregation and biofilm formation.

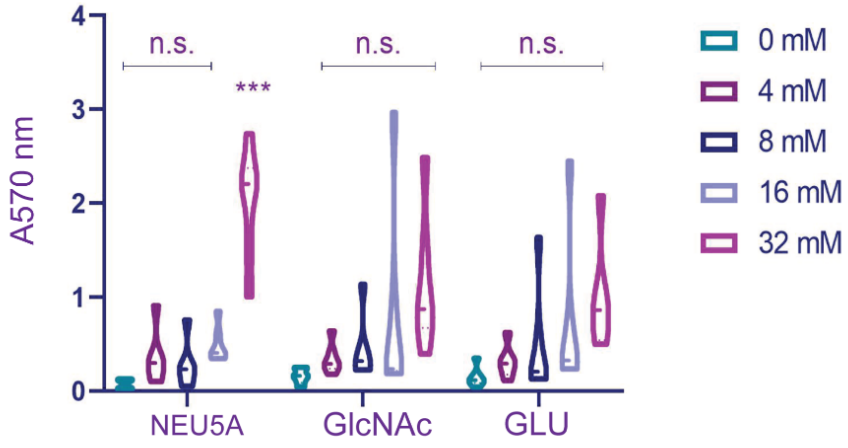

Figure 41. 32 mM NEU5A induces robust single-species biofilm formation by *C. difficile* R20291. Cultures of R20291 were incubated for 48 hrs at the indicated concentrations of NEU5A, GlcNAc, and GLU. Measurement of bacterial biomass using 0.1% crystal violet staining and 570 nm absorbance readings demonstrated that R20291 forms significantly more biofilm at 32 mM NEU5A. Production of biofilm in BHIS is independent of a GlcNAc and GLU gradient. Two-way ANOVA multiple comparison (cell means regardless of rows and columns) analysis of biomass produced at different concentrations of the unchained mucin monosaccharides., n.s., not significant, *** *P 0.0003.* Means and standard deviation of 6 biologicals are shown of two assays performed on different days.

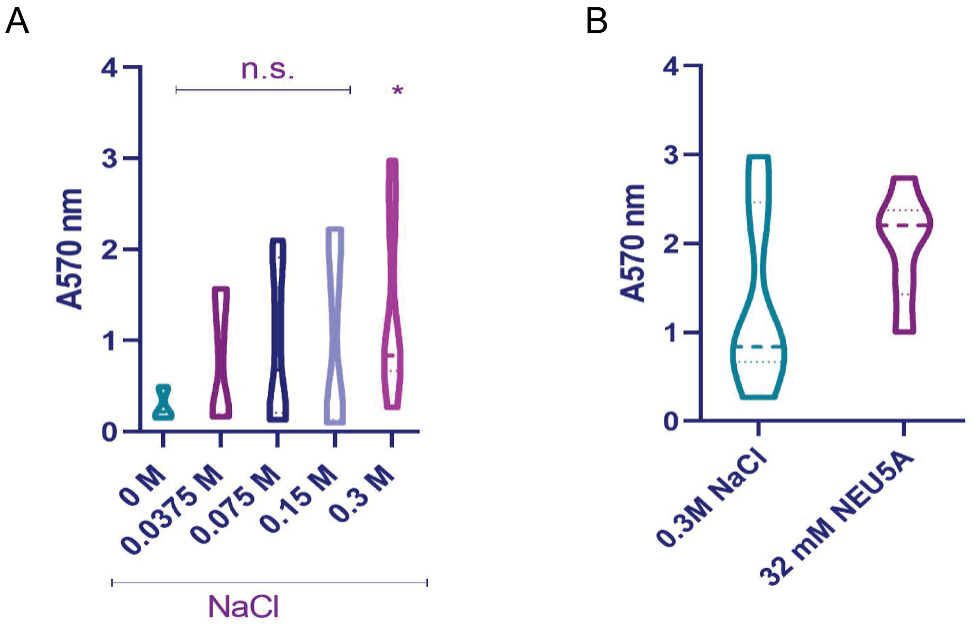

Figure 42. Effect of NaCl on biofilm production by *C. difficile* R20291. (A) Biofilm formation kinetics by R20291 in the presence of NaCl at the indicated concentrations using 0.1% CV staining procedure and measurement of biomass at 570 nm. Biofilm formation is comparable between 0 to 0.15 M non-sugar osmolyte but robust at 0.3 M NaCl. (B) R20291 produce biofilm in 32 mM NEU5A as well as in 0.3 M NaCl although at the population level, more independent biologicals produce more biomass in 32 mM NEU5A. Statistical significance determined by Unpaired t test., n.s., not significant, * *P 0.0355*. Means and standard deviation of 6 total biologicals are shown for two separate assays performed on different days.

SUMMARY

C. difficile is responsive to nutrient availability in its niche and we have found that the bacteria suppresses its movement in a nutritionally favorable environment. When added to a soft agar growth medium supplemented with either GLU or NEU5A, *C. difficile* can reduce motility at the population level, suggesting that the bacteria is sensing these free monosaccharides as a food source (317). In the presence of the non-metabolizable sugar ARA, *C. difficile* R20291 fails to exhibit any effect on motility over 24 hrs, confirming that the observed motility response is specific to sugars metabolizable by the bacteria (317). Notably, the molar concentration required to reduce R20291 motility is higher for GLU (55 mM at 1%) than for NEU5A (32 mM at 1%) (317). Unlike GLU, NEU5A supplies nitrogen and carbon as nutrients. Therefore, it remains to be elucidated whether the pronounced effect on motility exerted by NEU5A is specific or is a general read-out of the bacterium's global metabolic state (317). Since the organism codes for predicted chemotaxis gene products, we initially postulated that NEU5A-regulated motility suppression contributes to and/or is driven by bacterial directional motility in the presence of a NEU5A gradient (317). Engevik *et al*. recently demonstrated that *C. difficile* R20291 prefer NEU5A the least among other mucin monosaccharides, including GLU and GlcNAc (302). This finding suggests that R20291 does not readily respond to a NEU5A gradient when a plethora of significantly relevant metabolites are abundant in the niche. Therefore, we presume that *C. difficile* R20291 responds to NEU5A gradient strictly under circumstances where the metabolite profiles of the host have been changed as a consequence of intestinal dysbiosis. Post-cefaperozone treatment, a negative fold-change in GLU and GlcNAc have been reported in the gut of animal models, indicating that R20291 chemotaxis to NEU5A for survival when the levels of competing metabolites are low (300). Moreover, *C. difficile* R20291 may also reach NEU5A-rich sites independently of the chemotaxis mechanism (87).

Planktonic cells initiate biofilm formation to either resist adverse environmental conditions or to stay put in nutritionally favorable environments to establish colonization and infection (328). Based on our findings, *C. difficile* reduces unidirectional motility at higher NEU5A concentrations (317). Therefore, we postulated that NEU5A induces

motility suppression of R20291 while promoting single-species biofilm formation in a highly coordinated fashion, potentially under the regulation of the same signaling mechanism(s) such as the c-di-GMP signaling. We found that *C. difficile* R20291 forms biofilm in the presence of all monosaccharides tested. However, the bacteria form significantly higher amounts of biomass in 32 mM NEU5A than in the same concentration of GLU or GlcNAc. *C. difficile* is known to form biofilm in the presence of 0.3 M NaCl, which causes osmolarity stress to the pathogen (127). Based on our data, biofilm production by R20291 is influenced by osmolarity as well as nutrient availability. Unlike biofilm formation, however, *C. difficile* motility is influenced specifically by metabolizable nutrients rather than by osmolytes or factors contributing solely to changes in cellular osmolarity.

CHAPTER VI

CONCLUSIONS

This dissertation investigates the response of *Clostridioides difficile* to extracellular conditions. The (pp)pGpp-mediated stress response is a globally conserved mechanism that bacteria and some eukaryotes employ to respond to extracellular stresses (149). We have shown that the *C. difficile* genome encodes a long bifunctional RSH and a monofunctional RelQ enzyme that are members of the RSH superfamily (147,248). RSHCd contains two catalytic domains in the N-terminal end and regulatory domains in the C-terminal end, with a potential role in the reciprocal regulation of the enzyme's hydrolysis and synthesis activity (147). Unlike many of its Gram-positive RSH/Rel homologs, RSHCd does not bind GTP despite harboring the highly conserved RXKD motif in the amino acid sequence of its synthetase domain (147). The RXKD motif appears to influence RSHCd synthetase activity in the presence of high Mg^{2+} concentrations, suggesting that RSHCd-catalyzed pyrophosphate transfer reactions involve a single-divalent cation mechanism. However, the motif does not influence RSHCd substrate preference and utilization in a manner similar to RelSeq and RelMtb. Both RelSeq and RelMtb prefer GTP and readily produce pppGpp, suggesting that guanosine pentaphosphate alarmone has a physiological relevance to several Gram-positive organisms during the stringent response (160,243). In the contrary, RSHCd poorly binds GTP and does not accommodate pyrophosphate transfer from ATP to GTP (147).

RSHCd exclusively utilizes GDP as a substrate to synthesize the magic spot *in vitro* (147). We have shown that RSHCd synthetase activity is robust in a wide range of environmental pHs and that the enzyme can utilize a diverse array of metal cofactors that are structurally and chemically distinct (147). The failure of RSHCd to utilize GTP at an equimolar concentration of GDP and an excess in the same substrate pool suggests that the enzyme strictly utilizes GDP (147). We previously identified the magic spot produced by RSHCd as ppGpp since the enzyme exclusively utilized GDP under the conditions used (147,248). However, using RelQBs as a positive control, which utilizes GMP to

synthesize pGpp, we found that RSHCd-catalyzed alarmone migrates similar distances on PEI-cellulose plates as RelQBs-produced pGpp. The comparable mobility of the magic spot produced by RSHCd and RelQBs, notably, using two distinct substrates, lead us to conclude that RSHCd is synthesizing a three-phosphate alarmone instead of ppGpp via non-canonical mechanism(s). Additionally, a time-course analysis of RSHCd synthetase activity using HPLC also demonstrated that the signal of the triphosphate product increases with an increase in the reaction time, suggesting that the enzyme is producing putative pGpp in the presence of GDP and ATP (Appendix H). Future structural analysis using ^{31}Phosphorus NMR is necessary to confirm the identity of the triphosphate alarmone produced by RSHCd in the presence of GDP. Detection and quantification of alarmone accumulation *in vivo* is also imperative to establish that RSHCd produces pGpp via non-conventional mean(s). Like *Bacillus* species, *C. difficile* genome also encodes two putative NuDiX hydrolases that could potentially degrade pppGpp and ppGpp to pGpp, suggesting that *C. difficile* may synthesize the tetraphosphate and the pentaphosphate forms of magic spot under certain conditions (Appendix I).

To access the role of the CTD in regulating RSHCd synthetase activity, we have designed and cloned a synthetase-only gene called *rsh-rel* that codes for *C. difficile* RSH-REL enzyme. We found that the overexpression of *C. difficile rsh-rel* completely shuts down bacterial growth compared to *rsh*, which only partially inhibits growth. This suggests that expression of RSH-REL, lacking regulation by an intact hydrolase domain and/or the CTD, leads to the uncontrolled accumulation of the magic spot in bacterial cytoplasm (147). Notably, the toxicity associated with RSH-REL overexpression and subsequent magic spot production was attenuated by supplementing the bacterial growth medium with a combination of glucose and casamino acids (147). Like RSHCd, RSH-REL exclusively utilizes GDP to produce putative pGpp *in vitro*. We also examined the hydrolase activity of RSHCd in the presence of exogenous ppGpp and Mn^{2+} ion and found that RSHCd exhibits a relatively modest hydrolysis activity in isolation. Failure to detect hydrolysis product PPi via TLC suggests that the HD of RSHCd potentially requires activation regulation by branched-chain amino acids known to bind the ACT domain of several well-characterized Rel/RSH CTD (166).

Although the SR is a ubiquitous stress signaling pathway, factors contributing to the transcriptional regulation of *rsh* in diverse species vary dramatically (158). We found that *C. difficile rsh* is transcriptionally regulated by bacterial stationary phase onset and nutrient limitation (147). We also found that *rsh* transcription in *C. difficile* R20291 is induced by exposure to clindamycin and metronidazole (147). Interestingly, Relacin inhibits RSHCd synthetase activity *in vitro* but exerts no effect on bacterial accumulation *in vivo* (147). Exposure to antibiotics partially suppresses *C. difficile* R20291 accumulation from the intracellular production of (pp)pGpp and activation of the SR. Notably, the treatment of antibiotic-exposed *C. difficile* with 2 mM Relacin appeared to further suppress bacterial accumulation or load, suggesting that Relacin inhibits bacterial accumulation during the SR, presumably by inhibiting RSHCd-mediated putative pGpp synthesis (147). We have also confirmed the significance of *rsh* and *rsh* translation to *C. difficile* R20291 using a gene-silencing tool. Our data demonstrated that *rsh* translation in response to metronidazole is involved in bacterial antibiotic stress tolerance and survival. Furthermore, we have directly examined the significance of *rsh* gene in *C. difficile* R20291 virulence. Using ICelligence electrical cell impedance assay where R20291 and Madin-Darby canine kidney (MDCK) cells were co-cultured in gold microelectrode wells, we have shown that induction of asRNA specific to the mRNA of *C. difficile rsh* increases the lag time of MDCK cells to transition from proliferating to nonviable cells (Appendix J). While the MDCK cells are eventually killed from *C. difficile* toxicity (bacterial toxins lead to disruption of the mammalian epithelium monolayers and subsequent detachment from the assay wells causing reduction in impedance) and nutrient limitation in the growth medium, the observed delay in MDCK detachment or death corresponding to higher cellular index in the inducer-treated group indicates that *rsh* directly contributes to pathogenesis in *C. difficile* R20291 strain (Appendix J).

Finally, this dissertation also investigated nutrient-regulated mechanisms contributing to *C. difficile* host colonization. *C. difficile* is responsive to nutrients in the environment and as a motile organism, the bacteria utilize its motility machineries to respond to attractants and repellents accordingly (110). Based on a study by Theriot *et al*., antibiotic exposure alters the colonic microbiome and metabolome, creating an ideal niche for *C. difficile* germination and growth (300). Unchained NEU5A becomes abundant

and readily available to the pathogen post-cefoperazone treatment in the gut, suggesting that the bacteria utilize this mucin monosaccharide as a food source (300). Furthermore, Ng *et al.* demonstrated that *C. difficile* 630 genome carries a NEU5A catabolic operon like *S. typhimurium* and can metabolize free NEU5A, promoting higher pathogen densities within the intestinal lumen of mouse models (329). We have found that *C. difficile* R20291 suppresses its flagella-dependent motility at high NEU5A concentrations by decreasing bacterial displacement and swimming velocity (317). Notably, *C. difficile* does not attenuate motility by increasing its tumbling frequency (317). We hypothesized that the bacteria respond to NEU5A gradients in the host and maintain flagella-dependent chemotaxis to reach NEU5A-rich sites. However, a recent study demonstrated that NEU5A is one of the least preferred chemoattractants for *C. difficile*, indicating that R20291 cells respond to NEU5A gradient via chemotaxis only under conditions in which the levels of GLU and GlcNAc are substantially low (302).

While the chemotaxis mechanism largely governs the net direction of movement of bacteria for approaching attractants, it is not the only way pathogens can sense and move toward favorable environments (87). For instance, enterohemorrhagic *E. coli* can sense butyrate via positive transcriptional regulation of flagellar gene synthesis, which in turn enhances flagellum-driven motility of the pathogen to reach the surface of the intestinal mucosa (87,330). Furthermore, *V. cholerae* can sense high bile concentration using a two-component sensing and response system, which increases bacterial motility from the intestinal lumen to the bile-rich locations (87,331). This suggests that *C. difficile* R20291 could potentially rely on system(s) apart from chemotaxis to reach NEU5A-rich sites. Upon arriving at the target sites, the bacteria suspend flagella-driven motility but may or may not use flagella for other roles, including adhesion and biofilm formation during *C. difficile* infection. Purcell *et al.* reported that TFP contributes to biofilm formation by *C. difficile* in a c-di-GMP and class II_4 riboswitch-dependent manner (111). They also reported that c-di-GMP promotes TFP biosynthesis and surface motility, with the R20291 strain exhibiting significantly higher *pilA1* gene transcription corresponding to higher biofilm formation than 630/630Δ*erm* strain (111). Since c-di-GMP represses flagellum-mediated motility in *C. difficile* by down regulating the expression of genes in the *flgB* operon (including *sigD* that positively regulates toxin gene expression) and facilitates

autoaggregation and biofilm formation, we hypothesized that R20291 form biofilm in the presence of high NEU5A concentration and that NEU5A may be one of the many signals that impact cytoplasmic c-di-GMP pool and signaling in this organism.

Based on our quantification analyses using crystal violet assays and absorbance measurements at 570 nm, we found that *C. difficile* R20291 form biofilm in the presence of all sugar metabolites evaluated. Interestingly, R20291 cells appeared to form robust biofilm with significantly more biomass in the presence of 32 mM NEU5A than in GLU or GlcNAc at the same concentration. These findings indicate that *C. difficile* R20291 maintains colonization in the host by responding to NEU5A abundancy through robust single-species biofilm formation. However, the bacteria do not respond the same way to the same concentration of GLU and GlcNAc. Furthermore, our plate-based assays also revealed that biofilm formation by *C. difficile* R20291 is induced by osmolarity, while motility of the strain is not dependent on factors or monosaccharides such as ARA that impact cellular osmolarity. Overall, these findings indicate that motility suppression and biofilm formation of R20291 caused by 32 mM NEU5A may be inversely regulated by the same regulatory network(s) such as the c-di-GMP signaling. Recently, glucose-6-phopshate was shown to serve as a signal for *P. aeruginosa* SagS system to activate its motile-sessile switch function in a c-di-GMP-dependent manner (332). Glucose-6-phosphate increases diguanylate cyclase NicD expression, resulting in the corresponding increase in bacterial attachment and biofilm formation (332). Overall, this finding demonstrates the feasibility of our current hypothesis that NEU5A, much like glucose-6-phosphate, serves as a signal to induce R20291 biofilm formation via the c-di-GMP signaling network.

Using portable rose cell chambers to image bacterial aggregation upon incubation in buffered biofilm medium supplemented with 32 mM NEU5A, we have found that *C. difficile* R20291 form long chains of replicating cells (Appendix K) in a manner similar to *B. subtilis* during the production of ECM and biofilm formation (333). Notably, the chains appear to be longer when R20291 culture is treated with 0.3 M NaCl, with visibly fewer spores (Appendix K). We postulate that the deviation in cellular aggregation pattern and spore formation is attributable to the differential regulation of cell behaviors in the presence of a stress-inducing osmolyte versus a growth-facilitating food source. Future

characterization of R20291 biofilm architecture and matrix composition at 32 mM NEU5A using CLSM and TEM will provide more knowledge about the significance of this monosaccharide to *C. difficile* host colonization and pathogenesis. Furthermore, transcriptomic analyses with and without 32 mM NEU5A will provide mechanistic insights into the inverse regulation of motility and biofilm formation by R20291. We believe that the expression of genes involved in the biosynthesis of flagella (those in the F3 regulon and s*igD*) and/or genes regulating flagellar motility (*f*liC, *f*liD) along with those involved in chemotaxis will be downregulated in NEU5A-derived R20291 biofilms with a concurrent upregulation of TFP biosynthesis and assembly genes (such as *pilA1* and *pilB1*) (127). To determine if c-di-GMP signaling directly regulates the observed motility suppression and biofilm formation traits in *C. difficile* R20291 at elevated NEU5A concentrations, transcriptional profiling of genes encoding c-di-GMP cylases, class I and II riboswitches, and phosphodiesterases through microarray analyses or more advanced RNA sequencing technology will be useful. Additionally, we postulate that *spo0A*, with role(s) in biofilm formation and attachment by *C. difficile* and *C. perfringens* will be differentially expressed in R20291 biofilms ± 32 mM NEU5A (127). *spoOA* gene encodes SpoOA, the master regulator of sporulation in *Bacillus* and *Clostridium* species such that spoOA deletion attenuates biofilm formation (127,132). Upregulation of *spoOA* in R20291 biofilms at high NEU5A concentrations will suggest that NEU5A potentiates *C. difficile* pathogenesis by promoting sporulation and dissemination. While the role of c-di-GMP signaling in *C. difficile* sporulation remains to be elucidated, positive regulation of *spoOA* gene expression in R20291 biofilms in the presence of concentrated NEU5A will further denote that NEU5A serves as a signal during host microbial dysbiosis that primes *C. difficile* to sporulate rather than produce toxins.

As a concluding remark, we have shown the contributions of the stringent response mechanism in *Clostridioides difficile* tolerance and survival of extracellular stresses, providing significant implications toward the screening and/or designing of RSHCd-specific inhibitors with potency higher than that of Relacin's.

REFERENCES

1. Neumann-Schaal, M., Jahn, D., and Schmidt-Hohagen, K. (2019) Metabolism the difficile way: the key to the success of the pathogen *Clostridioides difficile*. *Front. Microbiol.* **10**, 219
2. Sebaihia, M., Wren, B. W., Mullany, P., Fairweather, N. F., Minton, N., Stabler, R., Thomson, N. R., Roberts, A. P., Cerdeño-Tárraga, A. M., and Wang, H. (2006) The multidrug-resistant human pathogen *Clostridium difficile* has a highly mobile, mosaic genome. *Nat. Genet.* **38**, 779-786
3. Bartlett, J. G., Chang, T.-W., and Onderdonk, A. B. (1978) Comparison of five regimens for treatment of experimental clindamycin-associated colitis. *J. Infect. Dis.* **138**, 81-86
4. Bartlett, J. G. (2006) Narrative review: the new epidemic of *Clostridium difficile*–associated enteric disease. *Ann. Intern. Med.* **145**, 758-764
5. Lessa, F. C., Mu, Y., Bamberg, W. M., Beldavs, Z. G., Dumyati, G. K., Dunn, J. R., Farley, M. M., Holzbauer, S. M., Meek, J. I., and Phipps, E. C. (2015) Burden of *Clostridium difficile* infection in the United States. *N. Engl. J. Med.* **372**, 825-834
6. Schaeffler, H., and Breitrueck, A. (2018) *Clostridium difficile*–From colonization to infection. *Front. Microbiol.* **9**, 646
7. Kuijper, E., Coignard, B., Tüll, P., difficile, E. S. G. f. C., States, E. M., Prevention, t. E. C. f. D., and Control. (2006) Emergence of *Clostridium difficile*-associated disease in North America and Europe. *Clin. Microbiol. Infect.* **12**, 2-18
8. Dubberke, E. R., and Olsen, M. A. (2012) Burden of *Clostridium difficile* on the healthcare system. *Clin. Infect. Dis.* **55**, S88-S92
9. Barbut, F. (2015) How to eradicate *Clostridium difficile* from the environment. *J. Hosp. Infect.* **89**, 287-295
10. Karen C, C., and John G, B. (2011) Biology of *Clostridium difficile*: implications for epidemiology and diagnosis. *Annu. Rev. Microbiol.* **65**, 501-521
11. Paredes-Sabja, D., Shen, A., and Sorg, J. A. (2014) *Clostridium difficile* spore biology: sporulation, germination, and spore structural proteins. *Trends. Microbiol.* **22**, 406-416

12. Rodriguez-Palacios, A., and LeJeune, J. T. (2011) Moist-heat resistance, spore aging, and superdormancy in *Clostridium difficile*. *Appl. Environ. Microbiol.* **77**, 3085-3091
13. Czepiel, J., Dróżdż, M., Pituch, H., Kuijper, E. J., Perucki, W., Mielimonka, A., Goldman, S., Wultańska, D., Garlicki, A., and Biesiada, G. (2019) *Clostridium difficile* infection. *Eur. J. Clin. Microbiol. Infect. Dis.* 1-11
14. Ofori, E., Ramai, D., Dhawan, M., Mustafa, F., Gasperino, J., and Reddy, M. (2018) Community-acquired *Clostridium difficile*: epidemiology, ribotype, risk factors, hospital and intensive care unit outcomes, and current and emerging therapies. *J. Hosp. Infect*. **99**, 436-442
15. Khanna, S., Pardi, D. S., Aronson, S. L., Kammer, P. P., Orenstein, R., Sauver, J. L. S., Harmsen, W. S., and Zinsmeister, A. R. (2012) The epidemiology of community-acquired *Clostridium difficile* infection: a population-based study. *Am. J. Gastroenterol.* **107**, 89
16. Guh, A. Y., Mu, Y., Winston, L. G., Johnston, H., Olson, D., Farley, M. M., Wilson, L. E., Holzbauer, S. M., Phipps, E. C., and Dumyati, G. K. (2020) Trends in US burden of *Clostridioides difficile* infection and outcomes. *N. Engl. J. Med.* **382**, 1320-1330
17. Sorg, J. A., and Sonenshein, A. L. (2008) Bile salts and glycine as cogerminants for *Clostridium difficile* spores. *J. Bacteriol.* **190**, 2505-2512
18. Zhu, D., Sorg, J. A., and Sun, X. (2018) *Clostridioides difficile* biology: sporulation, germination, and corresponding therapies for *C. difficile* infection. *Front. Cell. Infect. Microbiol.* **8**, 29
19. Voth, D. E., and Ballard, J. D. (2005) *Clostridium difficile* toxins: mechanism of action and role in disease. *Clin. Microbiol. Rev.* **18**, 247-263
20. Cohen, S. H., Tang, Y. J., and Silva Jr, J. (2000) Analysis of the pathogenicity locus in *Clostridium difficile* strains. *J. Infect. Dis.* **181**, 659-663
21. Moncrief, J. S., Barroso, L. A., and Wilkins, T. D. (1997) Positive regulation of *Clostridium difficile* toxins. *Infect. Immun.* **65**, 1105-1108
22. Tan, K. S., Wee, B. Y., and Song, K. P. (2001) Evidence for holin function of tcdE gene in the pathogenicity of *Clostridium difficile*. *J. Med. Microbiol.* **50**, 613-619

23. Nusrat, A., Giry, M., Turner, J., Colgan, S., Parkos, C., Carnes, D., Lemichez, E., Boquet, P., and Madara, J. (1995) Rho protein regulates tight junctions and perijunctional actin organization in polarized epithelia. *Proc. Natl. Acad. Sci.* **92**, 10629-10633

24. Nobes, C. D., and Hall, A. (1995) Rho, rac, and cdc42 GTPases regulate the assembly of multimolecular focal complexes associated with actin stress fibers, lamellipodia, and filopodia. *Cell*. **81**, 53-62

25. Freeman, J., Bauer, M., Baines, S. D., Corver, J., Fawley, W., Goorhuis, B., Kuijper, E., and Wilcox, M. (2010) The changing epidemiology of *Clostridium difficile* infections. *Clin. Microbiol. Rev.* **23**, 529-549

26. Riegler, M., Sedivy, R., Pothoulakis, C., Hamilton, G., Zacherl, J., Bischof, G., Cosentini, E., Feil, W., Schiessel, R., and LaMont, J. T. (1995) *Clostridium difficile* toxin B is more potent than toxin A in damaging human colonic epithelium *in vitro*. *J. Clin. Invest.* **95**, 2004-2011

27. Savidge, T. C., Pan, W.-h., Newman, P., O'Brien, M., Anton, P. M., and Pothoulakis, C. (2003) *Clostridium difficile* toxin B is an inflammatory enterotoxin in human intestine. *Gastroenterol.* **125**, 413-420

28. Guery, B., Galperine, T., and Barbut, F. (2019) *Clostridioides difficile*: diagnosis and treatments. *bmj*. **366**, l4609

29. He, M., Miyajima, F., Roberts, P., Ellison, L., Pickard, D. J., Martin, M. J., Connor, T. R., Harris, S. R., Fairley, D., and Bamford, K. B. (2013) Emergence and global spread of epidemic healthcare-associated *Clostridium difficile*. *Nat. Genet.* **45**, 109-113

30. Fatima, R., and Aziz, M. (2019) The hypervirulent strain of *Clostridium difficile*: NAP1/B1/027-a brief overview. *Cureus*. **11**

31. O'Connor, J. R., Johnson, S., and Gerding, D. N. (2009) *Clostridium difficile* infection caused by the epidemic BI/NAP1/027 strain. *Gastroenterol.* **136**, 1913-1924

32. Schwan, C., Stecher, B., Tzivelekidis, T., van Ham, M., Rohde, M., Hardt, W.-D., Wehland, J., and Aktories, K. (2009) *Clostridium difficile* toxin CDT induces

formation of microtubule-based protrusions and increases adherence of bacteria. *PLoS Pathog.* **5**, e1000626

33. McDonald, L. C., Killgore, G. E., Thompson, A., Owens Jr, R. C., Kazakova, S. V., Sambol, S. P., Johnson, S., and Gerding, D. N. (2005) An epidemic, toxin gene–variant strain of *Clostridium difficile*. *N. Engl. J. Med.* **353**, 2433-2441
34. Loo, V. G., Poirier, L., Miller, M. A., Oughton, M., Libman, M. D., Michaud, S., Bourgault, A.-M., Nguyen, T., Frenette, C., and Kelly, M. (2005) A predominantly clonal multi-institutional outbreak of *Clostridium difficile*–associated diarrhea with high morbidity and mortality. *N. Engl. J. Med.* **353**, 2442-2449
35. Masgala, A., Delis, S. G., and Dervenis, C. (2014) *Clostridium difficile* infection: an increasing postsurgical complication. *J. Infect. Dis. Ther.*
36. Khanna, S. (2021) Advances in *Clostridioides difficile* therapeutics. Taylor & Francis
37. Ley, R. E., Peterson, D. A., and Gordon, J. I. (2006) Ecological and evolutionary forces shaping microbial diversity in the human intestine. *Cell*. **124**, 837-848
38. Sekirov, I., Russell, S. L., Antunes, L. C. M., and Finlay, B. B. (2010) Gut microbiota in health and disease. *Physiol. Rev.* **90**, 859-904
39. Blaser, M. J. (2014) The microbiome revolution. *J. Clin. Invest.* **124**, 4162-4165
40. Lagier, J.-C. (2016) Gut microbiota and *Clostridium difficile* infections. *Hum. Microbiome. J.* **2**, 10-14
41. Vakili, B., Fateh, A., Aghdaei, H. A., Sotoodehnejadnematalahi, F., and Siadat, S. D. (2020) Intestinal Microbiota in Elderly Inpatients with *Clostridioides difficile* Infection. *Infect. Drug. Resist.* **13**, 2723-2731
42. Crobach, M. J., Vernon, J. J., Loo, V. G., Kong, L. Y., Péchiné, S., Wilcox, M. H., and Kuijper, E. J. (2018) Understanding *Clostridium difficile* colonization. *Clin. Microbiol. Rev.* **31**
43. Faden, H. (2020) Review and Commentary on the Importance of Bile Acids in the Life Cycle of *Clostridioides difficile* in Children and Adults. *J. Pediatr. Infect. Dis. Soc*

44. Winston, J. A., and Theriot, C. M. (2016) Impact of microbial derived secondary bile acids on colonization resistance against *Clostridium difficile* in the gastrointestinal tract. *Anaerobe*. **41**, 44-50
45. Francis, M. B., Allen, C. A., Shrestha, R., and Sorg, J. A. (2013) Bile acid recognition by the *Clostridium difficile* germinant receptor, CspC, is important for establishing infection. *PLoS Pathog*. **9**, e1003356
46. Gu, S., Chen, Y., Zhang, X., Lu, H., Lv, T., Shen, P., Lv, L., Zheng, B., Jiang, X., and Li, L. (2016) Identification of key taxa that favor intestinal colonization of *Clostridium difficile* in an adult Chinese population. *Microb. Infect.* **18**, 30-38
47. Kelly, C. P. (1996) Immune response to *Clostridium difficile* infection. *Eur. J. Gastroenterol. Hepatol.* **8**, 1048-1053
48. Mariat, D., Firmesse, O., Levenez, F., Guimarães, V., Sokol, H., Doré, J., Corthier, G., and Furet, J. (2009) The Firmicutes/Bacteroidetes ratio of the human microbiota changes with age. *BMC. Microbiol.* **9**, 123
49. Ogra, P. L. (2010) Ageing and its possible impact on mucosal immune responses. *Ageing Res. Rev.* **9**, 101-106
50. Hopkins, M., Sharp, R., and Macfarlane, G. (2001) Age and disease related changes in intestinal bacterial populations assessed by cell culture, 16S rRNA abundance, and community cellular fatty acid profiles. *Gut*. **48**, 198-205
51. Woodmansey, E. J. (2007) Intestinal bacteria and ageing. *J. Appl. Microbiol.* **102**, 1178-1186
52. Hung, Y.-P., Lin, H.-J., Wu, T.-C., Liu, H.-C., Lee, J.-C., Lee, C.-I., Wu, Y.-H., Wan, L., Tsai, P.-J., and Ko, W.-C. (2013) Risk factors of fecal toxigenic or non-toxigenic *Clostridium difficile* colonization: impact of Toll-like receptor polymorphisms and prior antibiotic exposure. *PloS One*. **8**, e69577
53. Loo, V. G., Bourgault, A.-M., Poirier, L., Lamothe, F., Michaud, S., Turgeon, N., Toye, B., Beaudoin, A., Frost, E. H., and Gilca, R. (2011) Host and pathogen factors for *Clostridium difficile* infection and colonization. *N. Engl. J. Med.* **365**, 1693-1703

54. Eyre, D. W., Griffiths, D., Vaughan, A., Golubchik, T., Acharya, M., O'Connor, L., Crook, D. W., Walker, A. S., and Peto, T. E. (2013) Asymptomatic *Clostridium difficile* colonisation and onward transmission. *PloS One*. **8**, e78445

55. Marciniak, C., Chen, D., Stein, A. C., and Semik, P. E. (2006) Prevalence of *Clostridium difficile* colonization at admission to rehabilitation. *Arch. Phys. Med. Rehabil.* **87**, 1086-1090

56. Hung, Y.-P., Lee, J.-C., Lin, H.-J., Liu, H.-C., Wu, Y.-H., Tsai, P.-J., and Ko, W.-C. (2015) Clinical impact of *Clostridium difficile* colonization. *J. Microbiol. Immunol. Infect.* **48**, 241-248

57. Jarmo, O., Veli-Jukka, A., and Eero, M. (2020) Treatment of *Clostridioides (Clostridium) difficile* infection. *Ann. Med.* **52**, 12-20

58. Boyce, J. M., Havill, N. L., Otter, J. A., McDonald, L. C., Adams, N. M., Cooper, T., Thompson, A., Wiggs, L., Killgore, G., and Tauman, A. (2008) Impact of hydrogen peroxide vapor room decontamination on *Clostridium difficile* environmental contamination and transmission in a healthcare setting. *Infect. Control Hosp. Epidemiol.* **29**, 723-729

59. Al-Jashaami, L. S., and DuPont, H. L. (2016) Management of *Clostridium difficile* infection. *Gastroenterol Hepatol.* **12**, 609

60. Deneve, C., Janoir, C., Poilane, I., Fantinato, C., and Collignon, A. (2009) New trends in *Clostridium difficile* virulence and pathogenesis. *Int. J. Antimicrob. Agents.* **33**, S24-S28

61. Stabler, R. A., He, M., Dawson, L., Martin, M., Valiente, E., Corton, C., Lawley, T. D., Sebaihia, M., Quail, M. A., and Rose, G. (2009) Comparative genome and phenotypic analysis of *Clostridium difficile* 027 strains provides insight into the evolution of a hypervirulent bacterium. *Genome Biol.* **10**, R102

62. Kelly, C. P., and LaMont, J. T. (2008) *Clostridium difficile*—more difficult than ever. *N. Engl. J. Med.* **359**, 1932-1940

63. Khanna, S., and Gerding, D. N. (2019) Current and Future Trends in *Clostridioides (Clostridium) difficile* Infection Management. *Anaerobe*

64. Curry, S. R. (2017) *Clostridium difficile*. *Clin. Lab. Medi.* **37**, 341-369

65. Babakhani, F., Bouillaut, L., Gomez, A., Sears, P., Nguyen, L., and Sonenshein, A. L. (2012) Fidaxomicin inhibits spore production in *Clostridium difficile. Clin. Infect. Dis.* **55**, S162-S169

66. Babakhani, F., Bouillaut, L., Sears, P., Sims, C., Gomez, A., and Sonenshein, A. L. (2012) Fidaxomicin inhibits toxin production in *Clostridium difficile*. *J. Antimicrob. Chemother.* **68**, 515-522

67. Bassères, E., Endres, B. T., Montes-Bravo, N., Pérez-Soto, N., Rashid, T., Lancaster, C., Begum, K., Alam, M. J., Paredes-Sabja, D., and Garey, K. W. (2021) Visualization of fidaxomicin association with the exosporium layer of *Clostridioides difficile* spores. *Anaerobe*. 102352

68. Marreddy, R. K., Wu, X., Sapkota, M., Prior, A. M., Jones, J. A., Sun, D., Hevener, K. E., and Hurdle, J. G. (2018) The fatty acid synthesis protein enoyl-ACP reductase II (FabK) is a target for narrow-spectrum antibacterials for C*lostridium difficile* infection. *ACS Infect. Dis.* **5**, 208-217

69. Cole, S. A., and Stahl, T. J. (2015) Persistent and Recurrent *Clostridium difficile* Colitis. *Clin. Colon. Rect. Surg.* **28**, 65-69

70. McFarland, L. V. (2008) Antibiotic-associated diarrhea: epidemiology, trends and treatment.

71. Shogbesan, O., Poudel, D. R., Victor, S., Jehangir, A., Fadahunsi, O., Shogbesan, G., and Donato, A. (2018) A systematic review of the efficacy and safety of fecal microbiota transplant for *Clostridium difficile* infection in immunocompromised patients. *Can. J. Gastroenterol. Hepatol.* **2018**

72. Khanna, S., and Pardi, D. (2020) Fecal Microbiota Transplantation for Recurrent *Clostridioides difficile* infection: The COVID-19 Era. *Am. J. Gastroenterol.*

73. McDonald, L. C., Gerding, D. N., Johnson, S., Bakken, J. S., Carroll, K. C., Coffin, S. E., Dubberke, E. R., Garey, K. W., Gould, C. V., and Kelly, C. (2018) Clinical practice guidelines for *Clostridium difficile* infection in adults and children: 2017 update by the Infectious Diseases Society of America (IDSA) and Society for Healthcare Epidemiology of America (SHEA). *Clin. Infect. Dis.* **66**, e1-e48

74. Boyle, M. L., Ruth-Sahd, L. A., and Zhou, Z. (2015) Fecal microbiota transplant to treat recurrent *Clostridium difficile* infections. *Crit. Care. Nurs.* **35**, 51-64

75. DeFilipp, Z., Bloom, P. P., Torres Soto, M., Mansour, M. K., Sater, M. R., Huntley, M. H., Turbett, S., Chung, R. T., Chen, Y.-B., and Hohmann, E. L. (2019) Drug-resistant *E. coli* bacteremia transmitted by fecal microbiota transplant. *N. Engl. J. Med.* **381**, 2043-2050

76. Guilfoyle, J., Considine, J., and Bouchoucha, S. L. (2020) Faecal microbiota transplantation (FMT) and the patient experience: A systematic review. *J. Clin. Nurs.*

77. Wilcox, M. H., Gerding, D. N., Poxton, I. R., Kelly, C., Nathan, R., Birch, T., Cornely, O. A., Rahav, G., Bouza, E., and Lee, C. (2017) Bezlotoxumab for prevention of recurrent *Clostridium difficile* infection. *N. Engl. J. Med.* **376**, 305-317

78. Gareau, M. G., Sherman, P. M., and Walker, W. A. (2010) Probiotics and the gut microbiota in intestinal health and disease. *Nat. Rev. Gastroenterol. Hepatol.* **7**, 503

79. Huebner, E. S., and Surawicz, C. M. (2006) Probiotics in the prevention and treatment of gastrointestinal infections. *Gastroenterol. Clin.* **35**, 355-365

80. Trejo, F. M., Minnaard, J., Perez, P. F., and De Antoni, G. L. (2006) Inhibition of *Clostridium difficile* growth and adhesion to enterocytes by Bifidobacterium supernatants. *Anaerobe.* **12**, 186-193

81. Valdés-Varela, L., Hernández-Barranco, A. M., Ruas-Madiedo, P., and Gueimonde, M. (2016) Effect of Bifidobacterium upon *Clostridium difficile* growth and toxicity when co-cultured in different prebiotic substrates. *Front. Microbiol.* **7**, 738

82. Naaber, P., Smidt, I., Štšepetova, J., Brilene, T., Annuk, H., and Mikelsaar, M. (2004) Inhibition of *Clostridium difficile* strains by intestinal *Lactobacillus* species. *J. Med. Mircobiol.* **53**, 551-554

83. Kim, S.-M., Park, H.-G., Song, W.-S., Jo, S.-H., Yang, Y.-H., and Kim, Y.-G. (2020) LC–MS/MS based observation of *Clostridium difficile* inhibition by *Lactobacillus rhamnosus* GG. *J. Ind. Eng. Chem*

84. Rossez, Y., Wolfson, E. B., Holmes, A., Gally, D. L., and Holden, N. J. (2015) Bacterial flagella: twist and stick, or dodge across the kingdoms. *PLoS Pathog*. **11**, e1004483

85. Harshey, R. M. (2003) Bacterial motility on a surface: many ways to a common goal. *Annu. Rev. Microbiol.* **57**, 249-273
86. Stevenson, E., Minton, N. P., and Kuehne, S. A. (2015) The role of flagella in *Clostridium difficile* pathogenicity. *Trends. Microbiol.* **23**, 275-282
87. Chaban, B., Hughes, H. V., and Beeby, M. (2015) The flagellum in bacterial pathogens: for motility and a whole lot more. in *Semin. Cell Dev. Biol*, Elsevier
88. Echazarreta, M., and Klose, K. (2019) Vibrio flagellar synthesis. *Front. Cell. Infect. Microbio*l. **9**, 131
89. Bolton, D. J. (2015) *Campylobacter* virulence and survival factors. *Food. Microbiol.* **48**, 99-108
90. Garrett, E. M. (2020) Characterization of a phase variable regulatory system and its impacts on *Clostridioides difficile* physiology. Ph.D. Thesis, The Uiversity of North Carolina-Chapel Hill
91. Nachamkin, I., Yang, X.-H., and Stern, N. J. (1993) Role of *Campylobacter jejuni* flagella as colonization factors for three-day-old chicks: analysis with flagellar mutants. *Appl. Environ. Microbiol.* **59**, 1269-1273
92. Richardson, K. (1991) Roles of motility and flagellar structure in pathogenicity of *Vibrio cholerae*: analysis of motility mutants in three animal models. *Infect. Immun.* **59**, 2727-2736
93. Dunne, C., Dolan, B., and Clyne, M. (2014) Factors that mediate colonization of the human stomach by *Helicobacter pylori*. *World J. Gastroenterol.* **20**, 5610
94. Postnova, T., Gómez-Duarte, O. G., and Richardson, K. (1996) Motility mutants of *Vibrio cholerae* 01 have reduced adherence *in vitro* to human small intestinal epithelial cells as demonstrated by ELISA. *Microbiology*. **142**, 2767-2776
95. Konkel, M. E., Klena, J. D., Rivera-Amill, V., Monteville, M. R., Biswas, D., Raphael, B., and Mickelson, J. (2004) Secretion of virulence proteins from *Campylobacter jejuni* is dependent on a functional flagellar export apparatus. *J. Bacteriol.* **186**, 3296-3303
96. Chevance, F. F., and Hughes, K. T. (2008) Coordinating assembly of a bacterial macromolecular machine. *Nat. Rev. Microbiol.* **6**, 455-465

97. Lowe, G., Meister, M., and Berg, H. C. (1987) Rapid rotation of flagellar bundles in swimming bacteria. *Nature*. **325**, 637-640

98. Lambert, C., Evans, K. J., Till, R., Hobley, L., Capeness, M., Rendulic, S., Schuster, S. C., Aizawa, S. I., and Sockett, R. E. (2006) Characterizing the flagellar filament and the role of motility in bacterial prey-penetration by *Bdellovibrio bacteriovorus. Mol. Microbiol.* **60**, 274-286

99. McKee, R. W., Mangalea, M. R., Purcell, E. B., Borchardt, E. K., and Tamayo, R. (2013) The second messenger cyclic Di-GMP regulates *Clostridium difficile* toxin production by controlling expression of sigD. *J. Bacteriol.* **195**, 5174-5185

100. El Meouche, I., Peltier, J., Monot, M., Soutourina, O., Pestel-Caron, M., Dupuy, B., and Pons, J.-L. (2013) Characterization of the SigD regulon of *C. difficile* and its positive control of toxin production through the regulation of tcdR. *PloS One*. **8**, e83748

101. Tasteyre, A., Barc, M.-C., Karjalainen, T., Dodson, P., Hyde, S., Bourlioux, P., and Borriello, P. (2000) A *Clostridium difficile* gene encoding flagellinThe GenBank accession numbers for the sequences reported in this paper are AF065259 (strain 79-685) and AF077341 (strain VPI 10463). *Microbiology*. **146**, 957-966

102. Martin, M. J., Clare, S., Goulding, D., Faulds-Pain, A., Barquist, L., Browne, H. P., Pettit, L., Dougan, G., Lawley, T. D., and Wren, B. W. (2013) The agr locus regulates virulence and colonization genes in *Clostridium difficile* 027. *J. Bacteriol.* **195**, 3672-3681

103. Twine, S. M., Reid, C. W., Aubry, A., McMullin, D. R., Fulton, K. M., Austin, J., and Logan, S. M. (2009) Motility and flagellar glycosylation in *Clostridium difficile*. *J. Bacteriol.* **191**, 7050-7062

104. Faulds-Pain, A., Twine, S. M., Vinogradov, E., Strong, P. C., Dell, A., Buckley, A. M., Douce, G. R., Valiente, E., Logan, S. M., and Wren, B. W. (2014) The post-translational modification of the *Clostridium difficile* flagellin affects motility, cell surface properties and virulence. *Mol. Microbiol.* **94**, 272-289

105. Guerry, P., Ewing, C. P., Schirm, M., Lorenzo, M., Kelly, J., Pattarini, D., Majam, G., Thibault, P., and Logan, S. (2006) Changes in flagellin glycosylation affect Campylobacter autoagglutination and virulence. *Mol. Microbiol.* **60**, 299-311

106. Valiente, E., Bouché, L., Hitchen, P., Faulds-Pain, A., Songane, M., Dawson, L. F., Donahue, E., Stabler, R. A., Panico, M., and Morris, H. R. (2016) Role of glycosyltransferases modifying type B flagellin of emerging hypervirulent *Clostridium difficile* lineages and their impact on motility and biofilm formation. *J. Biol. Chem.* **291**, 25450-25461

107. Baban, S. T., Kuehne, S. A., Barketi-Klai, A., Cartman, S. T., Kelly, M. L., Hardie, K. R., Kansau, I., Collignon, A., and Minton, N. P. (2013) The role of flagella in *Clostridium difficile* pathogenesis: comparison between a non-epidemic and an epidemic strain. *PloS One*. **8**, e73026

108. Hussain, H. A., Roberts, A. P., and Mullany, P. (2005) Generation of an erythromycin-sensitive derivative of *Clostridium difficile* strain 630 (630Δerm) and demonstration that the conjugative transposon Tn916ΔE enters the genome of this strain at multiple sites. *J. Med. Microbiol.* **54**, 137-141

109. Aubry, A., Hussack, G., Chen, W., KuoLee, R., Twine, S. M., Fulton, K. M., Foote, S., Carrillo, C. D., Tanha, J., and Logan, S. M. (2012) Modulation of toxin production by the flagellar regulon in *Clostridium difficile*. *Infect. Immun.* **80**, 3521-3532

110. Purcell, E. B., and Tamayo, R. (2016) Cyclic diguanylate signaling in Gram-positive bacteria. *FEMS Microbiol. Rev.* **40**, 753-773

111. Purcell, E. B., McKee, R. W., Bordeleau, E., Burrus, V., and Tamayo, R. (2016) Regulation of type IV pili contributes to surface behaviors of historical and epidemic strains of *Clostridium difficile*. *J. Bacteriol.* **198**, 565-577

112. Melville, S., and Craig, L. (2013) Type IV pili in Gram-positive bacteria. *Microbiol. Mol. Biol. Rev.* **77**, 323-341

113. Merz, A. J., So, M., and Sheetz, M. P. (2000) Pilus retraction powers bacterial twitching motility. *Nature*. **407**, 98-102

114. Conrad, J. C. (2012) Physics of bacterial near-surface motility using flagella and type IV pili: implications for biofilm formation. *Res. Microbiol.* **163**, 619-629

115. Mattick, J. S. (2002) Type IV pili and twitching motility. *Annu. Rev. Microbiol.* **56**, 289-314

116. Varga, J. J., Nguyen, V., O'Brien, D. K., Rodgers, K., Walker, R. A., and Melville, S. B. (2006) Type IV pili-dependent gliding motility in the Gram-positive pathogen *Clostridium perfringens* and other *Clostridia*. *Mol. Microbiol.* **62**, 680-694

117. Bordeleau, E., Purcell, E. B., Lafontaine, D. A., Fortier, L.-C., Tamayo, R., and Burrus, V. (2015) Cyclic di-GMP riboswitch-regulated type IV pili contribute to aggregation of *Clostridium difficile*. *J. Bacteriol.* **197**, 819-832

118. Hengge, R. (2009) Principles of cyclic-di-GMP signaling. *Nat. Rev. Microbiol*. **7**, 263-273

119. Purcell, E. B., McKee, R. W., McBride, S. M., Waters, C. M., and Tamayo, R. (2012) Cyclic diguanylate inversely regulates motility and aggregation in *Clostridium difficile*. *J. Bacteriol.* **194**, 3307-3316

120. McKee, R. W., Aleksanyan, N., Garrett, E. M., and Tamayo, R. (2018) Type IV pili promote *Clostridium difficile* adherence and persistence in a mouse model of infection. *Infect.* **86**

121. Uruén, C., Chopo-Escuin, G., Tommassen, J., Mainar-Jaime, R. C., and Arenas, J. (2021) Biofilms as Promoters of Bacterial Antibiotic Resistance and Tolerance. *Antibiotics*. **10**, 3

122. Verderosa, A. D., Totsika, M., and Fairfull-Smith, K. E. (2019) Bacterial biofilm eradication agents: a current review. *Front. Chem.* **7**, 824

123. Flemming, H.-C., and Wingender, J. (2001) Relevance of microbial extracellular polymeric substances (EPSs)-Part I: Structural and ecological aspects. *Water Sci. Technol.* **43**, 1-8

124. Ghosh, A., Jayaraman, N., and Chatterji, D. (2020) Small-Molecule Inhibition of Bacterial Biofilm. *ACS Omega*

125. Cohen, N. R., Lobritz, M. A., and Collins, J. J. (2013) Microbial persistence and the road to drug resistance. *Cell Host Microbe.* **13**, 632-642

126. Jung, S.-H., Ryu, C.-M., and Kim, J.-S. (2019) Bacterial persistence: Fundamentals and clinical importance. *J. Microbiol.* **57**, 829-835

127. Dapa, T., and Unnikrishnan, M. (2013) Biofilm formation by *Clostridium difficile. Gut Microbes.* **4**, 397-402

128. Lynch, M., Walsh, T. A., Marszalowska, I., Webb, A. E., MacAogain, M., Rogers, T. R., Windle, H., Kelleher, D., O'Connell, M. J., and Loscher, C. E. (2017) Surface layer proteins from virulent *Clostridium difficile* ribotypes exhibit signatures of positive selection with consequences for innate immune response. *BMC Evol. Biol.* **17**, 90

129. Rutherford, S. T., and Bassler, B. L. (2012) Bacterial quorum sensing: its role in virulence and possibilities for its control. *Cold Spring Harb. Perspect. Biol.* **2**, a012427

130. Lombardía, E., Rovetto, A. J., Arabolaza, A. L., and Grau, R. R. (2006) A LuxS-dependent cell-to-cell language regulates social behavior and development in *Bacillus subtilis*. *J. Bacteriol.* **188**, 4442-4452

131. Ohtani, K., Hayashi, H., and Shimizu, T. (2002) The luxS gene is involved in cell–cell signalling for toxin production in *Clostridium perfringens*. *Mol. Microbiol.* **44**, 171-179

132. Abee, T., Kovács, Á. T., Kuipers, O. P., and van der Veen, S. (2011) Biofilm formation and dispersal in Gram-positive bacteria. *Curr. Opin. Biotechnol.* **22**, 172-179

133. Semenyuk, E. G., Laning, M. L., Foley, J., Johnston, P. F., Knight, K. L., Gerding, D. N., and Driks, A. (2014) Spore Formation and Toxin Production in *Clostridium difficile* Biofilms. *PLoS One.* **9**, e87757

134. Dawson, L. F., Peltier, J., Hall, C. L., Harrison, M. A., Derakhshan, M., Shaw, H. A., Fairweather, N. F., and Wren, B. W. (2021) Extracellular DNA, cell surface proteins and c-di-GMP promote biofilm formation in *Clostridioides difficile*. *Sci. Rep.* **11**, 1-21

135. Vuotto, C., Donelli, G., Buckley, A., and Chilton, C. (2018) *Clostridium difficile* Biofilm. in *Updates on Clostridium difficile* in Europe*. Adv. Microbiol. Infect. Dis. Pub Health.* **8**, 97-115

136. Rupnik, M., Wilcox, M. H., and Gerding, D. N. (2009) *Clostridium difficile* infection: new developments in epidemiology and pathogenesis. *Nat. Rev. Microbiol.* **7**, 526-536

137. James, G. A., Chesnel, L., Boegli, L., deLancey Pulcini, E., Fisher, S., and Stewart, P. S. (2018) Analysis of *Clostridium difficile* biofilms: imaging and antimicrobial treatment. *J. Antimicrob. Chemother.* **73**, 102-108

138. Boix, V., Fedorak, R. N., Mullane, K. M., Pesant, Y., Stoutenburgh, U., Jin, M., Adedoyin, A., Chesnel, L., Guris, D., Larson, K. B., and Murata, Y. (2017) Primary Outcomes From a Phase 3, Randomized, Double-Blind, Active-Controlled Trial of Surotomycin in Subjects With *Clostridium difficile* Infection. *Open Forum Infect. Dis.* **4**

139. Lawley, T. D., Clare, S., Walker, A. W., Goulding, D., Stabler, R. A., Croucher, N., Mastroeni, P., Scott, P., Raisen, C., and Mottram, L. (2009) Antibiotic treatment of *Clostridium difficile* carrier mice triggers a supershedder state, spore-mediated transmission, and severe disease in immunocompromised hosts. *Infect. Immun.* **77**, 3661-3669

140. Goulding, D., Thompson, H., Emerson, J., Fairweather, N. F., Dougan, G., and Douce, G. R. (2009) Distinctive profiles of infection and pathology in hamsters infected with *Clostridium difficile* strains 630 and B1. *Infect. Immun.* **77**, 5478-5485

141. Semenyuk, E. G., Poroyko, V. A., Johnston, P. F., Jones, S. E., Knight, K. L., Gerding, D. N., and Driks, A. (2015) Analysis of Bacterial Communities during *Clostridium difficile* infection in the Mouse. *Infect. Immun.* **83**, 4383

142. Soavelomandroso, A. P., Gaudin, F., Hoys, S., Nicolas, V., Vedantam, G., Janoir, C., and Bouttier, S. (2017) Biofilm Structures in a Mono-Associated Mouse Model of *Clostridium difficile* Infection. *Front. Microbiol.* **8**

143. Normington, C., Moura, I. B., Bryant, J. A., Ewin, D. J., Clark, E. V., Kettle, M. J., Harris, H. C., Spittal, W., Davis, G., and Henn, M. R. (2021) Biofilms harbour *Clostridioides difficile*, serving as a reservoir for recurrent infection. *npj Biofilms and Microbiomes* **7**, 1-10

144. Conrad, J. C., Gibiansky, M. L., Jin, F., Gordon, V. D., Motto, D. A., Mathewson, M. A., Stopka, W. G., Zelasko, D. C., Shrout, J. D., and Wong, G. C. (2011) Flagella and pili-mediated near-surface single-cell motility mechanisms in *P. aeruginosa*. *Biophys. J.* **100**, 1608-1616

145. Martins, D., McKay, G., Sampathkumar, G., Khakimova, M., English, A. M., and Nguyen, D. (2018) Superoxide dismutase activity confers (p)ppGpp-mediated antibiotic tolerance to stationary-phase *Pseudomonas aeruginosa*. *Proc. Natl. Acad. Sci.* **115**, 9797

146. LeGrand, E. K., and Day, J. D. (2016) Self-harm to preferentially harm the pathogens within: non-specific stressors in innate immunity. *Proc. R. Soc. [Biol].* **283**. 20160266

147. Pokhrel, A., Poudel, A., Castro, K. B., Celestine, M. J., Oludiran, A., Rinehold, A. J., Resek, A. M., Mhanna, M. A., and Purcell, E. B. (2020) The (p)ppGpp synthetase RSH mediates stationary phase onset and antibiotic stress survival in *Clostridioides difficile*. *J. Bacteriol.*

148. Atkinson, G. C., Tenson, T., and Hauryliuk, V. (2011) The RelA/SpoT homolog (RSH) superfamily: distribution and functional evolution of ppGpp synthetases and hydrolases across the tree of life. *PloS One*. **6**, e23479

149. Irving, S. E., Choudhury, N. R., and Corrigan, R. M. (2020) The stringent response and physiological roles of (pp)pGpp in bacteria. *Nat. Rev. Microbiol.* 1-16

150. Steinchen, W., Schuhmacher, J. S., Altegoer, F., Fage, C. D., Srinivasan, V., Linne, U., Marahiel, M. A., and Bange, G. (2015) Catalytic mechanism and allosteric regulation of an oligomeric (p)ppGpp synthetase by an alarmone. *Proc. Natl. Acad. Sci.* **112**, 13348-13353

151. Sajish, M., Kalayil, S., Verma, S. K., Nandicoori, V. K., and Prakash, B. (2009) The significance of EXDD and RXKD motif conservation in Rel proteins. *J. Biol. Chem.* **284**, 9115-9123

152. Gaca, A. O., Kudrin, P., Colomer-Winter, C., Beljantseva, J., Liu, K., Anderson, B., Wang, J. D., Rejman, D., Potrykus, K., and Cashel, M. (2015) From (p) ppGpp to (pp)pGpp: characterization of regulatory effects of pGpp synthesized by the small alarmone synthetase of *Enterococcus faecalis*. *J. Bacteriol.* **197**, 2908-2919

153. Yang, N., Xie, S., Tang, N.-Y., Choi, M. Y., Wang, Y., and Watt, R. M. (2019) The Ps and Qs of alarmone synthesis in *Staphylococcus aureus. PloS One*. **14**, e0213630

154. Petchiappan, A., Naik, S. Y., and Chatterji, D. (2020) RelZ-mediated stress response in *Mycobacterium smegmatis*: pGpp synthesis and its regulation. *J. Bacteriol.* **202**

155. Ruwe, M., Kalinowski, J., and Persicke, M. (2017) Identification and functional characterization of small alarmone synthetases in *Corynebacterium glutamicum*. *Front. Microbiol.* **8**, 1601

156. Yang, J., Anderson, B. W., Turdiev, A., Turdiev, H., Stevenson, D. M., Amador-Noguez, D., Lee, V. T., and Wang, J. D. (2020) The nucleotide pGpp acts as a third alarmone in Bacillus, with functions distinct from those of (p) ppGpp. *Nat. Commun.* **11**, 1-11

157. Yang, J., Anderson, B. W., Turdiev, A., Turdiev, H., Stevenson, D. M., Amador-Noguez, D., Lee, V. T., and Wang, J. D. (2020) Systemic characterization of pppGpp, ppGpp and pGpp targets in Bacillus reveal NahA converts (p) ppGpp to pGpp to regulate alarmone composition and signaling. *bioRxiv*

158. Irving, S. E., and Corrigan, R. M. (2018) Triggering the stringent response: signals responsible for activating (p)ppGpp synthesis in bacteria. *Microbiology*. **164**, 268-276

159. Hogg, T., Mechold, U., Malke, H., Cashel, M., and Hilgenfeld, R. (2004) Conformational antagonism between opposing active sites in a bifunctional RelA/SpoT homolog modulates (p)ppGpp metabolism during the stringent response. *Cell*. **117**, 57-68

160. Mechold, U., Murphy, H., Brown, L., and Cashel, M. (2002) Intramolecular regulation of the opposing (p)ppGpp catalytic activities of Rel(Seq), the Rel/Spo enzyme from *Streptococcus equisimilis*. *J. Bacteriol.* **184**, 2878-2888

161. Bag, S., Das, B., Dasgupta, S., and Bhadra, R. K. (2014) Mutational analysis of the (p)ppGpp synthetase activity of the Rel enzyme of *Mycobacterium tuberculosis*. *Arch. Microbiol.* **196**, 575-588

162. Tamman, H., Van Nerom, K., Takada, H., Vandenberk, N., Scholl, D., Polikanov, Y., Hofkens, J., Talavera, A., Hauryliuk, V., and Hendrix, J. (2020) A nucleotide-switch mechanism mediates opposing catalytic activities of Rel enzymes. *Nat. Chem. Biol.* 1-7

163. Syal, K., Joshi, H., Chatterji, D., and Jain, V. (2015) Novel pppGpp binding site at the C-terminal region of the Rel enzyme from *Mycobacterium smegmatis*. *The FEBS. J.* **282**, 3773-3785

164. Gratani, F. L., Horvatek, P., Geiger, T., Borisova, M., Mayer, C., Grin, I., Wagner, S., Steinchen, W., Bange, G., and Velic, A. (2018) Regulation of the opposing (p) ppGpp synthetase and hydrolase activities in a bifunctional RelA/SpoT homologue from *Staphylococcus aureus*. *PLoS Genet.* **14**, e1007514

165. Ronneau, S., Caballero-Montes, J., Coppine, J., Mayard, A., Garcia-Pino, A., and Hallez, R. (2019) Regulation of (p)ppGpp hydrolysis by a conserved archetypal regulatory domain. *Nucleic Acids. Res.* **47**, 843-854

166. Fang, M., and Bauer, C. E. (2018) Regulation of stringent factor by branched-chain amino acids. *Proc. Natl. Acad. Sci.* **115**, 6446-6451

167. Lemos, J. A., Lin, V. K., Nascimento, M. M., Abranches, J., and Burne, R. A. (2007) Three gene products govern (p) ppGpp production by *Streptococcus mutans*. *Mol. Microbiol.* **65**, 1568-1581

168. Nanamiya, H., Kasai, K., Nozawa, A., Yun, C. S., Narisawa, T., Murakami, K., Natori, Y., Kawamura, F., and Tozawa, Y. (2008) Identification and functional analysis of novel (p) ppGpp synthetase genes in *Bacillus subtilis*. *Mol. Microbiol.* **67**, 291-304

169. Jimmy, S., Saha, C. K., Kurata, T., Stavropoulos, C., Oliveira, S. R. A., Koh, A., Cepauskas, A., Takada, H., Rejman, D., and Tenson, T. (2020) A widespread toxin− antitoxin system exploiting growth control via alarmone signaling. *Proc. Natl. Acad. Sci.* **117**, 10500-10510

170. Das, B., Pal, R. R., Bag, S., and Bhadra, R. K. (2009) Stringent response in *Vibrio cholerae*: genetic analysis of spoT gene function and identification of a novel (p) ppGpp synthetase gene. *Mol. Microbiol.* **72**, 380-398

171. Murdeshwar, M. S., and Chatterji, D. (2012) MS_RHII-RSD, a dual-function RNase HII-(p)ppGpp synthetase from *Mycobacterium smegmatis*. *J. Bacteriol.* **194**, 4003-4014

172. Ruwe, M., Rückert, C., Kalinowski, J., and Persicke, M. (2018) Functional Characterization of a Small Alarmone Hydrolase in *Corynebacterium glutamicum*. *Front. Microbiol.* **9**, 916
173. Boniecka, J., Prusińska, J., Dąbrowska, G. B., and Goc, A. (2017) Within and beyond the stringent response-RSH and (p)ppGpp in plants. *Planta*. **246**, 817-842
174. Ito, D., Ihara, Y., Nishihara, H., and Masuda, S. (2017) Phylogenetic analysis of proteins involved in the stringent response in plant cells. *J. Plant Res.* **130**, 625-634
175. Doshun, I., Hinata, K., Akira, O., Yuta, I., Toshio, S., Nakamura, N., Tsunaki, A., Shun-Ichiro, K., Suzuki, T., and Shinji, M. (2020) ppGpp functions as an alarmone in metazoa. *Commun. Biol.* **3**
176. Keasling, J., Bertsch, L., and Kornberg, A. (1993) Guanosine pentaphosphate phosphohydrolase of *Escherichia coli* is a long-chain exopolyphosphatase. *Proc. Natl. Acad. Sci.* **90**, 7029-7033
177. Sanyal, R., and Harinarayanan, R. (2020) Activation of RelA by pppGpp as the basis for its differential toxicity over ppGpp in *Escherichia coli. J. Biosci.* **45**, 28
178. Mechold, U., Potrykus, K., Murphy, H., Murakami, K. S., and Cashel, M. (2013) Differential regulation by ppGpp versus pppGpp in *Escherichia coli*. *Nucleic Acids. Res.* **41**, 6175-6189
179. Zhang, Y., Zborníková, E., Rejman, D., and Gerdes, K. (2018) Novel (p) ppGpp binding and metabolizing proteins of *Escherichia coli. MBio*. **9**, e02188-02117
180. Gao, A., Vasilyev, N., Kaushik, A., Duan, W., and Serganov, A. (2020) Principles of RNA and nucleotide discrimination by the RNA processing enzyme RppH. *Nucleic Acids. Res.* **48**, 3776-3788
181. Choi, M. Y., Wang, Y., Wong, L. L., Lu, B.-t., Chen, W.-y., Huang, J.-D., Tanner, J. A., and Watt, R. M. (2012) The two PPX-GppA homologues from *Mycobacterium tuberculosis* have distinct biochemical activities. *PLoS One*. **7**
182. Boutte, C. C., and Crosson, S. (2013) Bacterial lifestyle shapes stringent response activation. *Trends. Microbiol.* **21**, 174-180
183. Anderson, K. L., Roberts, C., Disz, T., Vonstein, V., Hwang, K., Overbeek, R., Olson, P. D., Projan, S. J., and Dunman, P. M. (2006) Characterization of the

Staphylococcus aureus heat shock, cold shock, stringent, and SOS responses and their effects on log-phase mRNA turnover. *J. Bacteriol.* **188**, 6739-6756

184. Zhang, T., Zhu, J., Wei, S., Luo, Q., Li, L., Li, S., Tucker, A., Shao, H., and Zhou, R. (2016) The roles of RelA/(p)ppGpp in glucose-starvation induced adaptive response in the zoonotic *Streptococcus suis*. *Sci. Rep.* **6**, 27169
185. Pulschen, A. A., Sastre, D. E., Machinandiarena, F., Crotta Asis, A., Albanesi, D., de Mendoza, D., and Gueiros-Filho, F. J. (2017) The stringent response plays a key role in *Bacillus subtilis* survival of fatty acid starvation. *Mol. Microbiol.* **103**, 698-712
186. Miethke, M., Westers, H., Blom, E.-J., Kuipers, O. P., and Marahiel, M. A. (2006) Iron starvation triggers the stringent response and induces amino acid biosynthesis for bacillibactin production in *Bacillus subtilis*. *J. Bacteriol.* **188**, 8655-8657
187. Colomer-Winter, C., Gaca, A., and Lemos, J. (2017) Association of metal homeostasis and (p) ppGpp regulation in the pathophysiology of *Enterococcus faecalis*. *Infect. Immun.* **85**, e00260-00217
188. Ronneau, S., and Hallez, R. (2019) Make and break the alarmone: regulation of (p ppGpp synthetase/hydrolase enzymes in bacteria. *FEMS Microbiol. Rev.* **43**, 389-400
189. Lin, C.-Y., Awano, N., Masuda, H., Park, J.-H., and Inouye, M. (2013) Transcriptional repressor HipB regulates the multiple promoters in *Escherichia coli*. *J. Mol. Microbiol. Biotechnol.* **23**, 440-447
190. Maisonneuve, E., Castro-Camargo, M., and Gerdes, K. (2013) (p)ppGpp Controls Bacterial Persistence by Stochastic Induction of Toxin-Antitoxin Activity. Elsevier
191. Cavanagh, A. T., Chandrangsu, P., and Wassarman, K. M. (2010) 6S RNA regulation of relA alters ppGpp levels in early stationary phase. *Microbiology*. **156**, 3791
192. Reiß, S., Pané-Farré, J., Fuchs, S., François, P., Liebeke, M., Schrenzel, J., Lindequist, U., Lalk, M., Wolz, C., and Hecker, M. (2012) Global analysis of the *Staphylococcus aureus* response to mupirocin. *Antimicrob. Agents Chemother.* **56**, 787-804

193. Hughes, J., and Mellows, G. (1978) Inhibition of isoleucyl-transfer ribonucleic acid synthetase in *Echerichia coli* by pseudomonic acid. *Biochem. J.* **176**, 305-318

194. Hughes, J., and Mellows, G. (1980) Interaction of pseudomonic acid A with *Escherichia coli* B isoleucyl-tRNA synthetase. *Biochem. J.* **191**, 209-219

195. Pisu, D., Provvedi, R., Espinosa, D. M., Payan, J. B., Boldrin, F., Palù, G., Hernandez-Pando, R., and Manganelli, R. (2017) The alternative sigma factors SigE and SigB are involved in tolerance and persistence to antitubercular drugs. *Antimicrob. Agents Chemother.* **61**

196. Sureka, K., Dey, S., Datta, P., Singh, A. K., Dasgupta, A., Rodrigue, S., Basu, J., and Kundu, M. (2007) Polyphosphate kinase is involved in stress-induced mprAB-sigE-rel signalling in Mycobacteria. *Mol. Microbiol.* **65**, 261-276

197. Eiamphungporn, W., and Helmann, J. D. (2008) The *Bacillus subtilis* σM regulon and its contribution to cell envelope stress responses. *Mol. Microbiol.* **67**, 830-848

198. Cao, M., Kobel, P. A., Morshedi, M. M., Wu, M. F. W., Paddon, C., and Helmann, J. D. (2002) Defining the *Bacillus subtilis* σW regulon: a comparative analysis of promoter consensus search, run-off transcription/macroarray analysis (ROMA), and transcriptional profiling approaches. *J. Mol. Biol.* **316**, 443-457

199. Geiger, T., Kästle, B., Gratani, F. L., Goerke, C., and Wolz, C. (2014) Two small (p) ppGpp synthases in *Staphylococcus aureus* mediate tolerance against cell envelope stress conditions. *J. Bacteriol.* **196**, 894-902

200. Pando, J. M., Pfeltz, R. F., Cuaron, J. A., Nagarajan, V., Mishra, M. N., Torres, N. J., Elasri, M. O., Wilkinson, B. J., and Gustafson, J. E. (2017) Ethanol-induced stress response of *Staphylococcus aureus*. *Can. J. Microbiol.* **63**, 745-757

201. Maciąg, M., Kochanowska, M., Łyżeń, R., Węgrzyn, G., and Szalewska-Pałasz, A. (2010) ppGpp inhibits the activity of *Escherichia coli* DnaG primase. *Plasmid*. **63**, 61-67

202. Frick, D. N., and Richardson, C. C. (2001) DNA primases. *Annu. Rev. Biochem.* **70**, 39-80

203. Wang, J. D., Sanders, G. M., and Grossman, A. D. (2007) Nutritional control of elongation of DNA replication by (p)ppGpp. *Cell*. **128**, 865-875

204. Gourse, R. L., Chen, A. Y., Gopalkrishnan, S., Sanchez-Vazquez, P., Myers, A., and Ross, W. (2018) Transcriptional responses to ppGpp and DksA. *Annu. Rev. Microbiol.* **72**, 163-184

205. Krásný, L., and Gourse, R. L. (2004) An alternative strategy for bacterial ribosome synthesis: *Bacillus subtilis* rRNA transcription regulation. *EMBO J.* **23**, 4473-4483

206. Kriel, A., Bittner, A. N., Kim, S. H., Liu, K., Tehranchi, A. K., Zou, W. Y., Rendon, S., Chen, R., Tu, B. P., and Wang, J. D. (2012) Direct regulation of GTP homeostasis by (p) ppGpp: a critical component of viability and stress resistance. *Mol. Cell.* **48**, 231-241

207. Hochstadt-Ozer, J., and Cashel, M. (1972) The Regulation of Purine Utilization in Bacteria V. Inhibition of purine hosphoribosyltransferase activities and purine uptake in isolated membrane vesicled by guanosine tetraphopshate. *J. Biol. Chem.* **247**, 7067-7072

208. Krásný, L., Tišerová, H., Jonák, J., Rejman, D., and Šanderová, H. (2008) The identity of the transcription+ 1 position is crucial for changes in gene expression in response to amino acid starvation in *Bacillus subtilis*. *Mol. Microbiol.* **69**, 42-54

209. Kästle, B., Geiger, T., Gratani, F. L., Reisinger, R., Goerke, C., Borisova, M., Mayer, C., and Wolz, C. (2015) rRNA regulation during growth and under stringent conditions in *Staphylococcus aureus*. *Environ. Microbiol.* **17**, 4394-4405

210. Sonenshein, A. L. (2005) CodY, a global regulator of stationary phase and virulence in Gram-positive bacteria. *Curr. Opin. Microbiol.* **8**, 203-207

211. Ahn, S. J., Kim, H. M., Desai, S., Deep, K., and Rice, K. C. (2020) Regulation of cid and lrg expression by CodY in *Streptococcus mutans*. *Microbiol Open*. e1040

212. Majerczyk, C. D., Dunman, P. M., Luong, T. T., Lee, C. Y., Sadykov, M. R., Somerville, G. A., Bodi, K., and Sonenshein, A. L. (2010) Direct targets of CodY in *Staphylococcus aureus*. *J. Bacteriol.* **192**, 2861-2877

213. Geiger, T., Francois, P., Liebeke, M., Fraunholz, M., Goerke, C., Krismer, B., Schrenzel, J., Lalk, M., and Wolz, C. (2012) The stringent response of *Staphylococcus aureus* and its impact on survival after phagocytosis through the induction of intracellular PSMs expression. *PLoS Pathog*. **8**, e1003016

214. Yoshida, M., Travers, A., and Clark, B. F. (1972) Inhibition of translation initiation complex formation by MS1. *FEBS Lett*. **23**, 163-166

215. Milon, P., Tischenko, E., Tomšic, J., Caserta, E., Folkers, G., La Teana, A., Rodnina, M. V., Pon, C. L., Boelens, R., and Gualerzi, C. O. (2006) The nucleotide-binding site of bacterial translation initiation factor 2 (IF2) as a metabolic sensor. *Proc. Natl. Acad. Sci.* **103**, 13962-13967

216. Steinchen, W., and Bange, G. (2016) The magic dance of the alarmones (p) ppGpp. *Mol. Microbiol.* **101**, 531-544

217. Corrigan, R. M., Bellows, L. E., Wood, A., and Gründling, A. (2016) ppGpp negatively impacts ribosome assembly affecting growth and antimicrobial tolerance in Gram-positive bacteria. *Proc. Natl. Acad. Sci.* **113**, E1710-E1719

218. Vinogradova, D. S., Zegarra, V., Maksimova, E., Nakamoto, J. A., Kasatsky, P., Paleskava, A., Konevega, A. L., and Milón, P. (2020) How the initiating ribosome copes with ppGpp to translate mRNAs. *PLoS Biol.* **18**, e3000593

219. Dalebroux, Z. D., Svensson, S. L., Gaynor, E. C., and Swanson, M. S. (2010) ppGpp conjures bacterial virulence. *Microbiol. Mol. Biol. Rev.* **74**, 171-199

220. Pizarro-Cerdá, J., and Tedin, K. (2004) The bacterial signal molecule, ppGpp, regulates Salmonella virulence gene expression. *Mol. Microbiol.* **52**, 1827-1844

221. Zhao, G., Weatherspoon, N., Kong, W., Curtiss, R., and Shi, Y. (2008) A dual-signal regulatory circuit activates transcription of a set of divergent operons in *Salmonella typhimurium*. *Proc. Natl. Acad. Sci.* **105**, 20924-20929

222. Nishio, M., Okada, N., Miki, T., Haneda, T., and Danbara, H. (2005) Identification of the outer-membrane protein PagC required for the serum resistance phenotype in *Salmonella enterica serovar Choleraesuis*. *Microbiology*. **151**, 863-873

223. Dasgupta, S., Das, S., Biswas, A., Bhadra, R. K., and Das, S. (2019) Small alarmones (p) ppGpp regulate virulence associated traits and pathogenesis of *Salmonella enterica serovar Typhi*. *Cell. Microbiol.* **21**, e13034

224. Gaynor, E. C., Wells, D. H., MacKichan, J. K., and Falkow, S. (2005) The *Campylobacter jejuni* stringent response controls specific stress survival and virulence-associated phenotypes. *Mol. Microbiol.* **56**, 8-27

225. Vogt, S. L., Green, C., Stevens, K. M., Day, B., Erickson, D. L., Woods, D. E., and Storey, D. G. (2011) The stringent response is essential for Pseudomonas aeruginosa virulence in the rat lung agar bead and *Drosophila melanogaster* feeding models of infection. *Infect. Immun.* **79**, 4094-4104

226. Xu, X., Yu, H., Zhang, D., Xiong, J., Qiu, J., Xin, R., He, X., Sheng, H., Cai, W., and Jiang, L. (2016) Role of ppGpp in *Pseudomonas aeruginosa* acute pulmonary infection and virulence regulation. *Microbiol. Res.* **192**, 84-95

227. Viducic, D., Ono, T., Murakami, K., Susilowati, H., Kayama, S., Hirota, K., and Miyake, Y. (2006) Functional analysis of spoT, relA and dksA genes on quinolone tolerance in *Pseudomonas aeruginosa* under nongrowing condition. *Microbiol. Immunol.* **50**, 349-357

228. Åberg, A., Shingler, V., and Balsalobre, C. (2006) (p)ppGpp regulates type 1 fimbriation of *Escherichia coli* by modulating the expression of the site-specific recombinase FimB. *Mol. Microbiol.* **60**, 1520-1533

229. He, H., Cooper, J. N., Mishra, A., and Raskin, D. M. (2012) Stringent response regulation of biofilm formation in *Vibrio cholerae*. *J. Bacteriol.* **194**, 2962-2972

230. Lemos, J. A., Brown, T. A., and Burne, R. A. (2004) Effects of RelA on key virulence properties of planktonic and biofilm populations of *Streptococcus mutans. Infect. Immun.* **72**, 1431-1440

231. Van Schaik, W., Prigent, J., and Fouet, A. (2007) The stringent response of *Bacillus anthracis* contributes to sporulation but not to virulence. *Microbiology*. **153**, 4234-4239

232. Raskin, D. M., Mishra, A., He, H., and Lundy, Z. (2020) Stringent response interacts with the ToxR regulon to regulate *Vibrio cholerae* virulence factor expression. *Arch. Microbiol.* 1-10

233. Wexselblatt, E., Oppenheimer-Shaanan, Y., Kaspy, I., London, N., Schueler-Furman, O., Yavin, E., Glaser, G., Katzhendler, J., and Ben-Yehuda, S. (2012) Relacin, a novel antibacterial agent targeting the stringent response. *PLoS Pathog.* **8**, 1002925

234. Kushwaha, G. S., Oyeyemi, B. F., and Bhavesh, N. S. (2019) Stringent response protein as a potential target to intervene persistent bacterial infection. *Biochimie.* **165**, 67-75

235. Wexselblatt, E., Kaspy, I., Glaser, G., Katzhendler, J., and Yavin, E. (2013) Design, synthesis and structure–activity relationship of novel Relacin analogs as inhibitors of Rel proteins. *Eur. J. Med. Chem.* **70**, 497-504

236. Syal, K., Flentie, K., Bhardwaj, N., Maiti, K., Jayaraman, N., Stallings, C. L., and Chatterji, D. (2017) Synthetic (p) ppGpp analogue is an inhibitor of stringent response in Mycobacteria. *Antimicrob. Agents Chemother.* **61**, 00443-00417

237. Tosa, T., and Pizer, L. I. (1971) Effect of serine hydroxamate on the growth of *Escherichia coli*. *J. Bacteriol.* **106**, e966-e971

238. Syal, K., Bhardwaj, N., and Chatterji, D. (2016) Vitamin C targets (p) ppGpp synthesis leading to stalling of long-term survival and biofilm formation in *Mycobacterium smegmatis*. *FEMS Microbiol. Lett.* **364**, fnw282

239. Reffuveille, F., De La Fuente-Nũnez, C., Mansour, S., and Hancock, R. E. (2014) A broad-spectrum antibiofilm peptide enhances antibiotic action against bacterial biofilms. *Antimicrob. Agents Chemother.* **58**, 5363-5371

240. De la Fuente-Núñez, C., Reffuveille, F., Haney, E. F., Straus, S. K., and Hancock, R. E. (2014) Broad-spectrum anti-biofilm peptide that targets a cellular stress response. *PLoS Pathog*. **10**, e1004152

241. Tkachenko, A. G., Kashevarova, N. M., Sidorov, R. Y., Nesterova, L. Y., Akhova, A. V., Tsyganov, I. V., Vaganov, V. Y., Shipilovskikh, S. A., Rubtsov, A. E., and Malkov, A. V. (2021) A synthetic diterpene analogue inhibits mycobacterial persistence and biofilm formation by targeting (p)ppGpp synthetases. *Cell Chem. Biol*

242. Potrykus, K., and Cashel, M. (2008) (p)ppGpp: Still Magical? *Annu. Rev. Microbiol.* **62**, 35-51

243. Avarbock, D., Avarbock, A., and Rubin, H. (2000) Differential Regulation of Opposing RelMtb Activities by the Aminoacylation State of a tRNA⊙ Ribosome⊙ mRNA⊙ RelMtb Complex. *Biochemistry*. **39**, 11640-11648

244. Gaca, A. O., Kajfasz, J. K., Miller, J. H., Liu, K., Wang, J. D., Abranches, J., and Lemos, J. A. (2013) Basal levels of (p)ppGpp in *Enterococcus faecalis*: the magic beyond the stringent response. *MBio*. **4**

245. Krishnan, S., and Chatterji, D. (2020) Pleiotropic Effects of Bacterial Small Alarmone Synthetases: Underscoring the Dual-Domain Small Alarmone Synthetases in *Mycobacterium smegmatis*. *Front. Microbiol.* **11**, 2499

246. Gaca, A. O., Colomer-Winter, C., and Lemos, J. A. (2015) Many means to a common end: the intricacies of (p)ppGpp metabolism and its control of bacterial homeostasis. *J. Bacteriol.* **197**, 1146-1156

247. Sajish, M., Tiwari, D., Rananaware, D., Nandicoori, V. K., and Prakash, B. (2007) A charge reversal differentiates (p)ppGpp synthesis by monofunctional and bifunctional Rel proteins. *J. Biol. Chem.* **282**, 34977-34983

248. Pokhrel, A., Poudel, A., and Purcell, E. B. (2018) A Purification and *In Vitro* Activity Assay for a (p) ppGpp Synthetase from *Clostridium difficile*. *JoVE (J. Vis. Exp.)*, e58547

249. Schneider, C. A., Rasband, W. S., and Eliceiri, K. W. (2012) NIH Image to ImageJ: 25 years of image analysis. *Nat. Methods.* **9**, 671-675

250. Svitil, A., Cashel, M., and Zyskind, J. (1993) Guanosine tetraphosphate inhibits protein synthesis *in vivo*. A possible protective mechanism for starvation stress in *Escherichia coli*. *J. Biol. Chem.* **268**, 2307-2311

251. Steinchen, W., Zegarra, V., and Bange, G. (2020) (p)ppGpp: Magic modulators of bacterial physiology and metabolism. *Front. Microbiol.* **11**, 2072

252. Buckstein, M. H., He, J., and Rubin, H. (2008) Characterization of nucleotide pools as a function of physiological state in *Escherichia coli*. *J. Bacteriol.* **190**, 718-726

253. Shyp, V., Tankov, S., Ermakov, A., Kudrin, P., English, B. P., Ehrenberg, M., Tenson, T., Elf, J., and Hauryliuk, V. (2012) Positive allosteric feedback regulation of the stringent response enzyme RelA by its product. *EMBO reports* **13**, 835-839

254. Gasteiger, E., Gattiker, A., Hoogland, C., Ivanyi, I., Appel, R. D., and Bairoch, A. (2003) ExPASy: the proteomics server for in-depth protein knowledge and analysis. *Nucleic Acids Res.* **31**, 3784-3788

255. Nugent, S., Kumar, D., Rampton, D., and Evans, D. (2001) Intestinal luminal pH in inflammatory bowel disease: possible determinants and implications for therapy with aminosalicylates and other drugs. *Gut*. **48**, 571-577

256. Trachsel, E., Redder, P., Linder, P., and Armitano, J. (2019) Genetic screens reveal novel major and minor players in magnesium homeostasis of *Staphylococcus aureus*. *PLoS Genet.* **15**, e1008336

257. Avarbock, D., Salem, J., Li, L.-s., Wang, Z.-m., and Rubin, H. (1999) Cloning and characterization of a bifunctional RelA/SpoT homologue from *Mycobacterium tuberculosis*. *Gene*. **233**, 261-269

258. Sobala, M., Bruhn-Olszewska, B., Cashel, M., and Potrykus, K. (2019) *Methylobacterium extorquens* RSH enzyme synthesizes (p) ppGpp and pppApp *in vitro* and *in vivo*, and leads to discovery of pppApp synthesis in *Escherichia coli. Front. Microbiol.* **10**, 859

259. Vashishtha, A. K., and Konigsberg, W. H. (2016) Effect of different divalent cations on the kinetics and fidelity of RB69 DNA polymerase. *Biochemistry*. **55**, 2661-2670

260. Vashishtha, A. K., Wang, J., and Konigsberg, W. H. (2016) Different divalent cations alter the kinetics and fidelity of DNA polymerases. *J. Biol. Chem.* **291**, 20869-20875

261. Park, J. O., Rubin, S. A., Xu, Y.-F., Amador-Noguez, D., Fan, J., Shlomi, T., and Rabinowitz, J. D. (2016) Metabolite concentrations, fluxes and free energies imply efficient enzyme usage. *Nat. Chem. Biol.* **12**, 482-489

262. Varik, V., Oliveira, S. R. A., Hauryliuk, V., and Tenson, T. (2017) HPLC-based quantification of bacterial housekeeping nucleotides and alarmone messengers ppGpp and pppGpp. *Sci. Rep.* **7**, 1-12

263. Gropp, M., Strausz, Y., Gross, M., and Glaser, G. (2001) Regulation of *Escherichia coli* RelA requires oligomerization of the C-terminal domain. *J. Bacteriol.* **183**, 570-579

264. Winther, K. S., Roghanian, M., and Gerdes, K. (2018) Activation of the stringent response by loading of RelA-tRNA complexes at the ribosomal A-site. *Mol. Cell.* **70**, 95-105. e104

265. Shin, J., Singal, B., Sony Subramanian Manimekalai, M., Wei Chen, M., Ragunathan, P., and Grüber, G. (2020) Atomic structure of, and valine binding to the regulatory ACT domain of the *Mycobacterium tuberculosis* Rel protein. *FEBS J*

266. Guan, Y., Zhu, Q., Huang, D., Zhao, S., Lo, L. J., and Peng, J. (2015) An equation to estimate the difference between theoretically predicted and SDS PAGE-displayed molecular weights for an acidic peptide. *Sci. Rep.* **5**, 1-11

267. Fung, D. K., Yang, J., Stevenson, D. M., Amador-Noguez, D., and Wang, J. D. (2020) Small Alarmone Synthetase SasA Expression Leads to Concomitant Accumulation of pGpp, ppApp, and AppppA in *Bacillus subtilis. Front. Microbiol.* **11**

268. Vinella, D., Albrecht, C., Cashel, M., and D'Ari, R. (2005) Iron limitation induces SpoT-dependent accumulation of ppGpp in *Escherichia coli*. *Mol. Microbiol.* **56**, 958-970

269. Hauryliuk, V., Atkinson, G. C., Murakami, K. S., Tenson, T., and Gerdes, K. (2015) Recent functional insights into the role of (p) ppGpp in bacterial physiology. *Nat. Rev. Microbiol.* **13**, 298-309

270. Kolter, R., Siegele, D. A., and Tormo, A. (1993) The stationary phase of the bacterial life cycle. *Annu. Rev. Microbiol.* **47**, 855-874

271. Emerson, J. E., Stabler, R. A., Wren, B. W., and Fairweather, N. F. (2008) Microarray analysis of the transcriptional responses of *Clostridium difficile* to environmental and antibiotic stress. *J. Med. Microbiol.* **57**, 757-764

272. Appelbaum, P. C., and Bozdogan, B. (2004) Vancomycin resistance in *Staphylococcus aureus*. *Clin. Lab. Med.* **24**, 381-402

273. Buckley, A. M., Jukes, C., Candlish, D., Irvine, J. J., Spencer, J., Fagan, R. P., Roe, A. J., Christie, J. M., Fairweather, N. F., and Douce, G. R. (2016) Lighting Up *Clostridium difficile*: Reporting Gene Expression Using Fluorescent Lov Domains. *Sci. Rep.* **6**, 23463

274. Aedo, S., and Tomasz, A. (2016) Role of the Stringent Stress Response in the Antibiotic Resistance Phenotype of Methicillin-Resistant *Staphylococcus aureus*. *Antimicrob. Agents Chemother.* **60**, 2311

275. Ooga, T., Ohashi, Y., Kuramitsu, S., Koyama, Y., Tomita, M., Soga, T., and Masui, R. (2009) Degradation of ppGpp by nudix pyrophosphatase modulates the transition of growth phase in the bacterium *Thermus thermophilus*. *J. Biol. Chem.* **284**, 15549-15556

276. Aspevall, O., Lundberg, A., Burman, L. G., Åkerlund, T., and Svenungsson, B. (2006) Antimicrobial susceptibility pattern of *Clostridium difficile* and its relation to PCR ribotypes in a Swedish university hospital. *Antimicrob. Agents Chemother.* **50**, 1890-1892

277. Acosta, R., and Lueking, D. R. (1987) Stringency in the absence of ppGpp accumulation in *Rhodobacter sphaeroides*. *J. Bacteriol.* **169**, 908-912

278. Andresen, L., Varik, V., Tozawa, Y., Jimmy, S., Lindberg, S., Tenson, T., and Hauryliuk, V. (2016) Auxotrophy-based High Throughput Screening assay for the identification of *Bacillus subtilis* stringent response inhibitors. *Sci. Rep.* **6**, 35824

279. Beljantseva, J., Kudrin, P., Jimmy, S., Ehn, M., Pohl, R., Varik, V., Tozawa, Y., Shingler, V., Tenson, T., and Rejman, D. (2017) Molecular mutagenesis of ppGpp: turning a RelA activator into an inhibitor. *Sci. Rep.* **7**, 1-10

280. Dutta, N. K., Klinkenberg, L. G., Vazquez, M.-J., Segura-Carro, D., Colmenarejo, G., Ramon, F., Rodriguez-Miquel, B., Mata-Cantero, L., Porras-De Francisco, E., and Chuang, Y.-M. (2019) Inhibiting the stringent response blocks *Mycobacterium tuberculosis* entry into quiescence and reduces persistence. *Sci. Adv.* **5**, eaav2104

281. Cohen, S. H., Gerding, D. N., Johnson, S., Kelly, C. P., Loo, V. G., McDonald, L. C., Pepin, J., and Wilcox, M. H. (2010) Clinical practice guidelines for *Clostridium difficile* infection in adults: 2010 update by the society for healthcare epidemiology of America (SHEA) and the infectious diseases society of America (IDSA). *Infect. Control Hosp. Epidemiol.* **31**, 431-455

282. Ozaki, E., Kato, H., Kita, H., Karasawa, T., Maegawa, T., Koino, Y., Matsumoto, K., Takada, T., Nomoto, K., and Tanaka, R. (2004) *Clostridium difficile* colonization in healthy adults: transient colonization and correlation with enterococcal colonization. *J. Med. Microbiol.* **53**, 167-172

283. Terveer, E. M., Crobach, M. J., Sanders, I. M., Vos, M. C., Verduin, C. M., and Kuijper, E. J. (2017) Detection of *Clostridium difficile* in feces of asymptomatic patients admitted to the hospital. *J. Clin. Microbiol.* **55**, 403-411

284. Guerrero, D., Becker, J., Eckstein, E., Kundrapu, S., Deshpande, A., Sethi, A., and Donskey, C. (2013) Asymptomatic carriage of toxigenic *Clostridium difficile* by hospitalized patients. *J. Hosp. infect.* **85**, 155-158

285. Leekha, S., Aronhalt, K. C., Sloan, L. M., Patel, R., and Orenstein, R. (2013) Asymptomatic *Clostridium difficile* colonization in a tertiary care hospital: admission prevalence and risk factors. *Am. J. Infect. Control.* **41**, 390-393

286. Bauer, M., Farid, A., Bakker, M., Hoek, R., Kuijper, E., and van Dissel, J. (2014) Patients with cystic fibrosis have a high carriage rate of non-toxigenic *Clostridium difficile*. *Clin. Microbiol. Infect.* **20**, O446-O449

287. Rousseau, C., Poilane, I., De Pontual, L., Maherault, A.-C., Le Monnier, A., and Collignon, A. (2012) *Clostridium difficile* carriage in healthy infants in the community: a potential reservoir for pathogenic strains. *Clin. Infect. Dis.* **55**, 1209-1215

288. Schwartz, K. L., Darwish, I., Richardson, S. E., Mulvey, M. R., and Thampi, N. (2014) Severe clinical outcome is uncommon in *Clostridium difficile* infection in children: a retrospective cohort study. *BMC Pediatr.* **14**, 28

289. van Dorp, S. M., Smajlović, E., Knetsch, C. W., Notermans, D. W., de Greeff, S. C., and Kuijper, E. J. (2017) Clinical and microbiological characteristics of *Clostridium difficile* infection among hospitalized children in the Netherlands. *Clin. Infect. Dis.* **64**, 192-198

290. Rajilić-Stojanović, M., Heilig, H. G., Molenaar, D., Kajander, K., Surakka, A., Smidt, H., and De Vos, W. M. (2009) Development and application of the human intestinal tract chip, a phylogenetic microarray: analysis of universally conserved phylotypes in the abundant microbiota of young and elderly adults. *Environ. Microbiol.* **11**, 1736-1751

291. Matamoros, S., Gras-Leguen, C., Le Vacon, F., Potel, G., and de La Cochetiere, M.-F. (2013) Development of intestinal microbiota in infants and its impact on health. *Trends. Microbiol.* **21**, 167-173

292. Bartlett, J. G. (2010) *Clostridium difficile*: progress and challenges. *Ann. N. Y. Acad. Sci.* **1213**, 62-69

293. Manges, A. R., Labbe, A., Loo, V. G., Atherton, J. K., Behr, M. A., Masson, L., Tellis, P. A., and Brousseau, R. (2010) Comparative metagenomic study of alterations to the intestinal microbiota and risk of nosocomial *Clostridum difficile*-associated disease. *J. Infect. Dis.* **202**, 1877-1884

294. Antharam, V. C., Li, E. C., Ishmael, A., Sharma, A., Mai, V., Rand, K. H., and Wang, G. P. (2013) Intestinal dysbiosis and depletion of butyrogenic bacteria in *Clostridium difficile* infection and nosocomial diarrhea. *J. Clin. Microbiol.* **51**, 2884-2892

295. Buffie, C. G., Jarchum, I., Equinda, M., Lipuma, L., Gobourne, A., Viale, A., Ubeda, C., Xavier, J., and Pamer, E. G. (2012) Profound alterations of intestinal microbiota following a single dose of clindamycin results in sustained susceptibility to *Clostridium difficile*-induced colitis. *Infect. Immun.* **80**, 62-73

296. Reeves, A. E., Theriot, C. M., Bergin, I. L., Huffnagle, G. B., Schloss, P. D., and Young, V. B. (2011) The interplay between microbiome dynamics and pathogen dynamics in a murine model of *Clostridium difficile* infection. *Gut Microbes*. **2**, 145-158

297. Zhang, L., Dong, D., Jiang, C., Li, Z., Wang, X., and Peng, Y. (2015) Insight into alteration of gut microbiota in *Clostridium difficile* infection and asymptomatic C. difficile colonization. *Anaerobe*. **34**, 1-7

298. Reeves, A. E., Koenigsknecht, M. J., Bergin, I. L., and Young, V. B. (2012) Suppression of *Clostridium difficile* in the gastrointestinal tracts of germfree mice inoculated with a murine isolate from the family Lachnospiraceae. *Infect. Immun.* **80**, 3786-3794

299. Macfarlane, G. T., and Macfarlane, S. (2012) Bacteria, colonic fermentation, and gastrointestinal health. *J. AOAC Int.* **95**, 50-60

300. Theriot, C. M., Koenigsknecht, M. J., Carlson Jr, P. E., Hatton, G. E., Nelson, A. M., Li, B., Huffnagle, G. B., Li, J. Z., and Young, V. B. (2014) Antibiotic-induced shifts in the mouse gut microbiome and metabolome increase susceptibility to *Clostridium difficile* infection. *Nat. Commun.* **5**, 3114

301. Hashimoto, T., Perlot, T., Rehman, A., Trichereau, J., Ishiguro, H., Paolino, M., Sigl, V., Hanada, T., Hanada, R., and Lipinski, S. (2012) ACE2 links amino acid malnutrition to microbial ecology and intestinal inflammation. *Nature.* **487**, 477-481
302. Engevik, M. A., Engevik, A. C., Engevik, K. A., Auchtung, J. M., Chang-Graham, A. L., Ruan, W., Luna, R. A., Hyser, J. M., Spinler, J. K., and Versalovic, J. (2020) Mucin-Degrading Microbes Release Monosaccharides That Chemoattract *Clostridioides difficile* and Facilitate Colonization of the Human Intestinal Mucus Layer. *ACS Infect. Dis.*
303. Mora-Uribe, P., Miranda-Cárdenas, C., Castro-Córdova, P., Gil, F., Calderón, I., Fuentes, J. A., Rodas, P. I., Banawas, S., Sarker, M. R., and Paredes-Sabja, D. (2016) Characterization of the adherence of *Clostridium difficile* spores: the integrity of the outermost layer affects adherence properties of spores of the epidemic strain R20291 to components of the intestinal mucosa. *Front. Cell. Infect. Microbiol.* **6**, 99
304. Eveillard, M., Fourel, V., Bare, M. C., Kernéis, S., Coconnier, M. H., Karjalainen, T., Bourlioux, P., and Servin, A. L. (1993) Identification and characterization of adhesive factors of *Clostridium difficile* involved in adhesion to human colonic enterocyte-like Caco-2 and mucus-secreting HT29 cells in culture. *Mol. Microbiol.* **7**, 371-381
305. Gomez-Trevino, M., Boureau, H., Karjalainen, T., and Bourlioux, P. (1996) *Clostridium difficile* adherence to mucus: results of an *in vivo* and *ex vivo* assay. *Microb. Ecol. Health Dis.* **9**, 329-334
306. Semenyuk, E. G., Poroyko, V. A., Johnston, P. F., Jones, S. E., Knight, K. L., Gerding, D. N., and Driks, A. (2015) Analysis of bacterial communities during *Clostridium difficile* infection in the mouse. *Infect. Immun.* **83**, 4383-4391
307. Tasteyre, A., Barc, M.-C., Collignon, A., Boureau, H., and Karjalainen, T. (2001) Role of FliC and FliD Flagellar Proteins of *Clostridium difficile* in Adherence and Gut Colonization. *Infect. Immun.* **69**, 7937-7940
308. Engevik, M. A., Engevik, K. A., Yacyshyn, M. B., Wang, J., Hassett, D. J., Darien, B., Yacyshyn, B. R., and Worrell, R. T. (2015) Human *Clostridium difficile* infection:

inhibition of NHE3 and microbiota profile. *Am. J. Physiol. Gastrointest. Liver Physiol.* **308**, G497-G509

309. Engevik, M. A., Yacyshyn, M. B., Engevik, K. A., Wang, J., Darien, B., Hassett, D. J., Yacyshyn, B. R., and Worrell, R. T. (2015) Human *Clostridium difficile* infection: altered mucus production and composition. *Am. J. Physiol. Gastrointest. Liver Physiol.* **308**, G510-G524
310. Jensen, P. H., Kolarich, D., and Packer, N. H. (2010) Mucin-type O-glycosylation–putting the pieces together. *FEBS J.* **277**, 81-94
311. Sicard, J.-F., Le Bihan, G., Vogeleer, P., Jacques, M., and Harel, J. (2017) Interactions of intestinal bacteria with components of the intestinal mucus. *Front. Cell. Infect. Microbiol.* **7**, 387
312. Hoskins, L. C., and Boulding, E. T. (1981) Mucin degradation in human colon ecosystems: evidence for the existence and role of bacterial subpopulations producing glycosidases as extracellular enzymes. *J. Clin. Invest.* **67**, 163-172
313. Reddi, G., Pruss, K., Cottingham, K. L., Taylor, R. K., and Almagro-Moreno, S. (2018) Catabolism of mucus components influences motility of *Vibrio cholerae* in the presence of environmental reservoirs. *PloS One*. **13**, e0201383
314. Hugdahl, M. B., Beery, J., and Doyle, M. (1988) Chemotactic behavior of *Campylobacter jejuni. Infect. Immun.* **56**, 1560-1566
315. Tu, Q. V., McGuckin, M. A., and Mendz, G. L. (2008) *Campylobacter jejuni* response to human mucin MUC2: modulation of colonization and pathogenicity determinants. *J. Med. Microbiol.* **57**, 795-802
316. Furter, M., Sellin, M. E., Hansson, G. C., and Hardt, W.-D. (2019) Mucus architecture and near-surface swimming affect distinct *Salmonella Typhimurium* infection patterns along the murine intestinal tract. *Cell Rep.* **27**, 2665-2678. e2663
317. Courson, D. S., Pokhrel, A., Scott, C., Madrill, M., Rinehold, A. J., Tamayo, R., Cheney, R. E., and Purcell, E. B. (2019) Single cell analysis of nutrient regulation of *Clostridioides (Clostridium) difficile* motility. *Anaerobe*. **59**, 205-211
318. Antunes, A., Martin-Verstraete, I., and Dupuy, B. (2011) CcpA-mediated repression of *Clostridium difficile* toxin gene expression. *Mol. Microbiol.* **79**, 882-899

319. Purcell, E. B., McKee, R. W., Courson, D. S., Garrett, E. M., McBride, S. M., Cheney, R. E., and Tamayo, R. (2017) A nutrient-regulated cyclic diguanylate phosphodiesterase controls *Clostridium difficile* biofilm and toxin production during stationary phase. *Infect. Immun.* **85**, 347-364

320. Wilson, K. H., and Perini, F. (1988) Role of competition for nutrients in suppression of *Clostridium difficile* by the colonic microflora. *Infect. Immun.* **56**, 2610-2614

321. Wadsworth, P. (2007) Studying mitosis in cultured mammalian cells. *Cold Spring Harb. Protoc*. **2**, pdb-prot4647

322. Swidsinski, A., Sydora, B. C., Doerffel, Y., Loening-Baucke, V., Vaneechoutte, M., Lupicki, M., Scholze, J., Lochs, H., and Dieleman, L. A. (2007) Viscosity gradient within the mucus layer determines the mucosal barrier function and the spatial organization of the intestinal microbiota. *Inflamm. Bowel Dis.* **13**, 963-970

323. Fan, Y., Wen, Z. T., Liao, S., Lallier, T., Hagan, J. L., Twomley, J. T., Zhang, J.-F., Sun, Z., and Xu, X. (2012) Novel amelogenin-releasing hydrogel for remineralization of enamel artificial caries. *J. Bioact. Compat. Polym.* **27**, 585-603

324. Lai, S. K., Wang, Y.-Y., Wirtz, D., and Hanes, J. (2009) Micro-and macrorheology of mucus. *Adv. Drug Deliv. Rev.* **61**, 86-100

325. Nakamura, S., Nakashio, S., Yamakawa, K., Tanabe, N., and Nishida, S. (1982) Carbohydrate fermentation by *Clostridium difficile*. *Microbiol. Immunol.* **26**, 107-111

326. Dubois, T., Tremblay, Y. D., Hamiot, A., Martin-Verstraete, I., Deschamps, J., Monot, M., Briandet, R., and Dupuy, B. (2019) A microbiota-generated bile salt induces biofilm formation in *Clostridium difficile*. *NPJ Biofilms Microbiomes.* **5**, 1-12

327. Xu, H., Zou, Y., Lee, H. Y., and Ahn, J. (2010) Effect of NaCl on the biofilm formation by foodborne pathogens. *J. Food Sci.* **75**, M580-M585

328. Jefferson, K. K. (2004) What drives bacteria to produce a biofilm? *FEMS Microbiol. Lett.* **236**, 163-173

329. Ng, K. M., Ferreyra, J. A., Higginbottom, S. K., Lynch, J. B., Kashyap, P. C., Gopinath, S., Naidu, N., Choudhury, B., Weimer, B. C., and Monack, D. M. (2013)

Microbiota-liberated host sugars facilitate post-antibiotic expansion of enteric pathogens. *Nature*. **502**, 96-99

330. Tobe, T., Nakanishi, N., and Sugimoto, N. (2011) Activation of motility by sensing short-chain fatty acids via two steps in a flagellar gene regulatory cascade in enterohemorrhagic *Escherichia coli*. *Infect. Immun.* **79**, 1016-1024
331. Krukonis, E. S., and DiRita, V. J. (2003) From motility to virulence: sensing and responding to environmental signals in *Vibrio cholerae*. *Curr. Opin. Microbiol.* **6**, 186-190
332. Park, S., Dingemans, J., Gowett, M., and Sauer, K. (2021) Glucose-6-Phosphate Acts as an Extracellular Signal of SagS To Modulate *Pseudomonas aeruginosa* c-di-GMP Levels, Attachment, and Biofilm Formation. *mSphere*. **6**
333. Chai, Y., Kolter, R., and Losick, R. (2010) Reversal of an epigenetic switch governing cell chaining in *Bacillus subtilis* by protein instability. *Mol. Microbiol.* **78**, 218-229

APPENDIX A

SUMMARY OF STRAINS AND PLASMIDS USED

Name	Description	Reference
Escherichia coli		
DH5α	F- φ80*lacZ*ΔM15 Δ(*lacZYA-argF*) U169 *recA1 endA1 hsdR*17, *phoA supE*44 *thi*-1 *gyrA*96 *relA1* λ^- *tonA*	New England Biolabs (NEB)
BL21	*fhuA2 [lon] ompT gal [dcm] ΔhsdS*	NEB
HB101		NEB
HB101 pRK24	HB101 transformed with pRK24	273
RT1255	pMMBneo::*R20291_rsh*-His6 in DH5α	248
RT1270	pMMBneo::*R20291_rsh*-His6 in BL21	248
Clostridioides difficile		
630	Wild type	
630Δ*erm*	Wild type 630 lacking erythromycin resistance gene *ermB*	108
R20291	Wild type	
CEP18	pRF185::*phiLOV2.12.1* in R20291	147
CEP19	pRF185::*phiLOV2.12.1* in 630Δ*erm*	147
CEP21	P*relQ630*Δ*erm::phiLOV2.12*.1 in R20291	147
CEP22	P*rsh630*Δ*erm::phiLOV2.12.1* in 630Δ*erm*	147
CEP23	*PrelQ630*Δ*erm*::*phiLOV2.*12.1 in 630Δ*erm*	147
CEP25	PrshR20291::*phiLOV2.12.1* in R20291	147
Plasmids		
pMMBneo	Low copy expression vector, *Ptac*, *neo* cassette, *KanR*	147
pRF185	*tetR*	273
pMMBneo::*R20291_rsh*-His6	R20291 *rsh* ligated into KpnI/PstI sites of pMMBneo	147

pMMBneo::*R20291_rshREL*-His6	*rel* amplified from R20291 *rsh* and ligated into KpnI/PstI sites of pMMBneo	147
pRF185::*phiLOV2.12.1*	*phiLOV2.1* downstream of tetracycline-inducible promoter ligated into BamHI/KpnI sites of pRF185	273
PrelQ630Δ*erm*::*phiLOV2.12.1*	Predicted promoter upstream of 630Δ*erm relQ* amplified and ligated into BamHI/KpnI sites of pRF185::phiLOV2.12.1	147
Prsh630Δ*erm*::*phiLOV2.12.1*	Predicted promoter upstream of 630Δ*erm rsh* amplified and ligated into BamHI/KpnI sites of pRF185::phiLOV2.12.1	147
PrshR20291::*phiLOV2.12.1*	Predicted promoter upstream of R20291 *rsh* amplified and ligated into BamHI/KpnI sites of pRF185::phiLOV2.12.1	147
pMSPT	Low copy expression vector	68
pMSPT::*as_rsh*	Antisense RNA to the mRNA of Cd*rsh* ligated into the SphI/XhoI sites of pMSPT	147
pBAD33	Low copy expression vector	
pBAD33::*rsh-rel*	*rsh-rel* amplified from full-length *rsh* and ligated into KpnI/PstI sites of pBAD33	147
pET24a	High copy expression vector	
pET24a*::rsh-rel*	*rsh-rel* amplified from full-length *rsh* and ligated into NdeI/XhoI sites of pET24a	147

APPENDIX B

SEQUENCES OF PRIMERS USED

Name	Sequence (5' to 3') Underlined region = restriction enzyme cut site	Reference
Cloning primers		
rsh_F KpnI	CAGGTACCGGTTATATGCATGATAAAGAAT TACAAG	248
rsh_R PstI	CCCTGCAGCTAATGGTGATGGTGATGGTGAT TTGTCATTCTATAAATAC	248
pRF185_F	CTGGACTTCATGAAAAACTAAAAAAAATATTG	147
pRF185_R	CACCGACGAGCAAGGCAAGACCG	147
phiLOV2.1_F	GCTAGCCCAGGTATGATTGAAAAAAGTTTTG TTATTACTG	147
phiLOV2.1_R	CATGGATCCTTATTAAACATGATCTG	147
Prsh_F BamHI	TATAGGATCCGGAAAGTTACCAGGTGAAGTT GA	147
Prsh_R KpnI	ATATGGTACCCCACCTATTTTGTATAAAATTT TAATATATATG	147
PrelQ_F BamHI	TATAGGATCCATGGCAAGCAAGTTATATCG	147
PrelQ_R KpnI	ATATGGTACCCCTTTATTTGTTTTTTATGACCT TC	147
relQ_F	CAAGAATTCCACTATGGAGCTTGTAATCA	147
relQ_R	CAAGGATCCCATATTGCTCACCCTTTATTTG	147
pMSPT_F	CTAAAGGGCAAAAGTGAGTATGG	147
pMSPT_R	GACGAGCAAGGCAAGACC	147
rsh_as_F	GGTATGCATGCTGCATAAAC	147
rsh_as_R	CCTAGCTCTCGAGACCAAC	147
rshREL_F KpnI	CAGGTACCATGAAAGAAGAAACTCAATCTG	147
rshREL_R PstI	CCCTGCAGCTAATGGTGATGGTGATGGTGA CTATTAAATACATCTTCTTTAAGTGC	147
pET24a::*rsh-rel*_F	GACCATATGAAAGAAGAAACTCAATC	This study
pET24a::*rsh-rel*_R	GTGCTCGAGACTATTAAATACATCTTC	This study

pBAD33::*rsh-rel*_F	CAGGTACCATGAAAGAAGAAACTCAATCTG	This study
pBAD33::*rsh-rel*_R	CCCTGCAGCTAATGGTGATGGTGACTATTAAATACATCTTCTTTAAGTGC	This study
qRT-PCR primers		
rpoCq_F	CTAGCTGCTCCTATGTCTCACATC	147
rpoCq_R	CCAGTCTCTCCTGGATCAACTA	147
rsh_qF	AAAATAGGTGGTTAT	147
rsh_qR	TCAATTTTATTATCCCTCCTTTGA	147
relQ_qF	CATTGCGGGTTCAAAGGAAAT	147
relQ_qR	CATTGCGGGTTCAAAGGAAAT	147

APPENDIX C

SIGNAL QUANTIFICATION USING A TLC AUTORADIOGRAM

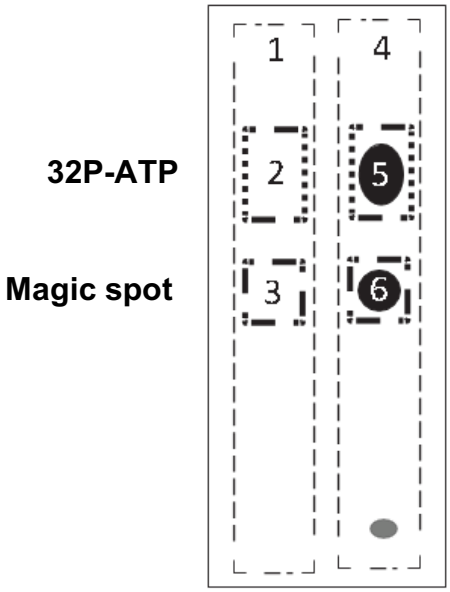

Signal quantification using a TLC autoradiogram. Regions of interest (ROIs) defining the total, 32P-ATP, and magic spot signal are shown for a blank lane and an experimental lane. Signal intensity within each blank ROI is subtracted from the experimental value, and the 32P-ATP and the magic spot signals are normalized to the total signal using the equations given to present the percentage of the total radioactive signal attributable to ATP hydrolysis and magic spot or putative 5'-pGpp-3' alarmone synthesis. Adapted from Pokhrel *et al.* 2018.

APPENDIX D

RSHCd PRODUCES PUTATIVE TRIPHOSPHATE ALARMONES

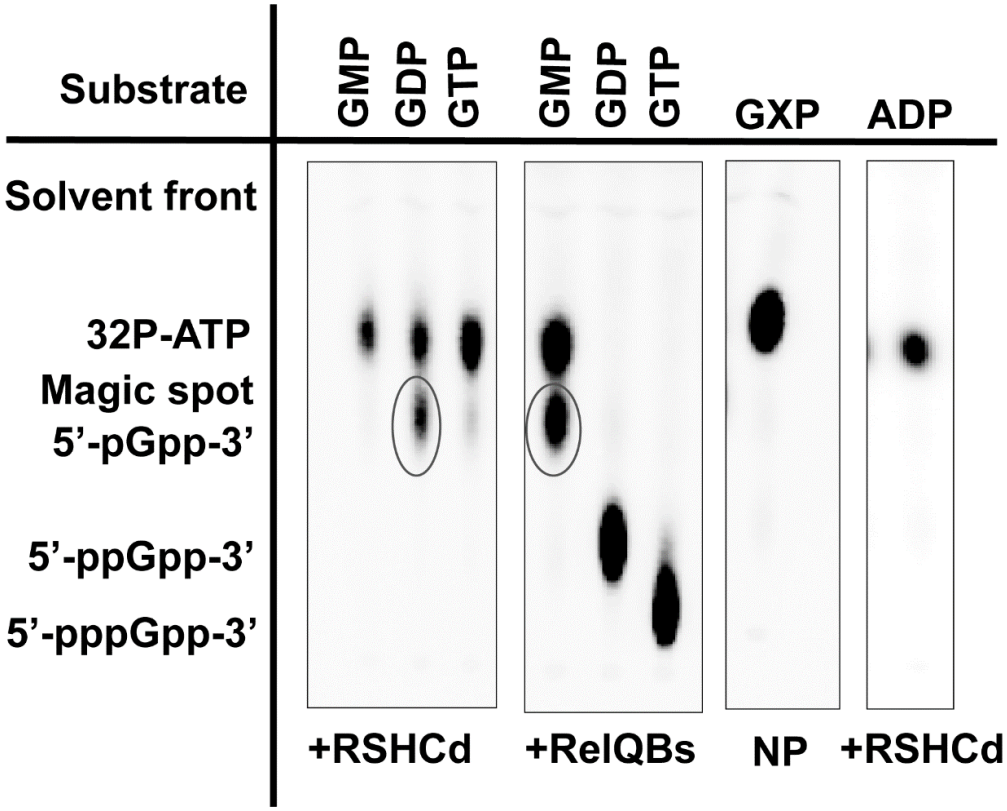

Autoradiograms of *in vitro* pyrophosphate transfer reactions catalyzed by RSHCd and RelQBs in the presence of GMP, GDP, GTP, and ADP (RSHCd only). RelQBs utilizes GMP, GDP, and GTP to produce 5'-pGpp-3', 5'-ppGpp-3', and 5'-pppGpp-3', respectively. RSHCd is unable to utilize GMP, GTP, and ADP. When either protein is lacking in the incubation mixture (where NP denotes no protein), magic spot is not synthesized. RSHCd-produced magic spot migrates similar distance with RelQBs-produced pGpp (black oval), suggesting that RSHCd-catalyzed magic spot could be pGpp. The first three autoradiograms (left to right) were produced by Asia Poudel and the last one by Astha Pokhrel (Poudel *et al.* manuscript in preparation).

APPENDIX E

SUBLETHAL CONCENTRATIONS OF ANTIBIOTICS USED

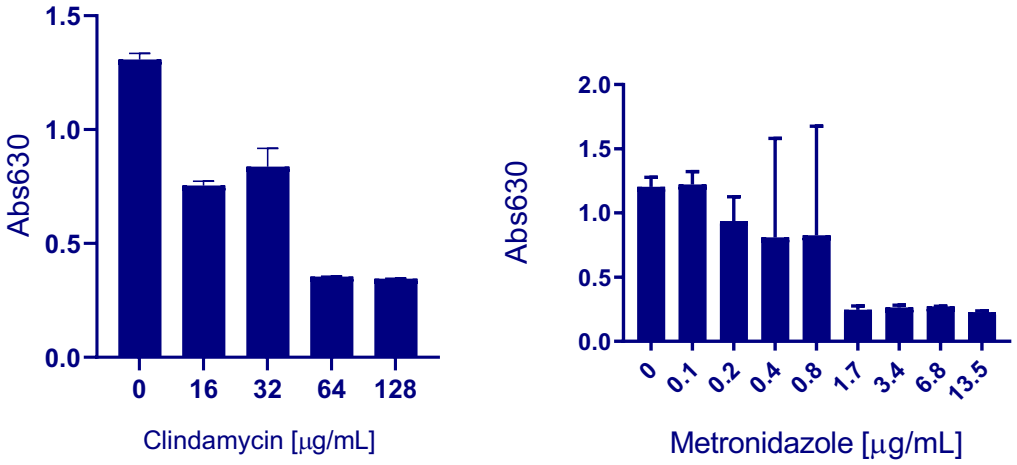

Sublethal concentration	Clindamycin (μg/mL)	Metronidazole (μg/mL)
0.25X	4.00	0.075
0.5X	8.00	0.15
1X	16.0	0.30

Sublethal concentrations of antibiotics metronidazole and clindamycin for *C. difficile* R20291 were determined using the standard minimum inhibitory concentration (MIC) technique. ON starter cultures of R20291 were inoculated 1:10 into fresh BHIS media treated with increasing concentrations of either antibiotic. Cells were incubated anaerobically at 37°C for 12 hrs to monitor cell accumulation and growth inhibition. The sublethal concentrations used in the study for four independent biologicals are shown. Adapted from Pokhrel *et al.* 2020.

APPENDIX F

SUBLETHAL CONCENTRATIONS OF ANHYDROTETRACYCLINE

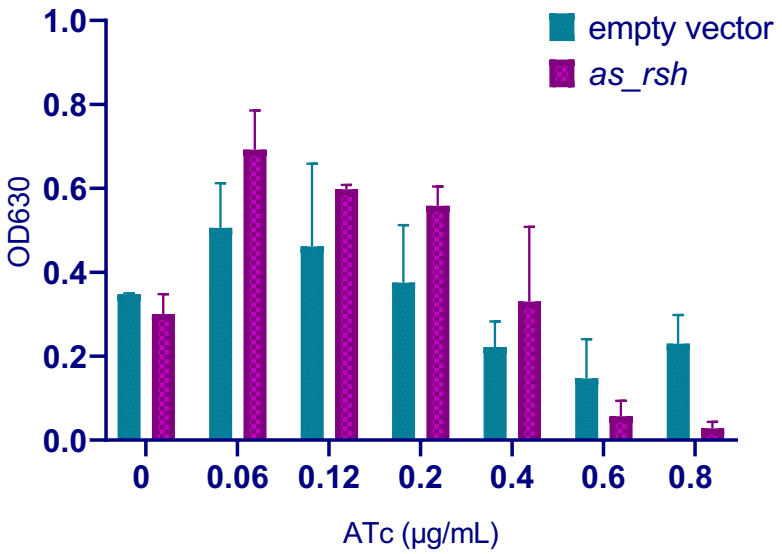

Minimum inhibitory concentration for ATc against *C. difficile* RNAi strains were analyzed in BHIS plus thiamphenicol (15 µg/mL) medium with increasing concentrations of ATc. ON starter cultures of RNAi strains were inoculated into media at the ratio of 1:20 and incubated anaerobically at 37°C for 24 hrs to monitoring growth inhibition. The MIC against empty vector (pMSPT) and asRNA vector (pMSPT*::as_rsh*) expressing strains are shown for two biological replicates. 0.5 µg/mL was determined to be the sublethal concentration of ATc against both RNAi strains to be used for end-point cell accumulation assays. Adapted from Pokhrel *et al.* 2020.

APPENDIX G

MOTILITY VIDEOS OF R20291 IN THE PRESENCE OF NEU5A

https://doi.org/10.1016/j.anaerobe.2019.102080.

Link is adapted from Courson *et al.* 2019.

APPENDIX H

TIME-COURSE ANALYSIS OF RSHCd ACTIVITY *IN VITRO*

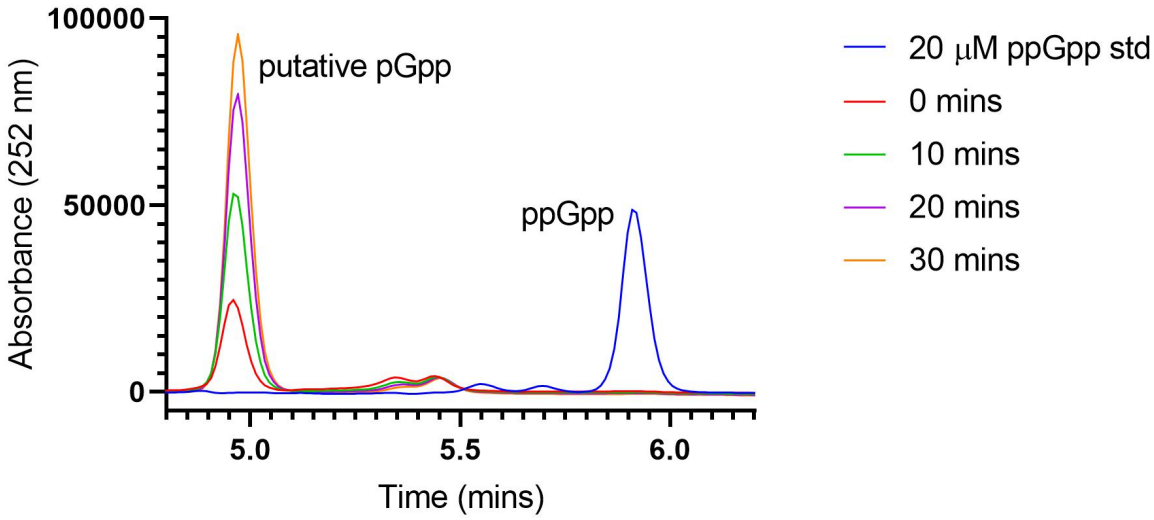

HPLC analysis of RSHCd-mediated three-phosphate alarmone production with increasing incubation time. Synthetase activity was performed in a buffer containing 10 mM Tris-HCl (pH 7.5 ± 0.5), 5 mM ammonium acetate, 2 mM KCl, 0.2 mM DTT, 0.12 mM ATP, 0.6 mM GDP, and 1.2 mM $MgCl_2$. Reaction was initiated by adding RSHCd at a final concentration of 3.0 μM and incubated at 37°C on a portable dry bath for a total duration of 30 mins. At 10 mins intervals, ~45 μL samples were transferred into VIVA SPIN 500 spin column (Corning) with a MWCO of 30 KDa and spun at 12,000 X g for 5 mins at 20°C. Filterates/samples were run through a strong anion exchange column the following day along with a 20 μM 5'-ppGpp-3' standard (Trilink) using a gradient elution profile. Absorbance at 252 nm was used to detect the standard (std) (blue peak) and the triphosphate compound at different time points. With increasing incubation time, there is an evident increase in the signal of putative pGpp as depicted in the chromatogram. This experiment was performed, and chromatogram produced by Astha Pokhrel (Poudel *et al.* manuscript in preparation).

APPENDIX I

C. DIFFICILE GENOME ENCODES FOR TWO PUTATIVE NUDIX ENZYMES

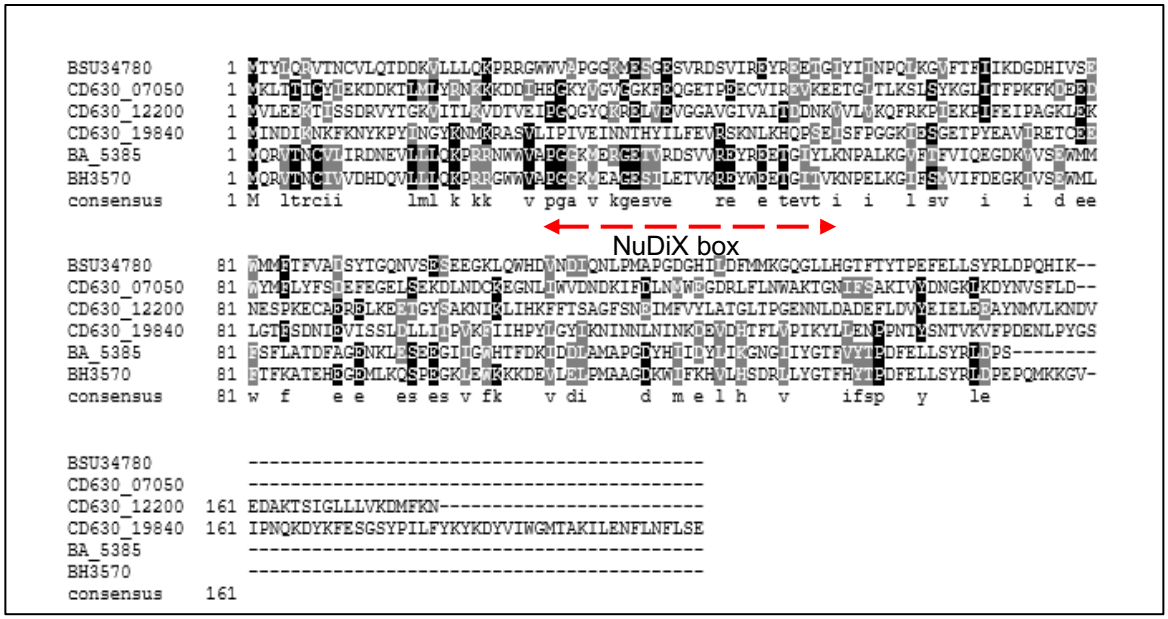

Protein sequence alignment of NahA (YvcI) homologs in different species including *C. difficile* strain 630. Multiple sequence alignment of YvcI homologs from *B. subtilis* (BSU_34780), *B. anthracis* (BA_5385), *B. halodurans* (BH_3570), and *C. difficile* 630 (CD630_07050, CD630_12200, CD630_19840). Alignment was obtained with BoxShade Server-EMBnet (with consensus lines). Numbers on the sides of the sequences indicate the residue numbers in the corresponding proteins. Dark shading (black) represents identical amino acid residues among sequences being aligned, whereas light shading (grey) represents amino acid residues with matching polarity. Protein accession numbers were retracted from Yang *et al.* 2020.

APPENDIX J

SIGNIFICANCE OF *RSH* GENE TO *C. DIFFICILE* TOXICITY

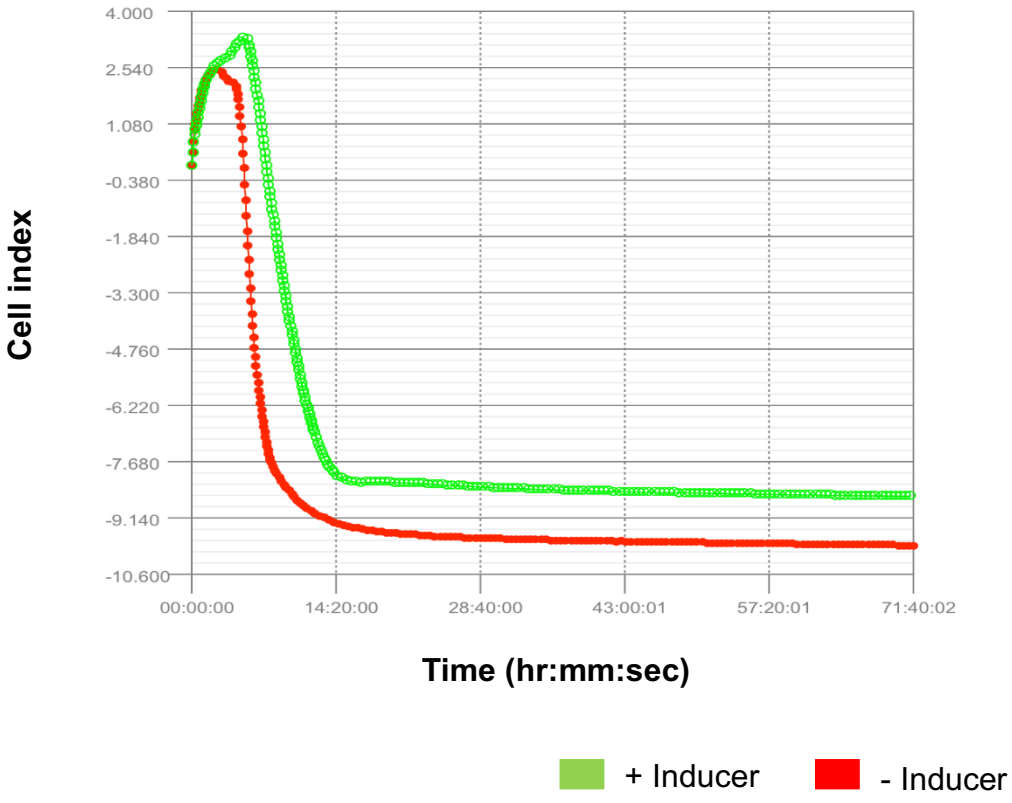

Significance of *rsh* in *C. difficile* virulence examined in real-time using iCeLLigence™ real-time cell analyzer (Agilent). The assays involved culturing 300 µL of MDCK cells (ATCC) in Dulbecco's modified eagle medium (DMEM) from VWR in the wells of the 16-well microtiter plates (with a gold microelectrode biosensor array) within a CO_2 incubator. Post-incubation, the apparatus was taken into the anaerobic chamber where MDCK cells were cultured in BHIS-Tm_{15} media with *as_rsh* expression vector carrying RNAi strain (R20291 variant), and with or without 0.5 µg/mL ATc. *C. difficile* toxicity was measured for a total of 72 hrs (5 mins interval for the first 24 hrs and 15 mins interval for the remaining 48 hrs).

APPENDIX K

MICROSCOPIC ANALYSIS OF R20291 AGGREGATION

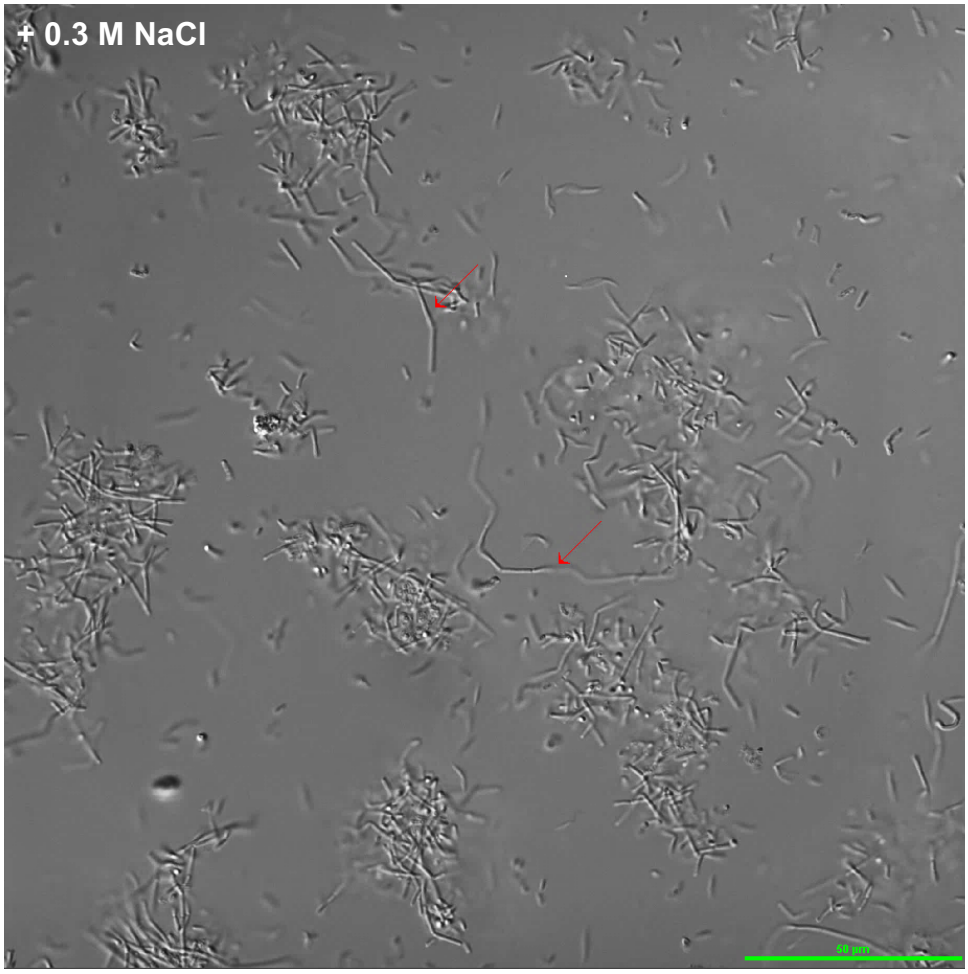

Portable rose cell chamber was injected with 1:100 dilution of ON starter culture of R20291 cells in buffered BHIS medium diluted with 0.3 M NaCl. The chamber was parafilmed and placed on the stage of a Nikon Ti-E inverted microscope. Live-cell DIC microscopy was performed to image R20291 aggregation in the presence of 0.3 M NaCl over a period of 48 hrs. Stage temperature was maintained at 36.5°C ± 0.5°C using a Nevtek Air Stream stage warmer. Red arrows indicate chaining of replicating cells for single-species biofilm formation. *C. difficile* produce biofilm in response to osmolarity stress. Scale bar shown is 50 µm.

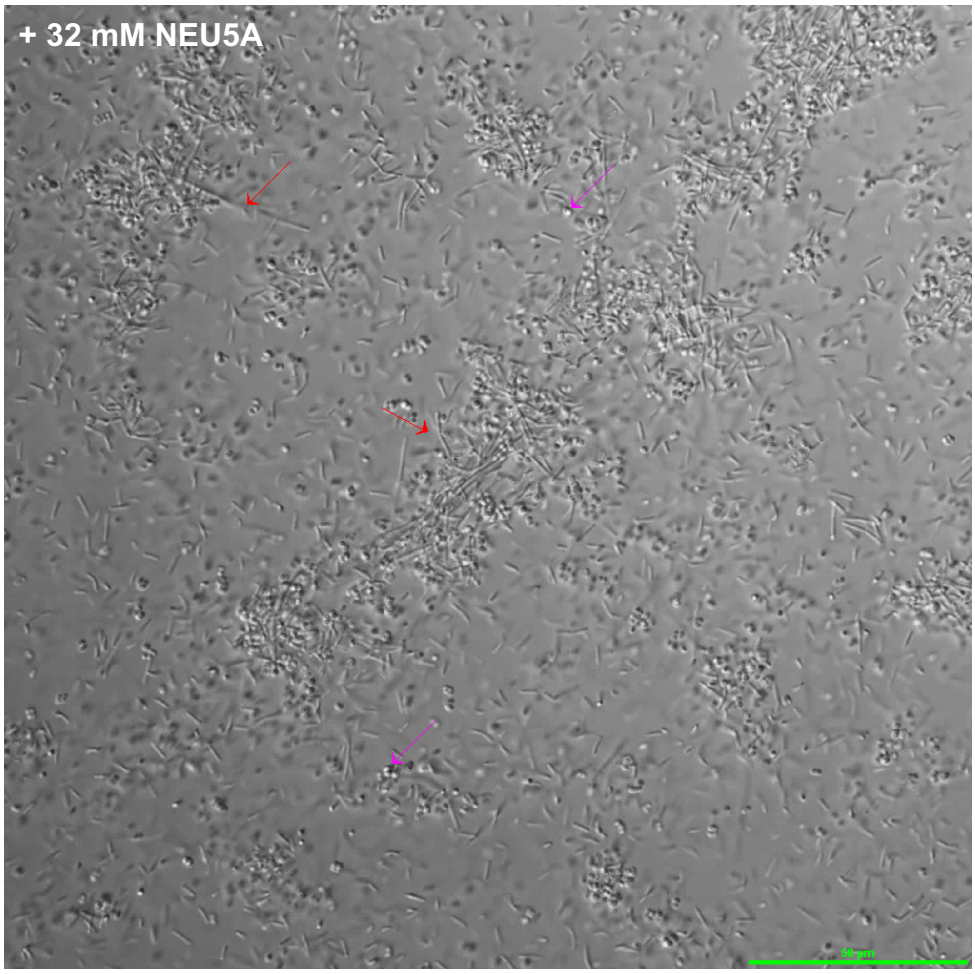

Portable rose cell chamber was injected with 1:100 dilution of ON starter culture of R20291 cells in buffered BHIS medium diluted with 32 mM NEU5A. The chamber was parafilmed and placed on the stage of a Nikon Ti-E inverted microscope. Live-cell DIC microscopy was performed to image R20291 aggregation in the presence of 32 mM NEU5A over a period of 48 hrs. Stage temperature was maintained at 36.5°C ± 0.5°C using a Nevtek Air Stream stage warmer. Red arrow(s) indicate replicating cells making contacts with one another to form extended, notably shorter chains for the initiation of single-species biofilm formation than in 0.3 M NaCl. Magenta arrows indicate spores. Unlike biofilm produced by R20291 in the presence of NaCl, the biofilm community of R20291 in 32 mM NEU5A may be dominated by spores. Scale bar shown is 50 μm.

APPENDIX L

PROPOSAL AND APPROVAL TO USE 32P

Old Dominion University
Radiation Safety Committee

Application for the Possession and Use of Radioactive Materials

Directions: This application is to be completed only by Authorized Users or persons applying concurrently for Authorized User status (RSO-1). *Complete in duplicate, sign both copies, and return* to the Environmental Health and Safety Office/Radiation Safety Office. When approved by the Radiation Safety Committee, one copy will be returned to the applicant to serve as his/her authorization. *This authorization expires two years from the approval date.* An amendment must be submitted for approval before any change in protocol.

1. **Applicant:** Erin Purcell

   Department: Chemistry and Biochemistry

2. **Application Type:** ☑ New ☐ Renewal ☐ Amendment

3. **Office:**

   Building Alfriend Room 201 Phone (757) 683-4240

4. **Location(s) of Proposed Use:**

   Building Alfriend Room(s) 206, 107 Phone none

5. **Radionuclides for Possession:**

   (a) **Radionuclide:** 32-P Possession Limit (mCi): 1.0

   Chemical/Physical Form: aqueous gamma-32-P ATP (adenosine triphosphate)

   (b) **Radionuclide:** _____ Possession Limit (mCi): _____

   Chemical/Physical Form: _____

   (c) **Radionuclide:** _____ Possession Limit (mCi): _____

   Chemical/Physical Form: _____

   (d) **Radionuclide:** _____ Possession Limit (mCi): _____

   Chemical/Physical Form: _____

   (e) **Radionuclide:** _____ Possession Limit (mCi): _____

   Chemical/Physical Form: _____

RSO-2 (rev. 7/02)

1

6. Sealed Sources Only:

Complete this part for each sealed source proposed for use. Low activity check sources and exempt check sources need not be listed.

(a) Source:

Radionuclide: _____ Half-life: _____

Activity: _____(mCi)

Principal radiation emitted (check one or more) and energy(s) of the emission(s):

☐ Alpha Energy _____(MeV)

☐ Beta Energy _____max. ___ (MeV)

☐ Gamma or x-ray Energy _____(MeV)

☐ Positron Energy _____(MeV)

Date calibrated: _____

Manufacturer: _____

Model No.: _____

Serial No.: _____

(b) Source description:

(c) Describe the proposed use(s) of the source giving particular attention to health and safety aspects:

7. Unsealed Sources Only:

Complete this part for *each* radionuclide proposed for use. Use a separate page for each radionuclide.

(a) Radionuclide:

Radionuclide 32-P Half-life 14.3 days

Principal radiation emitted (check one or more) and energy(s) of the emission(s):

- ☐ Alpha Energy _____(MeV)
- ☑ Beta Energy 1.71 max. (MeV)
- ☐ Gamma or x-ray Energy _____(MeV)
- ☐ Positron Energy _____(MeV)

(b) Experimental Protocol:

Outline experimental protocol, with particular attention to health and safety aspects of the proposed use. Use additional sheet(s) if necessary.

See attached page.

(c) Waste:

Estimate activity and volume (or number) of waste that will be generated by proposed use.

- ☑ Aqueous: Activity/Volume per month 0.005 mCi
- ☐ Other liquid (specify): Activity/Volume per month _____
- ☐ Liquid scintillation vials Activity/Number per month _____
- ☐ Animal carcasses Activity/Number per month _____
- ☑ Solid (dry)/Incinerable Activity/Volume per month 0.020 mCi
- ☐ Solid (dry)/Non-Incinerable Activity/Volume per month _____
- ☐ Other (specify): Activity/Volume/Number per month _____

(d) Associated Wastes:

If applicable, describe any mixed waste (e.g. carcinogenic, hazardous etc.) that will be generated as a result of proposed use

Experimental Protocol

Gamma-32-P ATP (adenosine triphosphate) will be used as a reagent for phosphotransfer experiments. Briefly, gamma-32-P ATP will be added to reaction mixes with crude cell extract or purified enzyme and either GDP (guanosine diphosphate) or GTP (guanosine triphosphate). At selected timepoints, aliquots of this reaction mixture will be spotted onto PEI cellulose plates and air dried. When experiments are complete, cellulose plates will be used for thin layer chromatography (TLC) in aqueous buffer buffer, dried, and exposed to a phosphorimager plate for visualization.

On occasion, radioactive guanosine tetraphosphate (ppGpp) formed when the beta and gamma phosphate from gamma-32-P ATP is transferred to a GDP substrate will be isolated from the TLC plates by cutting the radionuclide-containing portion of the TLC plate in water or buffer, precipitating the phosphate species in salt solution, and rehydrating the precipitated 32-P ppGpp. This purified 32-P ppGpp will be used as a substrate in subsequent TLC reactions performed as above.

Radionuclides will be stored in a locked acrylic container within a -20 degree freezer. This container will be transported to a radioactivity workstation and opened behind an acrylic shield to retrieve materials. Reaction mixes will be assembled with all components except for the radioactive substrate before experiments are initiated by adding the 32-P ATP. All steps involving radioactive materials—reaction assembly and spotting, running, and exposing the TLC plates--will occur behind plexiglass shielding. All work will occur over a disposable absorbant bench pad with a water resistant backing (bench diaper), which will be disposed in the radioactive solid waste after use. Personnel will wear appropriate PPE (gloves and labcoats) and will use a GM pancake detector to monitor for environmental contamination during and after the experiment.

We anticipate using roughly 0.25 mCi/month. These protocols will generate incinerable dry waste in the form of plastic tubes and pipet tips, bench pads and paper towels used for cleaning, and the TLC plates. Dry waste will be stored in a shielded container for EHS pickup. Reactions will be designed to occur in minimal volume, to limit the production of aqueous waste. When the TLC is performed properly, the radioactive phosphate species will remain on the cellulose plate and not enter the running buffer, but used buffer will be considered radioactive and stored and disposed of as aqueous radioactive waste, as will buffer or water used to soak and precipitate 32-P ppGpp. Aqueous radioactive waste will be stored in a shielded container for EHS pickup.

8. Equipment and Facilities:

(a) Instruments and Equipment:

Check available instruments and equipment

- ☐ Fume hood Room # _____
- ☑ Appropriate signs, tape and labeling
- ☑ Personal protective equipment (PPE)
  - ☑ Disposable gloves
  - ☑ Lab coats
  - ☐ Safety glasses
- ☑ Waterproof backed absorbent material for benches
- ☐ Remote pipette(s)
- ☐ Trays to contain spills
- ☐ Film badges
- ☑ Portable radiation detection instrument(s) Specify type GM pancake detector
- ☐ Liquid scintillation counter
- ☐ Gamma scintillation counter

(b) Facilities:

Attach a floor plan of areas where radioactive materials are used or stored showing fixtures such as sinks, hoods, benches, cold rooms etc., and major pieces of equipment such as refrigerators, freezers, centrifuges desks, radwaste containers etc. Indicate work areas, radioactive material storage areas, radioactive waste storage areas, entrances and exits. *Indicate room numbers.*

See attached page.

9. Security and Emergency Procedures:

(a) Security

Describe what provisions have been made to insure that radioactive materials are secure from unauthorized persons. Also describe a key control plan designed to restrict access to areas where radioactive materials are used and stored.

See attached page.

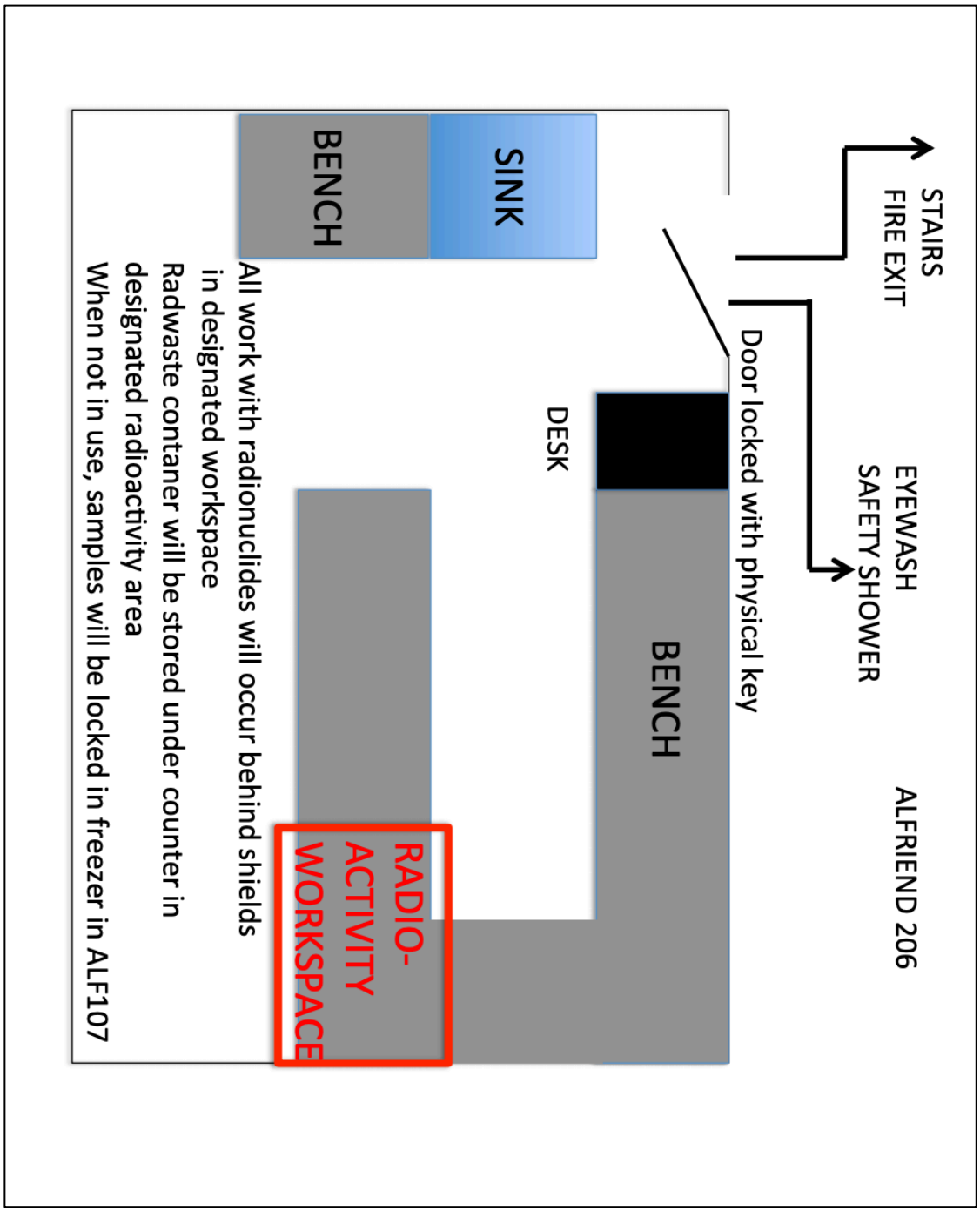
STAIRS
FIRE EXIT
EYEWASH
SAFETY SHOWER
ALFRIEND 206
Door locked with physical key
BENCH
DESK
SINK
BENCH
RADIO-
ACTIVITY
WORKSPACE
All work with radionuclides will occur behind shields
in designated workspace
Radwaste contaner will be stored under counter in
designated radioactivity area
When not in use, samples will be locked in freezer in ALF107

ALFRIEND 107

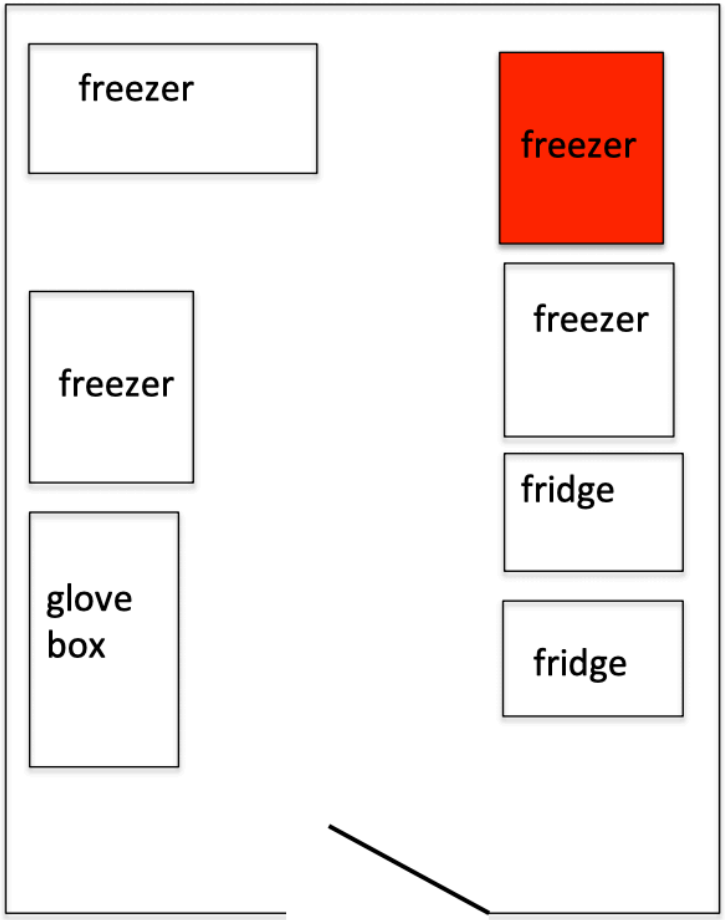

Future site of freezer in which radioactive material will be stores
Door locked with physical key

Door locked with numeric keypad

Security Procedures

Stock vials of gamma-32-ATP and any radionuclide products purified from TLC plates will be stored in an acylic lockbox secured to the inside of a -20 degree freezer (in Alfriend 107). Only qualified laboratory personnel will have either the key or the combination to the lock securing the box to the freezer and the separate lock to open the box. All work involving radionuclides will occur in Alfriend 206, which is kept locked when unoccupied. Only qualified laboratory personnel have the key to the room. A record of who has keys will be kept with other radiation safety documentation in a designated binder. Shielded waste will be stored in Alfriend 206.

Emergency Procedures

All radionuclides will be present as aqueous liquids, so spill procedures will be universal. Upon a spill, all work in the lab will be stopped and a sign placed on the door to prevent anyone from entering until the spill is cleaned up. Lab personnel, wearing appropriate PPE (lab coat, disposable gloves), keeping portable acrylic shields between their torsos/faces and the spill, will first use a Geiger coutner to define the area affected by the spill, then absorb all liquid with paper towels and dispose of them in the radioactive solid waste container. Personnel will then spray the affected area with radioactive spill cleaner (Count-Off or similar), absorb the liquid with paper towels, dispose of the paper towels in the radioactive waste, and survey the area with the Geiger counter. This procedure will be repeated until no radiation is detected. At this point, personnel will swipe the area with Kimwipes or filter paper to conduct a liquid scintillation test and ensure that there is no remaining contamination. After the area is confirmed to be clean of radioactivity, the sign will be removed from the door and normal laboratory operations will resume. The spill will be recorded in the use log and inventory to account for the radioactive material.

Laboratory monitoring

The lab will be monitored for radioactive contamination by liquid scintillation wipe tests (using the liquid scintillation counter owned by EHS) once monthly. The following surfaces within ALF206 will be tested:

- benchtop within radioactivity workspace
- floor within radioactivity workspace
- outside of radioactive waste containers
- pipets used within radioactivity workspace
- drawer handles within radioactivity workspace
- sink
- lab door handle

The radioactive workspace will be surveyed by GM pancake detector before and after each use of radionuclides.

Record keeping

Printed copies of materials pertaining to the use of radionuclides will be kept together in a designated binder, which will be kept on the reference shelf in ALF206. These will include:

- records of receipt of radionuclides
- use records—every time material is removed from the source vial, user will record the volume and activity removed. Every time materials are added to the dry or liquid waste container, the approximate activity added to that waste container will be recorded. After every use of radioactivity, the use logs will be updated so that the withdrawals of activity from the source vial equal the deposit of activity into the waste containers.
- Disposal records- whenever a source vial is discarded, it will be recorded and removed from the current inventory
- Records of monthly wipe tests
- All approvals from and communications with the radiation safety committee

(b) Emergency Procedures:

Describe the emergency procedure(s) that will be followed in case of a spill or accident. Describe decontamination procedures.

See attached page

(c) Emergency Contacts:

List two names and phone numbers to be called after hours in case of emergency.

Name Erin Purcell Phone (773) 354-2571

Name David Courson (spouse) Phone (773) 354-2570

10. Monitoring and Recordkeeping:

(a) Laboratory monitoring:

Describe your laboratory monitoring program. Include a description of your swipe survey schedule (specifically the frequency of surveys), areas to be surveyed, and documentation of surveys. *Note:* Survey frequency must be commensurate with the type(s), form(s), and activities of radionuclides proposed for use. For most applications swipe surveys must be conducted on a monthly basis. See the Radiation Safety Policy and Procedures Manual for guidance.

See attached page.S

(b) Recordkeeping:

Describe your method of inventory control and accounting, including records of receipt, use and disposal.

See attached page.

11. Personnel:

List all persons who will use or will be potentially exposed to radiation as the result of proposed use.

Erin B. Purcell (AU)

11. Certification:

The signature below affirms that the applicant has read and will comply with the rules, regulations, and procedures of the Old Dominion University Radiation Safety Committee and Radiation Safety Officer. The applicant accepts responsibility for maintaining current knowledge of those rules, regulations, and procedures and responsibility for the actions of those persons working under his/her authorization. Any changes in the use protocol, personnel and the location of use will be reported to the Radiation Safety Officer in a timely manner.

Signature Erin B Purcell **Date** Nov. 22, 2016

Radiation Safety Committee:

Approved / RSC Chair **Approved / RSO**

Approved / RSC Member **Approved / RSC Member**

Approved / RSC Member

(a) Dosimetry Indicated

- ☐ Whole Body
- ☒ Whole Body + Extremity
- ☐ Bioassay

(b) Special conditions attached to approval:

(c) Date of approval: 3/19/2018

(d) Expiration date: 3/18/2020

RSO-2 (rev. 7/02)

APPENDIX M

RIGHTS AND PERMISSIONS

jove

Hi Astha,

Thank you for publishing your article A Purification and *In Vitro* Activity Assay for a (p)ppGpp Synthetase from *Clostridium difficile* with JoVE.

You have permission to reuse the following material from it in your thesis or dissertation, pursuant to your Author License Agreement:

Figure(s):
Figure 1, 3, 4

Please ensure that JoVE is properly cited in the legends as well as the References: "This is adapted from Pokhrel, A., Poudel, A., Purcell, E. B. A Purification and *In Vitro* Activity Assay for a (p)ppGpp Synthetase from *Clostridium difficile*. *J. Vis. Exp.* (141), e58547, doi:10.3791/58547 (2018)."

Best regards,

Review
JoVE
617.674.1888
Follow us: Facebook | Twitter | LinkedIn
About JoVE

This message was sent to you by JoVE, the Journal of Visualized Experiments.
JoVE, One Alewife Center, Suite 200, Cambridge, MA 02140 | tel: 617.945.9051 | fax: 866.381.2236

Click the following links if you no longer want to receive emails from JoVE or to learn more about our policies.

Copyright Clearance Center | RightsLink®

Home | Help | Email Support | Astha Pokhrel

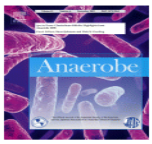

Single cell analysis of nutrient regulation of Clostridioides (Clostridium) difficile motility

Author:
David S. Courson,Astha Pokhrel,Cody Scott,Melissa Madrill,Alden J. Rinehold,Rita Tamayo,Richard E. Cheney,Erin B. Purcell

Publication: Anaerobe
Publisher: Elsevier
Date: October 2019

© 2019 Elsevier Ltd. All rights reserved.

Please note that, as the author of this Elsevier article, you retain the right to include it in a thesis or dissertation, provided it is not published commercially. Permission is not required, but please ensure that you reference the journal as the original source. For more information on this and on your other retained rights, please visit: https://www.elsevier.com/about/our-business/policies/copyright#Author-rights

BACK | CLOSE WINDOW

© 2021 Copyright - All Rights Reserved | Copyright Clearance Center, Inc. | Privacy statement | Terms and Conditions
Comments? We would like to hear from you. E-mail us at customercare@copyright.com

Relacin, a Novel Antibacterial Agent Targeting the Stringent Response

Ezequiel Wexselblatt, Yaara Oppenheimer-Shaanan, Ilana Kaspy, Nir London, Ora Schueler-Furman, Eylon Yavin, Gad Glaser, ...

PLOS

Citation: Wexselblatt E, Oppenheimer-Shaanan Y, Kaspy I, London N, Schueler-Furman O, Yavin E, et al. (2012) Relacin, a Novel Antibacterial Agent Targeting the Stringent Response. PLoS Pathog 8(9): e1002925. https://doi.org/10.1371/journal.ppat.1002925

Editor: Tomoko Kubori, Osaka University, Japan

Received: April 17, 2012; **Accepted:** August 9, 2012; **Published:** September 20, 2012

Copyright: © Wexselblatt et al. This is an open-access article distributed under the terms of the Creative Commons Attribution License, which permits unrestricted use, distribution, and reproduction in any medium, provided the original author and source are credited.

Funding: This work was supported by the European Research Council (ERC, erc.europa.eu) Starting Grant (209130) awarded to SBY, the Israeli National Academy of Science Foundation (ISF, www.isf.org.il) Grant (374/08) awarded to GG and the German-Israeli Foundation (GIF, www.gif.org.il) Grant (835/2004 and 943-334.9/2006) awarded to JK. The funders had no role in study design, data collection and analysis, decision to publish, or preparation of the manuscript.

Competing interests: The authors have declared that no competing interests exist.

Copyright Clearance Center | RightsLink®

Home | Help | Email Support | Sign in | Create Account

AMERICAN SOCIETY FOR MICROBIOLOGY

The (p)ppGpp Synthetase RSH Mediates Stationary-Phase Onset and Antibiotic Stress Survival in Clostridioides difficile

Author:
Astha Pokhrel,Asia Poudel,Kory B. Castro,Michael J. Celestine,Adenrele Oludiran,Alden J. Rinehold,Anthony M. Resek,Mariam A. Mhanna,Erin B. Purcell

Publication: Journal of Bacteriology

Publisher: American Society for Microbiology

Date: Sep 8, 2020

Copyright © 2020, American Society for Microbiology

Permissions Request

Authors in ASM journals retain the right to republish discrete portions of his/her article in any other publication (including print, CD-ROM, and other electronic formats) of which he or she is author or editor, provided that proper credit is given to the original ASM publication. ASM authors also retain the right to reuse the full article in his/her dissertation or thesis. For a full list of author rights, please see: http://journals.asm.org/site/misc/ASM_Author_Statement.xhtml

BACK | CLOSE WINDOW

© 2020 Copyright - All Rights Reserved | Copyright Clearance Center, Inc. | Privacy statement | Terms and Conditions
Comments? We would like to hear from you. E-mail us at customercare@copyright.com

Cyclic diguanylate signaling in Gram-positive bacteria

Author: Purcell, Erin B.; Tamayo, Rita
Publication: FEMS Microbiology Reviews
Publisher: Oxford University Press
Date: 2016-06-26

Copyright © 2016, Oxford University Press

Order Completed

Thank you for your order.

This Agreement between Old Dominion University ("You") and Oxford University Press ("Oxford University Press") consists of your license details and the terms and conditions provided by Oxford University Press and Copyright Clearance Center.

Your confirmation email will contain your order number for future reference.

License Number	4997830209532
License date	Jan 28, 2021

Printable Details

Licensed Content

Licensed Content Publisher	Oxford University Press
Licensed Content Publication	FEMS Microbiology Reviews

Order Details

Type of Use	Thesis/Dissertation
Requestor type	Educational Institution/Non-commercial/ Not for-profit
Format	Electronic

License date	Jan 28, 2021

Licensed Content

Licensed Content Publisher	Oxford University Press
Licensed Content Publication	FEMS Microbiology Reviews
Licensed Content Title	Cyclic diguanylate signaling in Gram-positive bacteria
Licensed Content Author	Purcell, Erin B.; Tamayo, Rita
Licensed Content Date	Jun 26, 2016
Licensed Content Volume	40
Licensed Content Issue	5

Order Details

Type of Use	Thesis/Dissertation
Requestor type	Educational Institution/Non-commercial/ Not for-profit
Format	Electronic
Portion	Figure/table
Number of figures/tables	3
Will you be translating?	No

About Your Work

Title	Evaluating the role of the stringent response mechanism in clostridioides difficile survival and pathogenesis
Institution name	Old Dominion University
Expected presentation date	Feb 2021

Additional Data

Portions	Figure 2.A, 2.B, 2.C, 2.D, 2.E

Requestor Location

Requestor Location	Old Dominion University 1049 W. 49th Street apt 203 NORFOLK, VA 23508 United States Attn: Astha Pokhrel

Tax Details

Publisher Tax ID	GB125506730

Copyright Clearance Center | RightsLink®

Home | Help | Email Support | Sign in | Create Account

Synthetic (p)ppGpp Analogue Is an Inhibitor of Stringent Response in Mycobacteria

Author:
Kirtimaan Syal,Kelly Flentie,Neerupma Bhardwaj,Krishnagopal Maiti,Narayanaswamy Jayaraman,Christina L. Stallings,Dipankar Chatterji

Publication: Antimicrobial Agents and Chemotherapy

Publisher: American Society for Microbiology

Date: May 24, 2017

Copyright © 2017, American Society for Microbiology

Permissions Request

ASM authorizes an advanced degree candidate to republish the requested material in his/her doctoral thesis or dissertation. If your thesis, or dissertation, is to be published commercially, then you must reapply for permission.

BACK CLOSE WINDOW

© 2021 Copyright - All Rights Reserved | Copyright Clearance Center, Inc. | Privacy statement | Terms and Conditions
Comments? We would like to hear from you. E-mail us at customercare@copyright.com

VITA

ASTHA POKHREL

Department of Chemistry and Biochemistry
Old Dominion University
Norfolk, VA 23529

EDUCATION

Ph.D. (Anticipated May 2021) in Chemistry and Biochemistry, Old Dominion University, Norfolk, VA, 2021

M.S. (May 2018) in Chemistry and Biochemistry, Old Dominion University, Norfolk, VA, 2018

B.Sc. (May 2015) in Biomolecular Sciences, Central Connecticut State University, New Britain, CT, 06110, 2015

PROFESSIONAL EXPERIENCE

- Graduate teaching assistant, Old Dominion University, Norfolk, VA, 2015-2021
- Graduate research assistant, Old Dominion University, Norfolk, VA, 2016-2017

PEER-REVIEWED PUBLICATIONS

- **Pokhrel, A.,** Poudel, A. and Purcell, E.B., 2018. A Purification and *In Vitro* Activity Assay for a (p)ppGpp Synthetase from *Clostridium difficile*. *JoVE (Journal of Visualized Experiments)*, (141), p.e58547.
- Courson, D.S., **Pokhrel, A.,** Scott, C., Madrill, M., Rinehold, A.J., Tamayo, R., Cheney, R.E. and Purcell, E.B., 2019. Single cell analysis of nutrient regulation of *Clostridioides (Clostridium) difficile* motility. *Anaerobe*, *59*, pp.205-211.
- **Pokhrel, A.,** Poudel, A., Castro, K.B., Celestine, M.J., Oludiran, A., Rinehold, A.J., Resek, A.M., Mhanna, M.A. and Purcell, E.B., 2020. The (p)ppGpp Synthetase RSH Mediates Stationary-Phase Onset and Antibiotic Stress Survival in *Clostridioides difficile*. *Journal of Bacteriology*, *2020* (19).